AN ABSTRACT OF THE DISSERTATION OF

Nicole Durfee for the degree of Doctor of Philosophy in Water Resources Science presented on July 12, 2022.

Title: Ecohydrologic Connections of Rangeland Ecosystems in Central and Eastern Oregon, USA

Abstract approved:

_____

Carlos G. Ochoa

In light of water scarcity and the impacts of climate change, there is an increased need to understand the interaction between land use characteristics and ecohydrologic processes in semiarid regions. Additionally, many semiarid and arid regions face various land management challenges, including woody plant encroachment, decreased snowpack, and increased stream temperatures. Therefore, a more comprehensive understanding of these processes is necessary for informing short-term land management approaches and long-term planning to help protect the resiliency of these systems.

The overarching goal of the studies presented here was to examine the ecohydrologic connections and environmental characteristics at two semiarid watersheds. The research for this dissertation sought to assess these connections in the context of two significant land management concerns: western juniper encroachment and increasing stream temperatures.

This dissertation is divided into four chapters. The research for the first two chapters of this dissertation took place at the Camp Creek Paired Watershed Study (CCPWS) in central Oregon, USA. This is a long-term study site established in 1993 in order to research the ecohydrologic impacts of western juniper (*Juniperus occidentalis*) encroachment and removal. The first chapter compares the seasonal water balance of a western juniper-dominated watershed to that of a sagebrush-

dominated watershed over a period of eight years. The second chapter examines multiple approaches to estimating evapotranspiration (ET) and characterizes the relationship between two vegetation indices [Normalized Difference Vegetation Index (NDVI) and the Normalized Difference Moisture Index (NDMI)] and soil moisture, ET, and springflow characteristics.

CCPWS consists of two adjacent watersheds of similar size and orientation and a riparian valley site located downstream of both watersheds. The majority of western juniper was removed from one watershed in 2005 and 2006 ('Mays WS'), and big sagebrush (*Artemisia tridentata*) is the dominant overstory vegetation. Western juniper is the dominant overstory in the other watershed ('Jensen WS').

Western juniper encroachment has been linked to reduced herbaceous productivity, altered soil moisture characteristics, altered streamflow timing, and soil erosion. Additionally, western juniper is costly and labor-intensive to remove. Cattle grazing is a key land use in central OR. In many semiarid regions of OR, reductions in herbaceous vegetative production and water availability can have ecological and economic impacts.

In order to better understand the potential hydrologic impacts of western juniper at this study site, a seasonal water balance approach was used. Eight years of streamflow, springflow, soil moisture, shallow groundwater levels, and meteorological data (precipitation, air temperature, and solar radiation) were measured. The Water Table Fluctuation Method was used to calculate shallow aquifer recharge. The Hargreaves-Samani equation was used to calculate potential evapotranspiration (PET). Seasonal ET was calculated using PET and as the sink term in the water balance approach. ET accounted for the largest portion of the water budget for both watersheds, although springflow and streamflow were greater at the sagebrush-dominated watershed compared to the juniper-dominated watershed. For both watersheds, greater groundwater recharge occurred and deep percolation occurred in snow-dominated years compared to rain-dominated years, even when total annual precipitation amounts were similar.

Specific data regarding ET are very limited in this region and in many semiarid areas. For the second chapter, satellite-based remote sensing data and readily

available sources were used to examine monthly ET, PET, NDVI, and NDMI for both watersheds at CCPWS. Additionally, the Soil and Water Assessment Tool (SWAT) was used to model monthly ET for both watersheds. Environmental indicators, specifically springflow, soil moisture, NDVI, and NDMI, related to ET were also examined. . A small unpiloted aerial vehicle (UAV) was used to collect thermal infrared and multispectral imagery (red, green, blue, near-infrared, and red-edge wavelengths) at a small plot in each watershed, which was used to calculate ET and NDVI at an hourly scale for a small plot at each watershed.

Considerable variability in seasonal and annual ET patterns and totals was found across the different watershed-scale ET models examined in this study. In general, ET rates peaked in May and June, but this was not the case for all models. For most of the watershed-scale ET models examined, total ET was greater at Jensen WS than Mays WS. A significant correlation was found between SWAT-modeled ET and NDMI, NDVI, and volumetric water content at Jensen WS. At Mays WS, a significant correlation was found between SWAT-modeled ET and volumetric water content, springflow, NDMI, and NDVI. A significant correlation was found between plot-scale hourly NDVI and ET. NDVI and springflow were also found to be significant predictors of ET at the plot scale.

Research for the third chapter also sought to characterize aspects of the water balance. Multiple land use practices and land cover types are present at this study site. Sagebrush steppe, including western juniper and perennial grasses, accounts for a large portion of the watershed. Ponderosa pine and mixed conifer forests dominate in the middle reaches of the watershed. Cattle grazing and forestry are two primary land use practices at this study site.

For the third manuscript, SWAT was used to model the monthly water balance for a 1280 ha watershed in eastern OR. A combination of on-site weather measurements (precipitation, air temperature, relative humidity, and solar radiation) and PRISM datasets were used to create the SWAT model. Two years were used as a "warm up" period for the model. A 10 m DEM was used for watershed delineation, National Land Cover Database (NLCD) data were used for land cover classification, and State Soil Geographic (STATSGO) data were used for soil type identification.

The SWAT-calibration and uncertainty program (SWAT-CUP) was used for calibration, sensitivity analysis, and validation. Streamflow data from 2021 and plant available water content (PAWC) from 2018, 2019, and 2021 were used for calibration. Streamflow data were limited and therefore only PAWC measurements were used for validation. Sensitivity analysis was conducted for calibration simulations using streamflow only, streamflow and PAWC, and PAWC only data.

Mean annual precipitation across the watershed from 2018 through 2021 was 377 mm yr^{-1}. ET accounted for the majority of the output of the water balance at 253 mm yr^{-1}, followed by water yield (123 mm yr^{-1}). Total modeled aquifer recharge was 10 mm yr^{-1}. Based on the sensitivity analysis, parameters related to snow cover, canopy cover, soil characteristics, and curve number were among the most influential parameters.

The fourth chapter characterizes stream temperature dynamics along a small spring-fed stream and tributary and builds upon the previous research in land cover and water balance characterization at the study site in eastern Oregon. In the Pacific Northwest of the U.S., increased stream temperatures are of particular concern because of their negative impacts on cold-water fish (such as salmonids). While the link between land cover change and stream temperature has been widely researched, particularly in more humid regions, more information is needed to understand these interactions in semiarid climates.

Stream temperature measurements were taken along the longitudinal gradient. Both the stream and tributary originate at a small spring. The daily mean, minimum, and maximum stream temperature were calculated along with the seven-day moving average (7DA), the seven-day moving average of the daily maximum (7DADM), and the diurnal range of stream temperatures. Land cover classification was performed using an object-oriented support vector machine approach. The land cover type (forested, sagebrush/shrubland, herbaceous, or non-vegetated) was examined within a 30 m buffer along the stream.

A support vector regression (SVR) approach was used to examine the relationship between stream temperature characteristics (specifically the 7DADM and the diurnal range) and environmental characteristics (mean air temperature, dew point

temperature, vapor pressure deficit, SWAT-modeled springflow, and land cover characteristics).

Excluding the headwater sites, stream temperatures were generally greater at lower elevation sites compared to higher elevation sites, but this did not hold true for all seasons or all locations. Water temperatures at the headwater springs varied very little across seasons or years. The average diurnal range in stream temperature of other sites varied between 1.8 and 5.8 °C and did not demonstrate an association with elevation. The SVR models indicated that air temperature, followed by sagebrush steppe land cover and forest cover were the primary predictors for 7DADM or diurnal stream temperatures. The SVR model for 7DADM (R^2=0.83) performed better overall than the SVR model for diurnal stream temperature (R^2=0.55).

The research profiled in this dissertation addresses the need for more research into the ecohydrologic processes in semiarid regions. Additionally, this research examined multiple approaches that can be applied in data-limited environments. The use of readily available data, such as PRISM, remote sensing imagery, or ET datasets, can help address these gaps in data, particularly when combined with in situ data. Results of this study contribute to the existing body of knowledge regarding the relationship between ecohydrologic processes and land use characteristics, which can provide insight into future research and land management decisions.

Ecohydrologic Connections of Rangeland Ecosystems in Central and Eastern Oregon, USA

by
Nicole Durfee

A DISSERTATION

submitted to

Oregon State University

in partial fulfillment of
the requirements for the
degree of

Doctor of Philosophy

Presented July 12, 2022
Commencement June 2023

Doctor of Philosophy dissertation of Nicole Durfee presented on July 12, 2022.

APPROVED:

Major Professor, representing Water Resources Science

Director of the Water Resources Graduate Program

Dean of the Graduate School

I understand that my dissertation will become part of the permanent collection of Oregon State University libraries. My signature below authorizes release of my dissertation to any reader upon request.

Nicole Durfee, Author

ACKNOWLEDGEMENTS

I would like to express my sincere appreciation to my adviser, Dr. Carlos Ochoa. Your guidance and mentorship have been invaluable throughout the process. Thank you for the energy and support that you have shown each of your students, and the opportunity to learn from your experience and knowledge. You have shown you are invested in the success of your students. Thank you for challenging me to be a better researcher and writer.

I would also like to express my sincere appreciation to my committee: Drs. Rebecca Flitcroft, Ivan Arismendi, Julia Jones, and Ricardo Mata-Gonzales. Your knowledge, guidance, and support have been a pivotal part of this experience. Thank you for your willingness to share your expertise and provide insight, as well as your patience and dedication.

I am also thankful for the unique learning opportunities that being a part of the Ecohydrology Lab has provided. My sincere thanks to the members of lab: Jordan Anderson, Derek Godwin, Daniel Gomez, and Nick Colter. It has been a pleasure to learn from each of you and your diverse scientific backgrounds.

My sincere thanks also go to the researchers and numerous students who have worked on these research projects. Thank you to Drs. Tim Deboodt, Mike Fisher, and John Buckhouse for your intensive research at the Camp Creek Paired Watershed Study. Also, I sincerely appreciate those who have assisted with data collection and/or analysis: Phil Caruso, Grace Ray, and Derek Godwin.

I would also like to acknowledge the Oregon Beef Council, who funded my PhD studies and has provided continued support for these research projects. I appreciate the continued support of the Hatfield High Desert Ranch and the ranch managers at Wilks Ranch.

My intense gratitude goes out to my family and friends. For my parents, thank you for supporting me even when it meant a drastic change in my career. To my friends, thank you for your kindness and support throughout the process, and providing me much needed company when I needed a break.

Most of all, thank you to my husband. Your unwavering support kept me going, even on the numerous occasions when I considered quitting. You have served in many roles throughout this process – from assisting with data collection to providing a listening ear. Thank you for your love, patience, positive attitude, and support throughout this entire process. I am looking forward to our next backpacking trip.

CONTRIBUTION OF AUTHORS

Dr. Carlos Ochoa contributed to the experimental design and research methods, analyses, and final review of all manuscripts. Dr. Samuel Rivera provided guidance and assistance regarding the use of the Soil and Water Assessment Tool (SWAT) and SWAT-Calibration and Uncertainty Program (SWAT-CUP). Dr. Gerrad Jones developed the Python code used for the support regression analysis in Chapter 4 and provided considerable assistance and guidance in model application and interpretation.

TABLE OF CONTENTS

TABLE OF CONTENTS (Continued)

Page

TABLE OF CONTENTS (Continued)

Page

TABLE OF CONTENTS (Continued)

Page

LIST OF FIGURES

LIST OF FIGURES (Continued)

Page

LIST OF TABLES

Table Page

LIST OF TABLES (Continued)

Page

LIST OF APPENDICES

Appendix Page

INTRODUCTION

1. Overview

The relationship between ecohydrologic processes and environmental characteristics (e.g., land use, climate patterns) has been examined in numerous studies and spans a wide array of topics. This includes research into the impacts of woody plant encroachment on elements of the water balance (e.g., [1,2]), the impacts of land use activities and/or climate characteristics on stream temperature (e.g. [3,4]) or streamflow (e.g.,[5,6]), and the relationship between declining snowpack and reduced groundwater recharge (e.g., [7,8]). Semiarid rangeland ecosystems face a number of related land management challenges, and understanding the underlying ecohydrologic processes is key to addressing these issues. However, more research is needed to understand these processes in semiarid regions specifically, as important drivers of the water balance have been shown to vary with climate and land use characteristics [9].

2. Hydrologic impacts of woody vegetation encroachment

Encroachment of woody vegetation is a concern in many regions of the world [10]. In particular, western juniper (*Juniperus occidentalis*) has expanded in range and density over 150 years throughout much of the western United States. Western juniper is found across 9 million acres of the intermountain west [11]. While a number of causes may be linked to the expansion of woody vegetation, juniper encroachment has been largely associated with the combination of reduced fire occurrence, wetter climate conditions, and land use practices, such as overgrazing [12,13].

Woody vegetation encroachment is particularly a concern in many semiarid systems as it may reduce water availability and herbaceous productivity in already water-scarce systems. Kormos et al. [14] found higher evapotranspiration rates and earlier snowmelt at juniper-dominated sites compared to sagebrush steppe sites. Increased juniper density has also been linked to reduced infiltration and increased runoff and erosion [15,16]. Further, the removal of western juniper has been associated with increased soil moisture accumulation over the winter [2] and increased vegetation cover [16]. Juniper encroachment has also been linked to decreased streamflow duration [17]. However, it is also important to note that the impacts of woody plant encroachment can also vary across regions with differing climate characteristics [18], species type, and level of encroachment [19].

The cumulative impacts of woody vegetation encroachment and climate change-related alterations in precipitation characteristics (e.g., shifts from snow-dominated to rain-dominated patterns), have the potential to influence the water balance and increase water scarcity [14,20,21]. Climate change is linked to reduced snowpack and earlier snowmelt [22,23] as well as shifts in ET rates [24] and soil moisture content [25]. However, in order to address the impacts of climate change and vegetation shifts and other land cover changes, it is necessary to understand the elements of the water balance (e.g., precipitation, groundwater recharge, streamflow, ET, and soil moisture storage).

3. Water Balance Characterization

Multiple methods have been used to characterize elements of the water budget, including direct measurements of water or energy fluxes and/or modeling approaches. ET is often calculated as the remainder of the water or energy balance. In the case of a water balance approach, ET is estimated by subtracting other outputs (e.g., soil moisture change, streamflow) from inputs (e.g., precipitation, irrigation). Energy balance approaches similarly estimate latent heat flux (to estimate ET) by subtracting other energy fluxes (e.g., sensible heat flux, ground heat flux) from incoming solar radiation.

The limitations of mass balance approaches are also an important consideration, including limitations in the spatial and temporal data available. For example, while precipitation data are often available for small to regional scales, topography influences precipitation patterns [26]. Additionally, rainfall interception and throughfall are influenced by climate and vegetation characteristics [27], which are difficult to characterize in a water balance method approach. Further, groundwater recharge and deep percolation are difficult to calculate, particularly across areas with varying topography and geologic characteristics. In particular, direct measurements of ET are often very limited and on-site measurements of fluxes through systems like eddy-covariance towers are often expensive and labor intensive. In snow-dominated semiarid regions (such as those in eastern and central OR), the majority of precipitation falls when ET is energy-limited and vegetation is often dormant or transpiring at significantly lower rates. Therefore, water balance approaches considering data at an annual scale may not accurately account for this

asynchrony. In contrast, daily water balances may not account for snowmelt and soil moisture recharge that occurs months after precipitation.

In data-limited areas, there are many challenges associated with characterizing the water balance. Remote sensing data and open access sources such as OpenET (https://openetdata.org/;[28]) provide alternative approaches that can be combined with on-site data. Several surface energy balance-based approaches, such as the Atmosphere-Land Exchange Inverse [ALEXI; [29,30]] or Mapping Evapotranspiration at High Resolution with Internalized Calibration [METRIC; [31–33]], utilize remote sensing data in order to model elements of the energy balance. Particularly in areas with homogenous agricultural land cover, ET is frequently estimated based on the reference ET (RET) or potential ET (PET) (see [34]) calculated from meteorological characteristics (e.g., wind speed, air temperature, solar radiation).

Environmental characteristics, such as vegetation density and production, also provide insight into water balance patterns. Readily available imagery, such as Landsat or Moderate Resolution Imaging Spectroradiometer (MODIS), can be used to calculate the Normalized Difference Vegetation Index (NDVI; [35]), which is linked to vegetation activity, biomass, and density. NDVI has been used as an indirect means of estimating ET in some environments (e.g., [36,37]), although vegetation type, climate, and seasonality should be taken into consideration.

4. Soil and Water Assessment Tool (SWAT) for water balance modeling

Modeling approaches, such as the Soil and Water Assessment Tool (SWAT, [38]), are another approach used to characterize the water balance. SWAT is a widely-used model that has been widely used for a variety of purposes, such as characterizing the impacts of land cover change (e.g., [39,40]), modeling streamflow rates (e.g., [41]) and snowmelt (e.g., [42]), and assessing how climate or soil characteristics can influence the water balance (e.g., [43]). SWAT has also been used at study sites of varying climate and land cover characteristics, including semiarid sites (e.g., [44,45]) and areas with multiple land uses present (e.g., [46,47]).

Multiple factors should also be considered when applying a model, such as SWAT, and interpreting the results. For instance, it is important to consider the overall objective and the related parameters (e.g., snowmelt timing for predicting streamflow). Parameter choice and

sensitivity analysis should be examined closely in order to prevent model overfitting and avoid equifinality.

Uncertainty in hydrologic models can result from many sources, including limited data, oversimplification, and parameter uncertainty [48]. While performance metrics may indicate good agreement between predicted and observed results, it is also important to consider the accuracy of other aspects of the model (e.g., soil moisture patterns when calibrating using streamflow). Calibration using multiple sites and variables has been shown to improve model results [49,50]. Sensitivity analysis of the parameters using in a model can also provide insight into the factors most impactful on the hydrology of a given area. Examples of approaches include the commonly-used Sequential Uncertainty Fitting version 2 (SUFI-2) or the Generalized Likelihood Uncertainty Estimation (GLUE, [51]) algorithms available within SWAT-Calibration Uncertainty Program (SWAT-CUP, [52,53]). While the limitations of models should be considered carefully, particularly when data are limited and in situations of complex geology [54], these approaches provide the potential to increase our understanding of land management concerns.

5. Environmental Characteristics and Stream Temperatures

Stream systems are an essential aspect of the water balance and an important water source in many semiarid and arid regions. In addition to water quantity, however, stream temperature is a significant water quality concern. In the United States, statistically significant increases in stream temperature have been observed in many areas [55]. Increased stream temperatures alter chemical and biological processes in stream, leading to reduced dissolved oxygen concentrations (e.g., [56]) and changes in nutrient cycling and production (e.g., [57]), and impact species distribution (e.g., [58]). Sub-lethal and lethal effects on salmonids and other coldwater fish [59] are also linked to increased stream temperatures. In order to address these concerns, it is necessary to understand the ecohydrologic processes that impact stream temperature.

Climate (e.g., arid compared to temperate climates), stream size [60], season [61] geomorphological characteristics, such as elevation, [62,63], stream discharge [64], shallow groundwater inflows [65] , substrate [66], flooding [67] and precipitation [68] have been found

to influence stream temperature. Stream order has also been associated with differences in stream temperature response to land cover changes, such as forestry operations [69]. In lower order streams, groundwater inputs can moderate stream temperature while mid-stream reaches often show a stronger correlation with climate [70]. Additionally, the increase in stream temperatures downstream along the longitudinal gradient tends to be greater in smaller streams compared to larger streams [71].

While multiple environmental characteristics can impact stream temperatures, the association between land use/land cover and stream temperature has been a subject of much research (e.g., [3,72–74]). Riparian shading, which influences the amount of solar radiation that reaches a stream, is strongly linked to stream temperature patterns (e.g., [75–78]). Removal of riparian vegetation has been associated to increased daily maximum and mean stream temperatures (e.g.,[79,80]) and reductions in diurnal stream temperature ranges (e.g., [76]). Additionally, streamflow volume and timing, which can be altered by irrigation withdrawals or similar practices [81,82], influence the stream temperature by affecting the thermal capacity of the stream. As a result, higher streamflow volume is often associated with lower stream temperatures (e.g., [68,83,84]).

Local processes and characteristics influence stream temperature and patterns in stream temperature profiles along a longitudinal gradient have been found to vary across systems [60]. Spatial characteristics, such as the length of riparian corridors, and the spatial resolution of stream temperature measurements [85] are an important consideration in assessing stream temperature patterns [86].

The assessment of stream temperature patterns, and predicting the future impacts of environmental changes, present a number of challenges. The stream temperature metric used (e.g., mean daily temperature vs. the moving average of the daily maximum) is an important consideration for both understanding how stream systems might respond to environmental shifts such as climate change (e.g., [87]) or removal of riparian shading (e.g., [88]). Spatial autocorrelation is another important consideration (see [89]) as many statistical approaches applied to stream temperature analysis assume independence. While regression approaches using air temperature to predict stream temperature are commonly utilized (e.g., [90–92]), they are sometimes limited in their ability to predict extreme stream temperatures and stream

temperatures over extended timeframes [93]. Additionally, the strength of the association between air and stream temperatures varies across systems [94].

While extensive research has addressed the stream temperature characteristics in humid environments, more research is needed into stream temperature dynamics in semiarid systems. This is particularly the case given the land use-related demands on water resources in these regions (e.g., water for irrigation or soil moisture for vegetation productivity). An improved understanding of the underlying drivers and influences of stream systems (and other aspects of the water balance) can be used to inform land management decisions in water-scarce regions.

6. Research Justification and Objectives

Each management issue addressed here has implications for water availability and/or quality. This dissertation explores the ecohydrologic processes associated with key management concerns impacting many semiarid regions. In particular, this research sought to address the relationships between land cover and land use on the water balance and stream temperature. Previous studies have examined these relationships, but a more comprehensive examination of the underlying ecohydrologic processes in semiarid systems is needed. Additionally, multiple approaches (e.g., mass balance approach, modeling) and multiple data sources (e.g., on-site measurements, remote sensing imagery) were used to achieve this

The overarching goal of this research was to provide a more comprehensive examination into the relationship between aspects of the water balance (e.g., evapotranspiration) and environmental characteristics. This research examined two significant water resource challenges faced in many semiarid systems: shifts in vegetation cover/ density (specifically juniper encroachment) and increasing stream temperatures. We hypothesized that variations in environmental characteristics would be associated with differences in ecohydrologic processes (e.g., evapotranspiration rates would vary with vegetation type and stream temperature would vary with land cover). Specific objectives of this research were to:

1) characterize the water balance of two unique semiarid systems in Oregon
2) examine multiple methods of modeling components of the water balance, including evapotranspiration (ET) and streamflow

3) characterize stream temperature dynamics along the longitudinal gradient of stream system in eastern OR

This dissertation is divided into four manuscripts. Research for the first two chapters occurred at the Camp Creek Paired Watershed Study (CCPWS) in central Oregon, USA. This is a long-term study site established in 1993 to examine the ecohydrologic impacts of western juniper encroachment. The site consists of two small watersheds of approximately 100 ha each, one dominated by western juniper and one in which big sagebrush is the dominant overstory, along with a downstream riparian valley.

For the first manuscript, the research examined characteristics of the water balance, including shallow groundwater recharge and discharge. We hypothesized that annual ET amounts would be larger, while other outputs of the water balance (e.g., springflow, streamflow) would be lower at the juniper-dominated watershed compared to the sagebrush-dominated watershed. Seven years of streamflow, soil moisture, precipitation, springflow, and shallow groundwater levels were used to develop a water balance model. Evapotranspiration was estimated using the potential evapotranspiration and the balance of the precipitation and the other outputs of the water balance (soil moisture storage, percolation, streamflow). Specific objectives of this research were to:

1) determine the partitioning of water budget components in a western juniper-dominated watershed and a sagebrush-dominated watershed
2) characterize shallow groundwater level fluctuations in response to seasonal precipitation

Research for the second manuscript also took place at CCPWS and builds upon research from the first manuscript. We hypothesized that larger rates of ET would be shown at the juniper-dominated sites, both at the watershed scale and the plot scale, and that these rates would vary with vegetation indices, soil moisture, and springflow. This research examined multiple approaches to estimating ET, including modeling using SWAT [38] and remote sensing-based energy balance approaches. Unpiloted aerial vehicles (UAVs) were also used to collect data

periodically at a small plot within each watershed. Ecohydrologic indicators, such as NDVI and the normalized difference moisture index (NDMI) were also calculated. Specific objectives of this research were to:

1) compare different approaches to modeling ET at different temporal and spatial scales at two small watersheds
2) assess the relationship between different ecohydrologic indicators and characteristics, specifically ET, springflow, soil moisture, NDVI, and NDMI

Research for the third manuscript took place at a 1280 ha semiarid watershed in eastern Oregon, USA. Multiple land use and land cover characteristics are present in this watershed, including cattle grazing and forestry. For this study, the water balance was modeled using SWAT. A combination of on-site weather data (including relative humidity, solar radiation, and air temperature) and Parameter-elevation Regressions on Independent Slopes Model (PRISM; [95]) datasets (air temperature and precipitation data) were used to build the model. SWAT-CUP [52,53] was used for model calibration, validation, and sensitivity analysis. Calibration was performed using streamflow and soil plant available water content (PAWC), and validated using PAWC (due to limited streamflow observations). We hypothesized that parameters associated with snow cover and soil moisture would be the most influential and that streamflow patterns would reflect patterns in snowmelt. Specific objectives of this study were to:

1) model the water balance of a snow-dominated semiarid watershed using SWAT
2) perform model parameter sensitivity

The final manuscript built upon the water balance model used in the previous study and was conducted at the same study site. For this research, the focus was on the relationships between environmental characteristics, including land cover, streamflow, air temperature, and stream temperatures. We characterized land cover characteristics within 30 m on either side of the stream channel using National Agricultural Imagery Program (NAIP) imagery and used SWAT to model daily streamflow rates. Additionally, surveys of stream channel condition were

performed at selected reaches. Stream temperature data were recorded along the longitudinal gradient of a small spring-fed stream and a tributary. PRISM data (including air temperature and vapor pressure deficit) were downloaded for each stream temperature site. A support vector regression approach was used to evaluate how well environmental parameters predicted the seven-day moving average of the daily maximum stream temperature and the diurnal range of stream temperature. We hypothesized that areas with greater amounts of forest cover in and near the riparian area would experience generally lower temperatures than sites of similar elevation with less forested cover. We also hypothesized that air temperature, streamflow, and forested cover would be key predictors of stream temperature patterns. Specific objectives of this study were to:

1) examine channel characteristics and condition at selected reaches along the system

2) characterize stream temperature patterns along the longitudinal gradient

3) assess the relationship between stream temperature and meteorological characteristics (e.g., air temperature and vapor pressure deficit), land cover, and streamflow

References

1. Bazan, R.A.; Wilcox, B.P.; Munster, C.; Gary, M. Removing Woody Vegetation Has Little Effect on Conduit Flow Recharge. *Ecohydrol.* **2013**, *6*, 435–443, doi:10.1002/eco.1277.
2. Mollnau, C.; Newton, M.; Stringham, T. Soil Water Dynamics and Water Use in a Western Juniper (Juniperus Occidentalis) Woodland. *Journal of Arid Environments* **2014**, *102*, 117–126, doi:10.1016/j.jaridenv.2013.11.015.
3. Sun, N.; Yearsley, J.; Voisin, N.; Lettenmaier, D.P. A Spatially Distributed Model for the Assessment of Land Use Impacts on Stream Temperature in Small Urban Watersheds. *Hydrological Processes* **2015**, *29*, 2331–2345, doi:10.1002/hyp.10363.
4. Daraio, J.A.; Bales, J.D. Effects of Land Use and Climate Change on Stream Temperature I: Daily Flow and Stream Temperature Projections. *J Am Water Resour Assoc* **2014**, *50*, 1155–1176, doi:10.1111/jawr.12179.
5. Adnan, N.A.; Atkinson, P.M. Exploring the Impact of Climate and Land Use Changes on Streamflow Trends in a Monsoon Catchment. *Int. J. Climatol.* **2011**, *31*, 815–831, doi:10.1002/joc.2112.
6. Dosdogru, F.; Kalin, L.; Wang, R.; Yen, H. Potential Impacts of Land Use/Cover and Climate Changes on Ecologically Relevant Flows. *Journal of Hydrology* **2020**, *584*, 124654, doi:10.1016/j.jhydrol.2020.124654.
7. Negm, A.; Abdrakhimova, P.; Hayashi, M.; Rasouli, K. Effects of Climate Change on Depression-Focused Groundwater Recharge in the Canadian Prairies. *Vadose Zone Journal* **2021**, *20*, e20153, doi:10.1002/vzj2.20153.

8. Lindquist, L.W.; Palmquist, K.A.; Jordan, S.E.; Lauenroth, W.K. Impacts of Climate Change on Groundwater Recharge in Wyoming Big Sagebrush Ecosystems Are Contingent on Elevation. *wnan* **2019**, *79*, 37–48, doi:10.3398/064.079.0104.
9. Li, Z.; Quiring, S.M. Identifying the Dominant Drivers of Hydrological Change in the Contiguous United States. *Water Resources Research* **2021**, *57*, e2021WR029738, doi:10.1029/2021WR029738.
10. Stevens, N.; Lehmann, C.E.R.; Murphy, B.P.; Durigan, G. Savanna Woody Encroachment Is Widespread across Three Continents. *Global Change Biology* **2017**, *23*, 235–244, doi:https://doi.org/10.1111/gcb.13409.
11. Miller, R.F.; Bates, J.D.; Svejcar, T.J.; Pierson, F.B.; Eddleman, L.E. *Biology, Ecology, and Management of Western Juniper (Juniperus Occidentalis)*; Oregon State University, Agricultural Experiment Station., 2005; Vol. Technical Bulletin 152;
12. Miller, R.F.; Rose, J.A. Historic Expansion of Juniperus Occidentalis (Western Juniper) in Southeastern Oregon. *The Great Basin Naturalist* **1995**, *55*, 37–45.
13. Caracciolo, D.; Istanbulluoglu, E.; Noto, L.V. An Ecohydrological Cellular Automata Model Investigation of Juniper Tree Encroachment in a Western North American Landscape. *Ecosystems* **2017**, *20*, 1104–1123, doi:10.1007/s10021-016-0096-6.
14. Kormos, P.R.; Marks, D.; Pierson, F.B.; Williams, C.J.; Hardegree, S.P.; Havens, S.; Hedrick, A.; Bates, J.D.; Svejcar, T.J. Ecosystem Water Availability in Juniper versus Sagebrush Snow-Dominated Rangelands. *Rangeland Ecology & Management* **2017**, *70*, 116–128, doi:10.1016/j.rama.2016.05.003.
15. Petersen, S.L.; Stringham, T.K. Infiltration, Runoff, and Sediment Yield in Response to Western Juniper Encroachment in Southeast Oregon. *Rangeland Ecology & Management* **2008**, *61*, 74–81, doi:10.2111/07-070R.1.
16. Pierson, F.B.; Bates, J.D.; Svejcar, T.J.; Hardegree, S.P. Runoff and Erosion after Cutting Western Juniper. *Rangeland Ecology & Management* **2007**, *60*, 285–292.
17. Zou, C.B.; Turton, D.J.; Will, R.E.; Engle, D.M.; Fuhlendorf, S.D. Alteration of Hydrological Processes and Streamflow with Juniper (Juniperus Virginiana) Encroachment in a Mesic Grassland Catchment. *Hydrol. Process.* **2014**, *28*, 6173–6182, doi:10.1002/hyp.10102.
18. Niemeyer, R.J.; Link, T.E.; Heinse, R.; Seyfried, M.S. Climate Moderates Potential Shifts in Streamflow from Changes in Pinyon-Juniper Woodland Cover across the Western U.S. *Hydrological Processes* **2017**, *31*, 3489–3503, doi:10.1002/hyp.11264.
19. Belay, T.A.; Totland, Ø.; Moe, S.R. Ecosystem Responses to Woody Plant Encroachment in a Semiarid Savanna Rangeland. *Plant Ecology* **2013**, *214*, 1211–1222.
20. Bradley, B.A. Assessing Ecosystem Threats from Global and Regional Change: Hierarchical Modeling of Risk to Sagebrush Ecosystems from Climate Change, Land Use and Invasive Species in Nevada, USA. *Ecography* **2010**, *33*, 198–208, doi:10.1111/j.1600-0587.2009.05684.x.
21. Creutzburg, M.K.; Halofsky, J.E.; Halofsky, J.S.; Christopher, T.A. Climate Change and Land Management in the Rangelands of Central Oregon. *Environmental Management* **2015**, *55*, 43–55, doi:10.1007/s00267-014-0362-3.
22. Regonda, S.K.; Rajagopalan, B.; Clark, M.; Pitlick, J. Seasonal Cycle Shifts in Hydroclimatology over the Western United States. *Journal of Climate* **2005**, *18*, 372–384, doi:10.1175/JCLI-3272.1.

23. Mote, P.W.; Hamlet, A.F.; Clark, M.P.; Lettenmaier, D.P. Declining Mountain Snowpack in Western North America. *Bulletin of the American Meteorological Society* **2005**, *86*, 39–50, doi:10.1175/BAMS-86-1-39.
24. Rasmussen, R.; Ikeda, K.; Liu, C.; Gochis, D.; Clark, M.; Dai, A.; Gutmann, E.; Dudhia, J.; Chen, F.; Barlage, M.; et al. Climate Change Impacts on the Water Balance of the Colorado Headwaters: High-Resolution Regional Climate Model Simulations. *Journal of Hydrometeorology* **2014**, *15*, 1091–1116, doi:10.1175/JHM-D-13-0118.1.
25. Hamlet, A.F.; Mote, P.W.; Clark, M.P.; Lettenmaier, D.P. Twentieth-Century Trends in Runoff, Evapotranspiration, and Soil Moisture in the Western United States. *Journal of Climate* **2007**, *20*, 1468–1486, doi:10.1175/JCLI4051.1.
26. Johansson, B.; Chen, D. The Influence of Wind and Topography on Precipitation Distribution in Sweden: Statistical Analysis and Modelling. *Int. J. Climatol.* **2003**, *23*, 1523–1535, doi:10.1002/joc.951.
27. Crockford, R.H.; Richardson, D.P. Partitioning of Rainfall into Throughfall, Stemflow and Interception: Effect of Forest Type, Ground Cover and Climate. *Hydrol. Process.* **2000**, *14*, 2903–2920, doi:10.1002/1099-1085(200011/12)14:16/17<2903::AID-HYP126>3.0.CO;2-6.
28. Melton, F.S.; Huntington, J.; Grimm, R.; Herring, J.; Hall, M.; Rollison, D.; Erickson, T.; Allen, R.; Anderson, M.; Fisher, J.B.; et al. OpenET: Filling a Critical Data Gap in Water Management for the Western United States. *JAWRA Journal of the American Water Resources Association* **2021**, *n/a*, 1–24, doi:10.1111/1752-1688.12956.
29. Anderson, M.; Gao, F.; Knipper, K.; Hain, C.; Dulaney, W.; Baldocchi, D.; Eichelmann, E.; Hemes, K.; Yang, Y.; Medellin-Azuara, J.; et al. Field-Scale Assessment of Land and Water Use Change over the California Delta Using Remote Sensing. *Remote Sensing* **2018**, *10*, 889, doi:10.3390/rs10060889.
30. Anderson, M.C.; Norman, J.M.; Mecikalski, J.R.; Otkin, J.A.; Kustas, W.P. A Climatological Study of Evapotranspiration and Moisture Stress across the Continental United States Based on Thermal Remote Sensing: 1. Model Formulation. *Journal of Geophysical Research: Atmospheres* **2007**, *112*, doi:10.1029/2006JD007506.
31. Allen, R.G.; Tasumi, M.; Trezza, R. Satellite-Based Energy Balance for Mapping Evapotranspiration with Internalized Calibration (METRIC)—Model. *J. Irrig. Drain Eng.* **2007**, *133*, 380–394, doi:10.1061/(ASCE)0733-9437(2007)133:4(380).
32. Allen, R.G.; Tasumi, M.; Morse, A.; Trezza, R. A Landsat-Based Energy Balance and Evapotranspiration Model in Western US Water Rights Regulation and Planning. *Irrig Drainage Syst* **2005**, *19*, 251–268, doi:10.1007/s10795-005-5187-z.
33. Allen, R.; Irmak, A.; Trezza, R.; Hendrickx, J.M.H.; Bastiaanssen, W.; Kjaersgaard, J. Satellite-Based ET Estimation in Agriculture Using SEBAL and METRIC. *Hydrol. Process.* **2011**, *25*, 4011–4027, doi:10.1002/hyp.8408.
34. Allen, R.G.; Pereira, L.S.; Raes, D.; Smith, M. Crop Evapotranspiration. Guidelines for Computing Crop Water Requirements. Irrigation and Drainage Paper 56, FAO, Rome, 300 p 1998.
35. Rouse, J.W.; Harlan, J.C.; Haas, R.H.; Schell, J.A.; Deering, D.W. Monitoring the Vernal Advancement and Retrogradiation (Green Wave Effect) of Natural Vegetation - NASA-CR-144661 **1974**.
36. Szilagyi, J. Vegetation Indices to Aid Areal Evapotranspiration Estimations. *J. Hydrol. Eng.* **2002**, *7*, 368–372, doi:10.1061/(ASCE)1084-0699(2002)7:5(368).

37. Szilagyi, J. Can a Vegetation Index Derived from Remote Sensing Be Indicative of Areal Transpiration? *Ecological Modelling* **2000**, *127*, 65–79, doi:10.1016/S0304-3800(99)00200-8.
38. Arnold, J.G.; Srinivasan, R.; Muttiah, R.S.; Williams, J.R. Large Area Hydrologic Modeling and Assessment Part I: Model Development1. *JAWRA Journal of the American Water Resources Association* **1998**, *34*, 73–89, doi:10.1111/j.1752-1688.1998.tb05961.x.
39. Baker, T.J.; Miller, S.N. Using the Soil and Water Assessment Tool (SWAT) to Assess Land Use Impact on Water Resources in an East African Watershed. *Journal of Hydrology* **2013**, *486*, 100–111, doi:10.1016/j.jhydrol.2013.01.041.
40. Ghaffari, G.; Keesstra, S.; Ghodousi, J.; Ahmadi, H. SWAT-Simulated Hydrological Impact of Land-Use Change in the Zanjanrood Basin, Northwest Iran. *Hydrological Processes* **2010**, *24*, 892–903, doi:10.1002/hyp.7530.
41. Demirel, M.C.; Venancio, A.; Kahya, E. Flow Forecast by SWAT Model and ANN in Pracana Basin, Portugal. *Advances in Engineering Software* **2009**, *40*, 467–473, doi:10.1016/j.advengsoft.2008.08.002.
42. Grusson, Y.; Sun, X.; Gascoin, S.; Sauvage, S.; Raghavan, S.; Anctil, F.; Sáchez-Pérez, J.-M. Assessing the Capability of the SWAT Model to Simulate Snow, Snow Melt and Streamflow Dynamics over an Alpine Watershed. *Journal of Hydrology* **2015**, *531*, 574–588, doi:10.1016/j.jhydrol.2015.10.070.
43. Muttiah, R.S.; Wurbs, R.A. Scale-Dependent Soil and Climate Variability Effects on Watershed Water Balance of the SWAT Model. *Journal of Hydrology* **2002**, *256*, 264–285, doi:10.1016/S0022-1694(01)00554-6.
44. Hosseini, S.; Khaleghi, M. Application of SWAT Model and SWAT-CUP Software in Simulation and Analysis of Sediment Uncertainty in Arid and Semi-Arid Watersheds (Case Study: The Zoshk–Abardeh Watershed). *Modeling Earth Systems and Environment* **2020**, *6*, doi:10.1007/s40808-020-00846-2.
45. Mosbahi, M.; Benabdallah, S.; Boussema, M.R. Hydrological Modeling in a Semi-Arid Catchment Using SWAT Model. *Journal of Environmental Science and Engineering* **2011**, *5*, 8.
46. Qiu, Z.; Wang, L. Hydrological and Water Quality Assessment in a Suburban Watershed with Mixed Land Uses Using the SWAT Model. *Journal of Hydrologic Engineering* **2014**, *19*, 816–827, doi:10.1061/(ASCE)HE.1943-5584.0000858.
47. Anand, J.; Gosain, A.K.; Khosa, R. Prediction of Land Use Changes Based on Land Change Modeler and Attribution of Changes in the Water Balance of Ganga Basin to Land Use Change Using the SWAT Model. *Science of The Total Environment* **2018**, *644*, 503–519, doi:10.1016/j.scitotenv.2018.07.017.
48. Moges, E.; Demissie, Y.; Larsen, L.; Yassin, F. Review: Sources of Hydrological Model Uncertainties and Advances in Their Analysis. *Water* **2020**, *13*, 28, doi:10.3390/w13010028.
49. Niraula, R.; Norman, L.M.; Meixner, T.; Callegary, J.B. Multi-Gauge Calibration for Modeling the Semi-Arid Santa Cruz Watershed in Arizona-Mexico Border Area Using SWAT. *Air, Soil and Water Research* **2012**, 41-.
50. Shah, S.; Duan, Z.; Song, X.; Li, R.; Mao, H.; Liu, J.; Ma, T.; Wang, M. Evaluating the Added Value of Multi-Variable Calibration of SWAT with Remotely Sensed Evapotranspiration Data for Improving Hydrological Modeling. *Journal of Hydrology* **2021**, *603*, 127046, doi:10.1016/j.jhydrol.2021.127046.
51. Beven, K.; Binley, A. The Future of Distributed Models: Model Calibration and Uncertainty Prediction. *Hydrological Processes* **1992**, *6*, 279–298, doi:10.1002/hyp.3360060305.

52. Abbaspour, K.C. SWAT-CUP: SWAT Calibration and Uncertainty Programs - A User Manual; Department of Systems Analysis, Integrated Assessment and Modelling (SIAM), Eawag. Swiss Federal Institute of Aquatic Science and Technology; Duebendorf, Switzerland. **2015**, 100.
53. Abbaspour, K.C.; Vaghefi, S.A.; Srinivasan, R. A Guideline for Successful Calibration and Uncertainty Analysis for Soil and Water Assessment: A Review of Papers from the 2016 International SWAT Conference. *Water* **2018**, *10*, 6, doi:10.3390/w10010006.
54. Abiodun, O.O.; Guan, H.; Post, V.E.A.; Batelaan, O. Comparison of MODIS and SWAT Evapotranspiration over a Complex Terrain at Different Spatial Scales. *Hydrology and Earth System Sciences; Katlenburg-Lindau* **2018**, *22*, 2775–2794, doi:http://dx.doi.org.ezproxy.proxy.library.oregonstate.edu/10.5194/hess-22-2775-2018.
55. Kaushal, S.S.; Likens, G.E.; Jaworski, N.A.; Pace, M.L.; Sides, A.M.; Seekell, D.; Belt, K.T.; Secor, D.H.; Wingate, R.L. Rising Stream and River Temperatures in the United States. *Frontiers in Ecology and the Environment* **2010**, *8*, 461–466, doi:10.1890/090037.
56. Ficklin, D.L.; Barnhart, B.L. SWAT Hydrologic Model Parameter Uncertainty and Its Implications for Hydroclimatic Projections in Snowmelt-Dependent Watersheds. *Journal of Hydrology* **2014**, *519*, 2081–2090, doi:10.1016/j.jhydrol.2014.09.082.
57. Rasmussen, J.J.; Baatrup-Pedersen, A.; Riis, T.; Friberg, N. Stream Ecosystem Properties and Processes along a Temperature Gradient. *Aquatic Ecology* **2011**, *45*, 231–242, doi:10.1007/s10452-010-9349-1.
58. Torgersen, C.E.; Price, D.M.; Li, H.W.; McIntosh, B.A. Multiscale Thermal Refugia and Stream Habitat Associations of Chinook Salmon in Northeastern Oregon. *Ecological Applications* **1999**, *9*, 301–319, doi:10.1890/1051-0761(1999)009[0301:MTRASH]2.0.CO;2.
59. Richter, A.; Kolmes, S.A. Maximum Temperature Limits for Chinook, Coho, and Chum Salmon, and Steelhead Trout in the Pacific Northwest. *Reviews in Fisheries Science* **2005**, *13*, 23–49, doi:10.1080/10641260590885861.
60. Fullerton, A.H.; Torgersen, C.E.; Lawler, J.J.; Faux, R.N.; Steel, E.A.; Beechie, T.J.; Ebersole, J.L.; Leibowitz, S.G. Rethinking the Longitudinal Stream Temperature Paradigm: Region-Wide Comparison of Thermal Infrared Imagery Reveals Unexpected Complexity of River Temperatures. *Hydrol. Process.* **2015**, *29*, 4719–4737, doi:10.1002/hyp.10506.
61. Mayer, T.D. Controls of Summer Stream Temperature in the Pacific Northwest. *Journal of Hydrology* **2012**, *475*, 323–335, doi:10.1016/j.jhydrol.2012.10.012.
62. Grabowski, Z.J.; Watson, E.; Chang, H. Using Spatially Explicit Indicators to Investigate Watershed Characteristics and Stream Temperature Relationships. *Science of The Total Environment* **2016**, *551–552*, 376–386, doi:10.1016/j.scitotenv.2016.02.042.
63. Isaak, D.J.; Hubert, W.A. A Hypothesis About Factors That Affect Maximum Summer Stream Temperatures Across Montane Landscapes1. *JAWRA Journal of the American Water Resources Association* **2001**, *37*, 351–366, doi:10.1111/j.1752-1688.2001.tb00974.x.
64. Woltemade, C.J.; Hawkins, T.W. Stream Temperature Impacts Because of Changes in Air Temperature, Land Cover and Stream Discharge: Navarro River Watershed, California, USA. *River Res. Applic.* **2016**, *32*, 2020–2031, doi:10.1002/rra.3043.
65. Ebersole, J.L.; Wiginton, P.J.; Leibowitz, S.G.; Van Sickle, J. Predicting the Occurrence of Cold-Water Patches at Intermittent and Ephemeral Tributary Confluences with Warm Rivers. *Freshwater Science* **2014**, *34*, 111–124, doi:10.1086/678127.

66. Johnson, S.L. Factors Influencing Stream Temperatures in Small Streams: Substrate Effects and a Shading Experiment. *Canadian Journal of Fisheries & Aquatic Sciences* **2004**, *61*, 913–923, doi:10.1139/F04-040.
67. Moore, R.D.; Nelitz, M.; Parkinson, E. Empirical Modelling of Maximum Weekly Average Stream Temperature in British Columbia, Canada, to Support Assessment of Fish Habitat Suitability. *Canadian Water Resources Journal / Revue canadienne des ressources hydriques* **2013**, *38*, 135–147, doi:10.1080/07011784.2013.794992.
68. Du, X.; Goss, G.; Faramarzi, M. Impacts of Hydrological Processes on Stream Temperature in a Cold Region Watershed Based on the SWAT Equilibrium Temperature Model. *Water* **2020**, *12*, 1112, doi:10.3390/w12041112.
69. Janisch, J.E.; Wondzell, S.M.; Ehinger, W.J. Headwater Stream Temperature: Interpreting Response after Logging, with and without Riparian Buffers, Washington, USA. *Forest Ecology and Management* **2012**, *270*, 302–313, doi:10.1016/j.foreco.2011.12.035.
70. Poole, G.C.; Berman, C.H. An Ecological Perspective on In-Stream Temperature: Natural Heat Dynamics and Mechanisms of Heat-Caused Thermal Degredation. *Environmental Management* **2001**, *27*, 787–802, doi:10.1007/s002670010188.
71. Caissie, D. The Thermal Regime of Rivers: A Review. *Freshwater Biology* **2006**, *51*, 1389–1406, doi:10.1111/j.1365-2427.2006.01597.x.
72. Horne, J.P.; Hubbart, J.A. A Spatially Distributed Investigation of Stream Water Temperature in a Contemporary Mixed-Land-Use Watershed. *Water* **2020**, *12*, 1756, doi:10.3390/w12061756.
73. He, M.; Hogue, T.S. Integrating Hydrologic Modeling and Land Use Projections for Evaluation of Hydrologic Response and Regional Water Supply Impacts in Semi-Arid Environments. *Environ Earth Sci* **2012**, *65*, 1671–1685, doi:10.1007/s12665-011-1144-3.
74. Borman, M.M.; Larson, L.L. A Case Study of River Temperature Response to Agricultural Land Use and Environmental Thermal Patterns. *Journal of Soil and Water Conservation* **2003**, *58*, 8–12.
75. Johnson, S.L.; Jones, J.A. Stream Temperature Responses to Forest Harvest and Debris Flows in Western Cascades, Oregon. *Canadian Journal of Fisheries and Aquatic Sciences* **2000**, *57*, 30–39, doi:10.1139/cjfas-57-S2-30.
76. Broadmeadow, S.B.; Jones, J.G.; Langford, T.E.L.; Shaw, P.J.; Nisbet, T.R. The Influence of Riparian Shade on Lowland Stream Water Temperatures in Southern England and Their Viability for Brown Trout. *River Res. Applic.* **2011**, *27*, 226–237, doi:10.1002/rra.1354.
77. Gomi, T.; Moore, R.D.; Dhakal, A.S. Headwater Stream Temperature Response to Clear-Cut Harvesting with Different Riparian Treatments, Coastal British Columbia, Canada. *Water Resour. Res.* **2006**, *42*, W08437, doi:10.1029/2005WR004162.
78. Simmons, J.A.; Anderson, M.; Dress, W.; Hanna, C.; Hornbach, D.J.; Janmaat, A.; Kuserk, F.; March, J.G.; Murray, T.; Niedzwiecki, J.; et al. A Comparison of the Temperature Regime of Short Stream Segments under Forested and Non-Forested Riparian Zones at Eleven Sites Across North America. *River Res. Applic.* **2015**, *31*, 964–974, doi:10.1002/rra.2796.
79. Kalny, G.; Laaha, G.; Melcher, A.; Trimmel, H.; Weihs, P.; Rauch, H.P. The Influence of Riparian Vegetation Shading on Water Temperature during Low Flow Conditions in a Medium Sized River. *Knowledge and Management of Aquatic Ecosystems* **2017**, *418*, 1–14.

80. Imholt, C.; Soulsby, C.; Malcolm, I. a.; Gibbins, C. n. Influence of Contrasting Riparian Forest Cover on Stream Temperature Dynamics in Salmonid Spawning and Nursery Streams. *Ecohydrol.* **2013**, *6*, 380–392, doi:10.1002/eco.1291.
81. Zeng, R.; Cai, X. Analyzing Streamflow Changes: Irrigation-Enhanced Interaction between Aquifer and Streamflow in the Republican River Basin. *Hydrol. Earth Syst. Sci.* **2014**, *18*, 493–502, doi:10.5194/hess-18-493-2014.
82. Essaid, H.I.; Caldwell, R.R. Evaluating the Impact of Irrigation on Surface Water - Groundwater Interaction and Stream Temperature in an Agricultural Watershed. *Science of the Total Environment* **2017**, *599–600*, 581–596.
83. Webb, B.W.; Clack, P.D.; Walling, D.E. Water–Air Temperature Relationships in a Devon River System and the Role of Flow. *Hydrological Processes* **2003**, *17*, 3069–3084, doi:10.1002/hyp.1280.
84. van Vliet, M.T.H.; Ludwig, F.; Zwolsman, J.J.G.; Weedon, G.P.; Kabat, P. Global River Temperatures and Sensitivity to Atmospheric Warming and Changes in River Flow. *Water Resour. Res.* **2011**, *47*, W02544, doi:10.1029/2010WR009198.
85. Fullerton, A.H.; Torgersen, C.E.; Lawler, J.J.; Steel, E.A.; Ebersole, J.L.; Lee, S.Y. Longitudinal Thermal Heterogeneity in Rivers and Refugia for Coldwater Species: Effects of Scale and Climate Change. *Aquat Sci* **2018**, *80*, 3, doi:10.1007/s00027-017-0557-9.
86. Allan, J.D. Landscapes and Riverscapes: The Influence of Land Use on Stream Ecosystems. *Annu. Rev. Ecol. Evol. Syst.* **2004**, *35*, 257–284, doi:10.1146/annurev.ecolsys.35.120202.110122.
87. Arismendi, I.; Johnson, S.L.; Dunham, J.B. Technical Note: Higher-Order Statistical Moments and a Procedure That Detects Potentially Anomalous Years as Two Alternative Methods Describing Alterations in Continuous Environmental Data. *Hydrol. Earth Syst. Sci.* **2015**, *19*, 1169–1180, doi:10.5194/hess-19-1169-2015.
88. Arismendi, I.; Groom, J.D. A Novel Approach for Examining Downstream Thermal Responses of Streams to Contemporary Forestry. *Science of The Total Environment* **2019**, *651*, 736–748, doi:10.1016/j.scitotenv.2018.09.208.
89. Isaak, D.J.; Peterson, E.E.; Ver Hoef, J.M.; Wenger, S.J.; Falke, J.A.; Torgersen, C.E.; Sowder, C.; Steel, E.A.; Fortin, M.-J.; Jordan, C.E.; et al. Applications of Spatial Statistical Network Models to Stream Data: Spatial Statistical Network Models for Stream Data. *WIREs Water* **2014**, *1*, 277–294, doi:10.1002/wat2.1023.
90. Neumann, D.W.; Rajagopalan, B.; Zagona, E.A. Regression Model for Daily Maximum Stream Temperature. *J. Environ. Eng.* **2003**, *129*, 667–674, doi:10.1061/(ASCE)0733-9372(2003)129:7(667).
91. Piotrowski, A.P.; Napiorkowski, J.J. Simple Modifications of the Nonlinear Regression Stream Temperature Model for Daily Data. *Journal of Hydrology* **2019**, *572*, 308–328, doi:10.1016/j.jhydrol.2019.02.035.
92. Segura, C.; Caldwell, P.; Sun, G.; McNulty, S.; Zhang, Y. A Model to Predict Stream Water Temperature across the Conterminous USA. *Hydrological Processes* **2015**, *29*, 2178–2195, doi:https://doi.org/10.1002/hyp.10357.
93. Arismendi, I.; Safeeq, M.; Dunham, J.B.; Johnson, S.L. Can Air Temperature Be Used to Project Influences of Climate Change on Stream Temperature? *Environ. Res. Lett.* **2014**, *9*, 084015, doi:10.1088/1748-9326/9/8/084015.

94. Arismendi, I.; Johnson, S.L.; Dunham, J.B.; Haggerty, R.; Hockman-Wert, D. The Paradox of Cooling Streams in a Warming World: Regional Climate Trends Do Not Parallel Variable Local Trends in Stream Temperature in the Pacific Continental United States. *Geophysical Research Letters* **2012**, *39*, doi:https://doi.org/10.1029/2012GL051448.
95. PRISM Climate Group, Oregon State University, Http://Prism.Oregonstate.Edu, Created 1 March 2019.

THE SEASONAL WATER BALANCE OF WESTERN JUNIPER-DOMINATED AND BIG SAGEBRUSH-DOMINATED WATERSHEDS

Durfee, N.; Ochoa, C.G. The Seasonal Water Balance of Western Juniper-Dominated and Big Sagebrush-Dominated Watersheds. *Hydrology* **2021**, *8*, 156, doi:10.3390/hydrology8040156.

The Seasonal Water Balance of Western Juniper-Dominated and Big Sagebrush-Dominated Watersheds

Abstract: The combined impacts of woody plant encroachment and climate variability have the potential to alter the water balance in many sagebrush steppe ecosystems in the Western USA, leading to reduced water availability in these already water-scarce regions. This study compared the water balance characteristics of two adjacent semiarid watersheds in central Oregon, USA: one dominated by big sagebrush and one dominated by western juniper. Precipitation, springflow, streamflow, shallow groundwater levels, and soil moisture were measured. The potential evapotranspiration was calculated using the Hargreaves–Samani method. Potential evapotranspiration and a water balance approach were used to calculate seasonal actual evapotranspiration. The shallow aquifer recharge was calculated using the Water Table Fluctuation Method. Evapotranspiration, followed by deep percolation, accounted for the largest portion (83% to 86% of annual precipitation) of water output for both watersheds. Springflow and streamflow rates were generally greater at the sagebrush-dominated watershed. Snow-dominated years showed greater amounts of groundwater recharge and deep percolation than years where a larger portion of precipitation fell as rain, even when total annual precipitation amounts were similar. This study's results highlight the role of vegetation dynamics, such as juniper encroachment, and seasonal precipitation characteristics, on water availability in semiarid rangeland ecosystems.

Keywords: water balance; groundwater; juniper encroachment; sagebrush steppe; rangelands

1. Introduction

Many areas of the Western US are facing severe drought conditions that have dramatically decreased the levels of water available for numerous production and ecological functions. Long-term deficits in available water associated with prolonged droughts and a changing climate threaten production systems and ecosystem resilience in many arid and semiarid regions worldwide. Reduced snowpack [1], shifts from snow to rain-dominated precipitation [2], and reduced groundwater recharge [3–5] can severely impact water availability for human and environmental use. Seasonal timing of precipitation is a key factor influencing the water balance, and therefore water availability, in sagebrush steppe ecosystems [6], particularly in regions with already variable precipitation patterns [7]. Shifts in plant functional types have

also been shown to alter the water balance of dryland ecosystems [8]. In particular, the encroachment of juniper (*Juniperus* spp.) in sagebrush steppe ecosystems has been associated with altered flow regimes [9], earlier snowmelt and increased evapotranspiration [10], and increased overland flow and erosion [11]. In the sagebrush steppe ecosystems of the Great Basin and Intermountain West, the combined effects of woody plant encroachment [10,12] and increased temperatures and precipitation variability associated with climate change [2,13] can alter the seasonal water balance.

A technique commonly used to assess water availability and the partitioning of water resources in a given area is the water-balance method (WBM). In the WBM, inflows (e.g., precipitation) offset outflows (e.g., runoff, evapotranspiration, and changes in soil water content). Some water budget components are relatively easy to measure (e.g., soil water content, precipitation, and runoff); other components, such as evapotranspiration, can be simulated based on available weather data. Evapotranspiration and deep percolation can also be calculated as the residual term, assuming all other components are known. The WBM approach has been used in a range of climates and ecosystems, such as sagebrush ecosystems [14], semiarid savannas [15], oak woodlands [16], and agricultural fields [17]. Additionally, the WBM has been used to examine climate change [3] and land use practices [18]. This approach has also been used to examine a broad range of temporal scales, including long-term examination of the water balance [15,19,20] and short-term precipitation events [21]. Similarly, the WBM has been applied across spatial scales from the watershed [22] to the larger catchment and continent scales [23]. Several studies have examined the water balance of semiarid shrublands in the Southwestern USA [19,24,25] and other semiarid regions of the world [26–29].

The partitioning of the water-balance components is less known in the western juniper (*Juniperus occidentalis*) and sagebrush (*Artemisia tridentata*) dominated settings in the Pacific Northwest region of North America. Some research has focused on variables such as soil water content (e.g., see [30–32]), runoff (e.g., see [30]), and transpiration (e.g., see [32–34]). Limited research has been conducted into the evapotranspiration (ET) of western juniper and sagebrush steppe ecosystems. The measurement of ET poses unique challenges. Methods using eddy-covariance or Bowen Ratio systems have been successfully applied in many studies (e.g., see [35–37]), as well as direct measurements of evaporation, such as pan evaporation measurement

(e.g., see [38]), or evapotranspiration, such as lysimeters [39], as well as sap flow approaches to measure transpiration (e.g., see [40]). However, the variation in ET across the landscape due to vegetation heterogeneity or topography cannot be captured without multiple monitoring systems, which are often costly or difficult to maintain in remote environments. Reference ET (ET_0) or potential evapotranspiration (PET), the amount of ET that would occur when moisture is not limited, is frequently used to estimate actual ET (ET_A). The Hargreaves–Samani equation [41] requires minimal climate data and has been successfully used to calculate PET in arid and semiarid regions [42,43]. Thornthwaite–Mather-type water-balance equations [44,45] have been used to estimate ET_A and other water-balance elements [46,47] and are particularly useful due to their simplicity and limited data requirements.

Surface water and groundwater interactions influence multiple ecological and hydrological relationships occurring in a landscape. Understanding these connections is critical for developing sound comprehensive resource management plans [48,49]. Surface water and groundwater cannot be seen as isolated components and are spatially and temporally variable in many systems [50]. In many instances, seasonal precipitation or irrigation inputs percolating below the effective rooting zone contribute to the replenishment of the shallow aquifer [30,51]. Groundwater recharge can be influenced by geologic characteristics, such as the presence of fractured bedrock or basalt [30,52], and precipitation timing and quantity [53] or vegetation [54].

Many rangeland ecosystems, including sagebrush and juniper woodlands, are not considered high water yielding sources mainly because of the low precipitation and the high evapotranspiration losses associated with these landscapes. Long-term groundwater recharge is assumed to be minimal in some areas of the US Southwest region [25,53,55], where the bulk of the precipitation that falls in the hot summer generally corresponds to vegetation productivity, and consequently with high evapotranspiration rates. However, the recharge of the shallow aquifer can be significant in winter precipitation-dominated systems where there is limited consumptive use from vegetation. Aquifer replenishment in response to seasonal water inputs can be more significant in regions overlying shallow aquifers characterized by permeable soils that allow rapid water infiltration and aquifer recharge [30].

Groundwater recharge can be calculated by using different methods [56], including soil-water budgets [56,57], isotope measurements [58], Darcy's equation [59], and groundwater-level

fluctuations [60]. Similar to the WBM described above, soil water budget approaches require information about other water-balance characteristics, such as ET_A, that may not be readily available. The use of tracers can be challenging in environments where regular sampling and analysis of tracer concentrations in the groundwater may not be possible. The Water Table Fluctuation Method (WTFM) is a commonly used approach that calculates recharge in unconfined aquifers based on groundwater level data [60]. The WTFM has been applied in several studies (e.g., see [61–63]) and is advantageous, particularly in data-limited environments, due to its simplicity.

It is increasingly recognized that woody vegetation expansion effects on hydrologic processes such as groundwater recharge must be better understood. While woody plant encroachment can influence groundwater recharge due to changes in infiltration rates, interception, and transpiration, among other factors, these impacts vary across spatial and temporal scales [64]. Moore et al. [65] found that removal of shrubs (primarily honey mesquite, *Prosopis glandulosa*) resulted in a slight increase in groundwater recharge at a study site in Southwest Texas; however, this varied with soil type and the amount of vegetation cover removed. Research addressing the effects of woody vegetation on water yield in cool climates is limited. Only a few studies (see, for example, [30,52]) have addressed vegetation and groundwater relationships in sagebrush- and juniper-dominated landscapes. More studies focused on the linkages between seasonal winter precipitation and water distribution throughout the landscape are needed to enhance base knowledge of the biophysical mechanisms that influence surface water and groundwater connectivity in rangeland ecosystems.

This research examined the water balance and the mechanisms of aquifer recharge and discharge at two adjacent watersheds in a semiarid region in central Oregon, USA. Specific objectives were to (1) determine the partitioning of water budget components in a western juniper-dominated watershed and a sagebrush-dominated watershed; and (2) characterize shallow groundwater level fluctuations in response to seasonal precipitation.

2. Materials and Methods

2.1. Site Description

This research was conducted at the Camp Creek Paired Watershed Study (CCPWS) site in central Oregon, USA. The CCPWS was established in 1993 to examine the potential impacts of juniper removal on hydrologic processes such as streamflow, soil water content, and groundwater. The CCPWS site includes two watersheds (WSs): Mays WS (116 hectares) and Jensen WS (96 hectares). The study site is located within the John Day ecological province [66]. Western juniper is the dominant overstory species at Jensen WS, while big sagebrush is the primary overstory species at Mays WS following juniper removal in 2005. Juniper canopy cover is 30% at the untreated Jensen WS and it is less than 1% at Mays WS [30,31,67]. Juniper density is 797 trees ha−1 at Jensen WS, of which 21% (167 trees ha−1) are estimated to be mature juniper, and 313 trees ha−1 at Mays WS where most junipers are at the sapling stage [67]. The density of mature juniper at the Mays WS is 9.5 trees ha−1 (unpublished data). Shrub cover, including big sagebrush and other species such as green rabbitbrush (*Chrysothamnus viscidiflorus*) and antelope bitterbrush (*Purshia tridentata*), is approximately 10% at the Jensen WS and 23% at the Mays WS [68]. At a study site approximately 9 km from CCPWS, Mollnau et al. [32] found that shrub density was approximately 2%. Similarly, Bates et al. [69] found that shrub cover was <1% at a study site in Southeastern Oregon, but this increased to 5.5% ± 1.3% 25 years after juniper removal. The CCPWS site consists of public and privately owned land and is largely used for cattle grazing. Most precipitation occurs as a mix of rain and snow during fall and winter. Long-term (1961–2016) average annual precipitation in the region is 322 mm, with daily snow depth reaching up to 480 mm [70].

Clarno and John Day formations dominate the geology in this region, with alluvium in the valleys. The low permeability of the deeper geologic strata has resulted in transient unconfined shallow aquifers that primarily follow surface topography and that are recharged during the winter precipitation and spring snowmelt runoff seasons [52]. The topography of Mays WS and Jensen WS are similar and are characterized by a relatively low gradient landscape. Elevation ranges from 1367 to 1524 m. The average slope is 24% for Mays WS and 25% for Jensen WS. The orientation of Mays WS is to the north–northwest, while Jensen WS is oriented to the north [71]. The soil series at CCPWS comprise Madeline Loam, Westbutte very stone loam, and Simas gravelly silt loam [71]. The Westbutte series covers approximately 50% of the area at Mays WS and 26% at Jensen WS. These soils are well-drained and moderately

deep [71,72]. Soils in the Madeline loam series are shallow and well-drained and cover 20% of the area at Mays and 48% at Jensen [71,72]. The Simas soils are very deep and well-drained and cover 21% at Jensen WS and 3% at Mays WS [71,72].

In 2005, the CCPWS site was instrumented to measure multiple hydrologic (e.g., soil water content, groundwater, and streamflow) and weather parameters. Since 2014, additional monitoring locations and equipment have been included to measure other variables (e.g., springflow and tree transpiration) and expand the spatial understanding of ecohydrologic processes within and downstream of the treated (Mays WS) and untreated (Jensen WS) watersheds (Figure 1). Data collected between 2013 and 2020 were used to calculate the different water budget components described in this study.

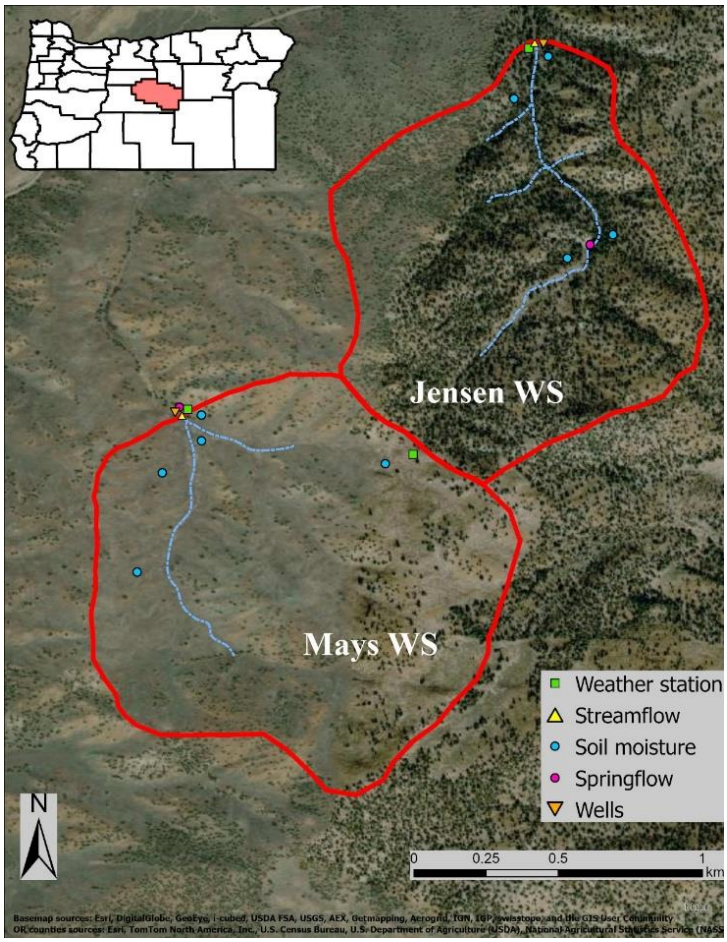

Figure 1. Location and instrumentation of the study site. This map was created by using ArcGIS® software by Esri. ArcGIS® and ArcMap™ are the intellectual property of Esri and are used herein under license. Copyright © Esri. All rights reserved. For more information about

Esri® software, please visit www.esri.com. Basemap credits: Esri, DigitalGlobe, GeoEye, icubed, USDA FSA, USGS, AEX, Getmapping, Aerogrid, IGN, IGP, swisstopo, and the GIS User Community. Oregon counties map credits: Esri, TomTom North America, Inc., US Census Bureau, US Department of Agriculture (USDA), and National Agricultural Statistics Service.

2.2. Water Balance

A water balance approach was used to calculate deep percolation (DP) below the top 0.8 m soil depth, which was assumed to be the effective rooting zone depth. This is based on observations made during soil water content sensor installation at multiple sites in the two watersheds, where it was noted that the soil's profile was less than 1 m depth [30]. For each watershed, the quarterly portioning of different water budget components for each water year from 2014 to 2020 were obtained based on measurements of precipitation (P), soil volumetric water content (θ), streamflow (Q), and weather data used for modeling evapotranspiration (ET_A). These components were assumed to represent processes within the unsaturated soil zone. The following water balance equation was used (Equation (1); all units are in mm day^{-1}).

$$DP = P - \Delta\vartheta - Q - ET_A \quad (1)$$

The seasonal water budget of the unsaturated soil layer zone was calculated by summing the daily values for each component. This was performed for each quarter of the water year, with the first quarter corresponding to October through December. A seasonal water budget approach was selected to contrast periods of differing precipitation and temperature characteristics. The annual water budget based on the water year (1 October through 30 September) was calculated by summing the quarterly values for each water balance component.

The seasonal patterns of precipitation were determined by using rain and snow data. Daily averaged levels of total P were calculated from data collected by using three tipping bucket rain gauges installed onsite at each watershed outlet, and the watershed divide. Rain data near the outlet of each watershed was primarily used. However, during brief periods of data unavailability (e.g., equipment failures), precipitation records from the watershed divide (Figure 1) were used. Snow depth data were obtained by using an ultrasonic snow depth recording sensor (Model TS-15S, Automata, Inc., Nevada City, CA, USA) installed at the outlet of Mays WS. We characterized the annual snow water equivalent (SWE) based on the snow depth sensor data and SWE: precipitation ratios derived from the nearest (Ochoco Meadows) SNOwpack TELemetry

Network (SNOTEL) [73], located approximately 51 km north at an elevation of 1655 m. The ratio of the SNOTEL SWE to snowpack depth at this station was multiplied by the snowpack depth at CCPWS to estimate monthly SWE.

Daily changes in soil volumetric water content ($\Delta\theta$) were obtained based on hourly records of θ from sensors installed at depths of 0.2, 0.5, and 0.8 m, as described in [30]. The $\Delta\theta$ was calculated for each soil depth, averaged across all three depths, and then divided by the total depth (0.8 m). The soil moisture stations used in this study are at locations representing different topographic and vegetation conditions within each watershed. At Jensen WS, soil moisture sensors are located in tree undercanopy and intercanopy sites at valley and upland sites. The stations at Mays WS, which is dominated by sagebrush, are likewise located in valley and upland sites (see [30]).

Streamflow (Q) was measured at the outlet of each watershed, using a type-H flume [74] equipped with a water level logger (Model HOBO U20-001-01, Onset Computer, Corp.; Bourne, MA, USA). Water stage data were collected every 15 min at the flume, and the manufacturer's pre-calibrated equations were used to estimate Q.

The Hargreaves–Samani equation [41] was used to calculate potential evapotranspiration (PET) (Equation (2)) in mm day^{-1}. Mean (T_{mean}), maximum (T_{max}), and minimum (T_{min}) air temperature and solar radiation (R_a) data were collected onsite. All temperatures are in °C. R_a is in MJ m^2 day^{-1}. Additionally, a radiation adjustment coefficient (k_{rs}) of 0.17 was used based on Samani [75]. Due to the close proximity of the two watersheds and their relatively small size, it was assumed that ambient conditions (e.g., air temperature) and solar radiation would be similar, and therefore PET values would also be similar.

$$PET = 0.0135 * k_{rs} * (T_{mean} + 17.8) * (T_{max} - T_{min})^{0.5} * 0.408 * R_a \quad (2)$$

Estimates of ET_A were obtained by using a modified Thornthwaite-type water balance equation, similar to that described by Alley [47] and Dingman [76] (Equations (3) and (4)). This approach was selected to reflect seasonal periods of energy-limited evapotranspiration (winter months) versus periods of water-limited evapotranspiration (generally late spring through fall).

$$\text{When } PET > P - \Delta\theta - Q, \text{then } ET_A = P - \Delta\theta - Q \quad (3)$$

$$\text{When } PET \leq P - \Delta\theta - Q, \text{then } ET_A = PET \quad (4)$$

2.3. Subsurface Flow and Shallow Aquifer Response to Seasonal Precipitation

Seasonal groundwater flow at each watershed was characterized by using data collected hourly with water level loggers (Model HOBO U20-001-01, Onset Computer, Corp.; Bourne, MA, USA) installed in five (Mays WS) and six (Jensen WS) shallow groundwater monitoring wells located near the outlet of each watershed (see Figure 1). The wells were located perpendicular to the stream channel and are numbered in order, generally from west to east (Mays WS wells, T1–T5; Jensen WS wells, U1–U6). The transect at Mays WS is 38 m across at an elevation of 1438 m and the transect at Jensen WS is 52 m across at an elevation of 1373 m. The Mays WS wells are primarily located in fractured rock substrate, while the Jensen WS wells are located in alluvium and fractured rock [68,77]. The maximum well depth was 8.2 m; however, some wells were somewhat shallower, with the bottom of all wells near or at the bedrock layer [30,77].

The recharge (Re_{GW}) of the shallow aquifer was estimated by using the WTFM [60]. The WTFM calculates recharge based on shallow, unconfined groundwater level fluctuations and specific yield (S_y) [60], where S_y is multiplied by the change in water table height (Δh) over time (Δt) (Equation (5)). Re was calculated at the daily time step (mm day^{-1}).

$$Re_{GW} = S_y \frac{\Delta h}{\Delta t} \quad (5)$$

The WTFM works best in shallow unconfined aquifers with sharp groundwater level rises and declines observed over short periods of time [60]. This is the case for the wells at our study site, where rapid changes in the water table are observed during the relatively short groundwater recharge season that peaks in early spring. Peak water level rises in the shallowest vs. the deepest wells ranged from 0.5 to 4.1 m at Mays WS and from 0.4 to 5.4 m at Jensen WS. For estimating groundwater recharge, the measurements of groundwater level, using a monitoring well, are believed to cover at least several tens of square meters [60]. Given that all monitoring wells used in this study are located within less than 50 m, in transects spanning across the entire valley bottom cross section, we used data from two of the deepest wells in each transect (T3 at Mays WS and U5 at Jensen WS) to calculate aquifer recharge. The assumption was that these two

wells would be representative of shallow groundwater dynamics occurring at the outlet of each watershed.

One of the challenges of using the WTFM is determining a representative value for S_y [56]. S_y indicates the volume of water drained out of the unconfined aquifer when the water table drops, and it is defined as the ratio of the volume of water that drains freely from a saturated substrate due to gravity forces to the total volume of the substrate [78]. To our knowledge, no shallow aquifer tests to determine S_y have been conducted in the region where our study site is located. Therefore, we used S_y values from the literature based on the medium gravel and tuff layers at Mays WS, and the fine-to-medium gravel at Jensen WS observed in the water table fluctuation zone during the installation of the wells (data not published). An average value of 0.23 for Mays WS and 0.26 for Jensen WS was obtained based on the S_y values for geological deposits reported by [76].

Springflow data were calculated based on a discharging spring in each watershed (Figure 1). The two relatively low flow springs have been reconditioned to be able to measure springflow [30]. A springbox (0.6 m diameter by 1.8 m depth) to capture and discharge water to a cattle trough was installed at each site [77]. Springflow was measured regularly (bi-weekly to quarterly) from 2004 to 2020, except for 2014 and 2015, when no data were collected. Manual springflow measurements were made at the discharge pipe outlet, using a timer and a 5 L bucket. In 2017, a water level logger (Model HOBO U20-001-01, Onset Computer, Corp.; Bourne, MA, USA) was installed in each springbox to measure springwater level fluctuations hourly.

The upslope contributing area for the spring in Mays WS (112 ha) is greater than Jensen WS (51 ha). The Mays WS spring is located near the outlet of the WS, while the Jensen WS spring is located further upslope in the upper portion of the watershed. Based on the Jensen WS spring location, springflow is assumed to contribute to intermittent streamflow, soil water content, and shallow groundwater within the watershed. The springflow at Mays WS is assumed to reflect groundwater outflow from the watershed.

A stage–discharge curve was calculated based on the manual measurements of springflow and springbox water level (stage). A high correlation (Pearson r = 0.95 for Mays WS and r = 0.95 for Jensen WS) was observed between springflow and spring water stage. A multilinear regression based on daily averaged θ in the contributing catchment was used to

estimate daily springflow volume in the years before installing the water level loggers in each watershed's springbox. Similar to the stage–discharge relationship, a relatively high correlation ($r = 0.84$ to 0.89 for Mays WS; $r = 0.81$ to 0.92 for Jensen WS) was observed between θ and springflow.

The Shapiro–Wilk test indicated that the springflow and groundwater level data were not normally distributed; therefore, nonparametric statistical analyses were used. The Mann–Whitney Rank-Sum test was used to compare mean seasonal springflow rates between the two watersheds. The Kruskal–Wallis One-Way Analysis of Variance on Ranks (ANOVA) and Dunn's Method were used to assess differences in groundwater level height for the 11 shallow groundwater wells. SigmaPlot® version 14.0 (Systat Software, Inc., San Jose, CA, USA) was used for all the statistical analyses.

3. Results

3.1. Water Balance

The annual water balance results by water year (October through September) for both watersheds are shown in Table 1. ET_A accounted for the largest portion of the annual water budget within both watersheds, averaging 83% of incoming precipitation at Mays WS and 86% of incoming precipitation at Jensen WS. At Mays WS, ET_A ranged from 210 to 260 mm yr^{-1} (mean of 242 mm yr^{-1}). The ET_A at Jensen WS ranged from 201 to 289 mm yr^{-1} (mean of 239 mm yr^{-1}). DP ranged from 5 to 121 mm yr^{-1} (mean of 50 mm yr^{-1}) at Mays WS and from 0 to 104 mm yr^{-1} (mean of 43 mm yr^{-1}) at Jensen WS.

Using data collected and described by Abdallah et al. [33] and density estimates from Durfee et al. [67], we estimated that transpiration associated with mature juniper at Jensen WS to be between 0.35 and 1.9 mm day^{-1} and between 0.03 and 0.16 mm day^{-1} at Mays WS for the time periods observed. The greater transpiration rate associated with juniper at Jensen WS is associated with the greater density of mature juniper in that WS. For saplings, estimated transpiration ranged from 0.01 to 0.09 mm day^{-1} at Mays WS and 0.01 to 0.18 mm day^{-1} at Jensen WS. Transpiration estimates were not available for the whole year, and therefore we did not calculate yearly juniper transpiration rates as a portion of the water budget.

Peaks in seasonal ET_A occurred during Q3 (April through June), which corresponds to periods of snowmelt. The average ET_A during Q3 was 107 mm at Mays WS and 101 mm at Jensen WS. Seasonal ET_A was generally lowest during Q2 (January through March), corresponding to periods of lowest temperatures and highest snowmelt. Mean ET_A at Mays WS was 28 mm and at Jensen WS was 39 mm during the second quarter.

Table 1. Water balance components by season and watershed. Each water year (October 31–September 30) is presented by quarter, with Q1 referring to October through December, etc.

		Mays WS					Jensen WS				
Water Year	PET	P	Q	Δθ	ET_A	DP	P	Q	Δθ	ET_A	DP
2014 Q1	48	36	0	−29	48	17	26	0	−18	44	0
2014 Q2	46	112	0	63	46	2	101	0	57	44	0
2014 Q3	234	67	0	−28	95	0	60	0	−26	86	0
2014 Q4	287	51	0	−15	65	0	31	0	−10	41	0
2014 Total	615	266	1	−9	255	19	218	0	2	215	0
2015 Q1	47	170	0	37	47	87	166	0	53	47	66
2015 Q2	57	69	24	21	24	0	78	0	16	57	6
2015 Q3	225	59	0	−31	91	0	55	0	−40	95	0
2015 Q4	287	43	0	−27	70	0	45	0	−28	72	0
2015 Total	615	342	24	−0.6	232	87	343	0	1	270	72
2016 Q1	44	129	0	26	44	59	112	0	42	44	25
2016 Q2	42	98	20	35	42	1	111	0	33	42	37
2016 Q3	232	69	4	−11	77	0	65	0	−29	94	0
2016 Q4	306	2	0	−43	44	0	12	0	−43	55	0
2016 Total	624	298	24	7	207	60	300	0	2	235	62
2017 Q1	44	117	0	−2	44	75	126	0	6	44	76
2017 Q2	38	169	26	86	38	19	156	2	89	38	28
2017 Q3	220	75	35	−44	84	0	74	2	−48	120	0
2017 Q4	332	15	1	−31	45	0	14	0	−33	47	0

2017 Total	634	376	62	10	210	94	369	4	13	249	104
2018 Q1	52	55	0	-10	52	13	68	0	-9	52	25
2018 Q2	44	61	0	51	10	0	73	0	50	23	0
2018 Q3	223	83	0	-26	109	0	80	1	-20	100	0
2018 Q4	364	28	0	-32	59	0	4	0	-22	26	0
2018 Total	683	226	0	-17	230	13	226	1	-1	201	25
2019 Q1	54.2	75	0	15	54	5	80	0	-1	54	27
2019 Q2	50	108	1	94	13	0	102	2	70	29	0
2019 Q3	207.9	83	27	-45	102	0	78	1	-29	106	0
2019 Q4	288.3	60	0	-31	91	0	72	0	-28	100	0
2019 Total	600.4	326	28	34	260	5	331	4	12	289	27
2020 Q1	45.6	88	0	17	46	25	70	0	12	46	13
2020 Q2	46	88	0	62	26	0	74	0	32	42	0
2020 Q3	187.9	81	0	-69	150	0	66	0	-39	105	0
2020 Q4	306.8	9	0	-26	35	0	8	0	-16	25	0
2020 Total	586.3	266	0	-15	256	25	218	0	-12	217	13

3.1.1. Snowpack and Precipitation Patterns

Annual precipitation was similar in the two watersheds. The average precipitation between the two watersheds was 293 mm yr^{-1}; ranging from 218 to 376 mm (Figure 2). Precipitation primarily fell during Q2 (January through March) (Figure 2), when ET is energy-limited. However, considerable variation was seen in seasonal precipitation patterns over the course of this study (see Table 1), even during years with similar amounts of total annual precipitation.

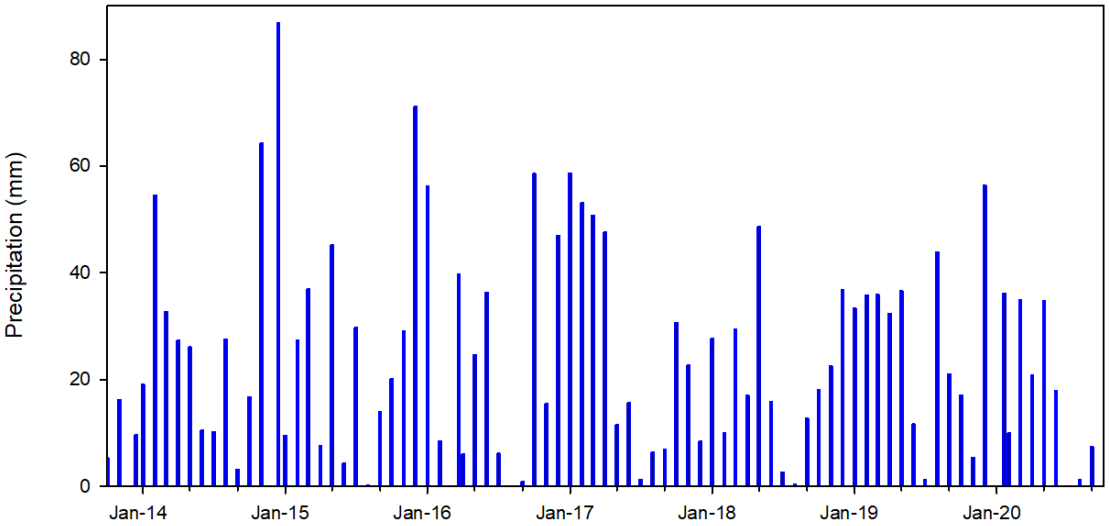

Figure 2. Average monthly precipitation (mm) of both watersheds.

In general, snow accumulated from November to January of each year, with snowmelt occurring in March or April (Figure 3). Annual variations in both snowfall and depth were observed across years during this study. Snowpack levels and SWE varied from year to year, even between years with similar total annual precipitation (e.g., 2014 and 2018). The 2017 water year showed the greatest SWE while the 2018 water year showed the least. SWE generally peaked in January (mean SWE of 40 mm) or February (mean SWE of 43 mm). Reflecting snowpack, SWE varied from 0.2 to 106 mm in January and from 3 to 100 mm in February. Mean

December SWE was 25 mm, ranging from 3 to 74 mm. Mean March SWE was 17 mm, ranging from 0.2 to 69 mm.

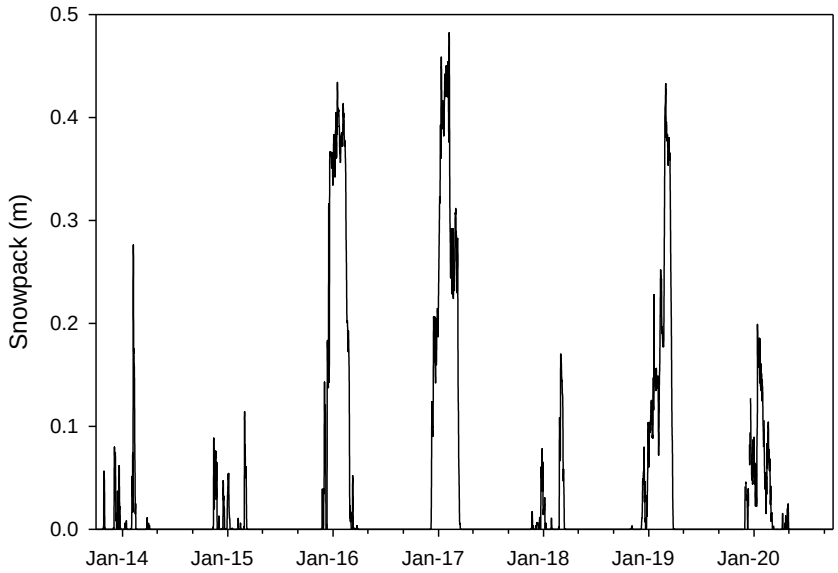

Figure 3. Snowpack depth at Mays WS.

3.1.2. Streamflow

On average, streamflow at Mays WS accounted for 5.8% of incoming precipitation, ranging from 0% to 17% for individual water years. At Jensen WS, streamflow accounted for an average of 0.3% of incoming precipitation, ranging from 0% to 1.1%.

In general, seasons of greatest streamflow corresponded to snowmelt and increased soil water content periods in March and April. In most years, streamflow peaked in Q2 (January through March) or Q3, generally corresponding to snowmelt. However, smaller streamflow amounts also periodically occurred in response to warmer season rainfall.

Years with the highest precipitation experienced the highest volume of streamflow (Figure 4). The timing of peak streamflow was similar in both watersheds, except for the 2019 water year, in which peak flow occurred at the Jensen WS several weeks sooner than it did at the Mays WS. In 2020, no streamflow was recorded at either WS; however, limited pooling was noted in the stream channel at both watersheds. Occasional convective summer storms resulted in streamflow during the summer months. During some of the larger summer storms, sediment accumulation in the flumes prevented accurate measurements of streamflow.

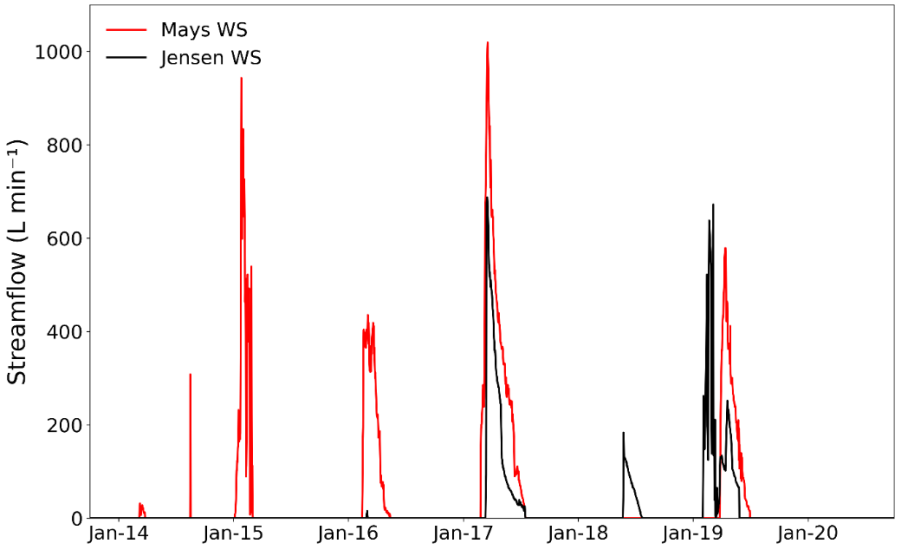

Figure 4. Streamflow in the sagebrush-dominated watershed (Mays WS) and the juniper-dominated watershed (Jensen WS).

3.1.3. Soil Water Content Change

The soil water content change (Δθ) accounted for between −7.3% and 10.3% of the annual water budget at Mays WS and −5.4% and 3.6% at Jensen WS. Across all water years, the average Δθ accounted for −0.2% of the annual water budget at Mays WS and 0.5% at Jensen WS.

While Δθ accounted for a small portion of the annual water budget (on average, 1 mm at Mays WS and 3 mm at Jensen WS), it did show large shifts from season to season (see Table 1). Seasonal Δθ ranged from −69 to 94 mm at Mays WS and from −48 to 89 mm at Jensen WS. In general, increased Δθ occurred during Q2 (mean of 59 mm at Mays WS and 49 mm at Jensen

WS), and decreased $\Delta\theta$ occurred in Q3 (mean of −36 mm at Mays WS and −33 mm at Jensen WS) and Q4 (mean of −29 mm at Mays WS and −26 mm at Jensen WS).

3.1.4. Seasonal PET

The mean annual PET was 623 mm yr^{-1} and ranged from 586 to 683 mm yr^{-1}. PET was on average 2.2 times greater than P on an annual basis. The balance of the water budget exceeded PET during Q1 for most years (see Table 1), which corresponds to the periods when increases in groundwater levels occurred. Given that the watersheds are adjacent to each other and experience similar temperature regimes and solar radiation, we assumed that PET was the same at both watersheds.

3.2. Subsurface Flow and Shallow Aquifer Response to Seasonal Precipitation

Similar to streamflow levels, the highest springflow rates obtained corresponded to periods of snowmelt in the spring and increased soil water content that typically occurred in winter and spring. Years with the highest precipitation generally experienced higher springflow rates, which peaked in Q3 (April through June) for most water years (Figure 5). Springflow rates were generally higher at Mays WS compared to Jensen WS. The mean springflow rate at Mays WS was 43.4 L min^{-1}, and it was 12.6 L min^{-1} at Jensen WS. The Mann–Whitney Rank Sum test indicated a statistically significant difference ($p \leq 0.001$, $U = 13748$) in median daily springflow rates between the two watersheds (5.4 L min^{-1} at Jensen WS vs. 20.6 L min^{-1} at Mays WS).

Based on the contributing area for each spring (112 ha at Mays WS and 51 ha at Jensen WS), the average daily springflow rate at Mays WS was 0.06 mm day^{-1} and at Jensen WS was 0.04 mm day^{-1}. The range in average daily springflow based on contributing area was 0 to 0.27 mm day^{-1} at Mays WS and 0 to 0.40 mm day^{-1} at Jensen WS.

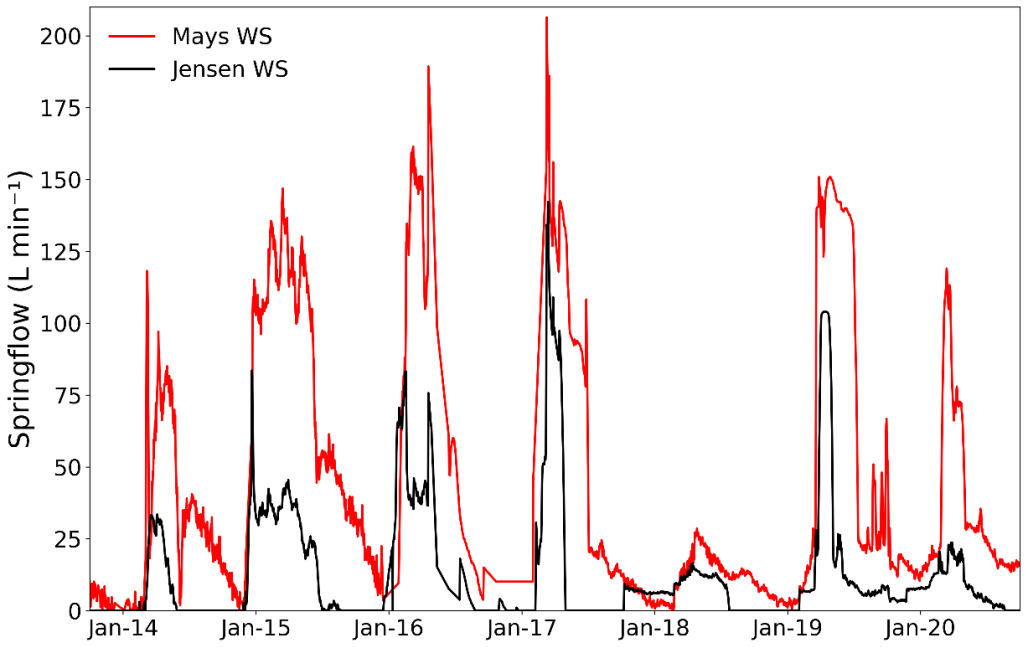

Figure 5. Daily average springflow (L min^{-1}) at both watersheds.

Manual measurements of springflow and water level records from the springbox were used to create a stage–discharge curve (Figure 6). The majority of observed springflow rates were less than 50 L min^{-1}, with springwell water levels less than 0.1 m at Mays WS and 0.2 m at Jensen WS.

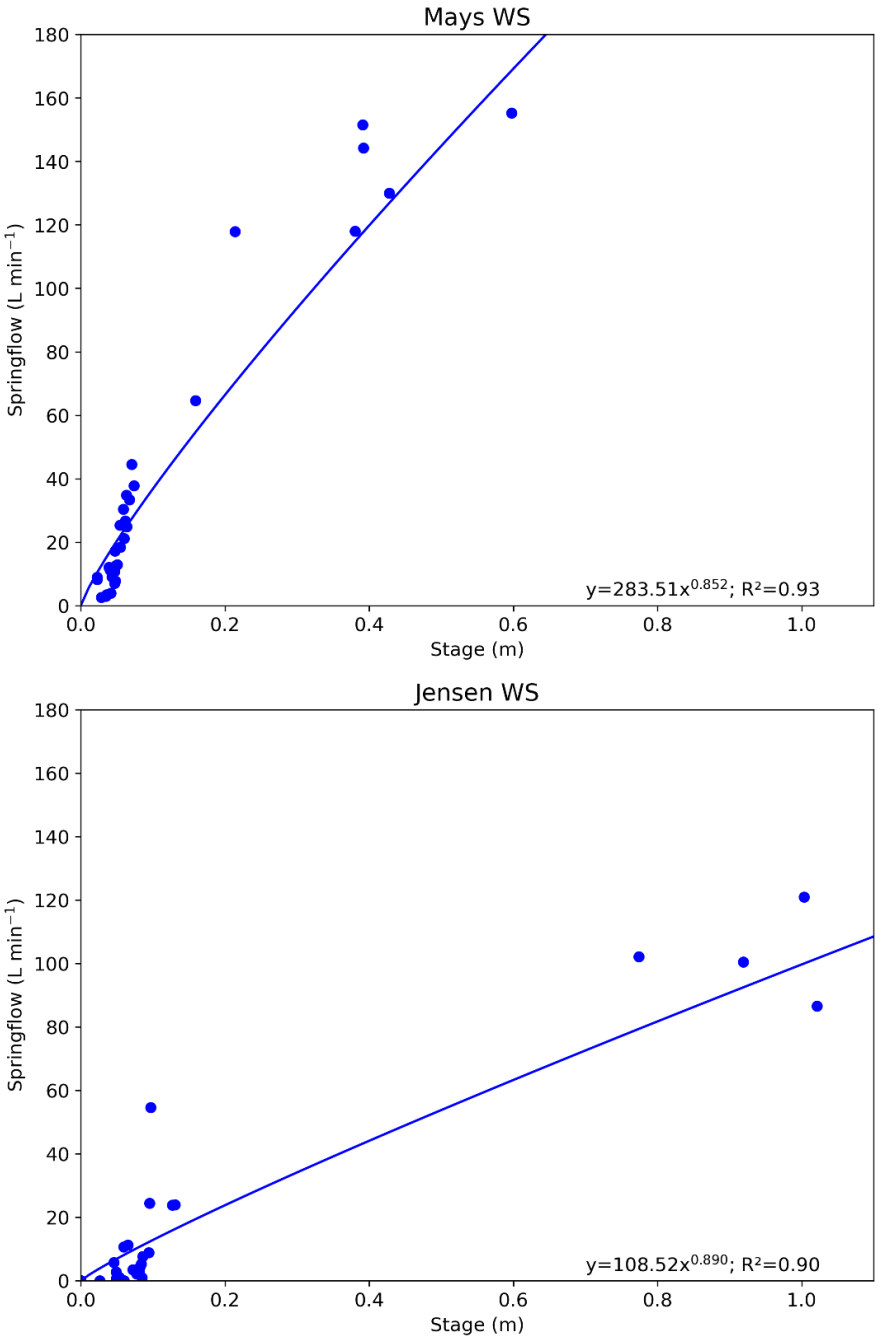

Figure 6. Stage–springflow discharge curve for the sagebrush-dominated watershed (Mays WS) and the juniper-dominated watershed (Jensen WS).

Shallow groundwater level fluctuations showed a seasonal response to winter precipitation and snowmelt. All wells in each transect showed similar responses every year, as illustrated in Figure 7 for 2016. A pattern of less pronounced but more frequent groundwater

level rises and declines was observed in the fractured basalt-dominated aquifer at Mays WS. A pattern of more pronounced and steadier groundwater level rises and declines was observed in the alluvium-dominated aquifer at Jensen WS. Peak groundwater levels at Mays WS were generally observed in February or March, while peak groundwater levels at Jensen were observed in late March or April every year (Figure 7).

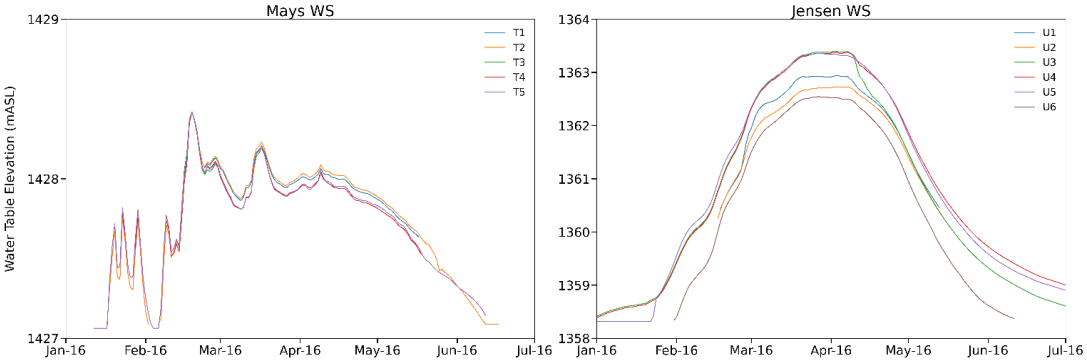

Figure 7. Shallow groundwater level fluctuations for year 2016 in the transect of wells in Mays WS and at Jensen WS.

The annual recharge of the shallow aquifer was highly variable in each watershed during the seven years evaluated (Table 2). Annual Re_{GW} ranged from 0 to 1371 mm in Mays WS (mean of 707 mm) and from 35 to 1441 mm in Jensen WS (mean of 808 mm). The ANOVA results showed mean annual Re_{GW} was not significantly different ($p > 0.05$) between the two watersheds. In general, the highest Re_{GW} values were obtained during the years with the greatest snowpack depths (see Figure 3).

Table 2. Annual groundwater recharge (Re_{GW}) and total precipitation (P) in the sagebrush-dominated watershed (Mays WS) and the juniper-dominated watershed (Jensen WS). All measurements are in mm.

	Mays WS		Jensen WS	
Water Year	Re_{GW}	P	Re_{GW}	P
2014	276	266	219	218
2015	862	342	659	343

2016	862	298	1311	300
2017	1263	376	1441	369
2018	0	226	35	226
2019	1371	326	1360	331
2020	318	266	632	218

4. Discussion

This research examined the seasonal variability of various water budget components (e.g., evapotranspiration, precipitation, and deep percolation) and shallow aquifer recharge in cool-climate rangeland ecosystems in a semiarid region in central Oregon, USA. Specifically, we sought to (1) determine the partitioning of several water budget components in a western-juniper-dominated watershed and a sagebrush-dominated watershed; and (2) characterize shallow groundwater-level fluctuations in response to seasonal precipitation.

Similar to other studies [79–82], this research highlights the importance of seasonal precipitation patterns in semiarid environments in driving the response of many water budget components and the replenishment of the local aquifer. Study results show that evapotranspiration (ET) accounted for 83% of total annual precipitation in the sagebrush-dominated watershed (Mays WS) and 86% in the juniper-dominated watershed (Jensen WS). This is similar to that reported for other snow-dominated rangelands in the region. For a study site in Southwestern Idaho, USA, Kormos et al. [10] modeled the ET of a juniper-dominated site to be 80% of incoming precipitation and ET at a sagebrush-dominated site to be 61% of incoming precipitation. Flerchinger and Cooley [55] found that ET accounted for 90% of annual precipitation for a semiarid subbasin in Southwestern ID, USA.

Limited research has been conducted into the ET of western juniper and sagebrush steppe ecosystems. Studies have largely focused on transpiration, particularly of western juniper. Mollnau et al. [32] found that mature western juniper stand transpiration rates at a site in Central Oregon were approximately 0.4 mm day^{-1} during summer months and that transpiration rates were largely associated with soil water content. Abdallah et al. [33] found that peak transpiration rates of western juniper trees ranged from 73 to 115 L day^{-1}, varying with seasonal and annual precipitation and soil water content. Calculations of sagebrush transpiration are very limited.

Valayamkunnath et al. [37] estimated sagebrush transpiration to be between 229 and 353 mm yr^{-1}, or 91–98% of the annual water budget, at a study site in Idaho.

Among the limitations of this study, the water balance method (WBM) approach applied cannot distinguish between precipitation that evaporates from juniper overstory, soil evaporation, or transpiration. As mature western juniper intercepts as much as 46% of precipitation at Jensen WS [30], there may be important differences in evaporation and transpiration rates not reflected by the WBM approach. Further, the WBM does not account for spatial variability (e.g., snowdrift, topographic variations in precipitation, or variations in vegetation cover) or connections between hydrologic processes (e.g., transmission losses in the stream channel and subsurface flow). It should be noted that for our study, streamflow measurements do not reflect potential stream channel transmission losses that may have occurred upslope of the flume at the outlet of the watershed.

Seasonal soil water storage is critical in sagebrush ecosystems [6]. Reduced soil water content has been associated with reduced net ecosystem exchange in sagebrush ecosystems in Wyoming [83]. In our study, the soil water content increased during the coldest and wettest months (January through March) at both watersheds and subsequently decreased in the following months. These seasonal increases corresponded to periods of highest annual precipitation and low PET. Additionally, we calculated daily soil water content change for a soil depth of 0.8 m, which we assumed represented the maximum rooting and soil depth for most of the two watersheds. This based on our observations of soil depth during sensor installation and the results of other studies [84,85]. However, the maximum rooting depth within each watershed may have varied due to specific site characteristics, including vegetation density and soil depth.

Winter precipitation and snowmelt runoff in the spring were reflected in the greater soil moisture and subsurface flows observed in both watersheds. Deep percolation (DP) below the root zone, calculated by using the WBM, and shallow aquifer recharge (Re_{GW}), estimated by using the WTFM, occurred during the wet season (winter–spring). Re_{GW} rates tended to decrease as juniper transpiration increased (based on data described by Abdallah et al. [33]); however, some interannual variability was shown. Seasonal variations in precipitation resulted in variations in DP and Re_{GW}, even during years when total precipitation amounts are similar. This was particularly the case in years when precipitation type was different (rain vs. snow). The

WBM used in this study calculates DP as the sink term but does not account for incoming precipitation that may percolate through fractures in the soil or for differences in rain vs. snow, and therefore may underestimate the amount of DP. A significant portion of the DP estimated was expected to reach the shallow aquifer in each watershed; however, it is difficult to equate to Re_{GW} given some DP can move laterally out of the watershed or through the spring system. As discussed in [51], fractured basalt substrates, like the one found at our study site, may not necessarily lead to recharge but could also result in lateral flows.

A key premise of WTFM is that the specific yield (S_y) is constant over a given area and timeframe. If these assumptions are not met, then the groundwater recharge calculations may not be accurate for a given area. The WTFM assumes that increases in shallow groundwater heights are associated with aquifer recharge, although other processes, such as evapotranspiration, can also result in shallow groundwater fluctuations [60]. In particular, assumptions regarding the baseline recession (the decrease in groundwater levels that would have occurred with no recharge) will influence recharge calculations. Similar to methods used by [61,86,87], we assumed daily increases in groundwater level would reflect recharge rates. While this approach has been found to underestimate recharge compared to other WTFM approaches [88], we used frequent measurements (recorded hourly for the majority of the study and averaged at the daily time step) to minimize these discrepancies.

The decline in groundwater levels, consequently less Re_{GW}, observed during late spring was attributed to a combination of less snowmelt runoff inputs and the increased vegetation water uptake during the warmer spring days. Annual Re_{GW} was, for most years, several times that of the total precipitation for the water year, indicating spatial heterogeneity in recharge rates. We attributed this Re_{GW} response to the wells' location at the watershed outlet, which may have accounted for the aggregate of subsurface flow coming out of the watersheds. However, it is difficult to extrapolate the results observed at the drainage outlet to the entire watershed, particularly with the varying topography, vegetation, and subsurface characteristics found at our study site.

In years with greater snowpack, streamflow and springflow levels were generally higher compared to rain-dominated years, even when annual precipitation amounts were nearly the same. As in Kormos et al. [10], significantly higher streamflow rates were observed in the

sagebrush-dominated watershed. This was the case in the two years (2016 and 2017) with greater snowpack depths. Also, higher springflow rates were obtained in the sagebrush-dominated watershed for all years evaluated. This was partly attributed to the greater subsurface flow residence time observed in the sagebrush-dominated watershed, as previously documented in [30]. While springflow has been relatively the same at the juniper-dominated watershed, springflow in the sagebrush-dominated watershed is twice that found before juniper removal in 2005 [30]. The smaller catchment area draining into the spring in the juniper-dominated watershed may have also contributed to the lower springflow rates observed. Streamflow and springflow accounted for a relatively small portion of incoming precipitation, yet, both play an important role in the ecohydrology of the site. For instance, springflow is an important water source for cattle and wildlife for most of the year. Also, transient streamflow and subsurface flow help maintain the hydrologic connectivity between the upland watersheds and the larger valley they drain into [30].

While additional research is needed into quantifying recharge and evapotranspiration rates, particularly across a heterogeneous landscape, the results of this study contribute to the understanding of how woody plant encroachment and climate variability collectively affect the water budget in sagebrush and western juniper ecosystems. Combining ground-based techniques and remote sensing can improve our understanding of the spatial and temporal patterns of vegetation and soil water content in these watersheds. Future research at this site includes the continued monitoring of ecohydrologic characteristics and modeling applications to expand local results to larger spatial domains.

5. Conclusions

This study examined seasonal water balance and subsurface flow dynamics in two rangeland watersheds, one dominated by western juniper and one dominated by big sagebrush, in central Oregon, USA. We assessed seven years of observations with varied meteorological conditions. A water balance method approach was used to quantify multiple components of the water budget in each watershed. The Water Table Fluctuation Method was used to calculate shallow aquifer recharge at the outlet of each watershed. Evapotranspiration accounted for most of the water budget, followed by deep percolation. Overall, greater springflow and streamflow

rates were observed in the sagebrush-dominated watershed. There were no statistically significant differences in groundwater recharge rates between the juniper-dominated site overlying alluvium substrate and the sagebrush-dominated site overlying fractured basalt. However, the significant springflow levels observed at the outlet of the sagebrush-dominated basin added to the total amount of subsurface flow coming out of the watershed. Aquifer recharge and springflow estimates were higher in both watersheds during the years with less potential evapotranspiration and greater snowpack. This study provides important information regarding the seasonal precipitation dynamics affecting the portioning of different water budget components and the mechanisms of shallow aquifer replenishment in juniper- vs. sagebrush-dominated landscapes. Further research is needed to expand on the temporal and spatial dynamics of the ecohydrologic processes and land management practices affecting water availability in cool climate rangeland ecosystems.

References

1. Bradford, J.B.; Schlaepfer, D.R.; Lauenroth, W.K. Ecohydrology of Adjacent Sagebrush and Lodgepole Pine Ecosystems: The Consequences of Climate Change and Disturbance. *Ecosystems* **2014**, *17*, 590–605. https://doi.org/10.1007/s10021-013-9745-1.
2. Palmquist, K.A.; Schlaepfer, D.R.; Bradford, J.B.; Lauenroth, W.K. Mid-Latitude Shrub Steppe Plant Communities: Climate Change Consequences for Soil Water Resources. *Ecology* **2016**, *97*, 2342–2354. https://doi.org/10.1002/ecy.1457.
3. Abdulla, F.; Eshtawi, T.; Assaf, H. Assessment of the Impact of Potential Climate Change on the Water Balance of a Semi-Arid Watershed. *Water Resour. Manag.* **2009**, *23*, 2051–2068. https://doi.org/10.1007/s11269-008-9369-y.
4. Eckhardt, K.; Ulbrich, U. Potential Impacts of Climate Change on Groundwater Recharge and Streamflow in a Central European Low Mountain Range. *J. Hydrol.* **2003**, *284*, 244–252. https://doi.org/10.1016/j.jhydrol.2003.08.005.
5. Meixner, T.; Manning, A.H.; Stonestrom, D.A.; Allen, D.M.; Ajami, H.; Blasch, K.W.; Brookfield, A.E.; Castro, C.L.; Clark, J.F.; Gochis, D.J.; et al. Implications of Projected Climate Change for Groundwater Recharge in the Western United States. *J. Hydrol.* **2016**, *534*, 124–138. https://doi.org/10.1016/j.jhydrol.2015.12.027.
6. Schlaepfer, D.R.; Lauenroth, W.K.; Bradford, J.B. Consequences of Declining Snow Accumulation for Water Balance of Mid-Latitude Dry Regions. *Glob. Chang. Biol.* **2012**, *18*, 1988–1997. https://doi.org/10.1111/j.1365-2486.2012.02642.x.
7. Konapala, G.; Mishra, A.K.; Wada, Y.; Mann, M.E. Climate Change Will Affect Global Water Availability through Compounding Changes in Seasonal Precipitation and Evaporation. *Nat. Commun.* **2020**, *11*, 3044. https://doi.org/10.1038/s41467-020-16757-w.
8. Bradford, J.B.; Schlaepfer, D.R.; Lauenroth, W.K.; Burke, I.C. Shifts in Plant Functional Types Have Time-Dependent and Regionally Variable Impacts on Dryland Ecosystem Water Balance. *J. Ecol.* **2014**, *102*, 1408–1418. https://doi.org/10.1111/1365-2745.12289.

9. Pierson, F.B.; Jason Williams, C.; Hardegree, S.P.; Clark, P.E.; Kormos, P.R.; Al-Hamdan, O.Z. Hydrologic and Erosion Responses of Sagebrush Steppe Following Juniper Encroachment,Wildfire, and Tree Cutting. *Rangel. Ecol. Manag.* **2013**, *66*, 274–289. https://doi.org/10.2111/REM-D-12-00104.1.
10. Kormos, P.R.; Marks, D.; Pierson, F.B.; Williams, C.J.; Hardegree, S.P.; Havens, S.; Hedrick, A.; Bates, J.D.; Svejcar, T.J. Ecosystem Water Availability in Juniper versus Sagebrush Snow-Dominated Rangelands. *Rangel. Ecol. Manag.* **2017**, *70*, 116–128. https://doi.org/10.1016/j.rama.2016.05.003.
11. Petersen, S.L.; Stringham, T.K. Infiltration, Runoff, and Sediment Yield in Response to Western Juniper Encroachment in Southeast Oregon. *Rangel. Ecol. Manag.* **2008**, *61*, 74–81. https://doi.org/10.2111/07-070R.1.
12. Bradley, B.A. Assessing Ecosystem Threats from Global and Regional Change: Hierarchical Modeling of Risk to Sagebrush Ecosystems from Climate Change, Land Use and Invasive Species in Nevada, USA. *Ecography* **2010**, *33*, 198–208. https://doi.org/10.1111/j.1600-0587.2009.05684.x.
13. Creutzburg, M.K.; Halofsky, J.E.; Halofsky, J.S.; Christopher, T.A. Climate Change and Land Management in the Rangelands of Central Oregon. *Environ. Manag.* **2015**, *55*, 43–55. https://doi.org/10.1007/s00267-014-0362-3.
14. Valayamkunnath, P.; Sridhar, V.; Zhao, W.; Allen, R.G. A Comprehensive Analysis of Interseasonal and Interannual Energy and Water Balance Dynamics in Semiarid Shrubland and Forest Ecosystems. *Sci. Total Environ.* **2019**, *651*, 381–398. https://doi.org/10.1016/j.scitotenv.2018.09.130.
15. Scott, R.L.; Biederman, J.A. Critical Zone Water Balance Over 13 Years in a Semiarid Savanna. *Water Resour. Res.* **2019**, *55*, 574–588. https://doi.org/10.1029/2018WR023477.
16. Lewis, D.; Singer, M.J.; Dahlgren, R.A.; Tate, K.W. Hydrology in a California Oak Woodland Watershed: A 17-Year Study. *J. Hydrol.* **2000**, *240*, 106–117. https://doi.org/10.1016/S0022-1694(00)00337-1.
17. Yang, Y.; Liu, D.L.; Anwar, M.R.; O'Leary, G.; Macadam, I.; Yang, Y. Water Use Efficiency and Crop Water Balance of Rainfed Wheat in a Semi-Arid Environment: Sensitivity of Future Changes to Projected Climate Changes and Soil Type. *Theor. Appl. Climatol.* **2016**, *123*, 565–580. https://doi.org/10.1007/s00704-015-1376-3.
18. Kundu, S.; Khare, D.; Mondal, A. Past, Present and Future Land Use Changes and Their Impact on Water Balance. *J. Environ. Manag.* **2017**, *197*, 582–596. https://doi.org/10.1016/j.jenvman.2017.04.018.
19. Chauvin, G.M.; Flerchinger, G.N.; Link, T.E.; Marks, D.; Winstral, A.H.; Seyfried, M.S. Long-Term Water Balance and Conceptual Model of a Semi-Arid Mountainous Catchment. *J. Hydrol.* **2011**, *400*, 133–143. https://doi.org/10.1016/j.jhydrol.2011.01.031.
20. Marc, V.; Robinson, M. The Long-Term Water Balance (1972–2004) of Upland Forestry and Grassland at Plynlimon, Mid-Wales. *Hydrol. Earth Syst. Sci.* **2007**, *11*, 44–60. https://doi.org/10.5194/hess-11-44-2007.
21. Ward, A.S.; Gooseff, M.N.; Voltz, T.J.; Fitzgerald, M.; Singha, K.; Zarnetske, J.P. How Does Rapidly Changing Discharge during Storm Events Affect Transient Storage and Channel Water Balance in a Headwater Mountain Stream? *Water Resour. Res.* **2013**, *49*, 5473–5486. https://doi.org/10.1002/wrcr.20434.
22. Wang, D.; Alimohammadi, N. Responses of Annual Runoff, Evaporation, and Storage Change to Climate Variability at the Watershed Scale. *Water Resour. Res.* **2012**, *48*. https://doi.org/10.1029/2011WR011444.

23. do Nascimento, M.G.; Herdies, D.L.; de Souza, D.O. The South American Water Balance: The Influence of Low-Level Jets. *J. Clim.* **2016**, *29*, 1429–1449. https://doi.org/10.1175/JCLI-D-15-0065.1.
24. Weltz, M.A.; Blackburn, W.H. Water Budget for South Texas Rangelands. *J. Range Manag.* **1995**, *48*, 45–52. https://doi.org/10.2307/4002503.
25. Wilcox, B.P.; Dowhower, S.L.; Teague, W.R.; Thurow, T.L. Long-Term Water Balance in a Semiarid Shrubland. *Rangel. Ecol. Manag.* **2006**, *59*, 600–606.
26. Bugan, R.; Jovanovic, N.; De Clercq, W. The Water Balance of a Seasonal Stream in the Semi-Arid Western Cape (South Africa). *WSA* **2012**, *38*, 201–212. https://doi.org/10.4314/wsa.v38i2.5.
27. Cantón, Y.; Villagarcía, L.; Moro, M.J.; Serrano-Ortíz, P.; Were, A.; Alcalá, F.J.; Kowalski, A.S.; Solé-Benet, A.; Lázaro, R.; Domingo, F. Temporal Dynamics of Soil Water Balance Components in a Karst Range in Southeastern Spain: Estimation of Potential Recharge. *Hydrol. Sci. J.* **2010**, *55*, 737–753. https://doi.org/10.1080/02626667.2010.490530.
28. Deus, D.; Gloaguen, R.; Krause, P. Water Balance Modeling in a Semi-Arid Environment with Limited in Situ Data Using Remote Sensing in Lake Manyara, East African Rift, Tanzania. *Remote Sens.* **2013**, *5*, 1651–1680. https://doi.org/10.3390/rs5041651.
29. Eilers, V.H.M.; Carter, R.C.; Rushton, K.R. A Single Layer Soil Water Balance Model for Estimating Deep Drainage (Potential Recharge): An Application to Cropped Land in Semi-Arid North-East Nigeria. *Geoderma* **2007**, *140*, 119–131. https://doi.org/10.1016/j.geoderma.2007.03.011.
30. Ochoa, C.; Caruso, P.; Ray, G.; Deboodt, T.; Jarvis, W.; Guldan, S. Ecohydrologic Connections in Semiarid Watershed Systems of Central Oregon USA. *Water* **2018**, *10*, 181. https://doi.org/10.3390/w10020181.
31. Ray, G.; Ochoa, C.G.; Deboodt, T.; Mata-Gonzalez, R. Overstory–Understory Vegetation Cover and Soil Water Content Observations in Western Juniper Woodlands: A Paired Watershed Study in Central Oregon, USA. *Forests* **2019**, *10*, 151. https://doi.org/10.3390/f10020151.
32. Mollnau, C.; Newton, M.; Stringham, T. Soil Water Dynamics and Water Use in a Western Juniper (Juniperus Occidentalis) Woodland. *J. Arid Environ.* **2014**, *102*, 117–126. https://doi.org/10.1016/j.jaridenv.2013.11.015.
33. Abdallah, M.A.B.; Durfee, N.; Mata-Gonzalez, R.; Ochoa, C.G.; Noller, J.S. Water Use and Soil Moisture Relationships on Western Juniper Trees at Different Growth Stages. **2020**, *26*, 1596.
34. Angell, R.F.; Miller, R.F. Simulation of Leaf Conductance and Transpiration in Juniperus Occidentalis. *For. Sci.* **1994**, *40*, 5–17.
35. Scott, R.L. Using Watershed Water Balance to Evaluate the Accuracy of Eddy Covariance Evaporation Measurements for Three Semiarid Ecosystems. *Agric. For. Meteorol.* **2010**, *150*, 219–225. https://doi.org/10.1016/j.agrformet.2009.11.002.
36. Todd, R.W.; Evett, S.R.; Howell, T.A. The Bowen Ratio-Energy Balance Method for Estimating Latent Heat Flux of Irrigated Alfalfa Evaluated in a Semi-Arid, Advective Environment. *Agric. For. Meteorol.* **2000**, *103*, 335–348. https://doi.org/10.1016/S0168-1923(00)00139-8.
37. Valayamkunnath, P.; Sridhar, V.; Zhao, W.; Allen, R.G. Intercomparison of Surface Energy Fluxes, Soil Moisture, and Evapotranspiration from Eddy Covariance, Large-Aperture Scintillometer, and Modeling across Three Ecosystems in a Semiarid Climate. *Agric. For. Meteorol.* **2018**, *248*, 22–47. https://doi.org/10.1016/j.agrformet.2017.08.025.

38. Yeşilırmak, E. Temporal Changes of Warm-Season Pan Evaporation in a Semi-Arid Basin in Western Turkey. *Stoch. Environ. Res. Risk Assess.* **2013**, *27*, 311–321. https://doi.org/10.1007/s00477-012-0605-x.
39. López-Urrea, R.; Martín de Santa Olalla, F.; Fabeiro, C.; Moratalla, A. Testing Evapotranspiration Equations Using Lysimeter Observations in a Semiarid Climate. *Agric. Water Manag.* **2006**, *85*, 15–26. https://doi.org/10.1016/j.agwat.2006.03.014.
40. Kume, T.; Otsuki, K.; Du, S.; Yamanaka, N.; Wang, Y.-L.; Liu, G.-B. Spatial Variation in Sap Flow Velocity in Semiarid Region Trees: Its Impact on Stand-Scale Transpiration Estimates. *Hydrol. Process.* **2012**, *26*, 1161–1168. https://doi.org/10.1002/hyp.8205.
41. Hargreaves, G.H.; Samani, Z.A. Reference Crop Evapotranspiration from Temperature. *Appl. Eng. Agric.* **1985**, *1*, 96–99. https://doi.org/10.13031/2013.26773.
42. Todorovic, M.; Karic, B.; Pereira, L.S. Reference Evapotranspiration Estimate with Limited Weather Data across a Range of Mediterranean Climates. *J. Hydrol.* **2013**, *481*, 166–176. https://doi.org/10.1016/j.jhydrol.2012.12.034.
43. Raziei, T.; Pereira, L.S. Estimation of ETo with Hargreaves–Samani and FAO-PM Temperature Methods for a Wide Range of Climates in Iran. *Agric. Water Manag.* **2013**, *121*, 1–18. https://doi.org/10.1016/j.agwat.2012.12.019.
44. Thornthwaite, C.; Mather, J. *The Water Balance, Climatology,VIII(1)*; Drexel Institute of Technology, Laboratory of Climatology: Centerton, NJ, USA, 1955.
45. Thornthwaite, C.W.; Mather, J.R. *Instructions and Tables for Computing Potential Evapotranspiration and the Water Balance*; Laboratory of Climatology: Centerton, NJ, USA, 1957; Volume 10, 132p.
46. Gudulas, K.; Voudouris, K.; Soulios, G.; Dimopoulos, G. Comparison of Different Methods to Estimate Actual Evapo-transpiration and Hydrologic Balance. *Desalination and Water Treatment* **2013**, *51*, 2945–2954, doi:10.1080/19443994.2012.748443.
47. Alley, W.M. On the Treatment of Evapotranspiration, Soil Moisture Accounting, and Aquifer Recharge in Monthly Water Balance Models. *Water Resources Research* **1984**, *20*, 1137–1149, doi:https://doi.org/10.1029/WR020i008p01137.
48. Barlow, P.; Leake, S. *Streamflow Depletion by Wells: Understanding and Managing Effects of Groundwater Pumping on Streamflow*; Circular 1376; US Geological Survey: Reston,VA, USA, 2012.
49. Taylor, R.G.; Scanlon, B.; Döll, P.; Rodell, M.; Van Beek, R.; Wada, Y.; Longuevergne, L.; Leblanc, M.; Famiglietti, J.S.; Edmunds, M.; et al. Ground Water and Climate Change. *Nat. Clim. Chang.* **2013**, *3*, 322–329. https://doi.org/10.1038/nclimate1744.
50. Sophocleous, M. Interactions between Groundwater and Surface Water: The State of the Science. *Hydrogeol. J.* **2002**, *10*, 52–67. https://doi.org/10.1007/s10040-001-0170-8.
51. Ochoa, C.G.; Fernald, A.G.; Guldan, S.J.; Tidwell, V.C.; Shukla, M.K. Shallow Aquifer Recharge from Irrigation in a Semiarid Agricultural Valley in New Mexico. *J. Hydrol. Eng.* **2013**, *18*, 1219–1230. https://doi.org/10.1061/(ASCE)HE.1943-5584.0000718.
52. Caruso, P.; Ochoa, C.G.; Jarvis, W.T.; Deboodt, T. A Hydrogeologic Framework for Understanding Local Groundwater Flow Dynamics in the Southeast Deschutes Basin, Oregon, USA. *Geosciences* **2019**, *9*, 57. https://doi.org/10.3390/geosciences9020057.
53. Seyfried, M.S.; Schwinning, S.; Walvoord, M.A.; Pockman, W.T.; Newman, B.D.; Jackson, R.B.; Phillips, F.M. Ecohydrological Control of Deep Drainage in Arid and Semiarid Regions. *Ecology* **2005**, *86*, 277–287. https://doi.org/10.1890/03-0568.
54. Ryel, R.J.; Caldwell, M.M.; Leffler, A.J.; Yoder, C.K. Rapid Soil Moisture Recharge to Depth by Roots in a Stand of Artemisia Tridentata. *Ecology* **2003**, *84*, 757–764. https://doi.org/10.1890/0012-9658(2003)084[0757:RSMRTD]2.0.CO;2.

55. Flerchinger, G.N.; Cooley, K.R. A Ten-Year Water Balance of a Mountainous Semi-Arid Watershed. *J. Hydrol.* **2000**, *237*, 86–99. https://doi.org/10.1016/S0022-1694(00)00299-7.
56. Scanlon, B.R.; Healy, R.W.; Cook, P.G. Choosing Appropriate Techniques for Quantifying Groundwater Recharge. *Hydrogeol. J.* **2002**, *10*, 347.
57. Kendy, E.; Gérard-Marchant, P.; Walter, M.T.; Zhang, Y.; Liu, C.; Steenhuis, T.S. A Soil-Water-Balance Approach to Quantify Groundwater Recharge from Irrigated Cropland in the North China Plain. *Hydrol. Process.* **2003**, *17*, 2011–2031. https://doi.org/10.1002/hyp.1240.
58. Okumura, A.; Hosono, T.; Boateng, D.; Shimada, J. Evaluations of the Downward Velocity of Soil Water Movement in the Unsaturated Zone in a Groundwater Recharge Area Using Δ18 O Tracer: The Kumamoto Region, Southern Japan. *Geol. Croat.* **2018**, *71*, 65–82. https://doi.org/10.4154/gc.2018.09.
59. Sammis, T.W.; Evans, D.D.; Warrick, A.W. Comparison of Methods to Estimate Deep Percolation Rates1. *JAWRA J. Am. Water Resour. Assoc.* **1982**, *18*, 465–470. https://doi.org/10.1111/j.1752-1688.1982.tb00013.x.
60. Healy, R.W.; Cook, P.G. Using Groundwater Levels to Estimate Recharge. *Hydrogeol. J.* **2002**, *10*, 91–109. https://doi.org/10.1007/s10040-001-0178-0.
61. Jassas, H.; Merkel, B. Estimating Groundwater Recharge in the Semiarid Al-Khazir Gomal Basin, North Iraq. *Water* **2014**, *6*, 2467–2481. https://doi.org/10.3390/w6082467.
62. Risser, D.W.; Gburek, W.J.; Folmar, G.J. Comparison of Recharge Estimates at a Small Watershed in East-Central Pennsylvania, USA. *Hydrogeol. J.* **2009**, *17*, 287–298.
63. Wang, X.; Zhang, G.; Xu, Y.J. Spatiotemporal Groundwater Recharge Estimation for the Largest Rice Production Region in Sanjiang Plain, Northeast China. *J. Water Supply Res. Technol.—AQUA* **2014**, *63*, 630–641. https://doi.org/10.2166/aqua.2014.024.
64. Acharya, B.S.; Kharel, G.; Zou, C.B.; Wilcox, B.P.; Halihan, T. Woody Plant Encroachment Impacts on Groundwater Recharge: A Review. *Water; Basel* **2018**, *10*, 1466. https://doi.org/10.3390/w10101466.
65. Moore, G.W.; Barre, D.A.; Owens, M.K. Does Shrub Removal Increase Groundwater Recharge in Southwestern Texas Semiarid Rangelands? *Rangel. Ecol. Manag.* **2012**, *65*, 1–10. https://doi.org/10.2111/REM-D-11-00055.1.
66. Anderson, E.W.; Borman, M.M.; Krueger, W.C. *The Ecological Provinces of Oregon: A Treatise on the Basic Ecological Geography of the State;* SR 990; Oregon Agricultural Experiment Station, Oregon State University: Corvallis, OR, USA, 1998.
67. Durfee, N.; Ochoa, C.G.; Mata-Gonzalez, R. The Use of Low-Altitude UAV Imagery to Assess Western Juniper Density and Canopy Cover in Treated and Untreated Stands. *Forests* **2019**, *10*, 296. https://doi.org/10.3390/f10040296.
68. Ray, G.L. Long-term Ecohydrologic Response to Western Juniper (Juniperus occidentalis) Control in Semiarid Watersheds of Central Oregon : A Paired Watershed Study. Master's Thesis, Oregon State University, Corvallis, OR, USA, 2015.
69. Bates, J.D.; Svejcar, T.; Miller, R.; Davies, K.W. Plant Community Dynamics 25 Years after Juniper Control. *Rangel. Ecol. Manag.* **2017**, *70*, 356–362. https://doi.org/10.1016/j.rama.2016.11.003.
70. Cooperative Climatological Data Summaries, Western Regional Climate Center. Available online: http://www.wrcc.dri.edu/cgi-bin/cliMAIN.pl?or0501 (accessed on 10 December 2020).
71. Fisher, M. Analysis of Hydrology and Erosion in Small, Paired Watersheds in a Juniper-Sagebrush Area of Central Oregon. Ph.D. Thesis, Oregon State University, Corvallis, OR, USA, 2004.

72. Soil Survey Staff Natural Resources Conservation Service Official Soil Series Descriptions (OSDs) | NRCS Soils. Available online: https://www.nrcs.usda.gov/wps/portal/nrcs/detail/soils/home/?cid=nrcs142p2_053587 (accessed on 13 May 2018).
73. USDA Natural Resources Conservation Service. SNOwpack TELemetry Network (SNOTEL). NRCS. 2021. Available online: https://data.nal.usda.gov/dataset/snowpack-telemetry-network-snotel (accessed on 18 September 2021).
74. Kilpatrick, F.A.; Schneider, V.R. *Use of Flumes in Measuring Discharge*; Techniques of Water-Resources Investigations; US Government Printing Office: Washington, DC, USA, 1983.
75. Samani, Z. Discussion of "History and Evaluation of Hargreaves Evapotranspiration Equation"by George H. Hargreaves and Richard G. Allen. *J. Irrig. Drain Eng.* **2004**, *130*, 447–448. https://doi.org/10.1061/(ASCE)0733-9437(2004)130:5(447.2).
76. Dingman, S.L. *Physical Hydrology*; 3rd ed.; Waveland Press, Inc.: Long Grove, IL, USA, 2015.
77. Deboodt, T.L. Watershed Response to Western Juniper Control. Ph.D. Thesis, Oregon State University, Corvallis, OR, USA, 2008.
78. Brooks, K.N.; Ffolliott, P.F.; Gregersen, H.M.; Debano, L.F. Groundwater. In *Hydrology and the Management of Watersheds*; Iowa State Press: Ames, IA, USA, 2003; pp. 107–121.
79. Dilts, T.E.; Weisberg, P.J.; Dencker, C.M.; Chambers, J.C. Functionally Relevant Climate Variables for Arid Lands: A Climatic Water Deficit Approach for Modelling Desert Shrub Distributions. *J. Biogeogr.* **2015**, *42*, 1986–1997. https://doi.org/10.1111/jbi.12561.
80. Lesica, P.; Kittelson, P.M. Precipitation and Temperature Are Associated with Advanced Flowering Phenology in a Semi-Arid Grassland. *J. Arid Environ.* **2010**, *74*, 1013–1017. https://doi.org/10.1016/j.jaridenv.2010.02.002.
81. Niemeyer, R.J.; Link, T.E.; Seyfried, M.S.; Flerchinger, G.N. Surface Water Input from Snowmelt and Rain Throughfall in Western Juniper: Potential Impacts of Climate Change and Shifts in Semi-Arid Vegetation. *Hydrol. Process.* **2016**, *30*, 3046–3060. https://doi.org/10.1002/hyp.10845.
82. Yaseef, N.R.; Yakir, D.; Rotenberg, E.; Schiller, G.; Cohen, S. Ecohydrology of a semi-arid forest: Partitioning among water balance components and its implications for predicted precipitation changes. *Ecohydrology* **2010**, *3*, 143–154. https://doi.org/10.1002/eco.65.
83. Kwon, H.; Pendall, E.; Ewers, B.E.; Cleary, M.; Naithani, K. Spring Drought Regulates Summer Net Ecosystem CO2 Exchange in a Sagebrush-Steppe Ecosystem. *Agric. For. Meteorol.* **2008**, *148*, 381–391. https://doi.org/10.1016/j.agrformet.2007.09.010.
84. Young, J.A.; Evans, R.A.; Easi, D.A. Stem Flow on Western Juniper (Juniperus Occidentalis) Trees. *Weed Sci.* **1984**, *32*, 320–327.
85. Sturges, D.L.; Trlica, M.J. Root Weights and Carbohydrate Reserves of Big Sagebrush. *Ecology* **1978**, *59*, 1282–1285.
86. Blarasin, M.; Quinodóz, F.B.; Cabrera, A.; Matteoda, E.; Alincastro, N.; Albo, G. Weekly and Monthly Groundwater Recharge Estimation in A Rural Piedmont Environment Using the Water Table Fluctuation Method. *Int. J. Environ. Agric. Res.* **2016**, *2*, 10.
87. Rutledge, A.T. *Computer Programs for Describing the Recession of Ground-Water Discharge and for Estimating Mean Ground-Water Recharge and Discharge from Streamflow Records-Update*; Water-Resources Investigations Report; Supercedes WRI 93-4121; US Geological Survey: Reston,VA, USA, 1998.

88. Delin, G.N.; Healy, R.W.; Lorenz, D.L.; Nimmo, J.R. Comparison of Local- to Regional-Scale Estimates of Ground-Water Recharge in Minnesota, USA. *J. Hydrol.* **2007**, *334*, 231–249. https://doi.org/10.1016/j.jhydrol.2006.10.010.

COMPARISON OF EVAPOTRANSPIRATION MODELS AND ECOHYDROLOGIC CHARACTERISTICS FOR A JUNIPER-DOMINATED WATERSHED AND A SAGEBRUSH-DOMINATED WATERSHED IN CENTRAL OREGON, USA

Comparison of Evapotranspiration Models and Ecohydrologic Characteristics for a Juniper-Dominated Watershed and a Sagebrush-Dominated Watershed in Central Oregon, USA

Abstract: More information is needed to understand how western juniper encroachment impacts evapotranspiration (ET). Direct measurements of ET are often difficult and cost-prohibitive at remote, data-scarce sites. The objective of this study is to compare methods of modeling ET for two small watersheds, one dominated by western juniper and one dominated by sagebrush, in central Oregon, USA. A secondary aim of this study is to characterize the relationship between Normalized Difference Vegetation Index (NDVI), Normalized Difference Moisture Index (NDMI), canopy cover, soil moisture, and ET. Landsat 8 imagery was used to calculate NDVI and NDMI. Monthly ET for the same time period was modeled using the Soil and Water Assessment Tool (SWAT). Regional ET was calculated using Moderate Resolution Imaging Spectroradiometer (MODIS) ET data. OpenET, an open access platform, was used to download ET modeled using Mapping Evapotranspiration at High Resolution with Internalized Calibration (METRIC), Operational Simplified Surface Energy Balance (SSEBop), and Disaggregation of the Atmosphere-Land Exchange Inverse (DisALEXI). A small unpiloted aerial vehicle (UAV) was used to collect thermal infrared and multispectral imagery at small plot within each watershed periodically over the course of a year. Soil moisture, canopy cover, and meteorological information were collected at the same time as the UAV flights. QWaterModel was used to estimate ET from the UAV-based thermal imagery. Estimates of average annual ET varied among approaches, although surface energy balance models estimated greater ET at the juniper-dominated watershed. Annual average NDVI and NDMI, respectively, are 0.25 and 0.04 at the juniper-dominated watershed and 0.23 and -0.02 at the sagebrush-dominated watershed. A significant correlation was found between monthly ET and NDVI for both watersheds. The results of this study provide insight into the relationship between environmental characteristics (e.g., springflow, NDVI) and ET in sagebrush steppe environments.

Keywords: sagebrush steppe; juniper encroachment; evapotranspiration; water balance; Normalized Difference Vegetation Index (NDVI)

1. Introduction

Evapotranspiration (ET) if often the largest output of the water balance. However, direct measurements of evapotranspiration are frequently not available. Limited data makes direct measurements of actual evapotranspiration difficult, particularly in water limited environments where potential ET (PET) generally exceeds available moisture. ET is dependent on multiple factors, such as vegetation cover and type, and is limited by moisture and energy. Therefore, ET is often calculated as either the residual term of the water balance or energy balance. In water balance approaches, direct measurements of incoming precipitation and streamflow are often used to calculate evapotranspiration. However, other outputs, such as deep percolation and groundwater recharge, are difficult to calculate and these measurements may not reflect spatial heterogeneity in watershed processes. Many hydrologic models, such as the Soil and Water Assessment Tool [SWAT;[1]], use a water balance approach to calculate ET and other components of the water balance.

Surface energy balance (SEB) methods using remote sensing data are also commonly used for estimating ET. The SEB approach focus on partitioning the separate energy fluxes (latent heat, sensible heat, and ground heat fluxes) from incoming solar radiation, but it is likewise difficult to accurately calculate each of these components. Some SEB methods utilize thermal infrared data and meteorological data to determine the land surface temperature and estimate the sensible heat flux. For example, the Mapping Evapotranspiration at High Resolution with Internalized Calibration [METRIC; [2–4]] uses satellite-based imagery, elevation characteristics, and on-site weather measurements to calculate ET as the residual of the energy balance and uses reference ET (RET) for calibration. The Operational Simplified Surface Energy Balance [SSEBop; [5,6]] uses RET, surface temperature, and air temperature to calculate actual ET. The Atmosphere-Land Exchange Inverse [ALEXI, [7,8]] is based on a two-source energy balance [TSEB; [9]] approach, in which vegetation and soil surfaces are evaluated separately. In addition to surface temperature, ALEXI utilizes land cover type, leaf area index, and soil characteristics, among other on-site characteristics (e.g., windspeed) to calculate ET. Research has also found that incorporating multiple remote-sensing based ET models can improve field scale ET estimates [10]. Additionally, much of the imagery required for these methods can be readily downloaded using sources such as Google Earth Engine

(https://earthengine.google.com/) or the USGS Earth Explorer (https://earthexplorer.usgs.gov/). Other readily available resources for estimating ET include Moderate Resolution Imaging Spectroradiometer (MODIS) products which calculate ET using remote sensing imagery, including albedo and land cover, and meteorological data.

Vegetation indices, such as the Normalized Difference Vegetation Index (NDVI), are associated with various plant physiological processes and phenology (e.g., [11]). In particular, NDVI has been widely used as an indirect means to estimate ET in agricultural areas (e.g., [12]) and in humid areas with high amounts of vegetation cover (e.g., [13]). However, NDVI does not provide indications of soil transpiration and the correlation between NDVI and transpiration varies between vegetation types and ecosystems. Past research has found that NDVI, when combined with soil moisture, can be successfully used to model actual ET in semiarid grasslands [14]. However, the relationship between NDVI and ET may vary across seasons. For example, [15] found that NDVI values were most strongly related to the previous month's ET. NDVI is also correlated with thermal emissivity [16], an important aspect of the energy balance. Other indices, such as the normalized difference water index (NDWI, [17]) or normalized difference moisture index (NDMI, [18]), can also be easily calculated with remote sensing data and provide an indication of moisture content. For example, [19] found that ET estimates improved in water-limited conditions when a surface energy balance approach was combined with NDWI.

The relationship between ET and PET (or RET) is a commonly used approach to estimating actual ET. Crop coefficients, which are based on PET or RET and on crop type and growing phase with adjustments for water stress (such as those discussed in [20]) have also been widely used to estimate ET for specific crop types. However, there is limited research that address the ratio between ET and PET in heterogenous, semiarid systems such as the sagebrush steppe in central Oregon, USA. Additionally, the ratio between ET and PET can vary on a seasonal [21,22] and annual basis [23], particularly in systems where the timing of precipitation and the growing season are asynchronous.

The combination of remote sensing-based and on-site data may yield important information about ET. [24] found that combining NIR, SWIR, and surface temperature can be used to estimate soil water availability, an important indicator of ET. Additionally, on-site data serves as an important means of assessing the accuracy of modeling approaches and

understanding hydrologic characteristics such as ET. However, direct measurements of ET are limited in many semiarid, snow-dominated environments. ET is a crucial piece of the water balance that impacts many land use activities in these regions, such as cattle grazing and agriculture, and is key to understanding streamflow and groundwater recharge patterns.

In order to address these challenges, we examined different approaches to calculating ET and PET at different temporal and spatial scales. We also examined environmental indicators related to ET, to include springflow, volumetric water content, NDVI, and NDMI. First, we used satellite-based remote sensing data and readily available sources of ET calculations to examine ET and PET at the monthly scale for two small watersheds and compared these results to calculations made using the Soil and Water Assessment Tool (SWAT) model. We also examined ET at an hourly scale for a small plot within each watershed, using high spatial resolution UAV-based thermal infrared and multispectral imagery, and surface soil moisture data. The objectives of this study were to 1) compare different approaches to modeling ET at different temporal and spatial scales at two small watersheds and 2) assess the relationship between different ecohydrologic indicators and characteristics, specifically ET, springflow, soil moisture, NDVI, and NDMI.

2. Methods

2.1 Site description

The Camp Creek Paired Watershed Study (CCPWS) is located in central OR, USA, approximately 30 km northeast of Brothers, Oregon. This has been the site of various studies (e.g., [25,26]) into the impact of western juniper encroachment on the ecohydrology of snow-dominated sagebrush ecosystems. This study built upon past research at this study site that examined the water balance at two small, adjacent watersheds: one dominated by western juniper ("Jensen WS") and one sagebrush-dominated watershed in which the majority of western juniper were removed 17 years earlier ("Mays WS"). Tree canopy cover, largely in the form of western juniper (*Juniperus occidentalis*), is approximately 31% at Jensen WS and <1% at Mays WS [27]. Big sagebrush (*Artemisia tridentata*) is the dominant overstory at Mays WS. Jensen WS is approximately 96 ha and ranges in elevation from 1367 m near the outlet to 1500 m at the top of the watershed. Mays WS is approximately 116 ha in area and ranges in elevation from 1430 m near the watershed outlet to 1524 m near the top of the watershed.

The climate in the region is characterized by cold, snowy winters and dry, warm summers. Long-term average annual precipitation is 322 mm yr^{-1} [28]. Most of the precipitation falls during the winter season as snow. From October 2013 through September 2021, the mean annual precipitation for both watersheds was 293 mm yr^{-1} based on on-site precipitation measurements.

During the winter months (December through February) for 2013 through 2021, the average minimum daily air temperature was -6.3 °C and the average maximum daily air temperature was 4.5 °C. During the summer months (June through August) for 2013 through 2021, the average minimum daily air temperature was 7.5 °C and the average maximum daily air temperature was 26.5 °C. Cattle grazing is the dominant land use at this study site and in the surrounding region. The study site consists of both privately owned land and land managed by the U.S. Bureau of Land Management.

2.2 Data Collection: Watershed Scale

Data collection included both on-site measurements and remote sensing-based measurements (Figure 1). Windspeed (model S-WSET-B; Onset Computer Corp., Bourne, MA, USA), relative humidity (model S-THB-M0002; Onset Computer Corp.), and ambient temperature (model S-THB-M0002; Onset Computer Corp.) were collected using on-site weather stations. An onsite pyranometer (model SP-421-SS, Apogee Instruments Inc., Logan, UT, USA) was used to measure incoming shortwave solar radiation. Rainfall data were collected using tipping-bucket rain gauges located at each watershed and near the divide between the two watersheds.

Soil volumetric water content (θ) was measured at two sites (one near the outlet and one located upslope) at Jensen WS and three sites at Mays WS (one near the outlet, one in the valley, and one located upslope). CS650 sensors (Campbell Scientific, Inc., Logan, UT, USA) were used at the three soil monitoring sites in Mays WS and the upland monitoring site at Jensen WS. At Jensen WS, θ data were collected using HydraProbe sensors (Stevens Water Monitoring Systems, Inc., Portland, OR, USA) at the monitoring site near the watershed outlet. The θ data were collected at depths of 0.2, 0.5, and 0.8 m at all stations.

A developed spring is located in each watershed. Springflow rates were estimated based on the approach described in [29], using the relationship between measured springflow rates and the water level at a nearby springbox well. A water level logger (Model HOBO U20-001-01, Onset Computer, Corp.; Bourne, MA, USA) was used to measure springbox-water height beginning in 2017. Prior to the installation of the water level logger, a regression using averaged θ was used to estimate springflow rates.

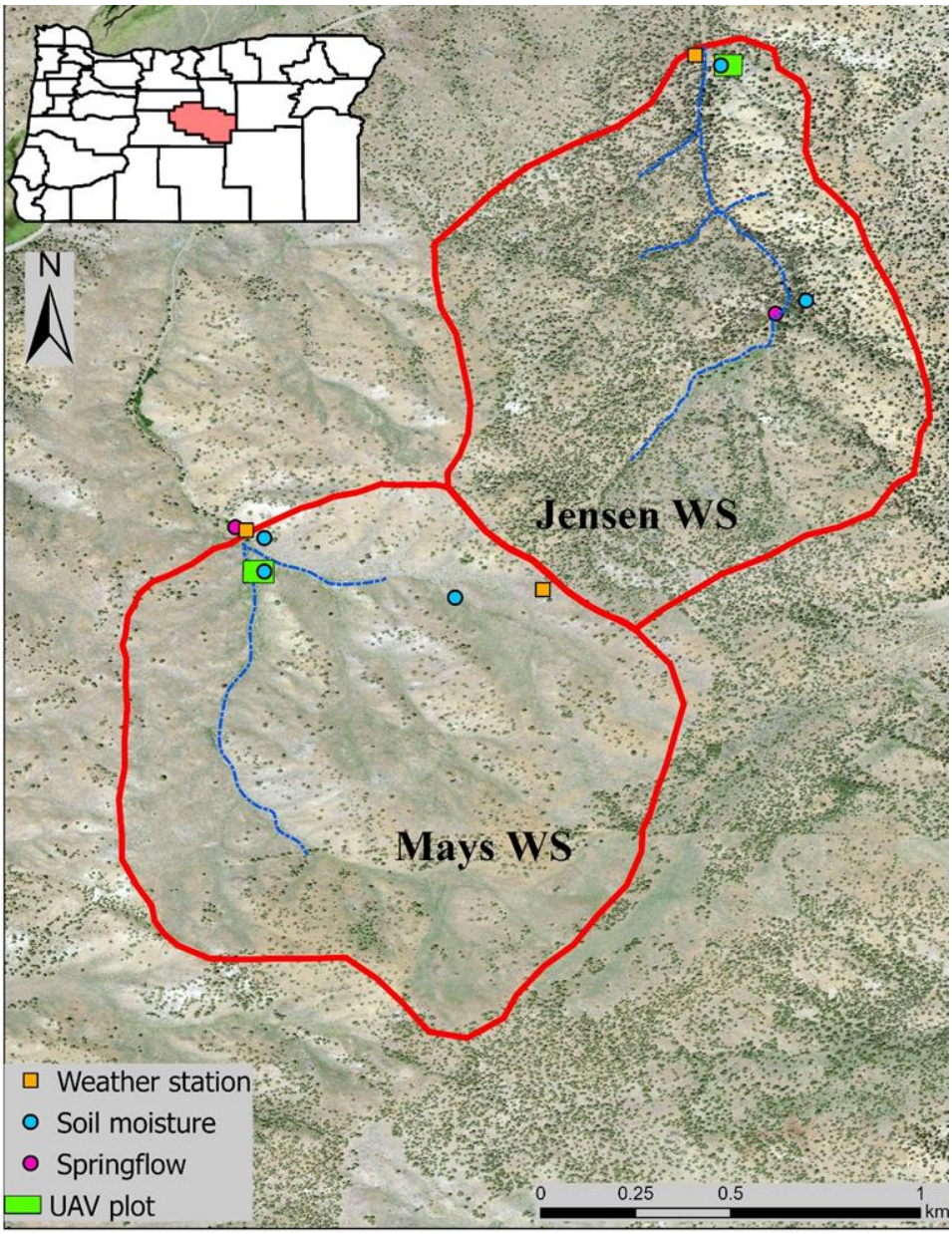

Figure 1. Location and instrumentation of Jensen WS and Mays WS. This map was created using ArcGIS® software by Esri. ArcGIS® and ArcMap™ are the intellectual property of Esri and are used herein under license. Copyright © Esri. All rights reserved. For more information about Esri® software, please visit www.esri.com. Basemap credits: U.S. Department of Agriculture (USDA), National Agriculture Imagery Program (NAIP); USDA-FSA-APFO Aerial Photography Field Office, publication date: 22 September 2016. Oregon counties map credits: Esri, TomTom North America, Inc., U.S. Census Bureau, U.S. Department of Agriculture (USDA), National Agricultural Statistics Service (NASS).

2.2.1 Data Collection: Watershed Scale NDVI, NDMI, and ET

Google Earth Engine (GEE; [30]) is a web-based platform used for geospatial analysis and visualization. GEE was used to extract the MODIS-based ET (MET) and PET (MPET) values from the MOD16A2.006 Evapotranspiration/Latent Heat Flux product [31] for both watersheds for October 2013 through December 2021. Each pixel value indicates the total ET or PET for an 8-day period, except for observations that occur at the end of the calendar year which are the sum of a 5- or 6-day period of observation. The spatial resolution of MODIS16A2.006 is 500 m. To estimate total monthly MET or MPET (both reported in kg m^{-2}), we first averaged the values of all pixels across each watershed for each observation. This value was converted from kg m^{-2} for each observation to mm day^{-1}. The average ET of the observations occurring within each month was then multiplied by the number of days in the month to estimate the monthly MET or MPET. GEE was also used to calculate Normalized Difference Moisture Index (NDMI; [18]) and Normalized Difference Vegetation Index (NDVI; [32]) for both watersheds for October 2013 through December 2021 using Landsat 8 data. A cloud mask was applied to select pixels without cloud cover and water. This resulted in observations not being available for some winter months. The Landsat 8 satellite collects data every 16 days. The spatial resolution of Landsat 8 shortwave bands is 30 m, while the Landsat 8 thermal infrared sensors have a spatial resolution of 100 m.

NDVI [32] is a commonly used index for assessing vegetation characteristics such as biomass, phenology, and vitality. It is based on the difference in reflectance between the near infrared (NIR) band and the red band (Equation 1). NIR is more strongly reflected by healthy vegetation and red wavelengths are more strongly absorbed. Decreased NIR reflectance and/or increased red reflectance may indicate that vegetation is water stressed, depending on vegetation characteristics and phenology. NDVI values range from -1 to 1. Higher values are associated with dense vegetation, values around zero are associated with bare soil, and negative values are associated with water or cloud cover. NDMI [18] provides an indication of vegetation water content and is based on the difference between NIR and shortwave infrared (SWIR) reflectance (Equation 2). For this study, we used the Landsat 8 band 6 SWIR, corresponding to a wavelength of 1.57 to 1.65 micrometers. At the extremes, NDMI can indicate completely bare soil (NDMI value of -1) to complete canopy, without water stress (NDMI value of 1). Values in the mid-

range (e.g., NDMI values of -0.2 to 0.2) indicate low to moderate amounts of canopy cover with high to low levels of water stress.

$$\frac{NIR - Red}{NIR + Red} \quad (1)$$

$$\frac{NIR - SWIR}{NIR + SWIR} \quad (2)$$

OpenET (see [33]) is an open-access, GEE-based platform that primarily uses Landsat 8 data and weather inputs (e.g., air temperature, wind speed, and solar radiation) to estimate monthly ET for the western region of the United States. Monthly modeled ET for January 2016 through December 2021 using METRIC, SSEBop, and DisALEXI was obtained from the OpenET website (https://openetdata.org/about/). The OpenET Ensemble ET (OET) for each watershed, which is the average of the monthly ET for the six models (METRIC, SSEBop, SIMS, PT-JPL, DisALEXI, and SEBAL) used in OpenET, with outlier estimates removed, were also obtained. Monthly reference ET (ORET) for the same period was also calculated. OpenET uses the Penman-Monteith equation for a grass surface to calculate RET. At the time of this research, January 2016 was the earliest date available within OpenET.

2.3 Watershed Scale: Soil and Water Assessment Tool-based ET

The Soil and Water Assessment Tool (SWAT, [1]) was also used to estimate ET (SWAT-ET) and PET (SWAT-PET) for both watersheds. SWAT is a physically-based hydrologic, semi-distributed model that has been used to calculate ET (e.g., [34,35]) and other aspects of the water balance. Inputs required for this model include a digital elevation model (DEM), soils information, and land use/cover, as well as meteorological information. A 10-m DEM was used to delineate the watershed boundaries and stream path. State Soil Geographic (STURGO) data was used for the soils' description. National Agricultural Imagery Program (NAIP) image was classified using the random trees classifier in ArcGIS Pro (Environmental Systems Research Institute (ESRI); Version 2.9; Redlands, CA, USA) to delineate land use. Land use was divided

into two main categories: range with shrub vegetation and evergreen forest (primarily western juniper). The ArcGIS interface for SWAT (ArcSWAT) was used in ArcGIS (ESRI, Version 10.7.1, Redlands, CA, USA) for this study. At the time of this study, ArcSWAT was not available for ArcGIS Pro.

Daily measurements of precipitation, minimum and maximum air temperature, relative humidity, and solar radiation for January 2010 through October 2021 were used to inform the model. The SWAT weather generator tool, which estimates values based on nearby monitoring stations, was used to estimate wind speed and to estimate observations for any periods of missing data. The slope in each watershed was divided into five categories, based on slope increments of 10 %. The minimum slope, land use, and soil coverage used to establish hydrologic response units was 10 %. Potential evapotranspiration in ArcSWAT was calculated using the Penman-Monteith equation. A monthly time step was used. The first three years were used as a "warm-up" period for the model. The monthly patterns of ET modeled by SWAT were compared to patterns of previous measurements of juniper transpiration [25] and to the results of a seasonal water balance study [29] for this study site. Attempts to calibrate the model using ephemeral streamflow and root-zone soil moisture measurements did not improve the results of the modeled monthly ET values and therefore the initial values modeled by ArcSWAT were used for analysis.

A multiple linear regression approach was used in SigmaPlot (Version 14, Systat Software, San Jose, CA, USA) to assess the relationship between NDVI, NDMI, and SWAT-based calculations of ET or OpenET Ensemble ET. Pearson's r was used to assess the correlation between NDVI, NDMI, θ, and springflow. A Kruskal-Wallis One Way Analysis of Variance (ANOVA) on Ranks was used to assess the differences in median values between ET calculated using METRIC, DisALEXI, MODIS, SSEBop, SWAT, and the OpenET Ensemble ET. Dunn's method was used to compare each ET method to the Ensemble ET.

2.4 Plot Scale: UAV-Based ET and NDVI

Multispectral (red, green, blue, red-edge, and near-infrared) imagery and thermal imagery were collected at a plot in each watershed using an Unpiloted Aerial Vehicle (UAV) on 11 days (Table 1). Multispectral imagery was collected using a MicaSense RedEdge camera (MicaSense,

Inc., Seattle, WA, USA). The thermal infrared (TIR) data was collected using a Zenmuse XT V2 (13 mm; DJI, Shenzhen, China) camera mounted to a Matrice 100 UAV (DJI, Shenzhen, China).

The thermal camera is radiometrically calibrated. The multispectral imagery was radiometrically calibrated using a calibration board and a downwelling light sensor. Visual imagery (red, blue, and green wavelengths) was collected using a Phantom 4 (DJI, Shenzhen, China) UAV for one flight. Due to processing limitations, the area of the thermal orthomosaic was reduced to approximately 3,000 m^2. No flights were conducted during the winter due to limited site access and snowpack. Flights were conducted approximately one and half hours after sunrise and at approximately noon. A flight altitude of approximately 60 to 70 m above ground level was used. During one flight, a battery malfunction resulted in only visual (red, green, blue wavelengths) and thermal imagery being collected. Two additional flights were excluded due to technological issues that occurred during flight. Therefore, more flight data were available for the Mays WS than at the Jensen WS.

Table 1. Dates of UAV flights. Data collection included multispectral imagery ("MS"), visual imagery (red, green, and blue wavelengths, "RGB"), thermal infrared imagery ("TIR"), surface soil moisture ("SM") and canopy density ("CD"). "WS" refers to the watershed where the data were collected. Morning flights occurred approximately 1.5 hours after sunrise and mid-day flights occurred around noon. In general, 2 to 3 flights were conducted, and total flight time was approximately 30 to 45 minutes for each observation.

Date	Time	Data collected	WS
23-Jul-2020	mid-day	MS, TIR, SM	Mays
6-Aug-2020	morning, mid-day	MS, TIR, SM	Jensen
20-Aug-2020	morning, mid-day	MS, TIR, SM, CD	Mays
2-Sep-2020	morning, mid-day	MS, TIR, SM	Jensen
3-Sep-2020	morning, mid-day	MS, TIR, SM	Mays
23-Sep-2020	mid-day	MS, TIR, SM	Jensen
29-Sep-2020	mid-day	RGB, TIR, SM	Mays
30-Sep-2020	morning, mid-day	MS, TIR, SM, CD	Jensen
1-Oct-2020	morning, mid-day	MS, TIR, SM, CD	Mays
14-Oct-2020	morning, mid-day	MS, TIR, SM	Mays
30-Apr-2021	morning, mid-day	MS, TIR, SM, CD	Jensen
18-Jun-2021	morning, mid-day	MS, TIR, SM, CD	Mays

The thermal and multispectral orthomosaics were created using AgiSoft Metashape (Agisoft LLC, St. Petersburg, Russia). MetaShape was used to radiometrically calibrate the multispectral imagery during the orthomosaic creation process. Each image contains metadata regarding the latitude, longitude, and elevation, which are then used for georeferencing. Additionally, for most multispectral and visible imagery, a minimum of four ground control points (GCPs) were used for geometric calibration. The latitude, longitude, and elevation of each GCP was measured using a submeter GPS (Model Geode GNS2, Juniper Systems Inc., Logan, UT, USA). The GCPs were not clearly visible in the thermal imagery and therefore the positional data were used instead. Additional georeferencing between the TIR and multispectral and visible orthomosaics was conducted in ArcGIS Pro to ensure alignment between the rasters. The approximate resolution was 0.09 m for the thermal orthomosaics and 0.05 m for the multispectral orthomosaics. The resolution for the orthomosaic with visible wavelengths only (red, green, and blue wavelengths) was 0.02 m.

The thermal orthomosaics created in MetaShape indicate brightness values ranging from 0 to 255. In order to create an orthomosaic reflecting temperature values in Kelvin, the thermal values were extracted from individual images using FLIR Tools (Teledyne FLIR LLC, Wilsonville, OR, USA). These values were then compared to brightness values for the same pixels within the orthomosaic. A minimum of 25 pixels were selected from each orthomosaic and a linear regression was used to determine the formula for converting from brightness values to temperature. The raster calculator tool in ArcGIS Pro (V 2.9; Environmental Systems Research Institute, Redlands, CA, USA) was used to convert the orthomosaics from brightness values to K.

NVDI (Equation 1) was calculated for each multispectral orthomosaic using the Raster Function NDVI tool in ArcGIS Pro. For the one orthomosaic of visual wavelengths only, the Visible Atmospherically Resistant Index (VARI) (Equation 3) was calculated.

$$VARI = \frac{Green - Red}{Green + Red - Blue} \quad (3)$$

In order to estimate evapotranspiration and other aspects of the energy balance (e.g., sensible heat flux) from the thermal images, the QWaterModel (version 1.3; [36]) tool in QGIS (Version 3.4.15, QGIS Geographic Information System, QGIS.org) was used. This tool is based on the Deriving Atmosphere from Turbulent Transport Useful to Dummies Using Temperature (DATTUTDUT) model [37]. QWaterModel creates a six-band raster with estimated net radiation, the latent heat flux, sensible heat flux, ground heat flux (all in Wm^{-2}), the evaporative fraction, and evapotranspiration (mm). The only required user inputs are a tagged image file (tif) containing thermal infrared (TIR) values in K. For this study, we provided the incoming solar radiation (in $W\ m^{-2}$) and air temperature (in K) data from an on-site weather station. QWaterModel also provides an estimate of mean albedo (α) based on the TIR raster. The surface emissivity (E_{surf}) was calculated based on NDVI from the Landsat 8 imagery for the same month (Equation 4).

$$E_{surf} = 1.0094 + 0.047\big(Ln(NDVI)\big) \quad (4)$$

The atmospheric emissivity (E_{atm}) was calculated based on actual vapor pressure (e_a) and E_{surf} (Equation 5) as described by [38]. T_A is air temperature in K.

$$E_{atm} = 1.24\left(\frac{e_a}{T_A}\right)^{0.14286} \quad (5)$$

The atmospheric transmissivity was left at the default value of 0.7. For flights conducted around solar noon, the ground heat flux (G) was assumed to be approximately 35% of the calculated incoming solar radiation, similar to methods used by [39,40] and described by [41]. For flights conducted approximately an hour and a half after sunrise, the ground heat flux (G) calculated by the QWaterModel model was used. In order to limit artefacts in the image, the maximum temperature was defined when very high TIR values associated with very reflective soils or a vehicle were present. The option to remove implausible output values was selected. A period of one hour was used. All images were previously georeferenced.

Hourly potential ET (PET) was calculated for each of the flights using the FAO-56 Penman-Monteith equation ([20]; Equation 6) with data from the on-site weather stations. The approach was modified to calculate hourly values, where ET_0 is the reference ET (mm hr^{-1}), Δ is the slope of the saturation vapor pressure curve (kPa $°C^{-1}$), R_n is the net radiation (MJ m^{-2} hr^{-1}), G is the ground heat flux (MJ m^{-2} hr^{-2}), γ is the psychrometric constant (kPa $°C^{-1}$), T is the mean hourly temperature (°C), μ_2 is the mean hourly windspeed at 2m (m s^{-1}), e_s is the saturated vapor pressure (kPa), and e_a is the actual vapor pressure (kPa). T_{mean} is the average hourly air temperature in °C. Calculations for saturated and unsaturated vapor pressure, the slope of the saturation vapor pressure curve, and the psychrometric constant were made based on the methods outlined by [20].

$$ET_0 = \frac{0.408\Delta(R_n - G) + \gamma \frac{37.5}{T + 273}\mu_2(e_s - e_a)}{\Delta + \gamma(1 + 0.34\mu_2)} \quad (6)$$

We estimated net radiation (R_n) using an approach similar to the method described by [42]. R_n (Equation 7) was estimated as the difference between net shortwave (R_{ns}, Equation 8) and net longwave (R_{nl}, Equation 9) solar radiation. R_{si} is the measured incoming shortwave radiation (Wm^{-2}), α is the albedo calculated using QWaterModel, T_p is the average pixel temperature from the TIR orthomosaic (K), and σ is the Stefan-Boltzman constant ($5.6704X\ 10^{-8}$ $Wm^{-2}K^4$).

$$R_n = R_{ns} + R_{nl} \quad (7)$$

$$R_{ns} = (1 - \alpha)R_{si} \quad (8)$$

$$R_{nl} = E_{atm}T_A^4\sigma - E_{surf}T_P^4\sigma \quad (9)$$

Topsoil (0.12 m) θ data were collected using a handheld portable moisture sensor (model CS659, Campbell Scientific) within a few hours of when the flights were conducted. The θ data were collected along five 45-m long line transects spaced 10 m apart with measurements spaced approximately 15 m apart along each line transect.

A CI-110 plant canopy imager (CID Bio-Science, Inc., Felix Instruments, Camas, WA, USA) was used to collect assess canopy cover (in %) on a seasonal basis. To assess canopy cover associated with big sagebrush (the predominant overstory vegetation at Mays WS), canopy imaging was conducted at a height of approximately 0.5 m off the ground. The primary overstory at Jensen WS is western juniper and therefore canopy cover was taken at heights of approximately 1 m, as very little vegetation fell below this height.

Pearson's r was used to examine the correlation between NDVI, θ, and ET at the plot scale. Multiple linear regression was used to assess how topsoil θ and NDVI predicted estimated ET at the plot scale. In order to assess differences in modeled canopy transpiration and soil evaporation, we selected 50 points, 25 representing overstory vegetation and 25 representing non-overstory surfaces (this included samples where small vegetation may not be discernable due to spatial resolution as well as open soil, rocky surfaces, etc.), within each mid-day image. Due to very slight differences in alignment between the NDVI and ET orthomosaics, points were selected using visual inspection of the imagery.

The 'Extract Multi Values to Points' tool in ArcGIS Pro was used to extract values at each sample location. Bilinear interpolation was applied during the extract process. The points were used to assess the average ET rate for overstory and non-overstory surfaces for each flight. Due to the reduced image quality of the morning TIR orthomosaics, this process was not conducted for imagery from the morning flights.

3. Results

3.1 Watershed-scale NDVI and NDMI

The NDVI and NDMI seasonal patterns were similar between the two watersheds (Figure 2), although larger seasonal peaks in watershed-scale NDVI were observed at Mays WS and larger peaks in watershed-scale NDMI were observed at Jensen WS. Mean seasonal NDVI and

NDMI values for each watershed are shown in Table 2. In general, negative NDVI values indicate cloud cover and/or water, therefore months where the mean NDVI was negative were excluded.

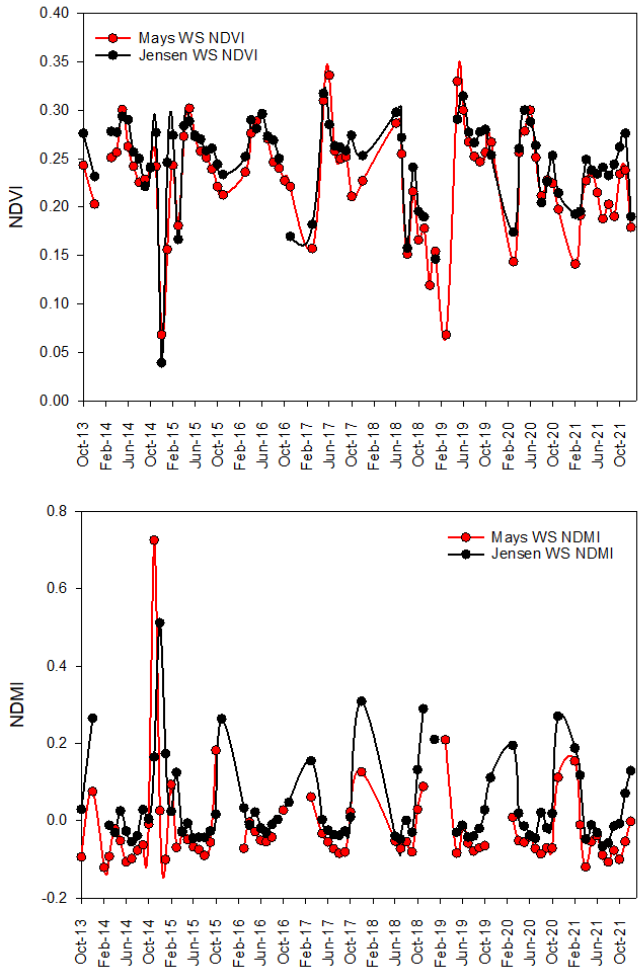

Figure 2. Average monthly NDVI and NDMI based on Landsat 8 imagery, for both watersheds, from October 2013 until October 2021.

Table 2. Average monthly NDMI and NDVI values for both WS for January 2016 through December 2021. Calculations are based on Landsat 8 imagery. The average monthly volumetric soil water content (θ) and springflow (spring, in average L min^{-1}) were calculated for January 2016 through September 2021. θ was calculated using the averaged soil water content at all measured soil depths for each soil moisture station in each watershed. For springflow, data from January through March 2021 was not available due to an equipment failure.

	Mays WS				Jensen WS			
Month	NDMI	NDVI	θ	Spring	NDMI	NDVI	θ	Spring
Jan	N/A	0.15	0.14	7.93	0.21	0.15	0.11	9.94
Feb	0.06	0.14	0.16	43.47	0.19	0.19	0.13	21.55
Mar	0.04	0.16	0.21	95.72	0.12	0.20	0.15	36.50
Apr	-0.06	0.25	0.23	88.70	-0.01	0.27	0.18	44.88
May	-0.05	0.29	0.21	72.40	-0.01	0.29	0.16	12.46
Jun	-0.04	0.29	0.18	60.63	-0.03	0.29	0.14	6.49
Jul	-0.07	0.25	0.15	26.63	-0.04	0.26	0.12	4.40
Aug	-0.08	0.22	0.13	18.24	-0.02	0.23	0.11	1.64
Sep	-0.08	0.23	0.12	16.40	-0.02	0.25	0.10	1.21
Oct	-0.03	0.22	0.11	11.96	0.04	0.25	0.10	2.12
Nov	0.05	0.22	0.12	9.27	0.16	0.22	0.11	2.53
Dec	0.06	0.18	0.12	6.84	0.22	0.22	0.10	3.31

Based on the calculations from Landsat 8 imagery, mean annual watershed NDVI was 0.23 at Mays WS and 0.25 at Jensen WS from October 2013 through December 2021. Mean annual NDMI was -0.02 at Mays WS and 0.04 at Jensen WS for the same period. In general, both NDVI and NDMI were greater at Jensen WS than Mays WS on a seasonal basis (Table 2). Peaks in seasonal NDVI were associated with peaks in seasonal soil moisture in both watersheds. Peaks in NDVI occurred in April through June. Peaks in NDMI were more substantial at Jensen WS, and generally occurred December through March.

At Mays WS, a significant correlation (at $p<0.05$) between monthly average NDVI and θ ($r=0.32$, $p=0.03$), NDVI and NDMI ($r=-0.26$, $p=0.03$), and springflow and θ ($r=0.79$, $p<0.001$). At Jensen WS, a significant correlation between NDVI and NDMI ($r=-0.66$, $p<0.001$), NDVI and θ ($r=0.35$, $p=0.01$), and θ and springflow ($r=0.74$, $p<0.001$).

3.2 Watershed-scale ET and PET

Considerable variability was shown between different ET models in both monthly ET and annual ET results. Average monthly ET (in mm) for January 2016 through December 2021 using METRIC, SSEBop, DisALEXI, and MET for both watersheds is displayed in Figure 3. The MET showed the least variability in monthly or seasonal ET compared to the other methods assessed. The other remote sensing-based approaches as well as the SWAT-ET indicated seasonal variation in ET. However, these seasonal variations were not consistent between models. Peak watershed ET tended to occur in March and April based on the DisALEXI model while for the OET (the average of all ET models used on the OpenET platform), SSEBop, and SWAT approaches, peak ET occurred between May and July.

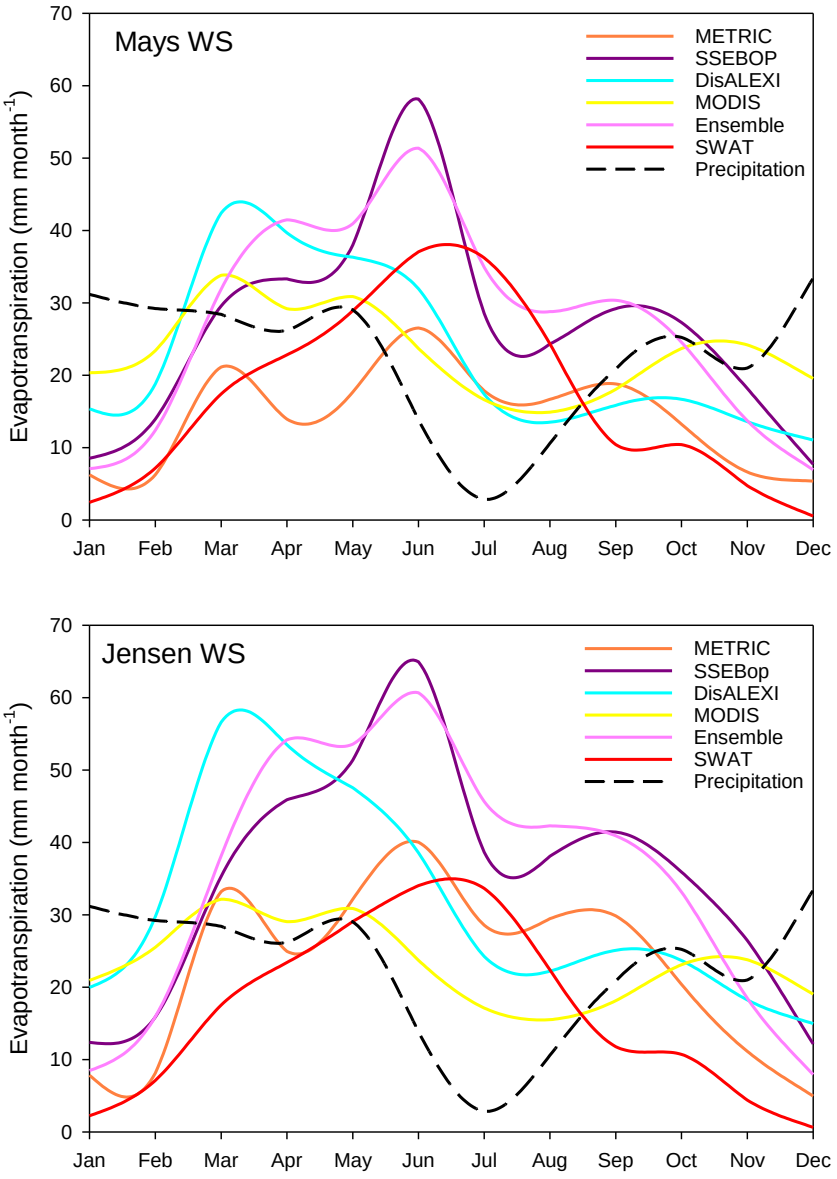

Figure 3. Average total monthly precipitation and ET for Jensen and Mays WS for January 2016 through December 2021.

For Jensen WS, a significant correlation was found between SWAT-ET values and NDMI (r=-0.63, p<0.001), NDVI (r=0.50, p<0.001), and θ (r=0.45, p<0.001). No significant correlation was found between the SWAT-ET values at Jensen WS and springflow (r=0.12, p=0.27). Similarly, a significant correlation was also found between the Jensen WS Ensemble ET values and NDMI (r=-0.62, p<0.001), NDVI (r=0.53, p<0.001), and θ (r=0.45, p<0.001), but not between the Ensemble ET values and springflow (r=0.13, p=0.30).

For Mays WS, a significant, correlation was found between the monthly SWAT-ET values and θ (r=0.45, p<0.001), springflow (r=0.33, p=0.001), NDMI (r=-0.35, p=0.003), and NDVI (r=0.53, p<0.001). The same pattern was shown between the Mays WS monthly Ensemble ET and θ (r=0.49, p<0.001), springflow (r=0.54, p<0.001), NDMI (r=-0.39, p=0.006), and NDVI (r=0.54, p<0.001).

Multiple linear regression was used to assess how well NDVI, NDMI, springflow, and θ predicted monthly SWAT-ET. At Mays WS, the overall regression model indicated that while the combination of NDVI, NDMI, springflow, and θ were significant (p=0.002) predictors of ET (r=0.60, R^2=0.36. F=5.07), NDVI (p=0.04) was the only significant predictor of SWAT-ET compared to NDMI (p=0.34), springflow (p=0.68), or θ (p=0.14). At Jensen WS, the overall regression indicated that the combination of NDVI, NDMI, springflow, and θ were also significant predictors (p<0.001) of monthly SWAT-ET (r=0.74, R^2=0.55, F=12.70), although NDMI (p=0.002) and θ (p=0.02) were the only significant predictors compared to NDVI (p=0.10) and springflow (p=0.54).

Excluding the SWAT- ET and MET, average annual estimated ET was greater at Jensen WS compared to Mays WS. Average annual ET for each watershed for January 2016 through December 2021 are shown in Tables 3 and 4. Excluding the SWAT-modeled ET values, higher ET values were calculated at Jensen WS compared to Mays WS. The Ensemble ET exhibited patterns most similar to the SSEBop model for both watersheds.

For both watersheds, the ANOVA indicated a significant difference (at $p \leq 0.001$) in median values among the watershed scale ET calculations. Based on Dunn's method, a significant difference between Ensemble ET and METRIC and SWAT-based calculations of ET at Mays WS were found. For Jensen WS, Dunn's method indicated a significant difference between Ensemble ET and SWAT, METRIC, and MODIS-based calculations of ET.

Table 3. Total annual ET for the selected approaches at Mays WS in mm yr^{-1}. For MODIS, one month of data were missing (indicated by "*") for 2019 and 2021. For 2017, two months of data were not available for MODIS (indicated by "**").

Year	Ensemble ET	METRIC	SSEBop	DisALEXI	MODIS	SWAT
2016	339	174	359	279	243*	197
2017	273	133	286	244	257**	198
2018	309	186	282	251	241*	210
2019	365	162	317	392	254*	243
2020	331	143	360	238	281	202
2021	331	224	296	232	274	164
Average	324	170	317	273	258	202

Table 4. Total annual ET for the selected approaches at Jensen WS in mm yr^{-1}. For MODIS, one month of data were missing (indicated by "*") for 2016, 2018, and 2019. For 2017, two months of data were not available for MODIS (indicated by "**").

Year	Ensemble ET	METRIC	SSEBop	DisALEXI	MODIS	SWAT
2016	423	276	440	347	274	194
2017	371	224	421	379	258**	187
2018	423	297	387	378	263	188
2019	454	266	416	505	260*	236
2020	427	268	445	320	276	184
2021	418	294	403	316	247*	190
Average	419	271	419	374	263	197

At Mays WS, the average annual MODIS PET (MPET) from January 2014 through December 2021, was 1468 mm yr^{-1}. At Jensen WS, the average annual MPET from January 2014 through December 2021, was 1491 mm yr^{-1}. Average annual OpenET RET for January 2016 through December 2021 was 1039 mm yr^{-1} at Mays WS and 1036 mm yr^{-1} at Jensen WS.

The average MPET and OpenET-based RET (ORET) by month for January 2016 through December 2021 are shown in Table 5. At Mays WS, the average ratio between MET and MPET was 0.33 and the ratio between OET and ORET was 0.35. At Jensen WS, the average ratio between MET and MPET was 0.34 and the ratio between OET and ORET was 0.45. The ratio

between MET and MPET was generally greatest during the winter months (December through February) for both watersheds and the least during the summer months. While both the MPET and ORET displayed seasonal differences, the ratio between OET and ORET tended to peak during late winter (February and March) and then again in early fall (October and November), with the lowest ratio between OET and ORET occurring during the summer months.

Table 5. Average monthly values for MODIS PET (MPET), OpenET reference ET (ORET), and the ratio of MODIS-ET (MET) to MPET and OpenET-ET (OET) to ORET. MPET and RET are in total mm per month. OET is the average ET of all ET models used in OpenET, with outliers removed.

	Mays WS				Jensen WS			
Month	MPET	MET/ MPET	RET	OET/ ORET	MPET	MET/ MPET	RET	OET/ ORET
Jan	30	0.72	25	0.26	30	0.74	23	0.34
Feb	43	0.61	34	0.36	46	0.57	33	0.5
Mar	92	0.37	57	0.55	89	0.37	57	0.67
Apr	146	0.21	90	0.46	152	0.2	90	0.6
May	185	0.17	126	0.32	185	0.17	127	0.42
Jun	213	0.11	155	0.33	214	0.11	156	0.39
Jul	246	0.07	183	0.19	247	0.07	183	0.25
Aug	214	0.07	158	0.18	214	0.07	158	0.27
Sep	143	0.13	100	0.31	143	0.13	100	0.42
Oct	91	0.27	56	0.44	95	0.25	56	0.6
Nov	52	0.49	33	0.41	54	0.46	32	0.57
Dec	26	0.78	20	0.33	22	0.91	20	0.39

SWAT-PET and the ratio between SWAT-ET and SWAT-PET were similar between the two watersheds. For January 2014 through December 2021, the average annual SWAT-PET was 578 mm yr^{-1} at Mays WS and 575 mm yr^{-1} at Jensen WS. The average annual ratio of SWAT- ET to PET was 0.56 at Mays WS and 0.55 at Jensen WS, ranging from 0.19 in September for both watersheds to 0.96 in January for both watersheds.

3.3 Plot scale

No major differences between the two watersheds were observed in plot-scale ET calculated using the thermal imagery. The mean energy balance components for each flight are shown in Table 6. Average estimated ET for all mid-day flights was 0.22 mm hr^{-1}. For all morning flights, the average estimated ET was 0.03 mm hr^{-1}. Average ET was similar for both watersheds, with the average mid-day ET rate at Mays WS being less than that of Jensen WS (0.20 mm hr^{-1} versus 0.24 mm hr^{-1}). Estimated PET for each flight was likewise very similar between the two watersheds, with estimated mid-day PET being 0.44 mm hr^{-1} at Mays WS and 0.45 mm hr^{-1} at Jensen WS. The ratio of ET to PET for mid-day flights was 0.56 at Jensen WS and 0.46 at Mays WS. For morning flights, the ratio of ET to PET was 0.64 at both watersheds.

Table 6. Energy balance components calculated using QWaterModel. "R_n" is net radiation, "LHF" is latent heat flux, "SHF" is sensible heat flux, "G" is ground heat flux. All fluxes are in W m^{-2}. Evapotranspiration (ET) and potential evapotranspiration (PET) are in mm hr^{-1}. "WS" the location of the flight: Mays WS (M) or the Jensen WS (J).

Date	Time	WS	R_n	LHF	SHF	G	ET	PET	ET/PET
23-Jul-2020	12:00	M	421	163	110	147	0.24	0.53	0.45
6-Aug-2020	07:25	J	8	7	1	1	0.01	0.05	0.2
6-Aug-2020	11:55	J	498	218	106	174	0.32	0.56	0.57
20-Aug-2020	07:30	M	38	26	7	5	0.04	0.04	1
20-Aug-2020	11:30	M	469	149	156	164	0.22	0.43	0.51
2-Sep-2020	07:30	J	33	24	5	4	0.04	0.04	1
2-Sep-2020	12:10	J	427	130	148	150	0.19	0.52	0.37
3-Sep-2020	07:22	M	57	39	10	8	0.06	0.06	1
3-Sep-2020	12:30	M	306	69	130	107	0.1	0.45	0.22
23-Sep-2020	12:00	J	334	141	77	117	0.21	0.46	0.46
29-Sep-2020	12:00	M	351	100	128	123	0.15	0.35	0.43
30-Sep-2020	08:00	J	41	29	7	5	0.04	0.06	0.67
30-Sep-2020	11:45	J	365	132	105	128	0.2	0.33	0.61
1-Oct-2020	08:30	M	6	5	0	0	0.01	0.02	0.5
1-Oct-2020	11:45	M	403	166	96	141	0.24	0.36	0.67
14-Oct-2020	08:50	M	7	6	1	1	0.01	0.04	0.25
14-Oct-2020	12:00	M	334	154	63	117	0.22	0.2	1.1
30-Apr-2021	07:20	J	33	25	4	4	0.04	0.06	0.67

30-Apr-2021	11:40	J	403	188	74	141	0.28	0.36	0.78
18-Jun-2021	07:10	M	32	25	4	3	0.04	0.09	0.44
18-Jun-2021	11:40	M	433	157	124	152	0.23	0.49	0.47

For the morning flights that took place on 1 October 2020 and 14 October 2020, approximately 60% of the pixels were excluded from analysis. On both of these days, a haze present in the image likely prevented accurate calculations of energy balance components in QWaterModel.

The NDVI, topsoil θ, and canopy cover at the plot scale are shown in Table 7. For the eleven mid-day observations, plot-scale NDVI and topsoil θ , and springflow were not found to be significant predictors of hourly ET rates (R^2=0.25, F=0.76, p=0.55) and no significant correlation was found between ET, NDVI, springflow, and topsoil θ at the plot scale. Excluding measurements made in April and May, the average topsoil θ across all flights was 4.7%. At Jensen WS, we observed a topsoil θ of 14.7% on 30 April 2021. Due to an equipment malfunction we were unable to conduct flights at Mays WS in April or May of 2021, when surface soil moisture was at its highest. The increased topsoil θ from fall to spring corresponded to an increase in the estimated canopy cover at Jensen WS (39% to 52%) and at Mays WS (30% to 37%). A slight increase in watershed-scale NDVI was noted between October and April/May (Table 7).

A difference in plot-scale NDVI (calculated using UAV-based multispectral imagery) and watershed-scale NDVI (calculated using Landsat 8 data) was found (Table 7). At Mays WS, the watershed scale estimates of NDVI were on average 0.10 greater than that of the plot-scale NDVI. At Jensen, the difference in plot-scale and watershed-scale NDVI was much less pronounced with the average difference between the two NDVI measurements being 0.01. In general, plot-scale NDVI was greater at Jensen WS (average 0.24 across all mid-day flights) compared to Mays WS (average 0.12 across all mid-day flights).

There was a noticeable difference in NDVI observed between the morning flights and the mid-day flights (Table 7). With the exclusion of the flight on 18 June 2021, morning NDVI was greater than mid-day NDVI.

Table 7. NDVI, shallow soil moisture (SM), daily springflow rate (spring, L min^{-1}) and canopy density (CD) for the UAV flights. NDVI (UAV) are the NDVI calculations for each flight at the plot scale. The NDVI(WS) indicates the average monthly NDVI for the respective watershed for the month the flight was conducted. On 29 September, a technological issue resulted in no multispectral data being recorded and therefore visual imagery (red, green, and blue wavelengths) was used and VARI was calculated instead of NDVI.

Date	WS	NDVI (UAV)	NDVI(WS)	SM	CD (%)	Spring
23-Jul-20	M	0.09	0.25	5.9		21.4
6-Aug-20	J	0.55/0.26	0.2	4.4		2.23
20-Aug-20	M	0.19/0.14	0.21	5.2	24	15.36
2-Sep-20	J	0.35/0.20	0.23	3.8		0
3-Sep-20	M	0.45/0.11	0.23	5.3		14.64
23-Sep-20	J	0.19	0.23	4.3		0
29-Sep-20	M	-0.04 (VARI)	0.23	5.1		7.05
30-Sep-20	J	0.48/0.27	0.23	3.8	39	0
1-Oct-20	M	0.23/0.12	0.22	4.3	29	7.24
14-Oct-20	M	0.46/0.12	0.22	4.9		6.5
30-Apr-21	J	0.63/0.27	0.25	14.7	52	10.7
1-May-21	M	(no UAV flights)	0.24	20.5	37	40.82
18-Jun-21	M	0.08/0.15	0.22	4.8	29	23.32

Based on the 50 sample points (25 representing overstory vegetation, 25 representing areas with bare ground, woody debris, or minimal detectable vegetation) selected from each mid-day orthomosaic, ET and NDVI values were greater for points of overstory vegetation (Table 8) with average overstory ET being generally greater at Mays WS (0.41 mm) compared to Jensen WS (0.35 mm). Average ET for non-overstory sample points was 0.13 mm at Jensen WS and 0.06 mm at Mays WS. Average NDVI for overstory points was 0.26 at Mays WS and 0.54 at Jensen WS. For points without overstory vegetation, the average NDVI was 0.06 at Mays WS and 0.10 at Jensen WS. For the flight where VARI was calculated instead of NDVI, there was not a sizeable difference in VARI for sample points with overstory vegetation versus those without (-0.03 vs. -0.04). Using the sample points (n=550), a significant correlation was found between NDVI and ET (r=0.58, $p<0.001$), springflow and ET (r=0.15, $p<0.001$), and between NDVI and springflow (r=-0.27, $p<0.001$). Based on the sample points, the multiple linear

regression found that NDVI (p<0.001) and springflow (p<0.001) were found to be significant predictors of ET.

Table 8. Average ET (in mm) and NDVI for selected points for each UAV flight. A total of 50 points in each mid-day orthomosaic were selected. Twenty-five points were selected at pixels where overstory vegetation was visible in the image (e.g., western juniper canopy, big sagebrush) and 25 points were selected at pixels where no overstory vegetation was visible. The non-overstory sample points included areas of bare ground, rocks, shadows, and tree boles. Small vegetation, such as perennial grasses, may also be present at the points because they were not visible due to spatial resolution or shadows.

		Overstory vegetation		Non-overstory	
Date	WS	ET	NDVI	ET	NDVI
23-Jul-20	Mays	0.50	0.28	0.00	0.11
6-Aug-20	Jensen	0.50	0.56	0.18	0.13
20-Aug-20	Mays	0.53	0.26	0.04	0.06
2-Sep-20	Jensen	0.30	0.49	0.04	0.07
3-Sep-20	Mays	0.39	0.23	-0.02	0.07
23-Sep-20	Jensen	0.36	0.57	0.12	0.07
29-Sep-20	Mays	0.27	-0.03 (VARI)	0.03	-0.04 (VARI)
30-Sep-20	Jensen	0.19	0.56	0.09	0.06
1-Oct-20	Mays	0.36	0.24	0.17	0.03
14-Oct-20	Mays	0.32	0.26	0.13	0.05
30-Apr-21	Jensen	0.39	0.53	0.24	0.16
18-Jun-21	Mays	0.53	0.31	0.07	0.05

4. Discussion

This research ought to improve our understanding ET and related environmental characteristics in sagebrush-steppe ecosystem in central Oregon, USA. The use of satellite-based remote sensing approaches has improved our ability to evaluate ET patterns; yet, limitations in spatial and/or temporal resolution create challenges for accurate modeling. This is particularly important in water-limited regions where increased water scarcity can have severe environmental

impacts. Specific objectives of this study were to 1) compare different approaches to modeling ET at different temporal and spatial scales and 2) assess the relationship between different ecohydrologic indicators and characteristics, specifically ET, springflow, soil moisture, NDVI, and NDMI.

For this study, we examined ET models at annual and monthly watershed scales and hourly plot scales. The MODIS ET and PET products (MOD16A2.006), the approach with the coarsest spatial resolution used in this study, provide calculations at a spatial resolution of 500 m and did not capture seasonal variation in ET values that were exhibited in other models. MODIS-ET products are likely more appropriate for larger spatial scale and regional uses, although it offers the advantage of high temporal resolution. The Landsat 8 data offers the advantage of higher spatial resolution (30 m for short-wave bands) but has a temporal resolution of 16 days. A mask was used in this study which excluded cloud-covered pixels from analysis which resulted in limited measurements of NDVI and NDMI being available for winter months and may indicate that the values are not entirely representative of seasonal characteristics during the winter. In addition to limited observations due to cloud conditions, it may also be the case that the spatial resolution was insufficient to assess changes in phenology and water stress conditions for small groundcover (e.g., perennial grasses).

The differences in ET estimates among the various approaches examined highlight the importance of model selection based on the study size, climate, and vegetation cover characteristics. Similar to the findings in this study, other research have also found the performance of ET models varies with vegetation type and phenology [43] and the availability of ground data [44], in addition to climatic factors. Additionally, it is important to note that SWAT is soil water-based approach and the OpenET models used here are energy balance-based approaches (although considerable variation was shown between OpenET results as well).

Past studies have also indicated the challenges of using SWAT and other ET models in dry climates (e.g., [45]). While initial calibration using on-site measurements of θ and ephemeral streamflow did not improve ET results when compared to transpiration measurements conducted in a past study at the same site [25] and a water balance-based approach [29], the use of additional ground-based measurements may improve the results of the SWAT model and reduce uncertainty.

Similar to the watershed-scale ET calculations, PET or RET calculations and the ratio between actual ET and PET or RET showed distinct differences between approaches. Further, while the use of a crop coefficient has been commonly used to estimate ET in many agricultural systems (e.g., [46,47]. Limited research has been conducted into determining a crop coefficient for sagebrush steppe ecosystems. Wight and Hanson [48] estimated the crop coefficient of a sagebrush community in Idaho, USA during the growing season to be 0.85, based on lysimeter measurements and the Jensen-Haise reference ET approach [49], which is considerably larger than the estimates of ET/PET and ET/RET during the growing season found in this study, regardless of the method used. In general, the average MODIS-PET and OpenET-RET at both watersheds were greater than estimates of PET calculated in a previous study using the Hargreaves-Samani approach [29].

Leaf area index has been shown to be strongly linked to the ratio between seasonal ET and PET [22] and may serve as another indicator of ET. NDVI, NDMI, leaf area index, soil moisture, and other ecohydrologic characteristics may provide additional means of estimating ET [14,50,51]. However, the results of this study indicate that approaches to using these indicators for predicting ET may be largely site-specific. For instance, we found that NDVI was an important predictor of ET at Mays WS while soil volumetric water content (θ) and NDMI were more important predictors at Jensen WS. Similarly, we found that springflow was only strongly correlated with NDVI, NDMI, or θ at Mays WS. Therefore, any estimates of ET should consider the myriad of factors related to ET (e.g., leaf area index, vegetation type, and θ) when developing a model to predict ET.

We also found differences in estimates of NDVI based on approach (Landsat 8 data versus UAV-based imagery). It is important to note that differences in sensors are also associated with differences in NDVI calculations [52]. Further, since we averaged NDVI from observations over a course of each month, it is not directly comparable to UAV-based data which captured data over the course of approximately an hour, due to the presence of clouds, precipitation patterns, or other meteorological factors at the time of flight. As the Landsat 8 data collects data at a 30 m scale (for NIR and red wavelengths) versus the sub-meter scale used by the UAV-based cameras, it may not be sufficient to discern bare ground and ground cover from small vegetation. We found that the NDVI calculations at the watershed scale (Landsat 8-based) and at

the plot scale (UAV-based imagery) were more similar at Jensen WS compared to Mays WS, which may indicate that the spatial resolution was a more important factor in areas with relatively smaller canopy size. It should also be considered if the UAV-plots are truly representative of the entire watershed for characterizing vegetation, land cover, and ET.

We also found that NDVI varied with the time of UAV flight (morning flights versus mid-day flights). Past studies have also found the ratio between NIR and red wavelengths varied with the time of observation [53] . With the exclusion of one flight, NDVI was greater for the morning flights compared to the mid-day flights. This is similar to [54], who found that NDVI values tended to be greater at the beginning and end of the day and [55] who found that vegetation indices varied with the time of day. Additionally, while [56] found that the performance of UAV-based cameras were similar to that of ground-based approaches, reflectance variations can lead to misleading vegetation index calculations. This suggests that the variations that we saw between NDVI in morning and mid-day flights were more likely a function of factors other than plant vigor and emphasizes the importance of considering when images are captured. The UAV-based calculations of ET were also larger than expected compared to the results of research conducted by Mollnau et al. [56] which estimated summertime western juniper stand transpiration to be 0.4 mm day^{-1}.

The results of this study highlight several key limitations in understanding ET in semiarid environments, particularly in snow-dominated systems, and the importance of considering approaches to calculating ET. While limited studies have been conducted to examine the transpiration of western juniper in central Oregon [25,57], additional research is also needed to understand the transpiration rates of other vegetation in these regions, to include big sagebrush and perennial grasses. Estimates of soil evaporation in semiarid environments are likewise also very limited. Future research could address these challenges by incorporating eddy covariance or Bowen ratio systems to gain a better understanding of the on-site characteristics related to evapotranspiration. Additionally, further information is needed to understand the relationship between on-site ecohydrologic characteristics (e.g., soil percolation, vegetation diversity and cover) and ET.

This study provides insight into the relationship between ET patterns and environmental characteristics at this study site. While it is an indirect indicator and will vary by location, the

results of this study suggest that certain environmental characteristics (e.g., soil moisture, NDVI) can be used estimate seasonal patterns in ET, although caution should be used. Additionally, the results of this study highlight the usefulness of incorporating readily-available datasets (such as OpenET) into ecohydrologic research in data limited environments.

An improved understanding of the factors related to ET has important implications for land management in this region. There is particular concern regarding how changes in ET related to western juniper encroachment may impact water availability and herbaceous productivity, two important factors for cattle grazing and ecosystem functions in the region. This study emphasizes the importance of considering the approach used to estimate ET, to include the spatial and temporal characteristics, as well as the need for more in-depth assessment of how ET rates may vary between western juniper dominated ecosystems and sagebrush-dominated ecosystems.

References

1. Arnold, J.G.; Moriasi, D.N.; Gassman, P.W.; Abbaspour, K.C.; White, M.J.; Srinivasan, R.; Santhi, C.; Harmel, R.D.; Griensven, A. van; Liew, M.W.V.; et al. SWAT: Model Use, Calibration, and Validation. *Transactions of the ASABE* **2012**, *55*, 1491–1508, doi:10.13031/2013.42256.
2. Allen, R.; Irmak, A.; Trezza, R.; Hendrickx, J.M.H.; Bastiaanssen, W.; Kjaersgaard, J. Satellite-Based ET Estimation in Agriculture Using SEBAL and METRIC. *Hydrol. Process.* **2011**, *25*, 4011–4027, doi:10.1002/hyp.8408.
3. Allen, R.G.; Tasumi, M.; Morse, A.; Trezza, R. A Landsat-Based Energy Balance and Evapotranspiration Model in Western US Water Rights Regulation and Planning. *Irrig Drainage Syst* **2005**, *19*, 251–268, doi:10.1007/s10795-005-5187-z.
4. Allen, R.G.; Tasumi, M.; Trezza, R. Satellite-Based Energy Balance for Mapping Evapotranspiration with Internalized Calibration (METRIC)—Model. *J. Irrig. Drain Eng.* **2007**, *133*, 380–394, doi:10.1061/(ASCE)0733-9437(2007)133:4(380).
5. Senay, G.B. Satellite Psychrometric Formulation of the Operational Simplified Surface Energy Balance (SSEBop) Model for Quantifying and Mapping Evapotranspiration. *Applied Engineering in Agriculture* **2018**, *34*, 555–566, doi:10.13031/aea.12614.
6. Senay, G.B.; Bohms, S.; Singh, R.K.; Gowda, P.H.; Velpuri, N.M.; Alemu, H.; Verdin, J.P. Operational Evapotranspiration Mapping Using Remote Sensing and Weather Datasets: A New Parameterization for the SSEB Approach. *JAWRA Journal of the American Water Resources Association* **2013**, *49*, 577–591, doi:10.1111/jawr.12057.
7. Anderson, M.; Gao, F.; Knipper, K.; Hain, C.; Dulaney, W.; Baldocchi, D.; Eichelmann, E.; Hemes, K.; Yang, Y.; Medellin-Azuara, J.; et al. Field-Scale Assessment of Land and Water Use Change over the California Delta Using Remote Sensing. *Remote Sensing* **2018**, *10*, 889, doi:10.3390/rs10060889.
8. Anderson, M.C.; Norman, J.M.; Mecikalski, J.R.; Otkin, J.A.; Kustas, W.P. A Climatological Study of Evapotranspiration and Moisture Stress across the Continental United

States Based on Thermal Remote Sensing: 1. Model Formulation. *Journal of Geophysical Research: Atmospheres* **2007**, *112*, doi:10.1029/2006JD007506.
9. Norman, J.M.; Kustas, W.P.; Humes, K.S. A Two-Source Approach for Estimating Soil and Vegetation Fluxes from Observations of Directional Radiometric Surface Temperature. *Agricultural and Forest Meteorology* **1995**, *80*.
10. Zhuang, Q.; Shao, H.; Guan, D. Operational Daily Evapotranspiration Mapping at Field Scale Based on SSEBop Model and Spatiotemporal Fusion of Multi-Source Remote Sensing Data. *PLOS ONE* **2022**, *17*, e0264133, doi:10.1371/journal.pone.0264133.
11. Chen, P.-Y.; Fedosejevs, G.; Tiscareño-LóPez, M.; Arnold, J.G. Assessment of MODIS-EVI, MODIS-NDVI and VEGETATION-NDVI Composite Data Using Agricultural Measurements: An Example at Corn Fields in Western Mexico. *Environ Monit Assess* **2006**, *119*, 69–82, doi:10.1007/s10661-005-9006-7.
12. French, A.N.; Hunsaker, D.J.; Sanchez, C.A.; Saber, M.; Gonzalez, J.R.; Anderson, R. Satellite-Based NDVI Crop Coefficients and Evapotranspiration with Eddy Covariance Validation for Multiple Durum Wheat Fields in the US Southwest. *Agricultural Water Management* **2020**, *239*, 106266, doi:10.1016/j.agwat.2020.106266.
13. Szilagyi, J. Can a Vegetation Index Derived from Remote Sensing Be Indicative of Areal Transpiration? *Ecological Modelling* **2000**, *127*, 65–79, doi:10.1016/S0304-3800(99)00200-8.
14. Del Grosso, S.J.; Parton, W.J.; Derner, J.D.; Chen, M.; Tucker, C.J. Simple Models to Predict Grassland Ecosystem C Exchange and Actual Evapotranspiration Using NDVI and Environmental Variables. *Agricultural and Forest Meteorology* **2018**, *249*, 1–10, doi:10.1016/j.agrformet.2017.11.007.
15. Szilagyi, J. Vegetation Indices to Aid Areal Evapotranspiration Estimations. *J. Hydrol. Eng.* **2002**, *7*, 368–372, doi:10.1061/(ASCE)1084-0699(2002)7:5(368).
16. Van De Griend, A.A.; Owe, M. On the Relationship between Thermal Emissivity and the Normalized Difference Vegetation Index for Natural Surfaces. *International Journal of Remote Sensing* **1993**, *14*, 1119–1131, doi:10.1080/01431169308904400.
17. Gao, B. NDWI—A Normalized Difference Water Index for Remote Sensing of Vegetation Liquid Water from Space. *Remote Sensing of Environment* **1996**, *58*, 257–266, doi:10.1016/S0034-4257(96)00067-3.
18. Wilson, E.H.; Sader, S.A. Detection of Forest Harvest Type Using Multiple Dates of Landsat TM Imagery. *Remote Sensing of Environment* **2002**, *80*, 385–396, doi:10.1016/S0034-4257(01)00318-2.
19. Huang, C.; Li, Y.; Gu, J.; Lu, L.; Li, X. Improving Estimation of Evapotranspiration under Water-Limited Conditions Based on SEBS and MODIS Data in Arid Regions. *Remote Sensing* **2015**, *7*, 16795–16814, doi:10.3390/rs71215854.
20. Allen, R.G.; Pereira, L.S.; Raes, D.; Smith, M. Crop Evapotranspiration. Guidelines for Computing Crop Water Requirements. Irrigation and Drainage Paper 56, FAO, Rome, 300 p 1998.
21. Liu, C.; Sun, G.; McNulty, S.G.; Noormets, A.; Fang, Y. Environmental Controls on Seasonal Ecosystem Evapotranspiration/Potential Evapotranspiration Ratio as Determined by the Global Eddy Flux Measurements. *Hydrol. Earth Syst. Sci.* **2017**, *21*, 311–322, doi:10.5194/hess-21-311-2017.

22. Peng, L.; Zeng, Z.; Wei, Z.; Chen, A.; Wood, E.F.; Sheffield, J. Determinants of the Ratio of Actual to Potential Evapotranspiration. *Global Change Biology* **2019**, *25*, 1326–1343, doi:10.1111/gcb.14577.
23. Lafleur, P.M.; Hember, R.A.; Admiral, S.W.; Roulet, N.T. Annual and Seasonal Variability in Evapotranspiration and Water Table at a Shrub-Covered Bog in Southern Ontario, Canada. *Hydrol. Process.* **2005**, *19*, 3533–3550, doi:10.1002/hyp.5842.
24. Holzman, M.E.; Rivas, R.E.; Bayala, M.I. Relationship between TIR and NIR-SWIR as Indicator of Vegetation Water Availability. *Remote Sensing* **2021**, *13*, 3371, doi:10.3390/rs13173371.
25. Abdallah, M.A.B.; Durfee, N.; Mata-Gonzalez, R.; Ochoa, C.G.; Noller, J.S. Water Use and Soil Moisture Relationships on Western Juniper Trees at Different Growth Stages. *Water* **2020**, *12*, 26.
26. Ochoa, C.; Caruso, P.; Ray, G.; Deboodt, T.; Jarvis, W.; Guldan, S. Ecohydrologic Connections in Semiarid Watershed Systems of Central Oregon USA. *Water* **2018**, *10*, 181, doi:10.3390/w10020181.
27. Ray, G.; Ochoa, C.G.; Deboodt, T.; Mata-Gonzalez, R. Overstory–Understory Vegetation Cover and Soil Water Content Observations in Western Juniper Woodlands: A Paired Watershed Study in Central Oregon, USA. *Forests* **2019**, *10*, 151, doi:10.3390/f10020151.
28. Western Regional Climate Center Available online: https://wrcc.dri.edu/cgi-bin/cliMAIN.pl?or0501.
29. Durfee, N.; Ochoa, C.G. The Seasonal Water Balance of Western Juniper-Dominated and Big Sagebrush-Dominated Watersheds. *Hydrology* **2021**, *8*, 156, doi:10.3390/hydrology8040156.
30. Gorelick, N.; Hancher, M.; Dixon, M.; Ilyushchenko, S.; Thau, D.; Moore, R. Google Earth Engine: Planetary-Scale Geospatial Analysis for Everyone. *Remote Sensing of Environment* **2017**, *202*, 18–27, doi:10.1016/j.rse.2017.06.031.
31. Running, S.W.; Mu, Q.; Zhao, M.; Moreno, A. User's Guide: MODIS Global Terrestrial Evapotranspiration (ET) Product (MOD16A2/A3 and Year-End Gap-Filled MOD16A2GF/A3GF) NASA Earth Observing System MODIS Land Algorithm (For Collection 6). Version 2.2 2019.
32. Rouse, J.W.; Harlan, J.C.; Haas, R.H.; Schell, J.A.; Deering, D.W. Monitoring the Vernal Advancement and Retrogradiation (Green Wave Effect) of Natural Vegetation - NASA-CR-144661 1974.
33. Melton, F.S.; Huntington, J.; Grimm, R.; Herring, J.; Hall, M.; Rollison, D.; Erickson, T.; Allen, R.; Anderson, M.; Fisher, J.B.; et al. OpenET: Filling a Critical Data Gap in Water Management for the Western United States. *JAWRA Journal of the American Water Resources Association* **2021**, *n/a*, 1–24, doi:10.1111/1752-1688.12956.
34. Abiodun, O.O.; Guan, H.; Post, V.E.A.; Batelaan, O. Comparison of MODIS and SWAT Evapotranspiration over a Complex Terrain at Different Spatial Scales. *Hydrology and Earth System Sciences; Katlenburg-Lindau* **2018**, *22*, 2775–2794, doi:http://dx.doi.org.ezproxy.proxy.library.oregonstate.edu/10.5194/hess-22-2775-2018.
35. Anand, J.; Gosain, A.K.; Khosa, R. Prediction of Land Use Changes Based on Land Change Modeler and Attribution of Changes in the Water Balance of Ganga Basin to Land Use Change Using the SWAT Model. *Science of The Total Environment* **2018**, *644*, 503–519, doi:10.1016/j.scitotenv.2018.07.017.

36. Ellsäßer, F.; Röll, A.; Stiegler, C.; Hendrayanto; Hölscher, D. Introducing QWaterModel, a QGIS Plugin for Predicting Evapotranspiration from Land Surface Temperatures. *Environmental Modelling & Software* **2020**, *130*, 104739, doi:10.1016/j.envsoft.2020.104739.
37. Timmermans, W.J.; Kustas, W.P.; Andreu, A. Utility of an Automated Thermal-Based Approach for Monitoring Evapotranspiration. *Acta Geophys.* **2015**, *63*, 1571–1608, doi:10.1515/acgeo-2015-0016.
38. Guzinski, R.; Nieto, H.; Jensen, R.; Mendiguren, G. Remotely Sensed Land-Surface Energy Fluxes at Sub-Field Scale in Heterogeneous Agricultural Landscape and Coniferous Plantation. *Biogeosciences* **2014**, *11*, 5021–5046, doi:10.5194/bg-11-5021-2014.
39. Li, F.; Kustas, W.P.; Prueger, J.H.; Neale, C.M.U.; Jackson, T.J. Utility of Remote Sensing–Based Two-Source Energy Balance Model under Low- and High-Vegetation Cover Conditions. *J. Hydrometeor.* **2005**, *6*, 878–891, doi:10.1175/JHM464.1.
40. Norman, J.M.; Kustas, W.P.; Prueger, J.H.; Diak, G.R. Surface Flux Estimation Using Radiometric Temperature: A Dual-Temperature-Difference Method to Minimize Measurement Errors. *Water Resources Research* **2000**, *36*, 2263–2274, doi:https://doi.org/10.1029/2000WR900033.
41. Kustas, W.P.; Daughtry, C.S.T. Estimation of the Soil Heat Flux/Net Radiation Ratio from Spectral Data. *Agricultural and Forest Meteorology* **1990**, *49*, 205–223, doi:10.1016/0168-1923(90)90033-3.
42. An, N.; Hemmati, S.; Cui, Y.-J. Assessment of the Methods for Determining Net Radiation at Different Time-Scales of Meteorological Variables. *Journal of Rock Mechanics and Geotechnical Engineering* **2017**, *9*, 239–246, doi:10.1016/j.jrmge.2016.10.004.
43. Zhuang, Q.; Link to external site, this link will open in a new window; Wang, H.; Xu, Y. Comparison of Remote Sensing Based Multi-Source ET Models over Cropland in a Semi-Humid Region of China. *Atmosphere; Basel* **2020**, *11*, 325, doi:http://dx.doi.org.ezproxy.proxy.library.oregonstate.edu/10.3390/atmos11040325.
44. Al Zayed, I.S.; Elagib, N.A.; Ribbe, L.; Heinrich, J. Satellite-Based Evapotranspiration over Gezira Irrigation Scheme, Sudan: A Comparative Study. *Agricultural Water Management* **2016**, *177*, 66–76, doi:10.1016/j.agwat.2016.06.027.
45. Chun, J.A.; Baik, J.; Kim, D.; Choi, M. A Comparative Assessment of SWAT-Model-Based Evapotranspiration against Regional-Scale Estimates. *Ecological Engineering* **2018**, *122*, 1–9, doi:10.1016/j.ecoleng.2018.07.015.
46. Eliades, M.; Bruggeman, A.; Djuma, H.; Christofi, C.; Kuells, C. Quantifying Evapotranspiration and Drainage Losses in a Semi-Arid Nectarine (Prunus Persica Var. Nucipersica) Field with a Dynamic Crop Coefficient (Kc) Derived from Leaf Area Index Measurements. *Water* **2022**, *14*, 734, doi:10.3390/w14050734.
47. Wang, Y.; Cai, H.; Yu, L.; Peng, X.; Xu, J.; Wang, X. Evapotranspiration Partitioning and Crop Coefficient of Maize in Dry Semi-Humid Climate Regime. *Agricultural Water Management* **2020**, *236*, 106164, doi:10.1016/j.agwat.2020.106164.
48. Wight, J.R.; Hanson, C.L. Crop Coefficients for Rangeland. *Journal of Range Management* **1990**, *43*, 482, doi:10.2307/4002349.
49. Jensen, M.E.; Haise, H.R. Estimating Evapotranspiration from Solar Radiation. *Proceedings of the American Society of Civil Engineers, Journal of the Irrigation and Drainage Division* **1963**, *89*, 15–41.

50. Joiner, J.; Yoshida, Y.; Anderson, M.; Holmes, T.; Hain, C.; Reichle, R.; Koster, R.; Middleton, E.; Zeng, F.-W. Global Relationships among Traditional Reflectance Vegetation Indices (NDVI and NDII), Evapotranspiration (ET), and Soil Moisture Variability on Weekly Timescales. *Remote Sensing of Environment* **2018**, *219*, 339–352, doi:10.1016/j.rse.2018.10.020.
51. Seevers, P.M.; Ottmann, R.W. Evapotranspiration Estimation Using a Normalized Difference Vegetation Index Transformation of Satellite Data. *Hydrological Sciences Journal* **1994**, *39*, 333–345, doi:10.1080/02626669409492754.
52. Huang, S.; Tang, L.; Hupy, J.P.; Wang, Y.; Shao, G. A Commentary Review on the Use of Normalized Difference Vegetation Index (NDVI) in the Era of Popular Remote Sensing. *J. For. Res.* **2021**, *32*, 1–6, doi:10.1007/s11676-020-01155-1.
53. de Souza, R.; Buchhart, C.; Heil, K.; Plass, J.; Padilla, F.M.; Schmidhalter, U. Effect of Time of Day and Sky Conditions on Different Vegetation Indices Calculated from Active and Passive Sensors and Images Taken from UAV. *Remote Sensing* **2021**, *13*, 1691, doi:10.3390/rs13091691.
54. Beneduzzi, H.M.; Souza, E.G.; Bazzi, C.L.; Schenatto, K. Temporal Variability in Active Reflectance Sensor-Measured NDVI in Soybean and Wheat Crops. *Eng. Agríc.* **2017**, *37*, 771–781, doi:10.1590/1809-4430-eng.agric.v37n4p771-781/2017.
55. Rasmussen, J.; Ntakos, G.; Nielsen, J.; Svensgaard, J.; Poulsen, R.N.; Christensen, S. Are Vegetation Indices Derived from Consumer-Grade Cameras Mounted on UAVs Sufficiently Reliable for Assessing Experimental Plots? *European Journal of Agronomy* **2016**, *74*, 75–92, doi:10.1016/j.eja.2015.11.026.
56. Mollnau, C.; Newton, M.; Stringham, T. Soil Water Dynamics and Water Use in a Western Juniper (Juniperus Occidentalis) Woodland. *Journal of Arid Environments* **2014**, *102*, 117–126, doi:10.1016/j.jaridenv.2013.11.015.

CHARACTERIZATION OF THE WATER BALANCE AT A SEMIARID WATERSHED IN EASTERN OREGON, USA USING THE SOIL AND WATER ASSESSMENT TOOL

Characterization of the water balance at a semiarid watershed in eastern Oregon, USA using the Soil and Water Assessment Tool

Abstract: The water balance is the foundation for many ecohydrologic processes and there is a need for an improved understanding of the drivers of the water balance, particularly in semiarid and arid regions. However, some aspects of the water balance are very difficult to directly measure (e.g., shallow groundwater recharge) and traditional water budget approaches may not adequately address spatial heterogeneity. Physically-based hydrologic models, such as the Soil and Water Assessment Tool (SWAT), provide another means of characterizing the water balance and have been widely used. In this study, we used SWAT to characterize the water balance for a semiarid watershed in eastern Oregon, USA in which several land cover types are present. A combination of on-site weather and Parameter-elevation Regressions on Independent Slopes Model (PRISM) were used in model development. The SWAT-Calibration and Uncertainty Program (SWAT-CUP) was used for model calibration, validation, and sensitivity analysis. Calibration with streamflow and plant available water content (PAWC) data and validation was performed with PAWC data only. The model performance was assessed using Nash-Sutcliffe efficiency (NS) and ranged from NS=0.68 to 0.93 for calibration and NS=0.81 to 0.85 for validation. Parameters related to snowpack and soil characteristics were found to be among the most influential on the modeled water balance. The results of this study highlight the importance of considering climate and site-specific characteristics, as well as calibration approaches, when modeling the water balance.

1. Introduction

The water balance is the basis for understanding many hydrologic processes within a watershed and improving land management practices. Many of the drivers of the water balance in snow-dominated, semiarid environments are less understood than those of rain-dominated, humid climates. Limited on-site data and multiple land cover characteristics, to include varying amounts of vegetation cover, make accurate representation of the water balance difficult in many of these regions. In light of these challenges, physically-based hydrologic models, such as the Soil and Water Assessment Tool (SWAT, [1]) have been widely uses to assess water balance components (e.g., [2,3]).

SWAT has been used to characterize diverse environments, including agricultural (e.g. [4,5]) and arid and semiarid landscapes ([6–8]). In addition to modelling the general components of the water balance, such as precipitation, streamflow, or evapotranspiration, SWAT also calculates aspects that are more difficult to directly measure such as soil percolation, aquifer recharge, and the contribution of shallow aquifer moisture to soil and plants. SWAT has also widely been applied to assess the impacts of land cover and management applications, such as urban expansion (e.g., [6]) and other shifts in land cover type (e.g., [9]), on the water balance.

While SWAT and other modeling approaches have been applied to areas with different climate characteristics, parameter sensitivity and model performance frequently vary between arid and humid climates. Muttiah and Wurbs [10] found that among six watersheds in Texas, USA, more humid climates showed greater sensitivity to climate and soil variations while the semiarid climates demonstrated more sensitivity with soil albedo and water capacity. Research has also found that climate is associated with differences in the performance of some hydrologic models [11,12]). Van Liew et al. [13] found that SWAT performed poorly at a desert rangeland site compared to more humid regions but also found that SWAT performed well at a mountainous rangeland site in Idaho for predicting streamflow. However, several studies have also found that the SWAT model performed satisfactorily to well in semiarid landscapes [7,14–16].

Limited on-site data is a challenge in many semiarid and arid regions. Alternatives to on-site measurements of precipitation and temperature, such as Parameter-elevation Regressions on Independent Slopes Model (PRISM; [17]), have been used successfully to address gaps in data (e.g., [18]). Studies have also illustrated how remote sensing data, such as Landsat (e.g., [19], MODIS (e.g., [20], or AMSR2 (e.g., [21]) can be integrated into the SWAT model and be used for model calibration.

In addition to model development, calibration procedures are an important area of research and approaches vary widely. While manual calibration can be performed in the SWAT model, this may be time-consuming compared to other approaches. Alternatively, programs such as the SWAT-Calibration and Uncertainty Procedures (SWAT-CUP; [22,23]) have widely been used for model calibration, validation, and sensitivity analysis. An in-depth examination of SWAT-CUP calibration and validation is provided in [24]. Abbaspour et al. [25] also outlined a

method for large-scale model calibration using SWAT-SUP and emphasized the importance that specific parameters have on variables, such as evapotranspiration or peak flow. Further, parameter calibration approaches should reflect watershed characteristics such as size and the complexity of topography, vegetation cover, and soil type. Programs, such as SWAT-CUP, allow the user to calibrate parameters based on specific soil type, slope characteristics, and vegetation, as well as other characteristics [26]. The best approach to calibration will likely depend on the study site in question and there is no replacement for an adequate understanding of hydrologic processes during model development and assessment.

Multisite and multivariable calibration approaches have shown promise in improving the performance of hydrologic models. Shah et al. [27] found that a SWAT model calibrated using only streamflow data had greater parameter uncertainty compared to a SWAT model calibrated using streamflow data and evapotranspiration data from Moderate Resolution Imaging Spectroradiometer (MODIS). Niraula et al. [28] found that using multiple streamflow measurements improved the accuracy of a SWAT model compared to when only streamflow measurements at the watershed outlet were used.

While streamflow is frequently used for model calibration and validation, streamflow data are often not available in arid and semiarid regions, particularly when streamflow is ephemeral or seasonal. Several studies have used soil moisture alone or in conjunction with streamflow to evaluate SWAT model performance (e.g., [29,30]). Rajib et al. [31] found that remote sensing-based measurements of surface moisture improved soil moisture calibration, particularly when combined with on-site measurements of root zone soil moisture. However, Kundu, Vervoot, and Ogtrop [32] found that calibration using soil moisture improved SWAT streamflow predictions at some locations, this varied with seasonal characteristics and topography.

The parameters used in calibration should reflect processes relevant to watershed characteristics and variables of interest, such as using the Soil Conservation Service curve number (SCS CN, [33]) in streamflow modeling. SWAT has effectively been used to model streamflow in snow-dominated regions [34,35] and snowpack parameters have been found to be particularly influential in these environments ((e.g., [36,37]). Further, land cover and vegetation characterization impact the water balance. The specific vegetation characteristics of land use

classification can also vary from region to region. For example, brush dominated rangeland areas in the Pacific Northwest USA region are frequently classified under the same land cover category as brush-dominated rangeland areas of the southwestern USA although the vegetation composition and density in these two regions varies. In light of these differences, several studies have also assessed vegetation parameters to improve SWAT models (e.g., [38,39]).

In addition to parameter selection, parameter sensitivity and uncertainty analysis are important factors in the assessment of model performance. Equifinality, such as when different parameter combinations yield similar results, is a key concern for hydrologic modeling. Ficklin and Barnhart [40] found that different parameter sets yielded similar calibration results but demonstrated differing projections of streamflow characteristics. Parameter sensitivity analysis can be used to avoid overfitting the model and to more aptly identify underlying processes within a watershed. Numerous factors contribute to uncertainty, to include the complexity of hydrologic processes as well as data scarcity. However, more research is needed into hydrologic modeling and parameter sensitivity analysis in semiarid and arid regions, particularly considering limited data.

This research sought to further examine the factors influencing the water balance in semiarid regions. We applied the Soil and Water Assessment Tool (SWAT) to estimate components of the water balance at a snow-dominated, semiarid watershed which encompasses differing land use and topographical characteristics. A combination of PRISM and on-site data were used along with a multisite, multivariable calibration approach. Specific objectives of this study were to: 1) model the water balance of a snow-dominated semiarid watershed using SWAT and 2) perform model parameter sensitivity.

2. Methods

2.1 Site Description

This study was conducted on a 1280-ha watershed (44.42° N, 117.91° W) located near Ironside, OR, USA. Elevation at the study site ranges from 1170 to 1953 m (Figure 1). Much of this study site is used for cattle grazing, with some timber production in the upper portions of the watershed. Sagebrush steppe accounts for a large portion of the land cover at the study site. Vegetation also includes western juniper, perennial bunchgrasses, and Ponderosa pine and mixed

conifer. Several perennial and seasonal streams run through the study site and generally flow from north to southeast. Multiple springs are located near the top of the watershed and the majority of streams within the study site are spring-fed.

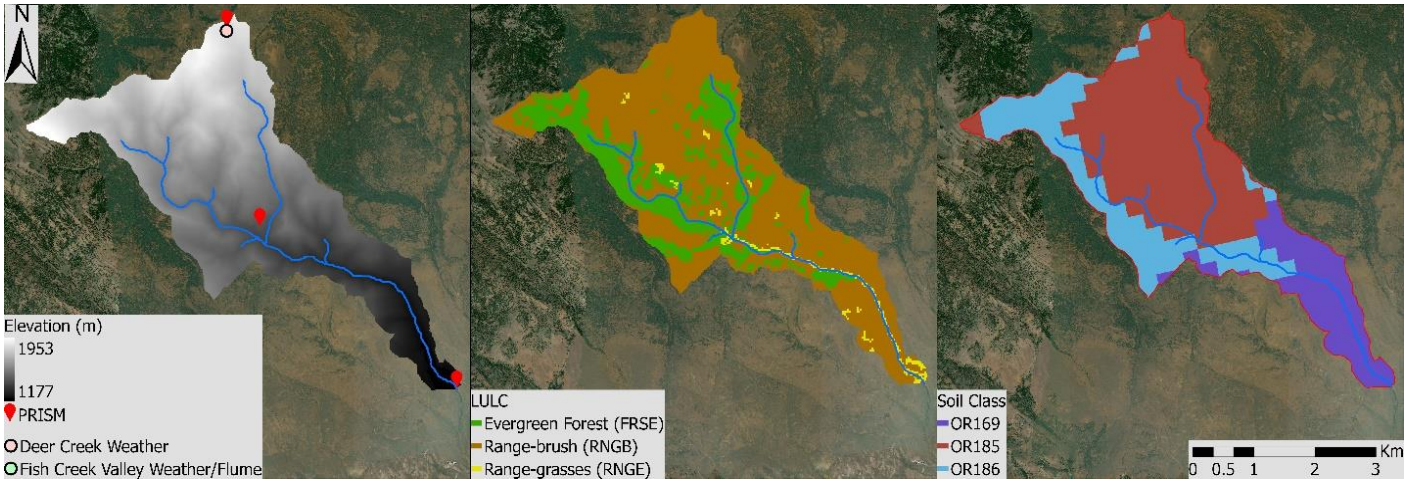

Figure 1. Study site data collection locations, elevation, land use, and soil type. Streams generally flow from the north to the south in this watershed and are intermittent in upslope regions. "PRISM" indicates the locations for which PRISM data were sourced. Streamflow measurements were taken near the Wilks Valley weather station. Descriptions of soil and soil land cover characteristics are provided in Tables 1 and 2, respectively. *Sources: Esri, DigitalGlobe, GeoEye, i-cubed, USDA FSA, USGS, AEX, Getmapping, Aerogrid, IGN, IGP, swisstopo, and the GIS User Community. This map was created using ArcGIS® software by Esri. ArcGIS® and ArcMap™ are the intellectual property of Esri and are used herein under license. Copyright © Esri. All rights reserved. For more information about Esri® software, please visit www.esri.com.*

The study site is located in a semiarid, snow-dominated region in eastern Oregon, USA. Based on on-site precipitation data and the PRISM precipitation data, the mean annual precipitation from 2016 to 2021 was 345 mm yr^{-1}. Some spatial variation in rainfall patterns was shown between sites, with slightly greater precipitation being observed at the upslope sites near the top of the watershed compared to the sites in the lower elevation valley areas (362 mm yr^{-1} vs. 264 mm yr^{-1}). For the years observed during this study, 2019 had the greatest watershed-wide annual precipitation (457 mm) and 2021 had the lowest annual precipitation (298 mm). Average daily maximum temperatures during the summer (July through September) were 26°C and average daily minimum temperatures during the winter (January through March) were -6°C. The geology of the watershed is primarily characterized by igneous, volcanic rock, such as rhyolite

lava flows and terrestrial tuffaceous sedimentary rock, and clastic sedimentary rock (Figure 2) [41,42].

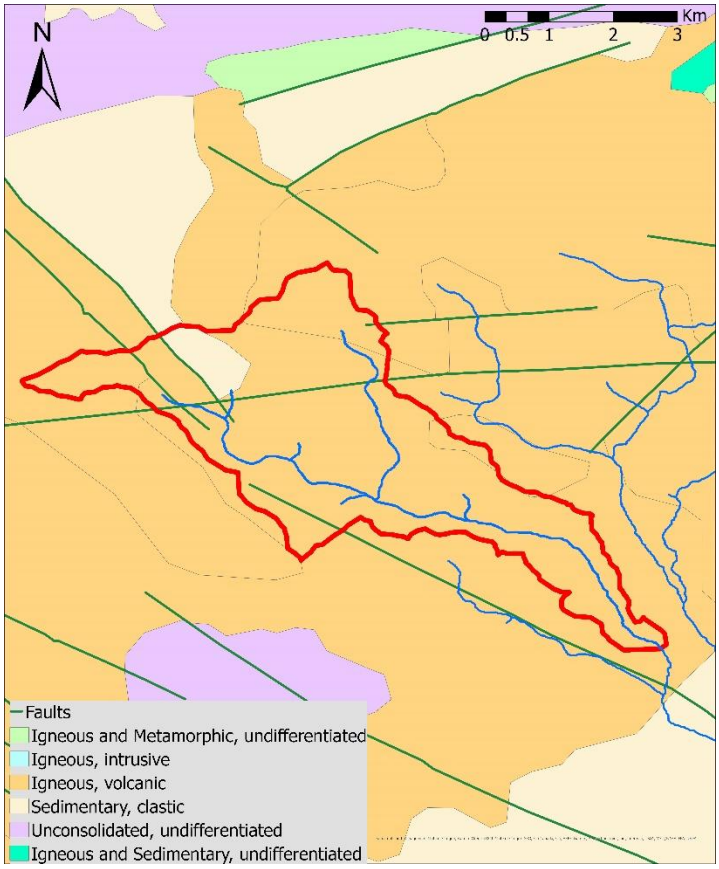

Figure 2. Geology of local area. Oregon geologic map data was obtained through the U.S. Geological Survey [43]. *This map was created using ArcGIS® software by Esri. ArcGIS® and ArcMap™ are the intellectual property of Esri and are used herein under license. Copyright © Esri. All rights reserved. For more information about Esri® software, please visit www.esri.com*

On site data collection began in 2018. The Deer Creek weather station ("Deer Creek") was installed in 2018 and is located at 1820 m near the top of the watershed. The Fish Creek Valley weather station ("Fish Creek Valley") was installed in 2019 and is located at approximately 1200 m elevation in a sagebrush-dominated area of the watershed, near the outlet of the study site used for this SWAT model. Wind speed and direction, air temperature, solar radiation, and precipitation were measured at both weather stations using similar equipment. A CR800 (Campbell Scientific, Inc., Logan, UT, USA) datalogger was used at both weather stations. A TE525 (Texas Electronics, Inc., Dallas, TX, USA) tipping bucket rain gauge was

used to measure precipitation. Relative humidity and air temperature were measured using a CS215 probe (Campbell Scientific, Inc., Logan, UT, USA). Incoming shortwave solar radiation was measured using the Apogee CS300 pyranometer (Apogee Instruments, Inc., Logan, UT, USA). A Young (R.M. Young Company, Travers City, MI, USA) model 03002 Wind Sentry anemometer and vane were used to measured wind speed and direction.

Soil moisture was collected using CS650 water content sensors (Campbell Scientific, Inc., Logan, UT, USA) beginning in October 2018 at the Deer Creek Site and in August 2019 at the Fish Creek Valley site. Hourly soil moisture data at 0.2 m and 0.5 m were collected at the Deer Creek and soil moisture data at Fish Creek Valley were collected at 0.2 m, 0.5 m, and 0.8 m. Three core soil samples were taken at each measurement depth in order to calculate bulk density and soil texture. The volumetric water content was calculated by averaging the water content at each depth and multiplying by the measured soil depth (0.5 m at the upper weather station and 0.8 m at the lower weather station). Soil texture analysis was conducted for both watersheds using the hydrometer method [44]. Bulk density was calculated using the soil core method as described in [45]. The field-based soil texture and bulk density data were used to estimate the permanent wilting point of the soils using the Retention Curve (RETC) computer program (Version 6.02, see [46] and [47]). Similar to the method described by [31], the soil moisture content was converted to plant available water content (PAWC) by subtracting the permanent wilting point from the measured volumetric water content. The monthly average PAWC was used for model calibration and validation.

Streamflow data was measured near the Fish Creek Valley weather station using a ramp-style flume installed in April of 2021 and equipped with a Hobo U20L pressure sensors (Onset Computer Corp., Bourne, MA, USA) to measure water level height. Streamflow volume was calculated based on water level height and the dimensions of the flume.

Streamflow measurements were used for model calibration, but insufficient streamflow data were available for validation. In order to address this, results were compared to modeled peak streamflow results. Manning's equation (Equation 1, [48]) was used to estimate peak flow rates based on stream channel measurements of depth and width, where n is the Manning's roughness coefficient, A is the channel area in m^2, R is the hydraulic radius (channel area divided by the wetted perimeter), and S is the slope.

$$Q = \left(\frac{1.00}{n}\right) * AR^{2/3}\sqrt{S} \quad (1)$$

A stream survey conducted in a 100-m reach at the location of the flume showed an average width of 2.0 m and average maximum depth of 0.3 m. The channel was classified as moderately entrenched.

Daily minimum and maximum air temperature and precipitation data for January 2016 until August 2021 from Parameter-elevation Regressions on Independent Slopes Model (PRISM, [17]) data were downloaded for five sites in the watershed (see Figure 1). Sites ranged from an elevation of 1162 m to 1953 m. Standard PRISM data have a spatial resolution of 4 km. Time series values can be directly downloaded from the PRISM website (https://prism.oregonstate.edu/explorer/bulk.php).

2.2 SWAT Description

SWAT is a semi-distributed, physically-based model that divides a given area into individual hydrologic response units (HRUs) based on land use, topography, and soil type. SWAT uses a soil water balance approach in which the final soil water content is equal to initial soil water content plus the sum of precipitation minus outflows (e.g., surface flow, percolation, and groundwater outflows). The ArcSWAT extension in ArcMap (Version 10.7.1; Environmental Systems Research Institute; Redlands, CA) was used to execute the SWAT model in this study. A simplified flowchart of the modeling process is provided in Figure 3.

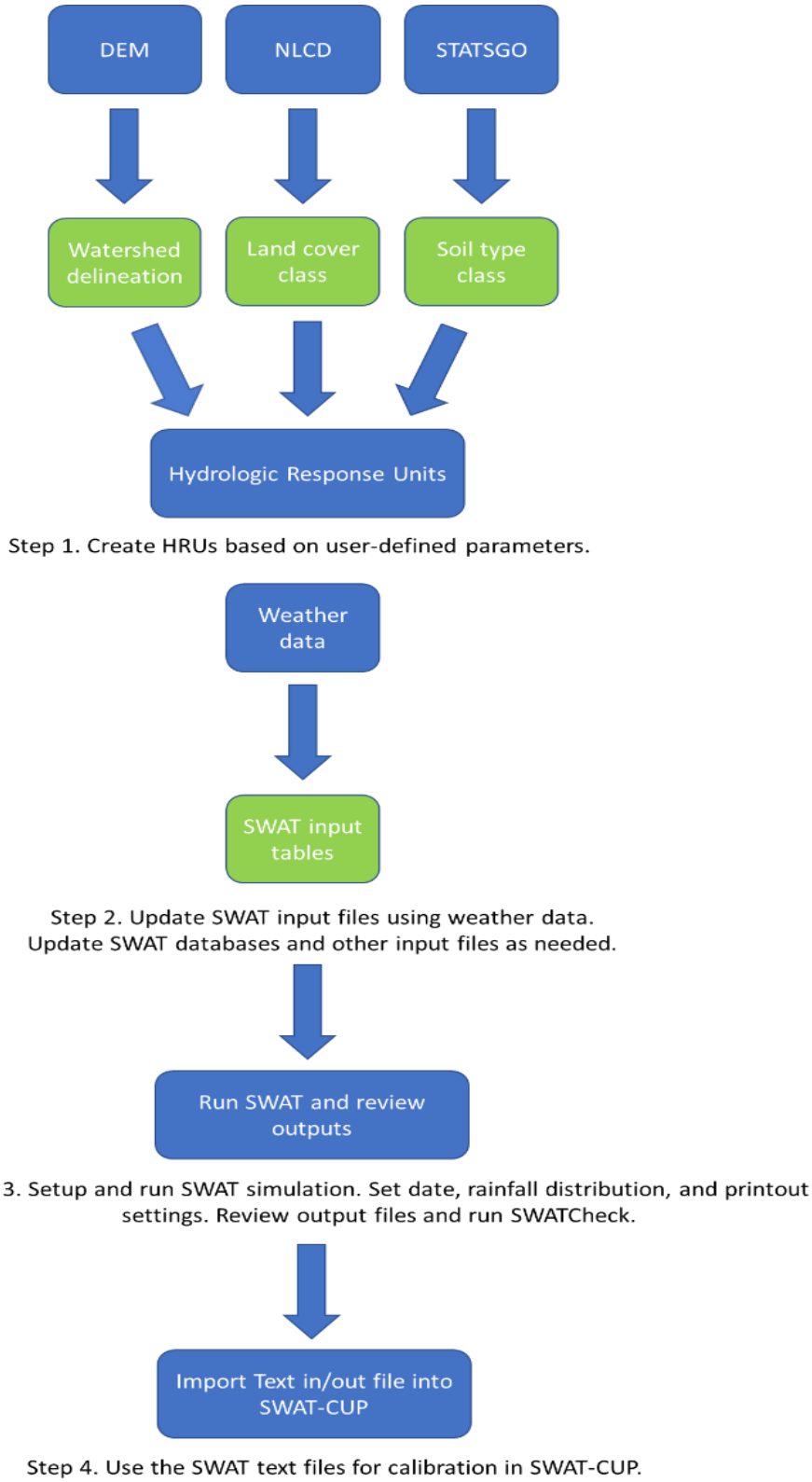

Figure 3. General flowchart for SWAT model creation. DEM refers to digital elevation model, NLCD refers to the National Land Cover Database, and STATSGO refers to the State Soil Geographic Dataset.

A 10-m resolution Digital Elevation Model (DEM) from the Oregon Spatial Data Library (https://spatialdata.oregonexplorer.info , [49]) was used to delineate the watershed. Elevation values were converted to meters using the ArcGIS Raster Calculator. The DEM and all other input rasters were projected to NAD 1983 UTM Zone 11 North. This watershed delineator divided the watershed into 12 subbasins and identified major stream systems within the watershed based on the DEM.

Land use classification was determined using the National Land Cover Database (NLCD; [50]) 2019 land cover dataset for the watershed. Resolution of the NLCD raster is 30 m. The NLCD datasets are available from the Multi-Resolution Land Characteristics website (https://www.mrlc.gov/data). A small section (<1 %) of the riparian area in the southern portion of the watershed was misclassified as low-density residential in the NLCD datasets. Our on-site observations indicate that this area is largely dominated by sagebrush vegetation and there is no residential development along this area of the reach. These portions of the NLCD raster were reclassified to rangeland-brush using the reclassify tool in ArcMap.

The State Soil Geographic (STATSGO) database was used as the soil input. Soil Survey Geographic Database (SSURGO) data were not available. STATSGO data is less detailed than SSURGO data but provides general information regarding rooting zone depth, hydrologic group, and soil texture. The primary soil types and texture characteristics are shown in Table 1.

Table 1. Soil class from the State Soil Geographic (STATSGO) database (http://www.fsl.orst.edu/pnwerc/wrb/metadata/soils/statsgo.pdf). Texture abbreviations are: very stony (STV), loam (L), very cobbly (CBV), silty clay loam (SICL), clay (C), unweathered bedrock (UWB), clay loam (CL), very gravelly (GRV), and sandy loam (SL). Land uses are classified as forest-evergreen (FRSE), rangeland-brush (RNGB), or rangeland-grasses (RNGE).

Soil Type	Soil Name	Hydrologic group	Texture	Land uses
OR 185	Ateron	D	STV-L-CBV-SICL-CBV-C-UWB	FRSE, RNGB, RNGE
OR 169	Ruckles	D	STV-CL-STV-C-UWB	FRSE, RNGB, RNGE
OR 186	Segundo	B	GRV-L-GRV-L-GRV-SL	FRSE, RNGB, RNGE

A minimum threshold of 5 % land cover area for land use, soils, and slope inputs was used for HRU definition. Percent slope was divided into five categories (Table 2) that reflect the

range in topography of the watershed. The CN2 numbers are generally based on shallow slopes up to 5 %. Based on these thresholds, 184 HRUs were created based on three NLCD land use categories, three soil types, and five slope categories (Table 2).

Table 2. Land use, soil, and slope categories after HRU delineation for the watershed. The "% of WS" indicates the percentage of area of the watershed for that land use category. Land uses are classified as forest-evergreen (FRSE), rangeland-brush (RNGB), or rangeland-grasses (RNGE).

Land Use Category	Area (ha)	% of WS
RNGB	914.9	71.9
FRSE	332.7	26.1
RNGE	25.5	2.0
Soil Category		
OR185	686.7	53.9
OR186	343.3	27.0
OR169	243.1	19.1
% Slope Category		
0-5	9.5	0.8
5-15	198.2	15.6
15-30	550.0	43.2
30-45	376.3	29.6
>45	139.1	10.9

Air temperature and precipitation data from PRISM were used for all years. On-site weather station data were used for minimum and maximum air temperature, precipitation, relative humidity, and wind speed from August 2019 until December 2021. The SWAT weather generator tool, which estimates values based on nearby monitoring stations, was used during limited periods when on site or PRISM data were not available. The Penman-Monteith approach was selected in ArcSWAT to calculate evapotranspiration.

For the SWAT model creation, data from 1 January 2016 to 31 December 2021 were used. Two years were used as a "warm up" period for the model. The daily curve number was calculated as a function of plant evapotranspiration (the "ICN" variable in SWAT). A SWAT model using the soil moisture method for daily curve number was also created but, based on initial results, the approach using the plant evapotranspiration modeled values that were closer to on-site observations. A skewed normal rainfall distribution was used.

2.3 SWAT-Calibration and Uncertainty (SWAT-CUP) Description

The SWAT Calibration and Uncertainty Program (SWAT-CUP; [22,23]) was used to perform parameter sensitivity, calibration, and validation. Streamflow (Q) for 2021 and PAWC for 2018, 2019, and 2021 were used for calibration, which included the years with the greatest and lowest recorded levels of precipitation during this study, and PAWC for 2020 was used for validation. Streamflow data were limited to observations during 2021.

The Sequential Uncertainty Fitting (SUFI-2) algorithm was used in SWAT-CUP to assess parameter uncertainty and sensitivity. SUFI-2 creates a 95 % simulation range (95PPU) based on user-selected parameters. SWAT-CUP uses two statistics, p-factor and r-factor, to assess the relationship between the simulation and the observations ([22]. The p-factor (ranging from 0 to 100 %) indicates the percentage of observations that fall within the modeled result while the r-factor (ranging from 0 to infinity) indicates the thickness of the 95 % probability range. Both factors will decrease as the range of parameters decreases [22]. Simulations which perfectly model data will have a p-factor of 1 and an r-factor of 0.

Within SWAT-CUP, several statistics can be chosen as the objective function in which the best performing model parameters for that statistic are selected. Nash-Sutcliffe (NS) was used as the objective function in this study.

The parameters selected for initial calibration in this study are shown in Table 3. These parameters were chosen based on the watershed characteristics (e.g., snow-dominated precipitation patterns) and factors that are known to influence streamflow (e.g., CN2) and soil moisture patterns (e.g., saturated hydraulic conductivity and soil albedo). Vegetation characteristics (e.g., CANMAX) were also included in the initial calibration. The curve number parameters (CN2) were further divided into the three land cover categories (RNGB, RNGE, and FRSE). These separations were made because of the link between CN2 and land cover. The CN2 parameter for RNGB was further subdivided into two groups based on the upper watersheds (reaches one through seven) and lower watersheds (reaches eight through 12), and then into three groups based on the average slope of the HRU. During later stages of calibration, it was noted that the average soil water content (SOL_AWC) was outside of expected ranges for some layers

and types of soil. Therefore, the SOL_AWC parameter was subdivided by hydrologic soil group (B or D) and soil layer.

In SWAT-CUP, the user can select one of three types of parameter changes: relative, replace, or absolute. When a relative change is indicated, which was used for the majority of parameters during this study, the original value is multiplied by a value plus one. For replace, the initial value is changed to a given value. For parameters such as CANMX and CH_K2 that were initially zero, the replace function was used for calibration. Caution should be used when the replace function is used for spatial variables, to include soil characteristics, as it will impact spatial variability. For absolute parameter changes, a given value is added to the original value. For each type of parameter change, the user selects the upper and lower limits of how much a parameter can change.

Sensitivity analysis was performed in SWAT-CUP using the global sensitivity analysis approach, which uses a multiple regression approach to determine parameter sensitivity. The *t*-statistic and *p*-value for each parameter are calculated during this process. As the range of calibration values impacts the sensitivity analysis results, multiple calibration runs were used to select parameters for calibration. Initial sensitivity analyses were run using only streamflow ("Q") for calibration, only PAWC, and using Q and PAWC. Each iteration for calibration used 500 simulations.

Using the SWAT-CUP sensitivity analysis, a threshold of $p \leq 10$ was used to identify parameters that were considered statistically significant (at $p \leq 0.05$) and those that were marginally significant (at $p \leq 0.10$). This threshold was selected because the results of the sensitivity analysis differed somewhat between calibration iterations, depending on the range of variation and parameters selected. In general, parameters that exceeded a *p*-value of 0.10 were removed from further calibration.

It was noted during several calibration iterations that the removal of some parameters (e.g., SNOCOVMX) that were excluded from calibration based on the $p \leq 0.10$ threshold resulted in reduced performance. In these cases, parameters were reintroduced to the calibration. The range of variation for each parameter was narrowed during the calibration process and parameters were removed when they were no longer considered statistically significant or marginally significant (at $p \leq 0.10$). After each iteration, the parameter ranges that yielded the best

NS values were used for each successive iteration. Parameter ranges were manually changed as necessary to ensure that parameters remained within an expected, realistic range. Therefore, the set of parameters used for the final calibration iteration and validation iteration were based on the results of previous calibrations and user knowledge of important hydrologic parameters (e.g., the influence of CN2 on Q). The parameter ranges yielding the best NS from the final calibration iteration were used for validation.

Table 3. Parameters used for sensitivity analysis. The extension (e.g., ".gw") indicates the SWAT file where the parameter is located. "Method" indicates the type of change applied to an existing parameter value. "Relative" indicates that the existing parameter value was multiplied by a given value plus one, "replace" indicates that the parameter value was replaced by a given value. The CN2 and CANMX parameters were separated by land use type for calibration. The CN2 parameter (indicated with "*") for the RNGB land cover was also divided by reaches based on location within the upper reaches (subbasins 1-7) or lower elevation reaches of the watershed (subbasins 8-12) and by slope. Sol_AWC ("**") was divided by hydrologic soil group (B or D) and layer (1 or 2-3).

Parameter	Explanation	Method	Land Use
ALPHA_BF.gw	Baseflow alpha factor	relative	(all)
CANMX.hru	Max canopy storage	replace	RNGB, RNGE, FRSE
CH_K2.rte	Effective hydraulic conductivity	replace	(all)
CH_N1.sub	Manning's roughness coefficient for tributary	relative	(all)
CH_N2.rte	Manning's roughness coefficient for main channel	relative	(all)
CN2.mgt*	Curve number	relative	RNGB, RNGE, FRSE
EPCO.hru	Plant uptake compensation factor	relative	(all)
ESCO.hru	Soil evaporation compensation factor	relative	(all)
EVRCH.bsn	Evaporation adjustment factor for reach	relative	(all)
GW_DELAY.gw	Groundwater delay time in days	relative	(all)
GW_REVAP.gw	Groundwater revap coefficient	relative	(all)
GWQMN.gw	Threshold depth of water in shallow aq required for return flow	relative	(all)
OV_N.hru	Manning's roughness coefficient for overland flow	relative	(all)
RCHRG_DP.gw	Deep aquifer percolation fraction	relative	(all)
REVAPMN.gw	Threshold depth of water in shallow aquifer required for revap or percolation to deep aquifer	relative	(all)
SFTMP.bsn	Snowfall temp (°C)	relative	(all)
SMFMN.bsn	Melt factor: Dec 21	relative	(all)

SMFMX.bsn	Melt factor: June 21	relative	(all)
SMTMP.bsn	Snowmelt base temp (°C)	relative	(all)
SNOCOVMX.bsn	Min snow water content at 100% snow cover	relative	(all)
SOL_ALB.sol	Moist soil albedo	relative	(all)
SOL_AWC.sol**	Average soil available water capacity	relative	(all)
SOL_K.sol	Saturated hydraulic conductivity (mm hr^{-1})	relative	(all)
SURLAG.hru	Surface runoff lag time	relative	(all)
TIMP.bsn	Snowpack temperature lag factor	relative	(all)
TRNSRCH.bsn	Portion of transmission losses from main channel that go into deep aquifer	replace	(all)

Model performance was assessed using the guidelines suggested by Moriasi et al. [51]. NS values between 0.75 and 1 were considered “very good”, between 0.65 and 0.75 were considered “good”, between 0.5 and 0.65 were considered “satisfactory”, and values below 0.5 were considered “unsatisfactory”.

3. Results

Peaks in the PAWC content generally corresponded to periods of snowmelt in April and May (Figures 4 and 5) and were generally greater at the Deer Creek site compared to the Fish Creek Valley site.

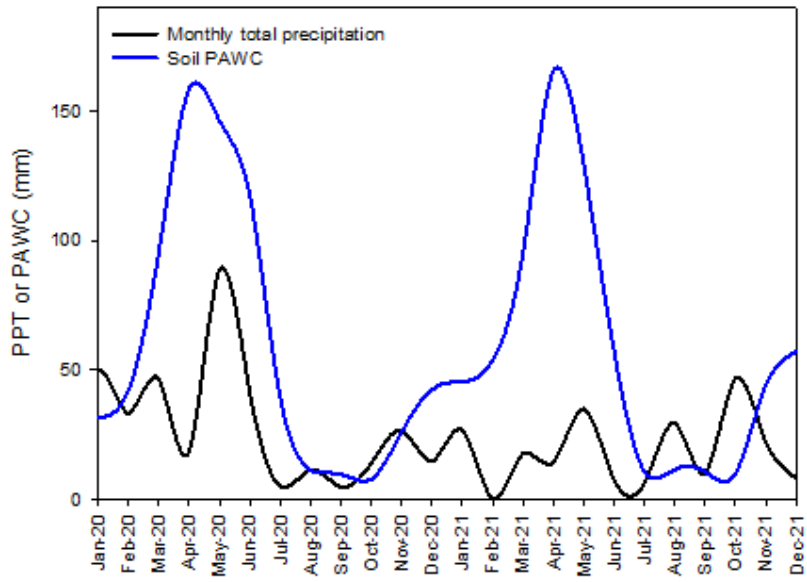

Figure 4. Total monthly precipitation (PPT) and average monthly PAWC for the Deer Creek site based.

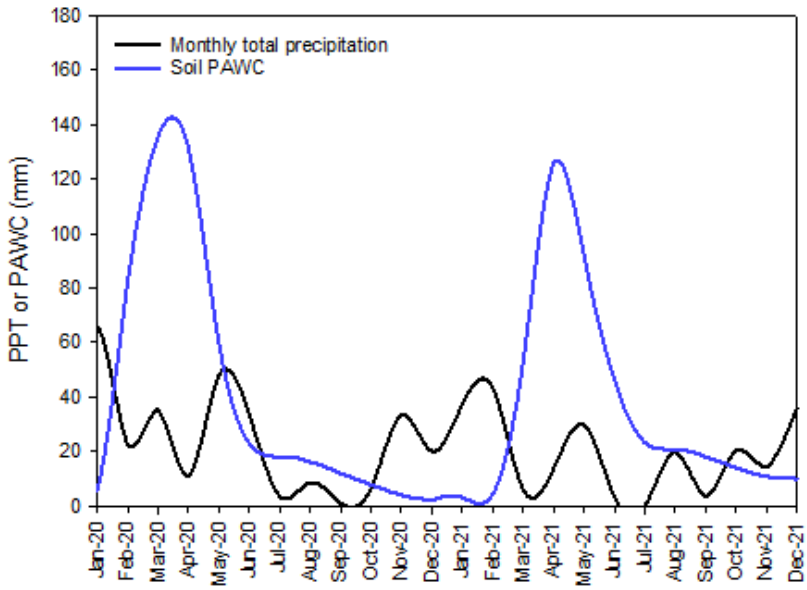

Figure 5. Total monthly precipitation (PPT) and average monthly PAWC for the Fish Creek Valley site.

The average monthly basin water balance values are shown in Table 4. Average annual ET was 253 mm (67% of incoming precipitation). Average annual water yield, which is the total of surface runoff and subsurface flow, was 126 mm (33% of average incoming precipitation). Snowfall accounted for 53% of incoming precipitation, with the majority of precipitation falling from November through May. Water moving from the shallow aquifer to soils and vegetation accounted for 16 mm, 4% of annual average incoming precipitation. Modeled average annual total groundwater recharge was 10 mm, 3% of average annual incoming precipitation.

Table 4. Average modeled monthly basin water balance values for 2018 through 2021. All values are in mm. "PPT" indicates precipitation, "Snow" refers to the average amount of precipitation that fell as freezing rain, sleet, or snow, "Surf Q" refers to surface runoff, "Lat Q" refers to lateral flow to streamflow, "Water Yield" indicates total of surface runoff and subsurface flow, "ET" refers to actual evapotranspiration, and "PET" refers to potential evapotranspiration.

Month	PPT	Snow	Surf Q	Lat Q	Water Yield	ET	PET
Jan	53	52	2	0	2	1	3
Feb	57	54	5	3	7	1	2
Mar	31	20	22	17	41	4	8
Apr	29	6	1	37	42	11	21
May	54	0	1	19	21	51	103
Jun	26	0	0	4	5	52	141
Jul	3	0	0	0	0	56	195
Aug	14	0	0	2	2	42	165
Sep	17	0	0	2	2	20	103
Oct	23	2	0	4	4	13	47
Nov	34	26	0	1	1	2	5
Dec	37	37	0	0	0	0	0

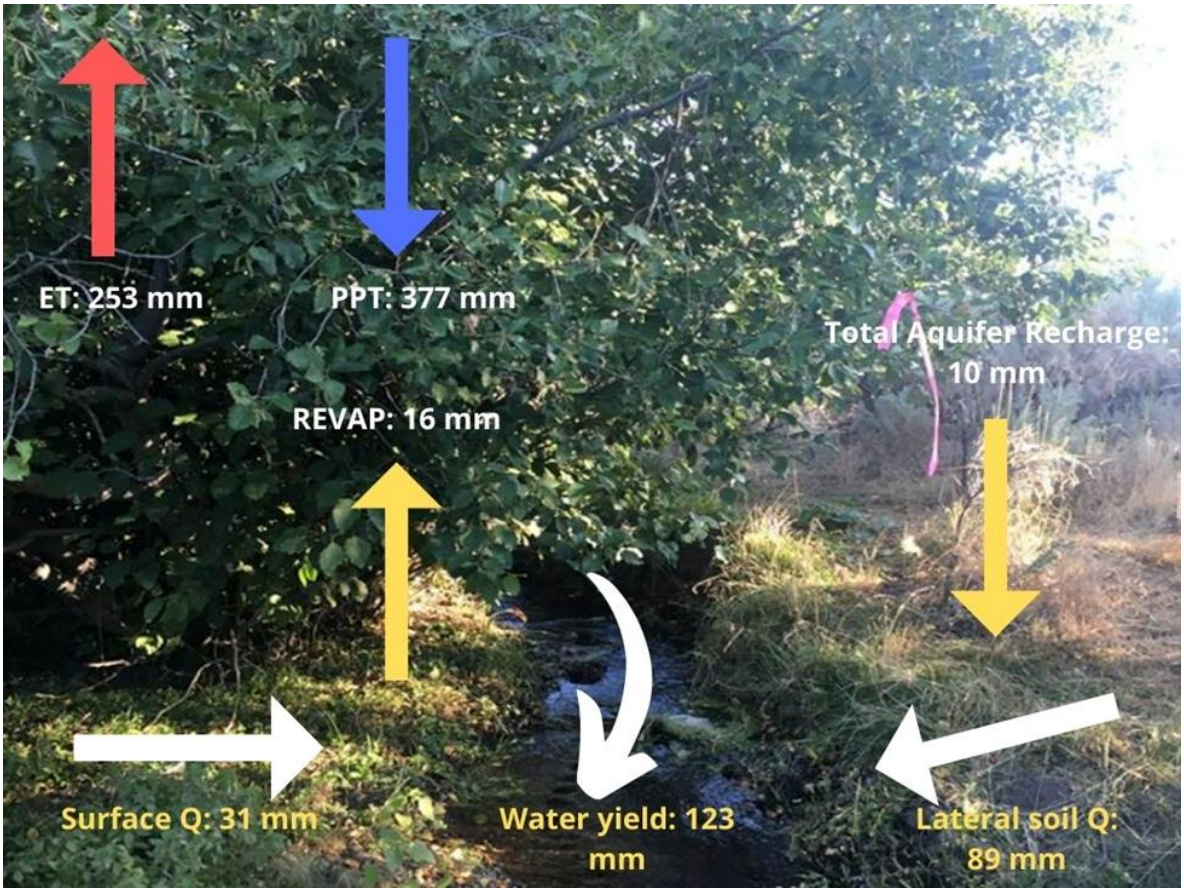

Figure 6. Average annual modeled basin water balance values for 2018 through 2021. All values are in mm yr^{-1}. "ET" refers to evapotranspiration, "PPT" refers to all precipitation, "REVAP" refers to moisture that moves from the shallow aquifer into the unsaturated zone, "Surface Q" refers to surface runoff, "Lateral soil Q" refers to subsurface flow through the soil, "water yield" refers to total water outflow in the form of surface and subsurface flow from the study area, and "total aquifer recharge" refers to all water that entered into the shallow or deep aquifer. Photo Credit: Carlos C. G. Ochoa.

Using Manning's equation and the characteristics and stream channel dimensions observed in our stream survey, we estimated the potential peak flow near the outlet of the study area to be 0.56 cms. The average monthly modeled streamflow rate was 0.02 cms with the highest monthly modeled streamflow rate occurring in April (0.08 cms) . The average monthly modeled streamflow rates are shown in Table 5.

Table 5. Modeled average monthly and annual streamflow rates (cms) for 2018 through 2021 at the Fish Creek Valley site.

Month	Streamflow
Jan	8.76E-04
Feb	5.98E-03
Mar	3.29E-02
Apr	8.33E-02
May	5.39E-02
Jun	2.55E-02
Jul	7.43E-03
Aug	2.18E-03
Sep	1.89E-03
Oct	2.99E-03
Nov	3.95E-03
Dec	1.55E-03
Annual	1.85E-02

The model used in this study yielded "very good" results based on the objective function (NS) for the calibration of Fish Creek Valley streamflow and Deer Creek PAWC and "good" results for the Fish Creek Valley PAWC (Table 6). Modeled streamflow rates and patterns were similar to those observed (Figure 7). The timing of seasonal PAWC peaks were generally modeled well under this approach although the model generally underpredicted peak PAWC (Figures 8 and 9).

Table 6. Results of the final calibration iteration. Nash-Sutcliffe (NS) was used as the objective function. P-factor indicates the percentage of observations that fall within the modeled result, r-factor is the width of the 95% probability range, R^2 is the coefficient of determination, bR^2 is the adjusted R^2, and MSE is the mean squared error.

Variable	p-factor	r-factor	R^2	NS	bR^2	MSE
Streamflow	0.56	0.11	0.96	0.93	0.88	0
Deer Creek PAWC	0.41	0.42	0.86	0.84	0.67	440
Fish Creek Valley PAWC	0.06	0.26	0.70	0.68	0.52	350

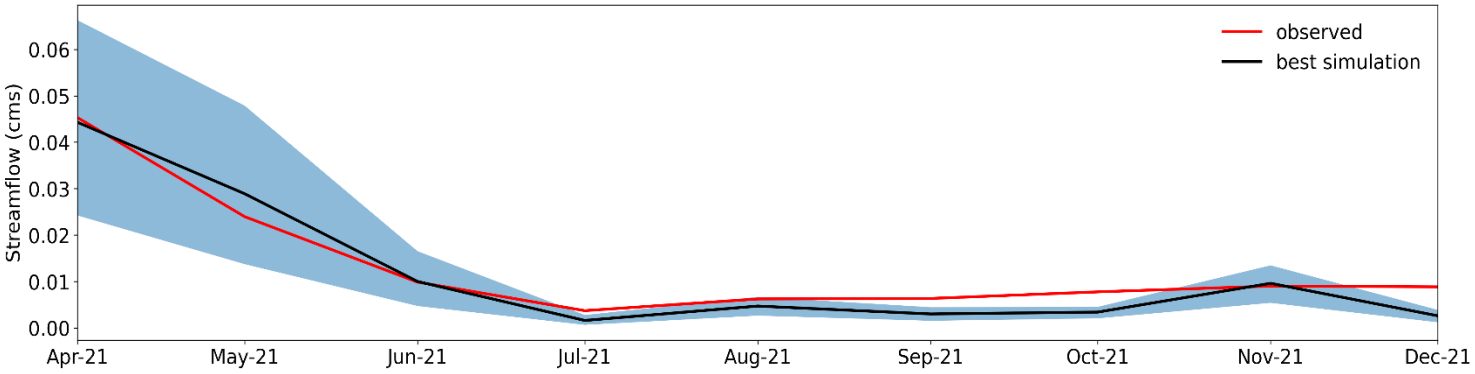

Figure 7. Streamflow observation and calibration results. The shaded blue area represents the 95% confidence range (95PPU). Streamflow data from 2021 were used for calibration. Streamflow data were not available for other years.

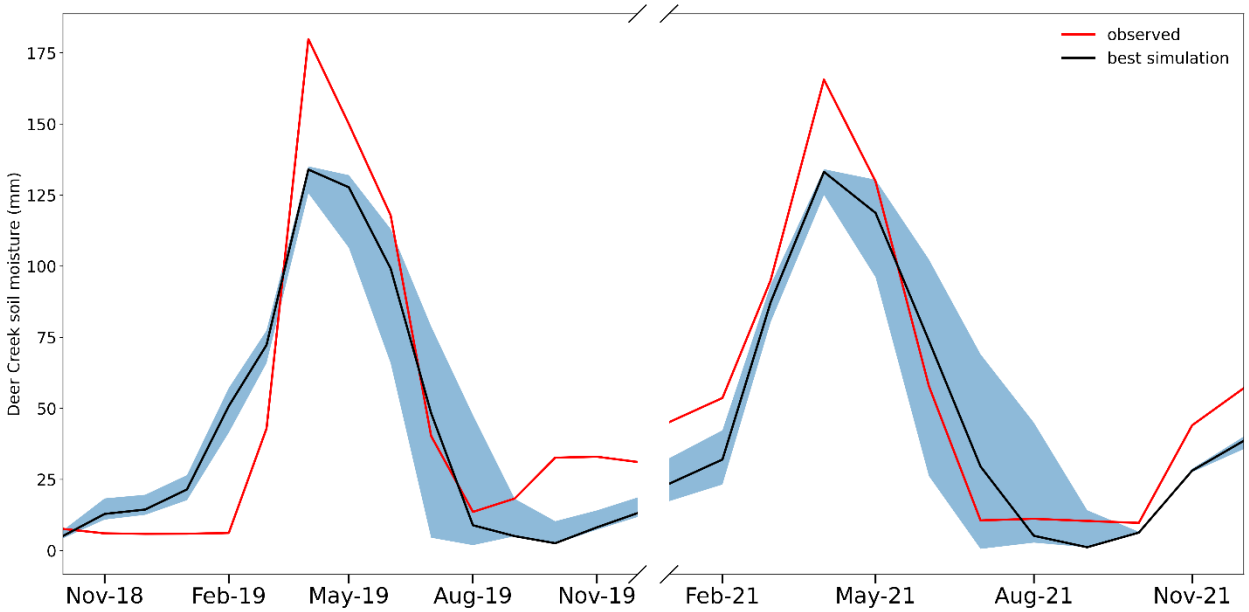

Figure 8. Deer Creek observation and calibration results. The shaded blue area represents the 95% confidence range (95PPU). Soil moisture data from 2018, 2019, and 2021 from the Deer Creek site were used for calibration.

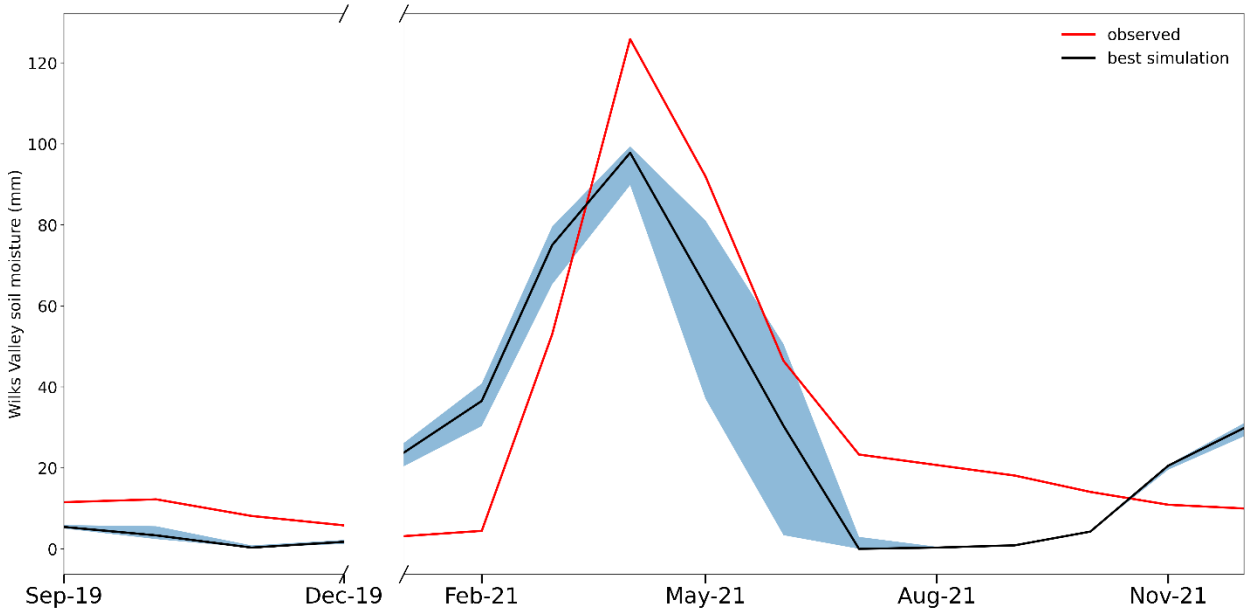

Figure 9. Fish Creek Valley observation and calibration results. The shaded blue area represents the 95% confidence range (95PPU). Soil moisture data from 2019 and 2021 from Fish Creek Valley were used for calibration.

Based on the NS value, the validation yielded “very good” results for PAWC at both sites (Table 7). Similar to the calibration results, the timing of peaks was generally modeled well but the modeled PAWC was generally lower than observed during peak periods of PAWC (Figures 10 and 11).

Table 7. Validation results. Nash-Sutcliffe (NS) was used as the objective function. P-factor indicates the percentage of observations that fall within the modeled result, r-factor is the width of the 95% range, R^2 is the coefficient of determination, bR^2 is the adjusted R^2, and MSE is the mean squared error.

Variable	p-factor	r-factor	R^2	NS	bR^2	MSE
Deer Creek	0.25	0.30	0.89	0.85	0.81	400
Fish Creek Valley	0.25	0.19	0.88	0.81	0.63	420

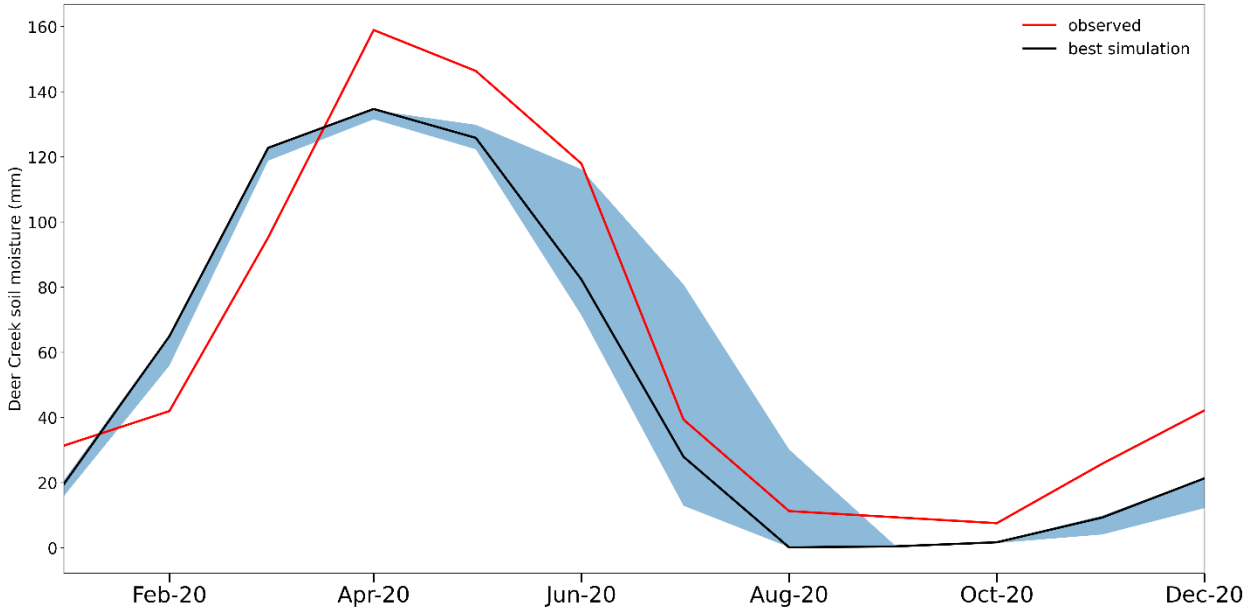

Figure 10. Deer Creek observation and validation results. The shaded blue area represents the 95% confidence range (95PPU).

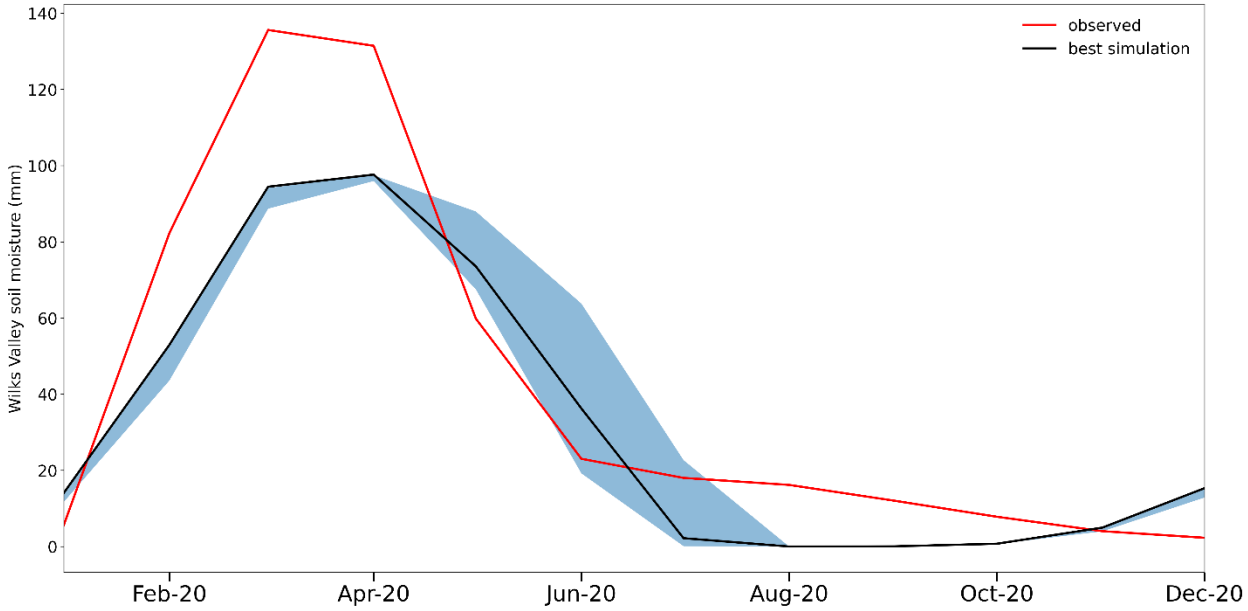

Figure 11. Fish Creek Valley observation and validation results. The shaded blue area represents the 95% confidence range (95PPU).

Based on the sensitivity analysis in SWAT-CUP, the parameters found to be statistically significant (at $p \leq 0.0.05$) or marginally statistically significant (at $p \leq 0.10$) are shown in Table 8. For the final calibration and validation, six parameters were used: SNOCOVMX, CN2, ESCO, CH_N1, SOL_AWC, and TRNSRCH. The average SNOCOVMX value was 255 mm. The average available soil water content for the study area was 0.24. The average available soil water content for all soils excluding unweather bedrock was 0.30. The final calibrated values for other parameters are listed in Table 8.

Table 8. Results of initial sensitivity analysis using SWAT-CUP for each variable and the final calibrated value for each parameter. The Sol_AWC indicates the average soil available water content for all layers across all soil types. "Q only" indicates that the streamflow was the only variable used during the sensitivity analysis, "Q and PAWC" indicates that streamflow and plant available water content were used during sensitivity analysis, and "PAWC only" indicates that plant available water content was the only variable used for sensitivity analysis. Units are shown where applicable. The extension (e.g., ".rte") indicates the SWAT file in which the parameter is located.

Variable	Parameter	*p*-value	Final value
Q only	CH_K2.rte	0.00	128 mm hr^{-1}
	CN2.mgt (FRSE)	0.00	35
	TRNSRCH.bsn	0.00	0.25
	ALPHA_BF.gw	0.00	0.15 $days^{-1}$
	SURLAG.hru	0.00	0.05 days
	SOL_K.sol	0.01	241 mm hr^{-1}
	CANMX.hru (RNGB)	0.03	15.3 mm
	CANMX.hru (RNGE)	0.05	4.2 mm
	CN2.mgt (RNGB, upper reaches, slopes ≥16%)	0.07	73
	CH_N1.sub	0.07	0.45
	CN2.mgt (RNGB, upper reaches, slopes 6-15%)	0.09	71
	REVAPMN.gw	0.10	500 mm
Q and PAWC	ESCO.hru	0.00	1
	TRNSRCH.bsn	0.00	0.25
	SOL_AWC.sol	0.00	0.24 (mm water/mm soil)
	CANMX.hru (RNGE)	0.01	4.2 mm
	ALPHA_BF.gw	0.01	0.15 $days^{-1}$
	SMTMP.bsn	0.02	1.1 °C
	TIMP.bsn	0.06	0.57
PAWC only	SOL_AWC.sol	0.00	0.24 (mm water/mm soil)
	ESCO.hru	0.00	1
	SMTMP.bsn	0.00	1.1 °C
	GW_REVAP.gw	0.02	0.02

The average watershed curve number (CN2) was 52. The average CN2 for the RNGB land cover, which accounts for 72% of the study area, was 73. The average CN2 for both the RNGE and FRSE land cover types was 35. Based on [52] , the estimated curve number for pinyon-juniper land cover is between 41 (‘good condition’) and 75 (‘poor condition’) for hydrologic group B and between 71 (‘good condition’) and 89 (‘poor condition’) for hydrologic group D. The estimated curve number for sagebrush areas with grass understory in hydrologic group B ranges from 35 (‘good condition’) to 67 (‘poor condition’) and for hydrologic group D ranges from 55 (‘good condition’) to 85 (‘poor condition’). For wooded areas, the curve number is expected to range between 55 (‘good condition’) and 66 (‘poor condition’) for hydrologic group B and between 77 (‘good condition’) and 83 (‘poor condition’) for hydrologic group D. The two soil moisture sites and the streamflow monitoring site were located within the RNGB land cover.

4. Discussion

This research sought to characterize the water balance and assess parameter sensitivity of a relatively small watershed in a snow-dominated semiarid region of eastern Oregon, USA. By understanding the water balance and the factors that impact hydrologic processes we can better address key water management issues in water-scarce rangeland ecosystems with limited on-site data.

We used a multisite, multivariable calibration approach for this study. The use of multiple variables at spatially distributed locations has been found to improve model calibration results [53,54]. The use of multisite and multivariable calibration may be particularly important, considering the presence of intermittent streams at this study site, and as spatial heterogeneity may not be accurately represented if only data at the study site outlet are used. For example, [55] found that streamflow predictions improved when multi-site calibration approaches were used in a heterogenous watershed. Even though limited streamflow data were available in this study, we noted that the model performance improved when streamflow data were included in the calibration compared to when we only used soil moisture data. It should be noted that observed streamflow rates were relatively low (0.01 to 0.4 cms) and that intermittent streamflow patterns were present in upslope locations. Further, in order to maintain parameter spatial heterogeneity,

we used a calibration approach that applied a relative change (the initial parameter value was multiplied by a given value plus one) for the majority of parameters.

Spatial and temporal variability in precipitation amounts were noted during this study. While this study represents a year of varying precipitation characteristics, it likely does not represent the full extent of seasonal and annual variability. Therefore, caution should be used when extrapolating the results of the model beyond the conditions observed. Further, even when years of varying precipitation characteristics are represented, there may be antecedent conditions which are not accounted for (e.g., soil moisture storage). However, by increasing the understanding of the key drivers of the water balance, we can better predict the influence of different weather or climatic patterns even when data are limited.

The application of SWAT and other surface hydrologic models is limited in areas with complex hydrogeology [56,57], such as when karst or volcanic geology are present [58]. While the primary objective of our study focused on the soil water balance and surface hydrology, given the presence of multiple spring-fed stream and fractured basalt at this study site, it should be noted that some aspects (e.g., deep percolation) may not be accurately represented. The SWAT model does not account for water sources external to the watershed (e.g., external subsurface flow) or interactions between HRUs; therefore, caution should be used when considering groundwater characteristics and groundwater-surface water interactions. Fully-distributed hydrologic models such as MODFLOW [59,60], have been widely used to model groundwater flow at larger, regional scales , and their use was beyond the scope of this study.

Parameter sensitivity varies with the variable of interest (e.g., PAWC, streamflow), the range of variation allowed for that parameter, and the objective function [61], among other factors. We noted that the results of the sensitivity analyses were not consistent between iterations and varied with the range of variation. For example, the SNOCOVMX parameter was initially removed from calibration based on the results of the sensitivity analysis but subsequent calibrations indicated reduced model performance. We attributed this to the initial range of variation used for the SNOCOVMX parameter in calibration. The parameter was used in later calibration iterations and model results improved. Therefore, the statistical significance of a parameter in the model may not necessarily equate to physical significance in actual hydrologic

processes. This may particularly be the case when other influential physical processes (e.g., subsurface flow) are not adequately represented.

Parameter sensitivity results indicated that snow-related parameters (e.g., SNOCOVMX and SMTMP) and soil characteristics (e.g., SOL_K) were among the most influential parameters for both variables. These results are similar to [10], who found that soil water content was a key factor in calculating the water balance of a semiarid site, and [36], who found that snow parameters were among the most influential parameters at a semiarid sage-steppe site. However, the sensitivity analyses indicated that the snow-related parameters were most influential when either the PAWC alone or when PAWC and streamflow were both being calibrated, not when streamflow only was being used for calibration. As expected, the curve number (CN2) and channel characteristics (e.g., Manning's roughness coefficients and baseflow) were found to be among the most influential parameters for calibrating streamflow. Similar to [34], we also found that the surface lag time (SURLAG) was one of the most sensitive parameters for streamflow calibration, although the final calibrated value was very low (0.05 days). Vegetation characteristics, specifically the maximum canopy storage (CANMX), were also indicated to be influential parameters for streamflow calibration.

While increased complexity does not necessarily result in a better model, it may be necessary to further subdivide some parameters. For example, we divided the curve number (CN2) parameter into separate groups based on land cover type and slope as, in general, steeper slopes experience greater runoff than shallower slopes. However, while we subdivided the soil available water content (SOL_AWC) parameter by hydrologic group and layer, we did not separate this parameter by texture (a key determinant in water content and hydraulic conductivity). The calibration data used in this study reflected different slope and elevation characteristics, but the locations of both weather stations were classified under the same land use type (rangeland-brush). While the average curve number appears representative of the watershed as a whole, it may not be representative of individual land cover types, particularly the forested areas. Therefore, this study could be further improved by including additional study sites in other land cover areas.

Although a particular model may yield good results based on the objective function, the model may not always realistically reflect physical processes [62]. During calibration and

validation careful consideration should be given to ensuring that parameter values are within a reasonable range. For example, during initial calibration attempts, we found that two key parameters, saturated hydraulic conductivity (SOL_K) and SOL_AWC, were outside of realistic ranges although objective function results were considered “good”. In these cases, the parameter ranges were manually adjusted. It should be emphasized that, in addition to the objective function results, the model objective (e.g., peak flow, water balance, etc.) and the parameter ranges should also be closely considered. Additionally, while we used one objective function (NS) for this study, past research has also indicated that multi-objective calibration approaches may decrease equifinality [63]. Further, in this study we used the Sequential Uncertainty Fitting Version 2 (SUFI-2) approach for uncertainty analysis in SWAT-CUP, but the applicability of approaches used for uncertainty analysis may vary based on site-specific characteristics [64].

Noting the objectives of this research and its limitations, model selection is also an important factor in modeling the water balance. For example, Pradhan et al. [12] found that an Artificial Neural Network (ANN) approach performed better in areas with high streamflow while SWAT performed better in areas with lower streamflow volume. Similarly, Demirel et al. [65] found that an ANN approach estimated peak flows better than the SWAT model for a basin in Portugal. While comparison of different models was beyond the scope of this project, it is important that model selection reflects the research objectives and the study site characteristics.

The approach used here can be expanded to larger geographic areas, incorporating a greater variation of topographical and land use characteristics. For example, while many of the streams in the region are ungauged, openly available data, such as through the USGS StreamStats database (https://streamstats.usgs.gov/ss/) or Oregon Water Resources Department (OWRD) hydrographic database (https://apps.wrd.state.or.us/apps/sw/hydro_near_real_time/) can be included into regional scale models in this area. Snowpack and snow water equivalent measurements available through sites such the Natural Resources Conservation Service SNOTEL database (https://www.nrcs.usda.gov/wps/portal/wcc/home/snowClimateMonitoring/snowpack/) can also be used to further improve model calibration for a larger regional scale. Models, such as MODFLOW, can be used to more fully address the complex hydrogeology and remote sensing

data, such as NASA's Soil Moisture Active Passive soil satellite, can be used to augment the on-site data available.

This study provides insight into the water balance and important hydrologic drivers at a semiarid, snow-dominated study site that can be used to inform future research and modeling approaches. SWAT is a versatile and robust model that may be used to address other key concerns in this region such as climate change, riparian land cover change, and water quality. Agricultural production is an important land use in this region, and SWAT has also been used to address key issues such as forage yield (e.g.[36]) and irrigation (e.g., [8]). From a land management standpoint, these data help improve our understanding of how different land use practices and environmental characteristics can impact water availability, both in the form of streamflow and soil moisture. The results of this research suggest that hydrologic models can improve our understanding of watershed processes and dynamics in semiarid, snow-dominated sites, provided that the model applications and limitations are understood.

References

1. Arnold, J.G.; Srinivasan, R.; Muttiah, R.S.; Williams, J.R. Large Area Hydrologic Modeling and Assessment Part I: Model Development1. *JAWRA Journal of the American Water Resources Association* **1998**, *34*, 73–89, doi:10.1111/j.1752-1688.1998.tb05961.x.
2. Desai, S.; Singh, D.K.; Islam, A.; Sarangi, A. Multi-Site Calibration of Hydrological Model and Assessment of Water Balance in a Semi-Arid River Basin of India. *Quaternary International* **2021**, *571*, 136–149, doi:10.1016/j.quaint.2020.11.032.
3. Uniyal, B.; Jha, M.K.; Verma, A.K. Assessing Climate Change Impact on Water Balance Components of a River Basin Using SWAT Model. *Water Resources Management* **2015**, *29*, 4767–4785, doi:http://dx.doi.org.ezproxy.proxy.library.oregonstate.edu/10.1007/s11269-015-1089-5.
4. Chen, Y.; Marek, G.W.; Marek, T.H.; Porter, D.O.; Brauer, D.K.; Srinivasan, R. Simulating the Effects of Agricultural Production Practices on Water Conservation and Crop Yields Using an Improved SWAT Model in the Texas High Plains, USA. *Agricultural Water Management* **2021**, *244*, 106574, doi:10.1016/j.agwat.2020.106574.
5. Lopes, T.R.; Zolin, C.A.; Mingoti, R.; Vendrusculo, L.G.; Almeida, F.T. de; Souza, A.P. de; Oliveira, R.F. de; Paulino, J.; Uliana, E.M. Hydrological Regime, Water Availability and Land Use/Land Cover Change Impact on the Water Balance in a Large Agriculture Basin in the Southern Brazilian Amazon. *Journal of South American Earth Sciences* **2021**, *108*, 103224, doi:10.1016/j.jsames.2021.103224.
6. Eshtawi, T.; Evers, M.; Tischbein, B. Quantifying the Impact of Urban Area Expansion on Groundwater Recharge and Surface Runoff. *Hydrological Sciences Journal* **2015**, 150527103244004, doi:10.1080/02626667.2014.1000916.

7. Mosbahi, M.; Benabdallah, S.; Boussema, M.R. Hydrological Modeling in a Semi-Arid Catchment Using SWAT Model. *Journal of Environmental Science and Engineering* **2011**, *5*, 8.
8. Wu, Y.; Li, C.; Zhang, C.; Shi, X.; Bourque, C.P.-A.; Zhao, S. Evaluation of the Applicability of the SWAT Model in an Arid Piedmont Plain Oasis. *Water Science and Technology* **2016**, *73*, 1341–1348, doi:10.2166/wst.2015.609.
9. Ghaffari, G.; Keesstra, S.; Ghodousi, J.; Ahmadi, H. SWAT-Simulated Hydrological Impact of Land-Use Change in the Zanjanrood Basin, Northwest Iran. *Hydrological Processes* **2010**, *24*, 892–903, doi:10.1002/hyp.7530.
10. Muttiah, R.S.; Wurbs, R.A. Scale-Dependent Soil and Climate Variability Effects on Watershed Water Balance of the SWAT Model. *Journal of Hydrology* **2002**, *256*, 264–285, doi:10.1016/S0022-1694(01)00554-6.
11. Kan, G.; He, X.; Ding, L.; Li, J.; Liang, K.; Hong, Y. Study on Applicability of Conceptual Hydrological Models for Flood Forecasting in Humid, Semi-Humid Semi-Arid and Arid Basins in China. *Water* **2017**, *9*, 719, doi:10.3390/w9100719.
12. Pradhan, P.; Tingsanchali, T.; Shrestha, S. Evaluation of Soil and Water Assessment Tool and Artificial Neural Network Models for Hydrologic Simulation in Different Climatic Regions of Asia. *Science of The Total Environment* **2020**, *701*, 134308, doi:10.1016/j.scitotenv.2019.134308.
13. Van Liew, M.W.; Veith, T.L.; Bosch, D.D.; Arnold, J.G. Suitability of SWAT for the Conservation Effects Assessment Project: Comparison on USDA Agricultural Research Service Watersheds. *Journal of Hydrologic Engineering* **2007**, *12*, 173–189, doi:10.1061/(ASCE)1084-0699(2007)12:2(173).
14. Brouziyne, Y.; Abouabdillah, A.; Bouabid, R.; Benaabidate, L.; Oueslati, O. SWAT Manual Calibration and Parameters Sensitivity Analysis in a Semi-Arid Watershed in North-Western Morocco. *Arab J Geosci* **2017**, *10*, 427, doi:10.1007/s12517-017-3220-9.
15. Ghoraba, S.M. Hydrological Modeling of the Simly Dam Watershed (Pakistan) Using GIS and SWAT Model. *Alexandria Engineering Journal* **2015**, *54*, 583–594, doi:10.1016/j.aej.2015.05.018.
16. Kiros, G.; Shetty, A.; Nandagiri, L. Performance Evaluation of SWAT Model for Land Use and Land Cover Changes under Different Climatic Conditions: A Review. *Hydrol Current Res* **2015**, *06*, doi:10.4172/2157-7587.1000216.
17. PRISM Climate Group, Oregon State University, Http://Prism.Oregonstate.Edu, Created 1 March 2019.
18. Gao, J.; Sheshukov, A.Y.; Yen, H.; White, M.J. Impacts of Alternative Climate Information on Hydrologic Processes with SWAT: A Comparison of NCDC, PRISM and NEXRAD Datasets. *CATENA* **2017**, *156*, 353–364, doi:10.1016/j.catena.2017.04.010.
19. Uniyal, B.; Dietrich, J.; Vasilakos, C.; Tzoraki, O. Evaluation of SWAT Simulated Soil Moisture at Catchment Scale by Field Measurements and Landsat Derived Indices. *Agricultural Water Management* **2017**, *193*, 55–70, doi:10.1016/j.agwat.2017.08.002.
20. Parajuli, P.B.; Jayakody, P.; Ouyang, Y. Evaluation of Using Remote Sensing Evapotranspiration Data in SWAT. *Water Resour Manage* **2018**, *32*, 985–996, doi:10.1007/s11269-017-1850-z.
21. Nilawar, A.; Calderella, C.; Lakhankar, T.; Waikar, M.; Munoz, J. Satellite Soil Moisture Validation Using Hydrological SWAT Model: A Case Study of Puerto Rico, USA. *Hydrology* **2017**, *4*, 45, doi:10.3390/hydrology4040045.

22. Abbaspour, K.C. SWAT-CUP: SWAT Calibration and Uncertainty Programs - A User Manual; Department of Systems Analysis, Integrated Assessment and Modelling (SIAM), Eawag. Swiss Federal Institute of Aquatic Science and Technology; Duebendorf, Switzerland. **2015**, 100.
23. Abbaspour, K.C.; Yang, J.; Maximov, I.; Siber, R.; Bogner, K.; Mieleitner, J.; Zobrist, J.; Srinivasan, R. Modelling Hydrology and Water Quality in the Pre-Alpine/Alpine Thur Watershed Using SWAT. *Journal of Hydrology* **2007**, *333*, 413–430, doi:10.1016/j.jhydrol.2006.09.014.
24. Abbaspour, K.C.; Vaghefi, S.A.; Srinivasan, R. A Guideline for Successful Calibration and Uncertainty Analysis for Soil and Water Assessment: A Review of Papers from the 2016 International SWAT Conference. *Water* **2018**, *10*, 6, doi:10.3390/w10010006.
25. Abbaspour, K.C.; Rouholahnejad, E.; Vaghefi, S.; Srinivasan, R.; Yang, H.; Kløve, B. A Continental-Scale Hydrology and Water Quality Model for Europe: Calibration and Uncertainty of a High-Resolution Large-Scale SWAT Model. *Journal of Hydrology* **2015**, *524*, 733–752, doi:10.1016/j.jhydrol.2015.03.027.
26. Arnold, J.G.; Moriasi, D.N.; Gassman, P.W.; Abbaspour, K.C.; White, M.J.; Srinivasan, R.; Santhi, C.; Harmel, R.D.; Griensven, A. van; Liew, M.W.V.; et al. SWAT: Model Use, Calibration, and Validation. *Transactions of the ASABE* **2012**, *55*, 1491–1508, doi:10.13031/2013.42256.
27. Shah, S.; Duan, Z.; Song, X.; Li, R.; Mao, H.; Liu, J.; Ma, T.; Wang, M. Evaluating the Added Value of Multi-Variable Calibration of SWAT with Remotely Sensed Evapotranspiration Data for Improving Hydrological Modeling. *Journal of Hydrology* **2021**, *603*, 127046, doi:10.1016/j.jhydrol.2021.127046.
28. Niraula, R.; Norman, L.M.; Meixner, T.; Callegary, J.B. Multi-Gauge Calibration for Modeling the Semi-Arid Santa Cruz Watershed in Arizona-Mexico Border Area Using SWAT. *Air, Soil and Water Research* **2012**, 41-.
29. Andrade, C.W.L. de; Montenegro, S.M.G.L.; Montenegro, A.A.A.; Lima, J.R. de S.; Srinivasan, R.; Jones, C.A. Soil Moisture and Discharge Modeling in a Representative Watershed in Northeastern Brazil Using SWAT. *Ecohydrology & Hydrobiology* **2019**, *19*, 238–251, doi:10.1016/j.ecohyd.2018.09.002.
30. Mengistu, A.G.; van Rensburg, L.D.; Woyessa, Y.E. Techniques for Calibration and Validation of SWAT Model in Data Scarce Arid and Semi-Arid Catchments in South Africa. *Journal of Hydrology: Regional Studies* **2019**, *25*, 100621, doi:10.1016/j.ejrh.2019.100621.
31. Rajib, M.A.; Merwade, V.; Yu, Z. Multi-Objective Calibration of a Hydrologic Model Using Spatially Distributed Remotely Sensed/in-Situ Soil Moisture. *Journal of Hydrology* **2016**, *536*, 192–207, doi:10.1016/j.jhydrol.2016.02.037.
32. Kundu, D.; Vervoort, R.W.; van Ogtrop, F.F. The Value of Remotely Sensed Surface Soil Moisture for Model Calibration Using SWAT. *Hydrological Processes* **2017**, *31*, 2764–2780, doi:10.1002/hyp.11219.
33. *Urban Hydrology for Small Watersheds*; U.S. Department of Agriculture, Natural Resources Conservation Service, Conservation Engineering Division, 1986;
34. Ahl, R.S.; Woods, S.W.; Zuuring, H.R. Hydrologic Calibration and Validation of SWAT in a Snow-Dominated Rocky Mountain Watershed, Montana, U.S.A. [1]. *JAWRA Journal of the American Water Resources Association* **2008**, *44*, 1411–1430, doi:10.1111/j.1752-1688.2008.00233.x.

35. Dhami, B.; Himanshu, S.K.; Pandey, A.; Gautam, A.K. Evaluation of the SWAT Model for Water Balance Study of a Mountainous Snowfed River Basin of Nepal. *Environ Earth Sci* **2018**, *77*, 21, doi:10.1007/s12665-017-7210-8.
36. Azimi, M.; Heshmati, Gh.A.; Farahpour, M.; Faramarzi, M.; Abbaspour, K.C. Modeling the Impact of Rangeland Management on Forage Production of Sagebrush Species in Arid and Semi-Arid Regions of Iran. *Ecological Modelling* **2013**, *250*, 1–14, doi:10.1016/j.ecolmodel.2012.10.017.
37. Grusson, Y.; Sun, X.; Gascoin, S.; Sauvage, S.; Raghavan, S.; Anctil, F.; Sáchez-Pérez, J.-M. Assessing the Capability of the SWAT Model to Simulate Snow, Snow Melt and Streamflow Dynamics over an Alpine Watershed. *Journal of Hydrology* **2015**, *531*, 574–588, doi:10.1016/j.jhydrol.2015.10.070.
38. Qiao, L.; Zou, C.B.; Will, R.E.; Stebler, E. Calibration of SWAT Model for Woody Plant Encroachment Using Paired Experimental Watershed Data. *Journal of Hydrology* **2015**, *523*, 231–239, doi:10.1016/j.jhydrol.2015.01.056.
39. White, J.; Stengel, V.; Rendon, S.; Banta, J. The Importance of Parameterization When Simulating the Hydrologic Response of Vegetative Land-Cover Change. *Hydrol. Earth Syst. Sci.* **2017**, *21*, 3975–3989, doi:10.5194/hess-21-3975-2017.
40. Ficklin, D.L.; Barnhart, B.L. SWAT Hydrologic Model Parameter Uncertainty and Its Implications for Hydroclimatic Projections in Snowmelt-Dependent Watersheds. *Journal of Hydrology* **2014**, *519*, 2081–2090, doi:10.1016/j.jhydrol.2014.09.082.
41. Brooks, H.C.; McIntyre, J.R.; Walkter, G.W. *Geology of the Oregon Part of the Baker 1° by 2° Quadrangle*; State of OR Department of Geology and Mineral Industries: Portland, OR, 1976; p. 28;.
42. Walker, G.W.; MacLeod, N.S.; Miller, R.J.; Raines, G.L.; Connors, K.A. *Spatial Digital Database for the Geologic Map of Oregon, Edition 2.0*; U.S. Geologic Survey: Menlo Park, CA, 2003;
43. Ludington, S.; Moring, B.C.; Miller, R.J.; Stone, P.A.; Bookstrom, A.A.; Bedford, D.R.; Evans, J.G.; Haxel, G.A.; Nutt, C.J.; Flyn, K.S.; et al. *Preliminary Integrated Geologic Map Databases of the United States: The Western States: California, Nevada, Arizona, Washington, Idaho, Utah (OFR 2005-1305), Version 1.3*; U.S. Geological Survey, 2003;
44. Bouyoucos, G.J. Hydrometer Method Improved for Making Particle Size Analyses of Soils. *Agron.j.* **1962**, *54*, 464–465, doi:10.2134/agronj1962.00021962005400050028x.
45. Burt, R.; Soil Survey Staff (ed.) *Soil Survey Field and Laboratory Methods Manual; Soil Survey Investigations Report No. 51; Version 2*; U.S. Department of Agriculture, Natural Resources Conservation Service, 2014; p. 487;.
46. van Genuchten, M.Th.; Leij, F.J.; Yates, S.R. *The RETC Code for Quantifying the Hydraulic Functions of Unsaturated Soils*; U.S. Salinity Laboratory, USDA, ARS, Riverside, California, 1991;
47. van Genuchten, M.Th.; Simunek, J.; Sejna, M. RETC for Windows, Version 6.02 2009.
48. Manning, R.; Griffith, J.P.; Pigot, T.F.; Vernon-Harcourt, L.F. On the Flow of Water in Open Channels and Pipes. *Transactions of the Institution of Civil Engineers of Ireland* **1890**, *20*, 161–207.
49. Oregon 10m Digital Elevation Model (DEM) Available online: https://spatialdata.oregonexplorer.info/geoportal/details;id=7a82c1be50504f56a9d49d13c7b4d9aa (accessed on 6 February 2020).

50. National Land Cover Dataset (NLCD) (accessed on 2 February 2020).
51. D. N. Moriasi; J. G. Arnold; M. W. Van Liew; R. L. Bingner; R. D. Harmel; T. L. Veith Model Evaluation Guidelines for Systematic Quantification of Accuracy in Watershed Simulations. *Transactions of the ASABE* **2007**, *50*, 885–900, doi:10.13031/2013.23153.
52. *National Engineering Handbook, Part 630 Hydrology, Chapter 9, Hydrologic Soil-Cover Complexes*; United States Department of Agriculture, National Resources Conservation Service, 2004;
53. Cao, W.; Bowden, W.B.; Davie, T.; Fenemor, A. Multi-Variable and Multi-Site Calibration and Validation of SWAT in a Large Mountainous Catchment with High Spatial Variability. *Hydrological Processes* **2006**, *20*, 1057–1073, doi:10.1002/hyp.5933.
54. X. Zhang; R. Srinivasan; M. Van Liew Multi-Site Calibration of the SWAT Model for Hydrologic Modeling. *Transactions of the ASABE* **2008**, *51*, 2039–2049, doi:10.13031/2013.25407.
55. Athira, P.; Sudheer, K.P. Calibration of Distributed Hydrological Models Considering the Heterogeneity of the Parameters across the Basin: A Case Study of SWAT Model. *Environ Earth Sci* **2021**, *80*, 131, doi:10.1007/s12665-021-09434-8.
56. Abiodun, O.O.; Guan, H.; Post, V.E.A.; Batelaan, O. Comparison of MODIS and SWAT Evapotranspiration over a Complex Terrain at Different Spatial Scales. *Hydrology and Earth System Sciences; Katlenburg-Lindau* **2018**, *22*, 2775–2794, doi:http://dx.doi.org.ezproxy.proxy.library.oregonstate.edu/10.5194/hess-22-2775-2018.
57. R. Jiang; Y. Li; Q. Wang; K. Kuramochi; A. Hayakawa; K. P. Woli; R. Hatano Modeling the Water Balance Processes for Understanding the Components of River Discharge in a Non-Conservative Watershed. *Transactions of the ASABE* **2011**, *54*, 2171–2180, doi:10.13031/2013.40656.
58. Le Moine, N.; Andréassian, V.; Perrin, C.; Michel, C. How Can Rainfall-Runoff Models Handle Intercatchment Groundwater Flows? Theoretical Study Based on 1040 French Catchments. *Water Resources Research* **2007**, *43*, doi:10.1029/2006WR005608.
59. Hughes, J.D.; Langevin, C.D.; Banta, E.R. *Documentation for the MODFLOW 6 Framework*; Techniques and Methods; U.S. Geological Survey: Reston, VA, 2017; Vol. 6-A57;.
60. Langevin, C.D.; Hughes, J.D.; Banta, E.R.; Niswonger, R.G.; Panday, S.; Provost, A.M. *Documentation for the MODFLOW 6 Groundwater Flow Model*; U.S. Geological Survey, 2017;
61. Sao, D.; Kato, T.; Tu, L.H.; Thouk, P.; Fitriyah, A.; Oeurng, C. Evaluation of Different Objective Functions Used in the SUFI-2 Calibration Process of SWAT-CUP on Water Balance Analysis: A Case Study of the Pursat River Basin, Cambodia. *Water* **2020**, *12*, 2901, doi:10.3390/w12102901.
62. Pfannerstill, M.; Bieger, K.; Guse, B.; Bosch, D.D.; Fohrer, N.; Arnold, J.G. How to Constrain Multi-Objective Calibrations of the SWAT Model Using Water Balance Components. *JAWRA Journal of the American Water Resources Association* **2017**, *53*, 532–546, doi:10.1111/1752-1688.12524.
63. Her, Y.; Seong, C. Responses of Hydrological Model Equifinality, Uncertainty, and Performance to Multi-Objective Parameter Calibration. *Journal of Hydroinformatics* **2018**, *20*, 864–885, doi:10.2166/hydro.2018.108.
64. Zhang, L.; Xue, B.; Yan, Y.; Wang, G.; Sun, W.; Li, Z.; Yu, J.; Xie, G.; Shi, H. Model Uncertainty Analysis Methods for Semi-Arid Watersheds with Different Characteristics: A Comparative SWAT Case Study. *Water* **2019**, *11*, 1177, doi:10.3390/w11061177.

65. Demirel, M.C.; Venancio, A.; Kahya, E. Flow Forecast by SWAT Model and ANN in Pracana Basin, Portugal. *Advances in Engineering Software* **2009**, *40*, 467–473, doi:10.1016/j.advengsoft.2008.08.002.

CHARACTERIZATION OF STREAM TEMPERATURE DYNAMICS IN A SEMIARID WATERSHED IN EASTERN OREGON, USA

Characterization of stream temperature dynamics in a semiarid watershed in eastern Oregon, USA

Abstract: Increasing stream temperatures are a concern in many areas of the world. However, more research is needed to understand the unique stream dynamics of semiarid systems. This study examined temperature patterns at a small stream and a tributary at a semiarid watershed in eastern Oregon, USA. Land cover at this site includes conifer and deciduous woodlands and sagebrush steppe. Multiple stream temperature sensors were located along the longitudinal gradient of the system, representing areas of different elevation, riparian cover, and streamflow volume. The daily mean, daily maximum, daily minimum, and moving averages of the daily max (7DADM) and daily mean (7DA) stream temperature were calculated. The diurnal range of stream temperature was also examined. A support vector machine (SVM) classifier was used to delineate land cover types in the riparian areas. A support vector regression (SVR) approach was used to assess the relationship between environmental characteristics (e.g., air temperature, riparian land cover) and 7DADM. Air temperature was found to explain the majority of stream temperature variation, followed by sagebrush steppe and forested cover. The SVR approach performed better at predicting 7DADM (R^2=0.83) than diurnal stream temperatures (R^2=0.55). The results of this study highlight the importance of considering multiple biotic and abiotic factors in assessing stream temperature patterns in semiarid systems.

Keywords: Stream temperature; rangelands; riparian; semiarid

1. Introduction

Stream temperature is a key water quality concern in many regions of the world and impacts biotic and abiotic processes and characteristics within the ecosystem [1,2]. The relationship between land use practices and stream temperature dynamics has also been an area of considerable research [3]. However, many sites, particularly in semiarid and arid regions, have limited on-site data available making addressing the complex relationships between environmental characteristics (including land use) and stream temperature dynamics challenging. Approaches that use a combination of techniques and data sources, such as on-site measurements

with satellite-based imagery, may provide greater insight into stream temperature dynamics in these regions by facilitating a more in-depth examination of stream characteristics.

Stream temperature is impacted by a combination of external factors (e.g., solar radiation) and stream channel characteristics (e.g., geomorphology, substrate, channel width) [4]. Heat fluxes in and out of the system are key drivers of stream temperature. This includes solar radiation, longwave radiation, convection, evaporation, conduction between the water and the stream bed, as well as groundwater inflows and outflows. In streams where groundwater inputs are present, stream temperature can be strongly influenced by groundwater advection [5]. Groundwater inputs, such as those from perennial springs or seeps, may buffer stream temperature changes [6]. Further, streamflow volume influences stream temperature by affecting the heat capacity and greater streamflow rates are associated with reduced temperatures in many study sites [7,8].

Riparian vegetation has been recognized as a critical factor in stream temperature dynamics in many systems (e.g. [9–11]), as increased shade reduces the amount of solar radiation reaching the channel [12,13]. The type of riparian vegetation, including deciduous vs. forested tree cover, has been shown to impact stream energy fluxes [14]. Past studies have also indicated the importance of addressing riparian canopy characteristics in conjunction with other factors, such as streamflow [15] and channel orientation [16].

Land use practices, particularly those that impact riparian areas, have the potential to impact energy fluxes and lead to altered stream temperature regimes. For example, [17] found that non-grazed reaches had denser riparian vegetation and experienced lower daily maximum temperatures compared to grazed reaches for a study site in CA. However, the impacts of grazing on riparian vegetation also vary with climate and grazing pressure [18]. Reductions in riparian vegetation have been associated with increased stream temperature in numerous locations (e.g., [12,13,19]) and those impacts are sometimes more pronounced in smaller streams, depending on hyporheic exchange [4]. Irrigation and groundwater withdrawals can lead to altered stream temperatures as well by reducing and/or altering streamflow [20,21].

Air temperature, along with characteristics such as streamflow (e.g.,[22]), land cover (e.g., [23]), and sun angle (e.g., [24], has frequently been used as a predictor of stream temperature (e.g., [25–27]). However, regression approaches may be limited in their ability to

predict temperature extremes or future conditions [28]. Additionally, air temperature may not be a sufficient predictor in areas with variable and significant groundwater inputs [5].

This study takes a systems-based approach to characterize stream temperature dynamics at a semiarid study site in eastern OR, USA. We hypothesized that air temperature, the amount of forest cover, and streamflow would be key factors in predicting stream temperature. We also anticipated that we would see greater diurnal range in stream temperatures at downstream sites compared to those further upstream. Specific objectives of this study were to 1) examine channel characteristics and condition at selected reaches along the system, 2) characterize stream temperature patterns along the longitudinal gradient, and 3) assess the relationship between stream temperature and meteorological characteristics (e.g., air temperature and vapor pressure deficit), land cover, and streamflow.

2. Methods

2.1 Site Description

This study took place at a semiarid watershed located outside of Ironside, OR, USA (44.42° N, 117.91° W). Based on data collected from on-site weather stations and using Parameter-elevation Regressions on Independent Slopes Model datasets (PRISM; [29]), the average annual precipitation from 2016 to 2021 was 345 mm yr^{-1}. Elevation at the study site ranges from 1076 to 1950 m. Perennial and seasonal streams are present in the watershed. Igneous, volcanic rock and clastic sedimentary rock are present throughout much of the study site [30,31]. Multiple springs and seeps are found at the study site, particularly in higher elevations of the watershed.

Land cover varies from sagebrush steppe/shrubland ecosystems in the upper most portions of the watershed and conifer forests in the mid-upper to middle reaches of the watershed and transitions into predominantly sagebrush-dominated areas with some deciduous riparian forest cover in the lower areas. The prominent land uses in the region are agricultural production, including dryland and irrigated pastures, cattle ranching, and forestry.

2.2 Data Collection

2.2.1 Stream Temperature

Stream temperature was recorded using two types of sensors, the HOBO Tidbit and Pendant MX Water Temperature Data Loggers (Onset Computer Corporation, Bourne, MA, USA). Stream temperature sensors were located along the longitudinal gradient of Fish Creek ("FC") and Deer Creek ("DC") (Figure 1), to include temperature sensors placed at the headwaters. FC and DC are spring-fed systems with snowmelt and runoff contributing to streamflow during the late spring. Stream temperature data used in this study began in October 2018 and ended in June 2022.

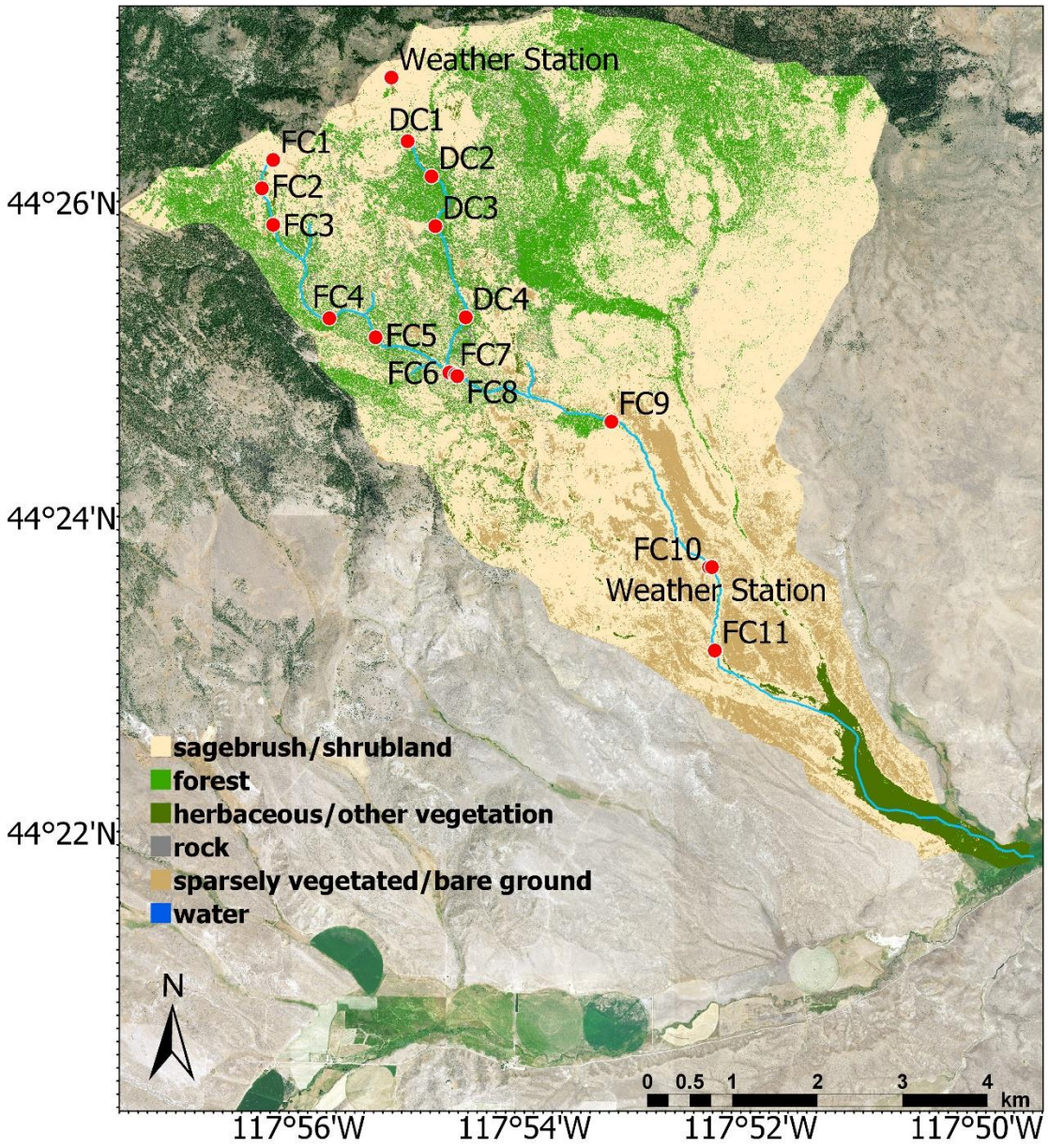

Figure 1. Locations of weather stations and stream temperature stations. Sensors along Fish Creek are indicated by "FC" and those along Deer Creek are indicated by "DC". A flume for monitoring streamflow is located near FC10. This map was created using ArcGIS® software by Esri. ArcGIS® and ArcMap™ are the intellectual property of Esri and are used herein under license. Copyright © Esri. All rights reserved. For more information about Esri® software, please visit www.esri.com. Basemap credits: U.S. Department of Agriculture (USDA), National Agriculture Imagery Program (NAIP); USDA-FSA-APFO Aerial Photography Field Office, publication date: 5 and 14 August 2020.

Stream temperature data were recorded hourly. The daily mean, daily maximum, daily minimum, seven-day moving average of the daily mean (7DA), and seven-day moving average of the daily maximum (7DADM) stream temperatures were calculated. Additionally, the diurnal stream temperature range was calculated for each site by subtracting the daily minimum stream temperature from the daily maximum stream temperature.

2.2.2 Proper Functioning Condition and Riparian Vegetation Assessment

A Proper Functioning Condition (PFC; [32]) assessment was conducted for two reaches in the study area: one near FC3 ("FC-Upper") and one near FC10 ("FC-Lower") in August 2019. The PFC is a qualitative, checklist-based approach to evaluating the physical functioning and condition of riparian or wetland areas for perennial or intermittent natural streams. A PFC includes an assessment of vegetation, channel morphology and characteristics, and woody debris. The PFC uses the Rosgen classification ([33]) to describe stream morphology.

Assessments of stream channel condition were conducted at the two 110 m reaches (FC-upper, FC-lower). Stream assessments at each reach included measurements of bankfull channel width, maximum bankfull depth, stream slope, and sinuosity. In addition to the PFC assessment, data regarding soil, litter, and vegetation cover by functional species were collected using the line-point intercept method [34] along three 30-m transects running perpendicular to the 110-m reaches. The three transects were established at 0, 55, and 110 m measured downstream along the reach.

2.2.3 PRISM Data

Parameter-elevation Regressions on Independent Slopes Model (PRISM; [29]) datasets were used to estimate the precipitation, minimum, mean, and maximum air temperature the minimum and maximum vapor pressure deficit, and the mean dewpoint temperature for each stream temperature sensor location using the bulk download time series page. The PRISM data used in this study have a spatial resolution of 4 km. PRISM data were used for creating the SWAT model and for the SVR model.

2.2.4 On-site Weather, Streamflow, and Soil Moisture Data Collection

On-site meteorological data were collected at two locations at the study site (Figure 1). The first weather station was installed in 2018 near the top of the watershed and a second weather station was installed in 2019 near FC10 (Figure 1). Data collected included air temperature and relative humidity (CS215 probe; Campbell Scientific, Inc., Logan, UT, USA), wind speed and direction, (model 03002; R.M. Young Company, Travers City, MI, USA), barometric pressure (CS100; Campbell Scientific, Inc., Logan, UT, USA), precipitation (TE525 tipping bucket; Texas Electronics, Inc., Dallas, TX, USA), and incoming shortwave radiation (Apogee CS300 pyranometer; Apogee Instruments, Inc., Logan, UT, USA). A CR800 (Campbell Scientific, Inc., Logan, UT, USA) datalogger was used.

Soil moisture data were also collected at both weather stations using CS650 water content sensors (Campbell Scientific, Inc., Logan, UT, USA). Hourly soil moisture data at 0.2 m and 0.5 m were collected at the upper-most weather station and at 0.2 m, 0.5 m, and 0.8 m at the weather station near FC10 (see Figure 1). Soil moisture measurements across the soil profile were averaged and then multiplied by the total depth of the soil profile (0.5 m or 0.8 m). The permanent wilting point of the soils was estimated using the Retention Curve (RETC) computer program (Version 6.02, see [35] and [36]) based on measurements of bulk density and soil texture data obtained at each weather station. The permanent wilting point was subtracted from the averaged soil moisture data to estimate the available water content (AWC), similar to the approach described by [37].

Measurements of streamflow data were obtained using a 0.6 m wide ramp-style flume equipped with a water level logger (Hobo Model U20L, Onset Computer Corporation, Bourne, MA, USA) beginning in April 2021. Streamflow measurements were calculated based on the height of the water and the dimensions of the flume (see [38]).

2.3 Soil and Water Assessment Tool

In order to estimate the streamflow in the watershed, we used the Soil Water Assessment Tool (SWAT) using the ArcSWAT extension in ArcMap 10.7.1 (Environmental Systems Research Institute; Redlands, CA). A daily timestep was used in the model. A combination of PRISM data and on-site weather station data was used to build the model. Weather data from 1 January 2016 until 31 December 2021 were used, with two years used as a “warm-up”. A 10-m

digital elevation model (https://spatialdata.oregonexplorer.info , [39]) was used to delineate the watershed. National Land Cover Database (NLCD; [40]) data from 2019 were used to identify land cover and the State Soil Geographic (STATSGO) data were used to delineate soil types within the model.

During watershed delineation, a stream path was not indicated in SWAT for FC1, FC2, or FC3 due to very limited streamflow in this area. Streamflow data were also not modeled for FC11 (the furthest downstream point) as the flume is located at FC10. FC10 was used as the outlet of the watershed for the SWAT model.

2.3.1 SWAT Calibration and Validation

The SWAT Calibration and Uncertainty Program (SWAT-CUP; [41,42]) was used to perform parameter sensitivity, calibration, and validation. Streamflow (Q) near FC10 for 2021 and on-site measurements of plant available water content located near the top of the watershed ("AWC_upslope") and near FC10 ("AWC_FC10") from 2018, 2019, and 2021 were used for calibration. Validation was performed using the available water content data from AWC_upslope and AWC_FC10 from 2020.

Nash-Sutcliff (NS) was used as the objective function. The range of parameters that indicated the best NS were used for subsequent iterations. An initial calibration iteration with 500 simulations was performed using only streamflow with 26 parameters (Appendix 1). Subsequent calibration iterations were performed using streamflow and soil moisture and a sensitivity analysis was performed using the Sequential Uncertainty Fitting (SUFI-2) algorithm. Based on the sensitivity analysis results, parameters considered statistically significant (at $p \leq 0.05$) were selected for further calibration. Additionally, based on the results of past studies at this site, we included soil available water content parameters separated into groups based on hydrologic soil type and layer into calibration. Parameters used for final calibration and validation are shown in Table 1.

Table 1. Parameters used in final calibration and validation of SWAT model.

Parameter	Definition
CN2	Curve number

CH_N1	Manning's roughness coefficient for tributary
SFTMP	Snowfall temp (°C)
SNOCOVMX	Minimum snow water content at 100% snow cover
SOL_AWC	Average soil available water capacity
SOL_K	Saturated hydraulic conductivity (mm hr^{-1})

2.4 Land Cover Classification

We assessed riparian cover characteristics along the length of the streams using U.S. Department of Agriculture National Agricultural Imagery Program (NAIP; [43]) imagery from 2020 downloaded from the U.S. Geological Survey Earth Resources Observation and Science website (https://earthexplorer.usgs.gov/). An object-based support vector machine (SVM) approach was used to classify the NAIP imagery using the Classification Wizard tool in ArcGIS Pro [Environmental Systems Research Institute (ESRI); Version 2.9; Redlands, CA, USA]. A segmented image was created for classification using the Segmentation tool in ArcGIS Pro. For the segmentation process, spectral detail and spatial detail were both set at 20 and the minimum segment size was 9 pixels. Training samples were created for the following categories: forested cover, sagebrush/shrubland, other vegetation (largely herbaceous vegetation), bare ground/sparsely vegetated, and rock/gravel. To train the SVM classifier, the following segment attributes were used: active chromaticity color, mean digital number, compactness, and rectangularity. A maximum of 500 samples per class were used in the SVM classification. The ArcGIS reclassification tool was used to correct areas that were misclassified. Following the initial classification, the majority filter tool in ArcGIS was applied using eight neighbors and a majority replacement threshold. Next, the boundary clean tool was applied to smooth the boundaries between individual classes. No sorting approach was used (this is the default).

Based on the above land classifications, three categories of land cover were used in the stream temperature models: forest cover, sagebrush/shrubland, and herbaceous/other vegetation. While tree cover and large areas of herbaceous cover are easy to delineate, the resolution of NAIP was insufficient to clearly delineate individual shrub-sized vegetations. Therefore, the

sagebrush/shrubland land cover class contain indicates areas that likely include a mixture of vegetation diversity and cover characteristics.

In order to assess riparian vegetation cover, 30 m wide buffers for 300 m upstream of each stream temperature sensor were created in ArcGIS. The percentage of pixels within these buffers classified as either forested ("30m_for"), sagebrush or other shrub cover ("30m_sage"), or herbaceous/other vegetation ("30m_herb") were calculated. For the stream temperature sensors located at the headwaters of Fish Creek and Deer Creek, the pixels that fell within a 30 m radius of the stream temperature sensor were used for analysis.

2.5 Support Vector Regression Model

To assess how well environmental characteristics predicted 7DADM or the diurnal stream temperature range, a support vector regression (SVR) approach, similar to the one described by [44], was used. The SVR analysis used data from October 2018 until November 2021. The two temperature stations located at the headwaters (DC1 and FC1) are located in springs and were excluded from the SVR analysis as the temperature patterns showed very little daily or seasonal change throughout the time period observed. The SVR used data from October 2018 until December 2021 as non-provisional data were not available beyond December 2021 at the time of this report.

We used ten parameters for the initial SVR analysis: elevation (in m), mean daily air temperature (in °C, "temp_mean"), mean daily dew point temperature ("TD_mean"), daily precipitation (in mm, "ppt"), daily minimum and maximum vapor pressure deficit in hPA ("VPD_min" or "VPD_max"), SWAT-modeled daily streamflow in cms ("Q"), and the three categories of vegetation cover ("30m_herb", "30m_sage ", and "30m_for"). These parameters were selected to represent key meteorological and land cover characteristics.

While SVR models are non-parametric, we assessed the skew of individual parameters to improve model performance. Parameters that had a |skew|>1 (ppt, Q, VPD_min, and VPD_max) were transformed using a natural log prior to being input into the model. Python was used to run the SVR model, based on algorithms from scikit learn (sklearn.svm.SVR; [45]). Half of the data were used for training and half were used for cross-validation of the model. A linear kernel was used.

To tune the model, the range for the regularization parameter (C) was set between 10^{-6} and 10^{2}. The R^2 for the training and testing datasets were compared for each training iteration (n=100) using a randomly selected value for C. If the difference in the coefficient of determination (R^2) between the training and testing values exceed 0.1, overfitting was assumed and the C-value was excluded from analysis. The C value which yielded the best R^2 was used for the final model (iterations=1000) and perform the sensitivity analysis.

The independent influence of each parameter was assessed during the sensitivity analysis. During this process, each parameter individually was allowed to vary by two standard deviations while the other parameters were held at a constant value. Overall model performance was assessed using the R^2 between observed and modeled values.

3. Results

3.1 Riparian Vegetation Assessment

The PFC assessment indicated that the FC-Upper reach was "functional-at risk" with an apparent downward trend. This rating was largely given because of the limited presence of stabilizing vegetation along the streamside. Minimal disturbance attributed to upstream or upland areas was found. Light to moderate streambank erosion was found but the stream was found to be vertically stable with no indications of significant erosion (i.e., degradation) or deposition. The Fish Creek-Upper had a bankfull width-depth ratio of 11.4 and an average entrenchment ratio of 1.4. The reach was determined to be a Stream Type "A" on the Rosgen scale, indicating a moderately sloped (4-10%), entrenched stream, with low sinuosity. Data collected from the three transects perpendicular to the reach indicated that 19% of the understory cover were grasses, 4% were forbs, and 1% were shrubs, while litter accounted for 42% and bare soil accounted for 28% of the surveyed site. Water accounted for 6% of the surveyed area.

The FC-Lower reach was found to be "functional-at risk" with no apparent trend. This reach was found to have a good diversity of vegetation types but limited vegetation age diversity. Some areas along this reach showed reduced vegetation growth associated with trampling, presumably from cattle or elk. The FC-Lower reach showed a stream slope of 2-4% with low sinuosity and moderate entrenchment (2.0 ratio), indicating a Rosgen Type B stream. Based on three 30 m transects, most of the understory cover was grass (19%), followed by shrubs (4%).

Litter accounted for 66% of the understory layer. Bare soil was found at 4% of the surveyed transect points, while rock and water each accounted for 3% of surveyed sites.

3.2 Streamflow

The SWAT model calculates streamflow based on stream reaches, therefore the same streamflow was indicated for multiple stream sensor locations when sensor locations fell within in the same reach. The average annual SWAT-modeled streamflow for the reach including DC1 through DC4 was 0.013 cms. For the reach including FC7, the modeled average annual streamflow was 0.039 cms. The modeled average annual streamflow was 0.019 cms at FC4. SWAT indicated that streamflow originated at FC4 and not at the spring (FC1). Observed flow from FC1 through FC4 is intermittent with areas of minimal surface flow during some seasons. The modeled annual streamflow was 0.023 cms at FC5, 0.045 cms at FC6, 0.039 cms at FC8, 0.048 cms at FC9, and 0.049 cms at FC 10.

Observed streamflow and modeled streamflow rates at the flume at FC10 are shown in Figure 2. The SWAT model indicated large very brief (1 to 2 day) early-season (March to April) peaks in streamflow that fell outside of the limited period of data collection. These peaks in streamflow exceeded observed streamflow conditions on-site. These brief periods of high streamflow were excluded from the SVR analysis.

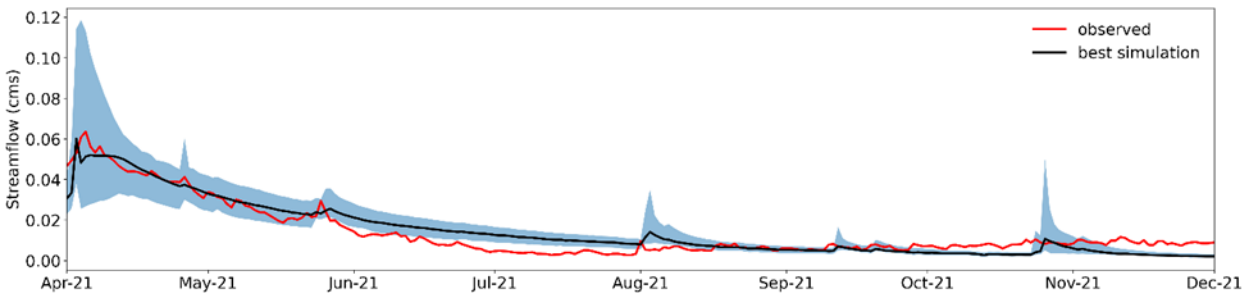

Figure 2. Modeled streamflow at FC10 versus observed streamflow. The shaded blue area represents the 95% confidence range

The NS calibration results ranged from 0.47 (AWC at FC10) to 0.86 (streamflow at FC10) (Table 2).

Table 2. SWAT calibration results for the coefficient of determination (R^2), Nash-Sutcliffe (NS), adjusted R^2, and mean squared error (MSE).

Variable	R^2	NS	bR^2	MSE
FC10 Streamflow	0.87	0.86	0.81	0.00
AWC Upslope	0.80	0.75	0.49	740.00
AWC FC10	0.49	0.47	0.28	690.00

As limited streamflow data were available, we used AWC data for validation. Based on NS, validation results ranged from 0.71 to 0.82 (Table 3).

Table 3. SWAT validation results.

Variable	R^2	NS	bR^2	MSE
AWC Upslope	0.89	0.82	0.66	530.00
AWC FC10	0.77	0.71	0.47	710.00

3.3 Stream Temperature Along Longitudinal Gradient

Water temperatures at the spring headwater sites (FC1 and DC1) were generally similar throughout the year (Tables 4 and 5, Figure 3). While summer stream temperatures were generally greater at lower elevation sites compared to higher elevation sites, this pattern did not hold true for seasonal stream temperatures or for all locations. For example, we saw an increase in summer 7DADM and 7DA from DC 1 to DC2 and a decrease in summer 7DADM and summer 7DA from DC2 to DC3. However, the annual 7DADM and 7DA were both greater at DC3 compared to DC2. The forest cover within 30 meters of the stream is 42% at DC2 and 72% at DC3. In contrast, we saw an increase in annual and summer 7DADM and summer 7DA between FC2 and FC3, where the forest cover increased from 17% at FC2 to 55% at FC3. However, annual and summer 7DADM were both lower at FC4 and compared to FC3.

Table 4. The 7-day moving average of the daily maximum stream temperature (7DADM) in °C, elevation, and vegetation cover characteristics for all sites from 20 September 2018 through 16 June 2022. Vegetation cover characteristics indicate the percentage of pixels classified as each land cover classification within an area 30 m wide, 300 m upstream of each sensor, except for the headwater stream locations (FC1 and DC1). For FC1 and DC1, the vegetation cover within a 30 m radius was used for characterization.

Location	Annual 7DADM	Summer 7DADM	Elevation (m)	% herbaceous/other	% shrub	% forest
FC1	9.1	9.5	1731	2	97	0
FC2	8.6	11.2	1667	7	67	17
FC3	9.7	17.5	1607	4	32	55
FC4	7.6	14.7	1506	6	45	37
FC5	6.6	15.2	1451	1	44	39
FC6	7.5	16.6	1376	4	57	25
FC7	9.4	20.2	1368	3	51	31
FC8	10.1	20.5	1364	3	51	32
FC9	8.4	15.7	1265	18	31	49
FC10	9.8	20.2	1185	2	83	9
DC1	8.2	8.9	1714	11	60	16
DC2	7.6	22.1	1665	9	31	42
DC3	8.1	15.4	1610	1	12	72
DC4	7.1	18.9	1450	<1	38	50

Table 5. The average 7-day moving average (7DA), mean daily, minimum (Min) daily, and maximum (Max) daily stream temperature in °C for selected sites. For 7DA and mean annual, data from 20 September 2018 through 16 June 2022 were used. Summer temperatures refer to measurements taken during July, August, and September and winter temperatures refer to measurements taken during January, February, and March for this same period.

Location	7DA-Summer	7DA-Annual	Mean-Summer	Mean-Annual	Max-Summer	Min-Winter
FC1	9.3	9	9.3	9	9.5	8.5
FC2	10.2	7.7	10.2	7.7	11.2	5.1
FC3	11.4	6.4	11.4	6.4	17.3	1.8
FC6	13.1	5.8	13.1	5.8	16.5	1
FC7	14.2	6.3	14.2	6.4	20.1	0.8
FC8	14	6.7	13.9	6.7	20.3	0.6
FC10	14.8	6.5	14.6	6.6	19.9	0.5
DC1	8.8	8.2	8.8	8.2	8.9	7.7
DC2	13.8	4.7	13.5	4.7	21.7	0.9
DC3	11.5	5.9	11.5	5.9	15.4	1.7

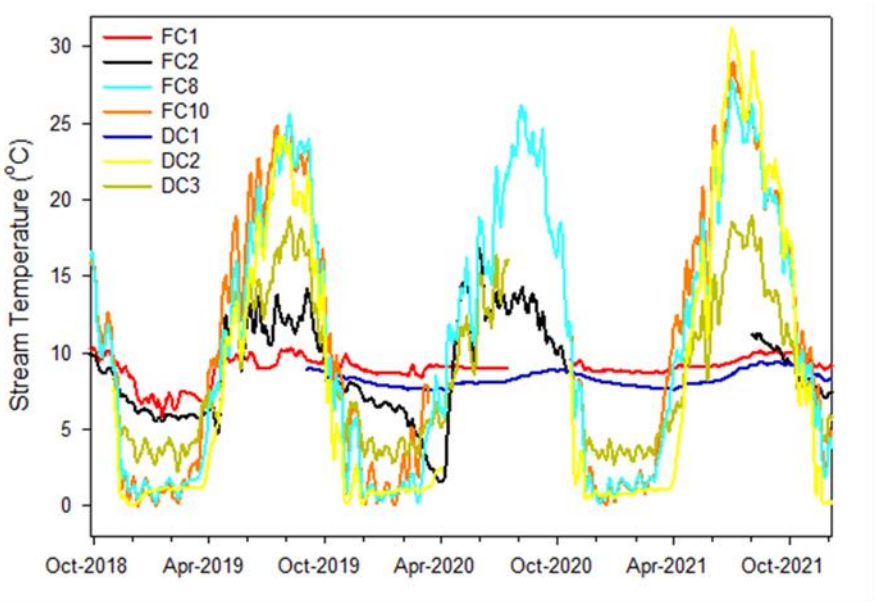

Figure 3. The 7-day moving average of the daily maximum stream temperature (7DADM) for selected sites.

Diurnal ranges in stream temperature for each quarter varied along the longitudinal gradient (Table 6). The headwater locations (springs) demonstrated the least variability in daily water temperature ranges. The mean daily range in stream temperatures was 0.3 °C at FC1 and 0.1 °C at DC1. By comparison, the mean daily range was 4.7 °C at DC2 and 3.9 °C at DC3. The mean daily range in stream temperatures was 4.9 at FC3, 3.0 at FC6, 5.8 at FC8, 3.1 at FC 9, and 5.6 at FC10. The largest ranges in daily stream temperatures were generally observed during the summer months (July through September).

Table 6. Average range in daily stream temperature for selected sites, by season and annually for 20 September 2018 through 16 June 2022. Quarter 1 (Q1) refers to January through March, and so on. “All” indicates the average of the daily temperature variation for the entire time period. Temperatures are in °C.

	FC1	FC2	FC3	FC4	FC6	FC8	FC9	FC10	DC1	DC2	DC3	DC4
Q1	0.2	0.5	3.0	1.7	1.3	2.0	2.0	2.7	0.1	0.3	2.6	1.1
Q2	0.3	3.7	5.5	5.3	4.6	8.6	6.2	9.9	0.0	6.6	5.4	4.9
Q3	0.4	1.7	8.5	6.4	6.3	10.6	3.7	9.6	0.1	13.0	6.4	6.9
Q4	0.3	1.0	3.6	2.1	1.4	3.1	1.3	3.1	0.1	1.8	2.2	1.5
All	0.3	1.8	4.9	3.5	3.0	5.8	3.1	5.6	0.1	4.7	3.9	3.1

Excluding the spring headwater locations (DC1 and FC1), seasonal stream temperature patterns generally followed daily air temperature patterns (Figure 4). As expected, patterns in VPD also followed air temperature, but exhibited a larger range in values.

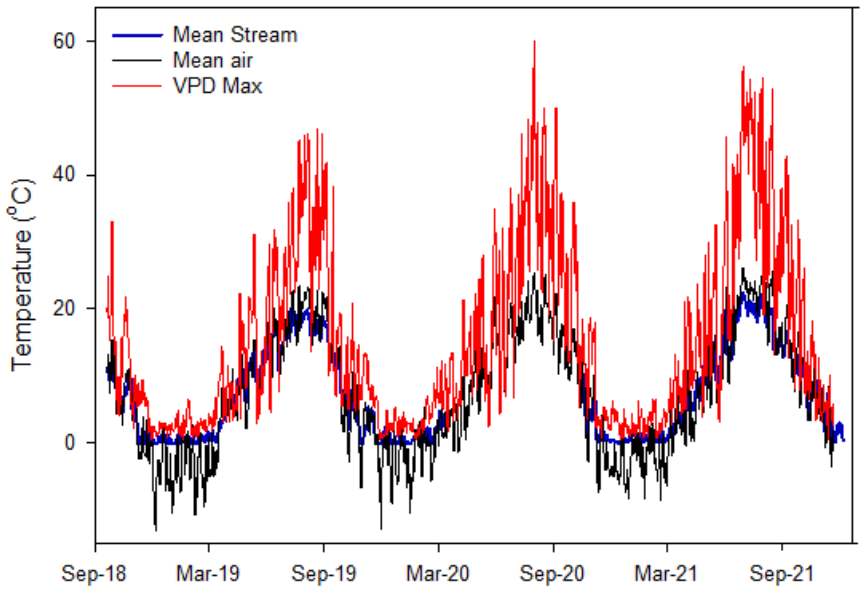

Figure 4. Mean stream temperature at FC10 and PRISM-based estimates of mean daily air temperature (“Mean air) and maximum vapor pressure deficit (VPD) for September 2018 through December 2021.

3.4 Support Vector Regression Model

The mean daily air temperature was the most important parameter in predicting 7DADM or the diurnal range, followed by sagebrush/shrubland land cover, forest cover, and daily maximum vapor pressure deficit (Figure 5). However, the SVR model was more effective at predicting 7DADM (R^2=0.83) compared to the diurnal range (R^2=0.55) of stream temperatures (Figure 6).

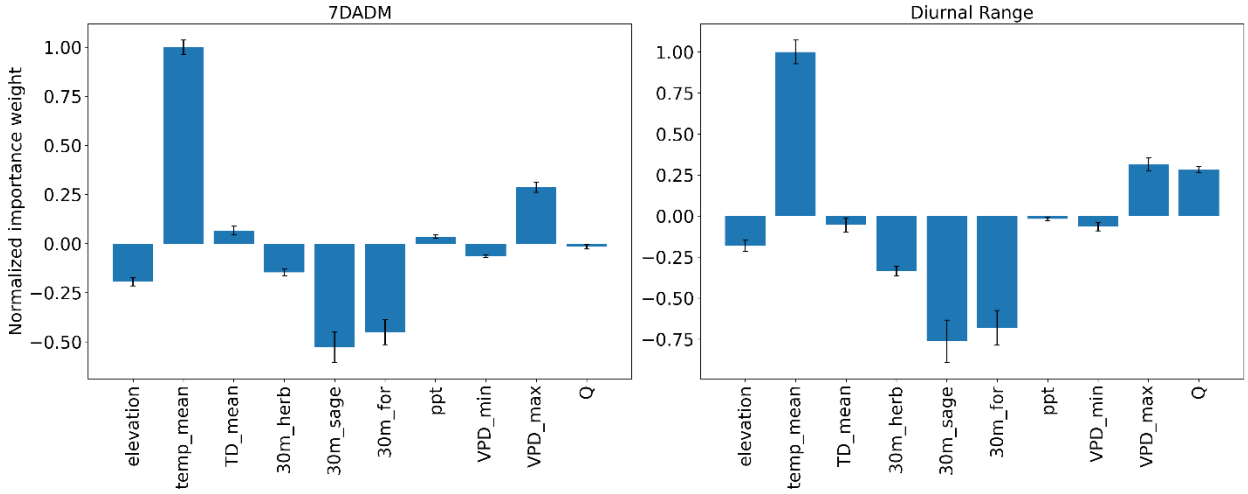

Figure 5. Weighted importance of each parameter for the 7DADM and diurnal-range SVR models.

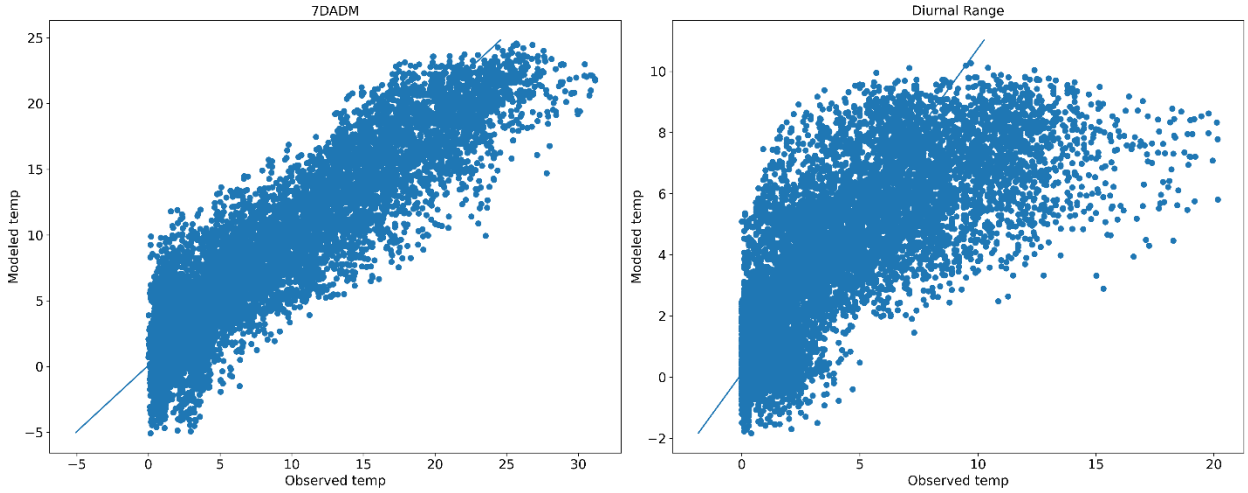

Figure 6. Scatterplots of modeled versus observed stream temperature values for both SVR models.

For both the 7DADM and diurnal range SVR approaches, peak modeled values tended to be lower than peak observed values (Figures 7 and 8). Additionally, as we used a linear model, the SVR model did not account for stream temperature patterns at freezing temperatures and predicted a continual decrease in stream temperatures.

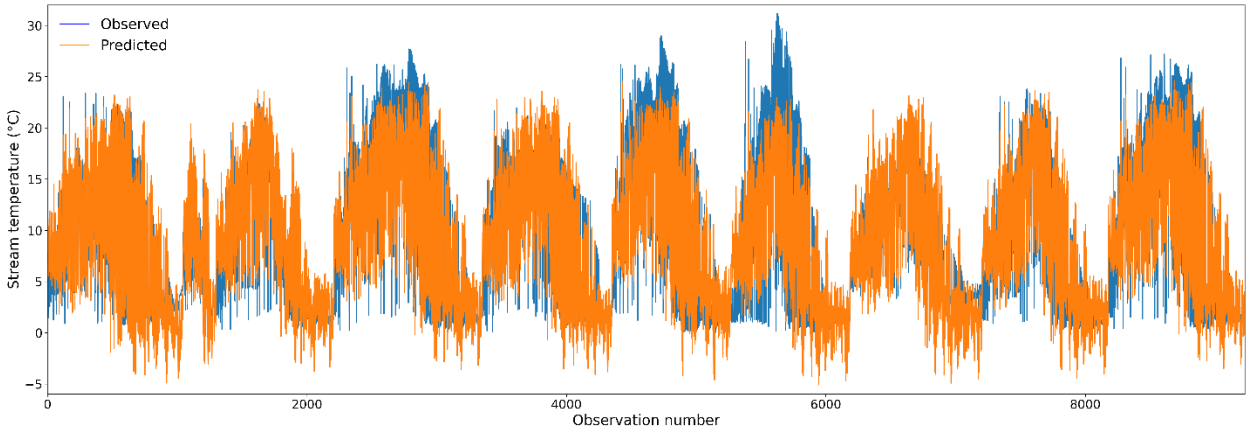

Figure 7. Comparison of observed and predicted stream temperatures for the 7DADM SVR model. “Observed” refers to on-site measurements of stream temperature. “Predicted” refers to the average modeled value across all iterations.

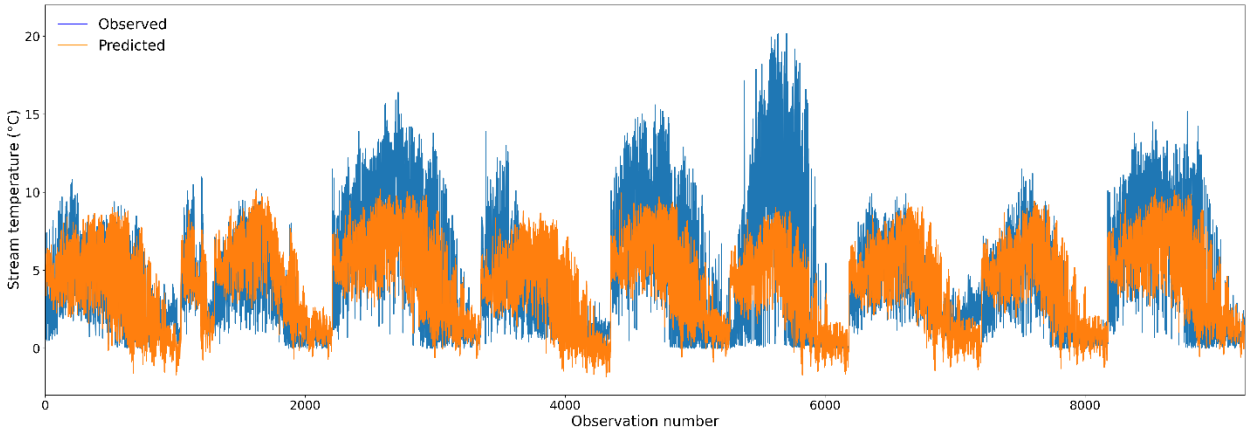

Figure 8. Comparison of observed and SVR-predicted stream temperatures diurnal ranges. “Observed” refers to on-site measurements of stream temperature ranges. “Predicted” refers to the average modeled value across all iterations.

4. Discussion

This study was a preliminary examination of stream temperature and ecohydrologic characteristics at a semiarid watershed in eastern Oregon. Stream temperature patterns were assessed along the longitudinal gradient, and included areas with varying land cover, streamflow, and meteorological (e.g., air temperature, precipitation) characteristics. Additionally, we assessed the stream condition at two reaches in the study site. Specific objectives of this study were to 1) examine channel characteristics and condition at selected reaches along the system, 2) characterize stream temperature patterns along the longitudinal gradient, and 3) assess the relationship between stream temperature and meteorological characteristics (e.g., air temperature and vapor pressure deficit), land cover, and streamflow.

Similar to other studies [27,46], we found that air temperature was the strongest predictor of stream temperature. Sagebrush/shrubland and forest cover were found to be the second and third most important predictors of stream temperature, respectively, with greater amounts of either being associated with decreased stream temperature. It is important to note, that stream and air temperature are influenced by solar radiation. Additionally, while several past studies have found that forest cover is associated with cooler stream temperatures (e.g., [47,48]), sagebrush also provides, to varying degrees, shade when growing near the stream. However, the density of vegetation in sagebrush steppe areas varies throughout the watershed, although we assumed a relatively vegetation density in the areas nearest the stream. The association between sagebrush/shrubland and stream temperature in this study may be because larger amounts of shrubland cover are found near the headwaters (although sagebrush steppe is found throughout the watershed) where stream temperatures tended to be cooler. Additionally, more herbaceous vegetation is present in the lower elevation reaches where stream temperatures are highest.

The spatial (1 m) and temporal (on average, every 3 years during the growing season) resolution of the NAIP imagery is another important consideration. Due to the limitations of image spatial resolution used for classification, individual sagebrush canopy could not be discerned while forested cover is clearer. Therefore, areas delineated as sagebrush/shrubland may likely have heterogenous cover and vegetation characteristics (e.g., the density of sagebrush shrubs and/or perennial grasses may be greater in some areas than others which fall under the same land cover classification).

We also anticipated that streamflow would be more strongly associated with stream temperatures, based on the results of past studies [44] and because of the link between streamflow and stream heat capacity. This lack of association between streamflow and stream temperature may also be the result of generally low flows throughout most of the year. However, we also have limited direct measurements of on-site streamflow. In particular, very large increases in streamflow over the course of a few days, which then rapidly receded, were modeled. While direct measurements of streamflow were not available during these time periods, on-site observations of streamflow at similar times do not align with these results. Therefore, caution should be applied when interpreting these results as the model may be overfitted for the period of observed streamflow data and not representative for the entire timeframe of the model. We found that model results improved when we included streamflow data compared to when we used only PAWC data. Additionally, another study that examined the SWAT model at this site using a monthly timestep, indicated smaller increases in seasonal streamflow during the same time period (unpublished data). However, this may also be associated with the timestep used as brief, rapid changes will not be as pronounced with monthly estimates of streamflow. The results, although preliminary, indicate that more streamflow data are needed for calibration and validation but also that there may be processes (e.g., connections between groundwater and surface water) that are not adequately represented in this model.

Both Deer Creek and Fish Creek originate at a relatively small, low-flow, spring-fed perennial stream. As expected, water temperatures at the springs in the headwaters were relatively stable through the year. We anticipated that the springflow would provide a moderating influence on stream temperatures and expected larger diurnal ranges in stream temperature moving downstream. However, the diurnal stream temperatures did not display a clear association with downstream position. The diurnal ranges, and stream temperatures in general along this reach, may also be impacted by subsurface flows in addition to riparian cover. Other characteristics, such as aspect, stream entrenchment, and width/depth ratios are also key factors in stream temperature that were not addressed in this study.

The PFC surveys used in study also provide important insight into the stream channel and riparian conditions, which can impact water quality (including stream temperature). For example, trampling or heavy vegetation grazing can lead to streambank erosion and subsequently alter

stream channel dimensions and result in increased stream temperatures by creating wider, shallower streams. However, monitoring is needed at this study site in order to assess longer-term trends in function and condition.

The results of this study highlight some of the uses, and limitations, of regression-based approaches. The SVR approach used here can easily be adapted to multiple circumstances. While we used a linear approach in this study, the kernel type used in SVR can be adjusted for non-linear conditions. This may be particularly useful in areas with sub-zero stream temperatures or greater maximum stream temperatures. However, while the SVR model using 7DADM performed satisfactorily, the results of the SVR for diurnal stream temperature performed less well. In particular, the diurnal stream temperature model underpredicted the range of diurnal stream temperature fluctuation. For both approaches, it is also important to consider how well these models may perform in future conditions and along other stream reaches (particularly mid-order streams). More research and data are needed to evaluate these conditions at this watershed. Further, hyporheic exchange is difficult to measure and quantify in these approaches but may be an important factor influencing stream temperature.

Although continued monitoring is needed, , the results of the study suggest that air temperature and land cover characteristics are important considerations for stream temperature management in semiarid sites. Given the strong relationship between air temperature and stream temperature, future studies should consider the impacts of climate change on stream temperature at this site. Lastly, the surface water-groundwater connections present at this site may be an important factor in stream temperature dynamics. Yet, these connections are difficult to quantify and incorporate into stream temperature model used here and therefore future research may also seek to examine the hydrogeologic framework at the study site.

References

1. Ficklin, D.L.; Stewart, I.T.; Maurer, E.P. Effects of Climate Change on Stream Temperature, Dissolved Oxygen, and Sediment Concentration in the Sierra Nevada in California. *Water Resources Research* **2013**, *49*, 2765–2782, doi:10.1002/wrcr.20248.
2. Rasmussen, J.J.; Baatrup-Pedersen, A.; Riis, T.; Friberg, N. Stream Ecosystem Properties and Processes along a Temperature Gradient. *Aquatic Ecology* **2011**, *45*, 231–242, doi:10.1007/s10452-010-9349-1.

3. Webb, B.W.; Hannah, D.M.; Moore, R.D.; Brown, L.E.; Nobilis, F. Recent Advances in Stream and River Temperature Research. *Hydrological Processes* **2008**, *22*, 902–918, doi:10.1002/hyp.6994.
4. Poole, G.C.; Berman, C.H. An Ecological Perspective on In-Stream Temperature: Natural Heat Dynamics and Mechanisms of Heat-Caused Thermal Degredation. *Environmental Management* **2001**, *27*, 787–802, doi:10.1007/s002670010188.
5. Tague, C.; Farrell, M.; Grant, G.; Lewis, S.; Rey, S. Hydrogeologic Controls on Summer Stream Temperatures in the McKenzie River Basin, Oregon. *Hydrological Processes* **2007**, *21*, 3288–3300, doi:10.1002/hyp.6538.
6. Caldwell, T.G.; Wolaver, B.D.; Bongiovanni, T.; Pierre, J.P.; Robertson, S.; Abolt, C.; Scanlon, B.R. Spring Discharge and Thermal Regime of a Groundwater Dependent Ecosystem in an Arid Karst Environment. *Journal of Hydrology* **2020**, *587*, 124947, doi:10.1016/j.jhydrol.2020.124947.
7. van Vliet, M.T.H.; Ludwig, F.; Zwolsman, J.J.G.; Weedon, G.P.; Kabat, P. Global River Temperatures and Sensitivity to Atmospheric Warming and Changes in River Flow. *Water Resour. Res.* **2011**, *47*, W02544, doi:10.1029/2010WR009198.
8. Webb, B.W.; Clack, P.D.; Walling, D.E. Water–Air Temperature Relationships in a Devon River System and the Role of Flow. *Hydrological Processes* **2003**, *17*, 3069–3084, doi:10.1002/hyp.1280.
9. Broadmeadow, S.B.; Jones, J.G.; Langford, T.E.L.; Shaw, P.J.; Nisbet, T.R. The Influence of Riparian Shade on Lowland Stream Water Temperatures in Southern England and Their Viability for Brown Trout. *River Res. Applic.* **2011**, *27*, 226–237, doi:10.1002/rra.1354.
10. Johnson, S.L.; Jones, J.A. Stream Temperature Responses to Forest Harvest and Debris Flows in Western Cascades, Oregon. *Canadian Journal of Fisheries and Aquatic Sciences* **2000**, *57*, 30–39, doi:10.1139/cjfas-57-S2-30.
11. Simmons, J.A.; Anderson, M.; Dress, W.; Hanna, C.; Hornbach, D.J.; Janmaat, A.; Kuserk, F.; March, J.G.; Murray, T.; Niedzwiecki, J.; et al. A Comparison of the Temperature Regime of Short Stream Segments under Forested and Non-Forested Riparian Zones at Eleven Sites Across North America. *River Res. Applic.* **2015**, *31*, 964–974, doi:10.1002/rra.2796.
12. Gomi, T.; Moore, R.D.; Dhakal, A.S. Headwater Stream Temperature Response to Clear-Cut Harvesting with Different Riparian Treatments, Coastal British Columbia, Canada. *Water Resour. Res.* **2006**, *42*, W08437, doi:10.1029/2005WR004162.
13. Janisch, J.E.; Wondzell, S.M.; Ehinger, W.J. Headwater Stream Temperature: Interpreting Response after Logging, with and without Riparian Buffers, Washington, USA. *Forest Ecology and Management* **2012**, *270*, 302–313, doi:10.1016/j.foreco.2011.12.035.
14. Dugdale, S.J.; Malcolm, I.A.; Kantola, K.; Hannah, D.M. Stream Temperature under Contrasting Riparian Forest Cover: Understanding Thermal Dynamics and Heat Exchange Processes. *Science of The Total Environment* **2018**, *610–611*, 1375–1389, doi:10.1016/j.scitotenv.2017.08.198.
15. Essaid, H.I.; Caldwell, R.R. Evaluating the Impact of Irrigation on Surface Water - Groundwater Interaction and Stream Temperature in an Agricultural Watershed. *Science of the Total Environment* **2017**, *599–600*, 581–596.
16. Garner, G.; Malcolm, I.A.; Sadler, J.P.; Hannah, D.M. The Role of Riparian Vegetation Density, Channel Orientation and Water Velocity in Determining River Temperature Dynamics. *Journal of Hydrology* **2017**, *553*, 471–485, doi:10.1016/j.jhydrol.2017.03.024.

17. Nusslé, S.; Matthews, K.R.; Carlson, S.M. Mediating Water Temperature Increases Due to Livestock and Global Change in High Elevation Meadow Streams of the Golden Trout Wilderness. *PLOS ONE* **2015**, *10*, e0142426, doi:10.1371/journal.pone.0142426.
18. Oles, K.M.; Weixelman, D.A.; Lile, D.F.; Tate, K.W.; Snell, L.K.; Roche, L.M. Riparian Meadow Response to Modern Conservation Grazing Management. *Environmental Management* **2017**, *60*, 383–395, doi:10.1007/s00267-017-0897-1.
19. Studinski, J.; Hartman, K.; Niles, J.; Keyser, P. The Effects of Riparian Forest Disturbance on Stream Temperature, Sedimentation, and Morphology. *Hydrobiologia* **2012**, *686*, 107–117, doi:10.1007/s10750-012-1002-7.
20. Alger, M.; Lane, B.A.; Neilson, B.T. Combined Influences of Irrigation Diversions and Associated Subsurface Return Flows on River Temperature in a Semi-Arid Region. *Hydrological Processes* **2021**, *35*, e14283, doi:10.1002/hyp.14283.
21. Zeng, R.; Cai, X. Analyzing Streamflow Changes: Irrigation-Enhanced Interaction between Aquifer and Streamflow in the Republican River Basin. *Hydrol. Earth Syst. Sci.* **2014**, *18*, 493–502, doi:10.5194/hess-18-493-2014.
22. Mayer, T.D. Controls of Summer Stream Temperature in the Pacific Northwest. *Journal of Hydrology* **2012**, *475*, 323–335, doi:10.1016/j.jhydrol.2012.10.012.
23. Segura, C.; Caldwell, P.; Sun, G.; McNulty, S.; Zhang, Y. A Model to Predict Stream Water Temperature across the Conterminous USA. *Hydrological Processes* **2015**, *29*, 2178–2195, doi:https://doi.org/10.1002/hyp.10357.
24. Piotrowski, A.P.; Napiorkowski, J.J. Simple Modifications of the Nonlinear Regression Stream Temperature Model for Daily Data. *Journal of Hydrology* **2019**, *572*, 308–328, doi:10.1016/j.jhydrol.2019.02.035.
25. Gu, C.; Anderson, W.P.; Colby, J.D.; Coffey, C.L. Air-stream Temperature Correlation in Forested and Urban Headwater Streams in the Southern Appalachians. *Hydrological Processes* **2015**, *29*, 1110–1118, doi:10.1002/hyp.10225.
26. Li, H.; Deng, X.; Kim, D.-Y.; Smith, E.P. Modeling Maximum Daily Temperature Using a Varying Coefficient Regression Model. *Water Resources Research* **2014**, *50*, 3073–3087, doi:https://doi.org/10.1002/2013WR014243.
27. Mohseni, O.; Stefan, H.G.; Erickson, T.R. A Nonlinear Regression Model for Weekly Stream Temperatures. *Water Resources Research* **1998**, *34*, 2685–2692, doi:https://doi.org/10.1029/98WR01877.
28. Arismendi, I.; Safeeq, M.; Dunham, J.B.; Johnson, S.L. Can Air Temperature Be Used to Project Influences of Climate Change on Stream Temperature? *Environ. Res. Lett.* **2014**, *9*, 084015, doi:10.1088/1748-9326/9/8/084015.
29. PRISM Climate Group, Oregon State University, Http://Prism.Oregonstate.Edu, Created 1 March 2019.
30. Brooks, H.C.; McIntyre, J.R.; Walkter, G.W. *Geology of the Oregon Part of the Baker 1° by 2° Quadrangle*; State of OR Department of Geology and Mineral Industries: Portland, OR, 1976; p. 28;.
31. Walker, G.W.; MacLeod, N.S.; Miller, R.J.; Raines, G.L.; Connors, K.A. *Spatial Digital Database for the Geologic Map of Oregon, Edition 2.0*; U.S. Geologic Survey: Menlo Park, CA, 2003;

32. U.S. Department of the Interior *Riparian Area Management: Proper Functioning Condition Assessment for Lotic Areas. Technical Reference 1737-15*; Bureau of Land Management, National Operations Center: Denver, CO, 2015;
33. Rosgen, D.L.; Silvey, H.L. *Applied River Morphology*; Wildland Hydrology Books: Fort Collins, CO, 1996;
34. *Monitoring Manual for Grassland, Shrubland, and Savanna Ecosystems*; Herrick, J.E., Jornada Experimental Range, Eds.; USDA - ARS Jordana Experimental Range ; Distributed by the University of Arizona Press: Las Cruces, N.M. : Tucson, Ariz, 2005; ISBN 978-0-9755552-0-0.
35. van Genuchten, M.Th.; Leij, F.J.; Yates, S.R. *The RETC Code for Quantifying the Hydraulic Functions of Unsaturated Soils*; U.S. Salinity Laboratory, USDA, ARS, Riverside, California, 1991;
36. van Genuchten, M.Th.; Simunek, J.; Sejna, M. RETC for Windows, Version 6.02 2009.
37. Rajib, M.A.; Merwade, V.; Yu, Z. Multi-Objective Calibration of a Hydrologic Model Using Spatially Distributed Remotely Sensed/in-Situ Soil Moisture. *Journal of Hydrology* **2016**, *536*, 192–207, doi:10.1016/j.jhydrol.2016.02.037.
38. Bos, M.G., Replogle, J.A., & Clemmens, A.J. Flow measuring flumes for open channel systems. John Wiley and Sons Inc: New York, NY, USA, 1984; ISBN Z-0471-80637-4
39. Oregon 10m Digital Elevation Model (DEM) Available online: https://spatialdata.oregonexplorer.info/geoportal/details;id=7a82c1be50504f56a9d49d13c7b4d9aa (accessed on 6 February 2020).
40. National Land Cover Dataset (NLCD) (accessed on 2 February 2020).
41. Abbaspour, K.C. SWAT-CUP: SWAT Calibration and Uncertainty Programs - A User Manual; Department of Systems Analysis, Integrated Assessment and Modelling (SIAM), Eawag. Swiss Federal Institute of Aquatic Science and Technology; Duebendorf, Switzerland. **2015**, 100.
42. Abbaspour, K.C.; Yang, J.; Maximov, I.; Siber, R.; Bogner, K.; Mieleitner, J.; Zobrist, J.; Srinivasan, R. Modelling Hydrology and Water Quality in the Pre-Alpine/Alpine Thur Watershed Using SWAT. *Journal of Hydrology* **2007**, *333*, 413–430, doi:10.1016/j.jhydrol.2006.09.014.
43. National Agriculture Imagery Program Digital Ortho Photo Image 2020.
44. Durfee, N.; Ochoa, C.G.; Jones, G. Stream Temperature and Environment Relationships in a Semiarid Riparian Corridor. *Land* **2021**, *10*, 519, doi:10.3390/land10050519.
45. Pedregosa, F.; Varoquaux, G.; Gramfort, A.; Michel, V.; Thirion, B.; Grisel, O.; Blondel, M.; Prettenhofer, P.; Weiss, R.; Dubourg, V.; et al. Scikit-Learn: Machine Learning in Python. *Machine Learning in Python* **2011**, *12*, 2825–2830.
46. Morrill, J.C.; Bales, R.C.; Conklin, M.H. Estimating Stream Temperature from Air Temperature: Implications for Future Water Quality. *J. Environ. Eng.* **2005**, *131*, 139–146, doi:10.1061/(ASCE)0733-9372(2005)131:1(139).
47. Bowler, D.E.; Mant, R.; Orr, H.; Hannah, D.M.; Pullin, A.S. What Are the Effects of Wooded Riparian Zones on Stream Temperature? *Environmental Evidence* **2012**, *1*, 3, doi:10.1186/2047-2382-1-3.
48. Horne, J.P.; Hubbart, J.A. A Spatially Distributed Investigation of Stream Water Temperature in a Contemporary Mixed-Land-Use Watershed. *Water* **2020**, *12*, 1756, doi:10.3390/w12061756.

Appendix 1

Parameter	Definition
ALPHA_BF.gw	Baseflow alpha factor
CANMX.hru	Maximum canopy storage, grouped by land use
CH_K2.rte	Effective hydraulic conductivity
CH_N1.sub	Manning's roughness coefficient for tributary, grouped by land use
CH_N2.rte	Manning's roughness coefficient for main channel
CN2.mgt	Curve number, grouped by watershed, land use, and range of slope
EPCO.hru	Plant uptake compensation factor
ESCO.hru	Soil evaporation compensation factor
EVRCH.bsn	Evaporation adjustment factor for reach
GW_DELAY.gw	Groundwater delay time in days
GW_REVAP.gw	Groundwater revap coefficient
GWQMN.gw	Threshold depth of water in shallow aquifer required for return flow
OV_N.hru	Manning's roughness coefficient for overland flow
RCHRG_DP.gw	Deep aquifer percolation fraction
REVAPMN.gw	Threshold depth of water in shallow aquifer required for revap/percolation to deep aquifer
SFTMP.bsn	Snowfall temp (°C)
SMFMN.bsn	Melt factor on Dec 21
SMFMX.bsn	Melt factor on June 21
SMTMP.bsn	Snowmelt base temp (°C)
SNOCOVMX.bsn	Min snow water content at 100% snow cover
SOL_ALB.sol	Albedo of moist soil
SOL_AWC.sol	Average soil available water capacity, grouped by soil type and layer
SOL_K.sol	Saturated hydraulic conductivity (mm hr^{-1})
SURLAG.hru	Surface runoff lag time
TIMP.bsn	Snowpack temperature lag factor
TRNSRCH.bsn	Portion of transmission losses from main channel that go into deep aquifer

GENERAL CONCLUSIONS

GENERAL CONCLUSIONS

This dissertation examined ecohydrologic connections at two semiarid study sites. In particular, this research sought to expand our understanding of these processes regarding two significant land management challenges faced in similar regions: woody vegetation encroachment and increasing stream temperatures. For both study sites, the water balance was characterized in order to establish the basic framework for future research. This research also examined different approaches to characterizing the water balance and its components.

This dissertation consists of four manuscripts. The first two manuscripts took place at the Camp Creek Paired Watershed Study (CCPWS), which was established in 1993 to examine the ecohydrologic impacts of western juniper encroachment and removal. For the research in these two manuscripts, we focused on examining the water balance components for two small, adjacent watersheds: one dominated by western juniper and one in which the majority of juniper had been removed 17 years earlier.

For the first manuscript, a mass balance approach was used to characterize aspects of the seasonal water balance. On-site measurements of spring flow, streamflow, soil moisture, precipitation, solar radiation, and shallow groundwater levels were examined. Evapotranspiration (ET) was calculated using potential evapotranspiration (PET) and the water balance.

Evapotranspiration accounted for the majority of the water budget, followed by deep percolation. No significant differences were found in shallow groundwater recharge rates between the two watersheds. However, we did find that groundwater recharge rates were lower in years with reduced snowpack compared to years of greater snowpack, even when the annual precipitation amounts were similar. We also found that springflow and streamflow rates were generally lower at the juniper-dominated watershed compared to the sagebrush-dominated watershed. Therefore, results of this study suggest that the combination of western juniper encroachment and reduced snowpack may lead to reduced groundwater recharge and decreased water yield.

The second manuscript examined different methods of estimating ET and examined the relationship between ET and several related environmental characteristics: springflow, soil moisture, the Normalized Difference Vegetation Index (NDVI), and the Normalized Difference Moisture Index (NDMI). OpenET was used to download ET data for three commonly-used

models: Mapping Evapotranspiration at High Resolution with Internalized Calibration (METRIC), Operational Simplified Surface Energy Balance (SSEBop), and Disaggregation of the Atmosphere-Land Exchange Inverse (DisALEXI). A small unpiloted aerial vehicle (UAV) was used to capture multispectral (red, green, blue, near-infrared, and red-edge wavelengths) and thermal imagery during the summer, fall, and spring for one year. The QWaterModel, along with on-site measurements of solar radiation and air temperature, were used to estimate ET at these study plots. The Soil and Water Assessment Tool (SWAT) was used to model ET for both watersheds.

Variations in overall ET rates and seasonal timing was demonstrated among the approaches examined. Estimates of ET using METRIC, SSEBop, and DisALEXI were substantially larger at the juniper-dominated watershed compared to the sagebrush dominated watershed. Annual mean NDVI and NDMI were both greater at the juniper-dominated watershed compared to the sagebrush-dominated watershed. A significant correlation was found between watershed-scale monthly ET and NDVI, NDVI and soil moisture, NDVI and NDMI, and springflow and soil moisture for both watersheds. ET calculated using UAV-based thermal imagery did not indicate major differences in ET between plots at the two watersheds.

The results of the first two chapters emphasize the potential advantages and challenges in using water balance and energy balance-based approaches to estimating ET. For example, the water balance-based approach did not indicate considerable differences in ET between the two watersheds while the energy balance-based approaches calculated larger rates of ET at the juniper-dominated watershed. Therefore, consideration should be given to the particular strengths and weaknesses of each approach when using these methods to inform land management.

The third manuscript sought to characterize the water balance at a semiarid site in eastern OR using the SWAT model and to examine the most sensitive parameters in the water balance calibration. A combination of PRISM and on-site meteorological data were used in model creation. A multisite, multivariable approach was used in calibration. The SWAT-Calibration and Uncertainty Program (SWAT-CUP) was used for calibration, validation, and sensitivity analysis. Parameter sensitivity was performed for calibrations using streamflow only, plant available water content (PAWC) only, and a combination of streamflow and PAWC. Calibration

was performed using streamflow and PAWC, but due to limited streamflow data, only PAWC data were used for model validation. Model performance ranged from NS=0.68 to 0.93 for calibration and NS=0.81 to 0.85 for validation. Snowpack cover and soil characteristics were among the most influential parameters in calibration. While the model generally captured patterns in seasonal PAWC, more data are needed to verify the performance of the model over longer timeframes. The results of this study further highlight that reductions in snowpack cover may be particularly impactful on the ecohydrology of semiarid regions and warrant further examination.

The final manuscript also took place at the eastern Oregon study site used in the third manuscript and examined a key water quality concern in many regions: increasing stream temperatures. Stream temperature sensors were located along the longitudinal gradient at sites with varying land cover, streamflow, and meteorological conditions. This research built upon the water balance characterization used in the third manuscript in order to model daily streamflow rates. PRISM data were downloaded for each stream temperature site. A support vector machine (SVM) approach was used to delineate land cover in a 30 m area on either side of the stream. The daily minimum, maximum, and mean stream temperatures and 7-day moving average of the daily max (7DADM) and daily mean (7DA) stream temperature were calculated, as well as the diurnal range in stream temperature. A support vector regression (SVR) approach was used to evaluate the relationship between selected environmental parameters (e.g., land cover type, air temperature) and the 7DADM and diurnal stream temperature.

Based on the SVR, air temperature was the primary predictor of stream temperature, followed by the percentage of sagebrush steppe and forest cover. A negligible relationship was found between streamflow and 7DADM, with a somewhat larger relationship being found between streamflow and the diurnal range. The results of this study emphasize the importance of considering ambient conditions and riparian vegetation when addressing stream temperature, although more research is needed to better understand how the characteristics of headwater streams might impact stream temperature dynamics of larger, higher-order systems.

The results of this research contribute to our understanding of the ecohydrologic connections in semiarid sites in central and eastern, Oregon. In particular, this dissertation sought to address the need for a greater understanding of the water balance in semiarid regions, as well

to provide a greater examination of two key land management challenges faced in similar areas. The methodology applied in these studies can also be adapted and applied to other research sites. Through a more in-depth examination of these issues, more informed land management and research can be developed.

Bibliography

1. Bazan, R.A.; Wilcox, B.P.; Munster, C.; Gary, M. Removing Woody Vegetation Has Little Effect on Conduit Flow Recharge. *Ecohydrol.* **2013**, *6*, 435–443, doi:10.1002/eco.1277.
2. Mollnau, C.; Newton, M.; Stringham, T. Soil Water Dynamics and Water Use in a Western Juniper (Juniperus Occidentalis) Woodland. *Journal of Arid Environments* **2014**, *102*, 117–126, doi:10.1016/j.jaridenv.2013.11.015.
3. Sun, N.; Yearsley, J.; Voisin, N.; Lettenmaier, D.P. A Spatially Distributed Model for the Assessment of Land Use Impacts on Stream Temperature in Small Urban Watersheds. *Hydrological Processes* **2015**, *29*, 2331–2345, doi:10.1002/hyp.10363.
4. Daraio, J.A.; Bales, J.D. Effects of Land Use and Climate Change on Stream Temperature I: Daily Flow and Stream Temperature Projections. *J Am Water Resour Assoc* **2014**, *50*, 1155–1176, doi:10.1111/jawr.12179.
5. Adnan, N.A.; Atkinson, P.M. Exploring the Impact of Climate and Land Use Changes on Streamflow Trends in a Monsoon Catchment. *Int. J. Climatol.* **2011**, *31*, 815–831, doi:10.1002/joc.2112.
6. Dosdogru, F.; Kalin, L.; Wang, R.; Yen, H. Potential Impacts of Land Use/Cover and Climate Changes on Ecologically Relevant Flows. *Journal of Hydrology* **2020**, *584*, 124654, doi:10.1016/j.jhydrol.2020.124654.
7. Negm, A.; Abdrakhimova, P.; Hayashi, M.; Rasouli, K. Effects of Climate Change on Depression-Focused Groundwater Recharge in the Canadian Prairies. *Vadose Zone Journal* **2021**, *20*, e20153, doi:10.1002/vzj2.20153.
8. Lindquist, L.W.; Palmquist, K.A.; Jordan, S.E.; Lauenroth, W.K. Impacts of Climate Change on Groundwater Recharge in Wyoming Big Sagebrush Ecosystems Are Contingent on Elevation. *wnan* **2019**, *79*, 37–48, doi:10.3398/064.079.0104.
9. Li, Z.; Quiring, S.M. Identifying the Dominant Drivers of Hydrological Change in the Contiguous United States. *Water Resources Research* **2021**, *57*, e2021WR029738, doi:10.1029/2021WR029738.
10. Stevens, N.; Lehmann, C.E.R.; Murphy, B.P.; Durigan, G. Savanna Woody Encroachment Is Widespread across Three Continents. *Global Change Biology* **2017**, *23*, 235–244, doi:https://doi.org/10.1111/gcb.13409.
11. Miller, R.F.; Bates, J.D.; Svejcar, T.J.; Pierson, F.B.; Eddleman, L.E. *Biology, Ecology, and Management of Western Juniper (Juniperus Occidentalis)*; Oregon State University, Agricultural Experiment Station., 2005; Vol. Technical Bulletin 152;
12. Miller, R.F.; Rose, J.A. Historic Expansion of Juniperus Occidentalis (Western Juniper) in Southeastern Oregon. *The Great Basin Naturalist* **1995**, *55*, 37–45.
13. Caracciolo, D.; Istanbulluoglu, E.; Noto, L.V. An Ecohydrological Cellular Automata Model Investigation of Juniper Tree Encroachment in a Western North American Landscape. *Ecosystems* **2017**, *20*, 1104–1123, doi:10.1007/s10021-016-0096-6.
14. Kormos, P.R.; Marks, D.; Pierson, F.B.; Williams, C.J.; Hardegree, S.P.; Havens, S.; Hedrick, A.; Bates, J.D.; Svejcar, T.J. Ecosystem Water Availability in Juniper versus Sagebrush Snow-Dominated Rangelands. *Rangeland Ecology & Management* **2017**, *70*, 116–128, doi:10.1016/j.rama.2016.05.003.
15. Petersen, S.L.; Stringham, T.K. Infiltration, Runoff, and Sediment Yield in Response to Western Juniper Encroachment in Southeast Oregon. *Rangeland Ecology & Management* **2008**, *61*, 74–81, doi:10.2111/07-070R.1.

16. Pierson, F.B.; Bates, J.D.; Svejcar, T.J.; Hardegree, S.P. Runoff and Erosion after Cutting Western Juniper. *Rangeland Ecology & Management* **2007**, *60*, 285–292.
17. Zou, C.B.; Turton, D.J.; Will, R.E.; Engle, D.M.; Fuhlendorf, S.D. Alteration of Hydrological Processes and Streamflow with Juniper (Juniperus Virginiana) Encroachment in a Mesic Grassland Catchment. *Hydrol. Process.* **2014**, *28*, 6173–6182, doi:10.1002/hyp.10102.
18. Niemeyer, R.J.; Link, T.E.; Heinse, R.; Seyfried, M.S. Climate Moderates Potential Shifts in Streamflow from Changes in Pinyon-Juniper Woodland Cover across the Western U.S. *Hydrological Processes* **2017**, *31*, 3489–3503, doi:10.1002/hyp.11264.
19. Belay, T.A.; Totland, Ø.; Moe, S.R. Ecosystem Responses to Woody Plant Encroachment in a Semiarid Savanna Rangeland. *Plant Ecology* **2013**, *214*, 1211–1222.
20. Bradley, B.A. Assessing Ecosystem Threats from Global and Regional Change: Hierarchical Modeling of Risk to Sagebrush Ecosystems from Climate Change, Land Use and Invasive Species in Nevada, USA. *Ecography* **2010**, *33*, 198–208, doi:10.1111/j.1600-0587.2009.05684.x.
21. Creutzburg, M.K.; Halofsky, J.E.; Halofsky, J.S.; Christopher, T.A. Climate Change and Land Management in the Rangelands of Central Oregon. *Environmental Management* **2015**, *55*, 43–55, doi:10.1007/s00267-014-0362-3.
22. Regonda, S.K.; Rajagopalan, B.; Clark, M.; Pitlick, J. Seasonal Cycle Shifts in Hydroclimatology over the Western United States. *Journal of Climate* **2005**, *18*, 372–384, doi:10.1175/JCLI-3272.1.
23. Mote, P.W.; Hamlet, A.F.; Clark, M.P.; Lettenmaier, D.P. Declining Mountain Snowpack in Western North America. *Bulletin of the American Meteorological Society* **2005**, *86*, 39–50, doi:10.1175/BAMS-86-1-39.
24. Rasmussen, R.; Ikeda, K.; Liu, C.; Gochis, D.; Clark, M.; Dai, A.; Gutmann, E.; Dudhia, J.; Chen, F.; Barlage, M.; et al. Climate Change Impacts on the Water Balance of the Colorado Headwaters: High-Resolution Regional Climate Model Simulations. *Journal of Hydrometeorology* **2014**, *15*, 1091–1116, doi:10.1175/JHM-D-13-0118.1.
25. Hamlet, A.F.; Mote, P.W.; Clark, M.P.; Lettenmaier, D.P. Twentieth-Century Trends in Runoff, Evapotranspiration, and Soil Moisture in the Western United States. *Journal of Climate* **2007**, *20*, 1468–1486, doi:10.1175/JCLI4051.1.
26. Johansson, B.; Chen, D. The Influence of Wind and Topography on Precipitation Distribution in Sweden: Statistical Analysis and Modelling. *Int. J. Climatol.* **2003**, *23*, 1523–1535, doi:10.1002/joc.951.
27. Crockford, R.H.; Richardson, D.P. Partitioning of Rainfall into Throughfall, Stemflow and Interception: Effect of Forest Type, Ground Cover and Climate. *Hydrol. Process.* **2000**, *14*, 2903–2920, doi:10.1002/1099-1085(200011/12)14:16/17<2903::AID-HYP126>3.0.CO;2-6.
28. Melton, F.S.; Huntington, J.; Grimm, R.; Herring, J.; Hall, M.; Rollison, D.; Erickson, T.; Allen, R.; Anderson, M.; Fisher, J.B.; et al. OpenET: Filling a Critical Data Gap in Water Management for the Western United States. *JAWRA Journal of the American Water Resources Association* **2021**, *n/a*, 1–24, doi:10.1111/1752-1688.12956.
29. Anderson, M.; Gao, F.; Knipper, K.; Hain, C.; Dulaney, W.; Baldocchi, D.; Eichelmann, E.; Hemes, K.; Yang, Y.; Medellin-Azuara, J.; et al. Field-Scale Assessment of Land and Water Use Change over the California Delta Using Remote Sensing. *Remote Sensing* **2018**, *10*, 889, doi:10.3390/rs10060889.

30. Anderson, M.C.; Norman, J.M.; Mecikalski, J.R.; Otkin, J.A.; Kustas, W.P. A Climatological Study of Evapotranspiration and Moisture Stress across the Continental United States Based on Thermal Remote Sensing: 1. Model Formulation. *Journal of Geophysical Research: Atmospheres* **2007**, *112*, doi:10.1029/2006JD007506.
31. Allen, R.G.; Tasumi, M.; Trezza, R. Satellite-Based Energy Balance for Mapping Evapotranspiration with Internalized Calibration (METRIC)—Model. *J. Irrig. Drain Eng.* **2007**, *133*, 380–394, doi:10.1061/(ASCE)0733-9437(2007)133:4(380).
32. Allen, R.G.; Tasumi, M.; Morse, A.; Trezza, R. A Landsat-Based Energy Balance and Evapotranspiration Model in Western US Water Rights Regulation and Planning. *Irrig Drainage Syst* **2005**, *19*, 251–268, doi:10.1007/s10795-005-5187-z.
33. Allen, R.; Irmak, A.; Trezza, R.; Hendrickx, J.M.H.; Bastiaanssen, W.; Kjaersgaard, J. Satellite-Based ET Estimation in Agriculture Using SEBAL and METRIC. *Hydrol. Process.* **2011**, *25*, 4011–4027, doi:10.1002/hyp.8408.
34. Allen, R.G.; Pereira, L.S.; Raes, D.; Smith, M. Crop Evapotranspiration. Guidelines for Computing Crop Water Requirements. Irrigation and Drainage Paper 56, FAO, Rome, 300 p 1998.
35. Rouse, J.W.; Harlan, J.C.; Haas, R.H.; Schell, J.A.; Deering, D.W. Monitoring the Vernal Advancement and Retrogradiation (Green Wave Effect) of Natural Vegetation - NASA-CR-144661 1974.
36. Szilagyi, J. Vegetation Indices to Aid Areal Evapotranspiration Estimations. *J. Hydrol. Eng.* **2002**, *7*, 368–372, doi:10.1061/(ASCE)1084-0699(2002)7:5(368).
37. Szilagyi, J. Can a Vegetation Index Derived from Remote Sensing Be Indicative of Areal Transpiration? *Ecological Modelling* **2000**, *127*, 65–79, doi:10.1016/S0304-3800(99)00200-8.
38. Arnold, J.G.; Srinivasan, R.; Muttiah, R.S.; Williams, J.R. Large Area Hydrologic Modeling and Assessment Part I: Model Development1. *JAWRA Journal of the American Water Resources Association* **1998**, *34*, 73–89, doi:10.1111/j.1752-1688.1998.tb05961.x.
39. Baker, T.J.; Miller, S.N. Using the Soil and Water Assessment Tool (SWAT) to Assess Land Use Impact on Water Resources in an East African Watershed. *Journal of Hydrology* **2013**, *486*, 100–111, doi:10.1016/j.jhydrol.2013.01.041.
40. Ghaffari, G.; Keesstra, S.; Ghodousi, J.; Ahmadi, H. SWAT-Simulated Hydrological Impact of Land-Use Change in the Zanjanrood Basin, Northwest Iran. *Hydrological Processes* **2010**, *24*, 892–903, doi:10.1002/hyp.7530.
41. Demirel, M.C.; Venancio, A.; Kahya, E. Flow Forecast by SWAT Model and ANN in Pracana Basin, Portugal. *Advances in Engineering Software* **2009**, *40*, 467–473, doi:10.1016/j.advengsoft.2008.08.002.
42. Grusson, Y.; Sun, X.; Gascoin, S.; Sauvage, S.; Raghavan, S.; Anctil, F.; Sáchez-Pérez, J.-M. Assessing the Capability of the SWAT Model to Simulate Snow, Snow Melt and Streamflow Dynamics over an Alpine Watershed. *Journal of Hydrology* **2015**, *531*, 574–588, doi:10.1016/j.jhydrol.2015.10.070.
43. Muttiah, R.S.; Wurbs, R.A. Scale-Dependent Soil and Climate Variability Effects on Watershed Water Balance of the SWAT Model. *Journal of Hydrology* **2002**, *256*, 264–285, doi:10.1016/S0022-1694(01)00554-6.
44. Hosseini, S.; Khaleghi, M. Application of SWAT Model and SWAT-CUP Software in Simulation and Analysis of Sediment Uncertainty in Arid and Semi-Arid Watersheds (Case Study: The Zoshk–Abardeh Watershed). *Modeling Earth Systems and Environment* **2020**, *6*, doi:10.1007/s40808-020-00846-2.

45. Mosbahi, M.; Benabdallah, S.; Boussema, M.R. Hydrological Modeling in a Semi-Arid Catchment Using SWAT Model. *Journal of Environmental Science and Engineering* **2011**, *5*, 8.
46. Qiu, Z.; Wang, L. Hydrological and Water Quality Assessment in a Suburban Watershed with Mixed Land Uses Using the SWAT Model. *Journal of Hydrologic Engineering* **2014**, *19*, 816–827, doi:10.1061/(ASCE)HE.1943-5584.0000858.
47. Anand, J.; Gosain, A.K.; Khosa, R. Prediction of Land Use Changes Based on Land Change Modeler and Attribution of Changes in the Water Balance of Ganga Basin to Land Use Change Using the SWAT Model. *Science of The Total Environment* **2018**, *644*, 503–519, doi:10.1016/j.scitotenv.2018.07.017.
48. Moges, E.; Demissie, Y.; Larsen, L.; Yassin, F. Review: Sources of Hydrological Model Uncertainties and Advances in Their Analysis. *Water* **2020**, *13*, 28, doi:10.3390/w13010028.
49. Niraula, R.; Norman, L.M.; Meixner, T.; Callegary, J.B. Multi-Gauge Calibration for Modeling the Semi-Arid Santa Cruz Watershed in Arizona-Mexico Border Area Using SWAT. *Air, Soil and Water Research* **2012**, 41-.
50. Shah, S.; Duan, Z.; Song, X.; Li, R.; Mao, H.; Liu, J.; Ma, T.; Wang, M. Evaluating the Added Value of Multi-Variable Calibration of SWAT with Remotely Sensed Evapotranspiration Data for Improving Hydrological Modeling. *Journal of Hydrology* **2021**, *603*, 127046, doi:10.1016/j.jhydrol.2021.127046.
51. Beven, K.; Binley, A. The Future of Distributed Models: Model Calibration and Uncertainty Prediction. *Hydrological Processes* **1992**, *6*, 279–298, doi:10.1002/hyp.3360060305.
52. Abbaspour, K.C. SWAT-CUP: SWAT Calibration and Uncertainty Programs - A User Manual; Department of Systems Analysis, Integrated Assessment and Modelling (SIAM), Eawag. Swiss Federal Institute of Aquatic Science and Technology; Duebendorf, Switzerland. **2015**, 100.
53. Abbaspour, K.C.; Vaghefi, S.A.; Srinivasan, R. A Guideline for Successful Calibration and Uncertainty Analysis for Soil and Water Assessment: A Review of Papers from the 2016 International SWAT Conference. *Water* **2018**, *10*, 6, doi:10.3390/w10010006.
54. Abiodun, O.O.; Guan, H.; Post, V.E.A.; Batelaan, O. Comparison of MODIS and SWAT Evapotranspiration over a Complex Terrain at Different Spatial Scales. *Hydrology and Earth System Sciences; Katlenburg-Lindau* **2018**, *22*, 2775–2794, doi:http://dx.doi.org.ezproxy.proxy.library.oregonstate.edu/10.5194/hess-22-2775-2018.
55. Kaushal, S.S.; Likens, G.E.; Jaworski, N.A.; Pace, M.L.; Sides, A.M.; Seekell, D.; Belt, K.T.; Secor, D.H.; Wingate, R.L. Rising Stream and River Temperatures in the United States. *Frontiers in Ecology and the Environment* **2010**, *8*, 461–466, doi:10.1890/090037.
56. Ficklin, D.L.; Barnhart, B.L. SWAT Hydrologic Model Parameter Uncertainty and Its Implications for Hydroclimatic Projections in Snowmelt-Dependent Watersheds. *Journal of Hydrology* **2014**, *519*, 2081–2090, doi:10.1016/j.jhydrol.2014.09.082.
57. Rasmussen, J.J.; Baatrup-Pedersen, A.; Riis, T.; Friberg, N. Stream Ecosystem Properties and Processes along a Temperature Gradient. *Aquatic Ecology* **2011**, *45*, 231–242, doi:10.1007/s10452-010-9349-1.
58. Torgersen, C.E.; Price, D.M.; Li, H.W.; McIntosh, B.A. Multiscale Thermal Refugia and Stream Habitat Associations of Chinook Salmon in Northeastern Oregon. *Ecological Applications* **1999**, *9*, 301–319, doi:10.1890/1051-0761(1999)009[0301:MTRASH]2.0.CO;2.
59. Richter, A.; Kolmes, S.A. Maximum Temperature Limits for Chinook, Coho, and Chum Salmon, and Steelhead Trout in the Pacific Northwest. *Reviews in Fisheries Science* **2005**, *13*, 23–49, doi:10.1080/10641260590885861.

60. Fullerton, A.H.; Torgersen, C.E.; Lawler, J.J.; Faux, R.N.; Steel, E.A.; Beechie, T.J.; Ebersole, J.L.; Leibowitz, S.G. Rethinking the Longitudinal Stream Temperature Paradigm: Region-Wide Comparison of Thermal Infrared Imagery Reveals Unexpected Complexity of River Temperatures. *Hydrol. Process.* **2015**, *29*, 4719–4737, doi:10.1002/hyp.10506.
61. Mayer, T.D. Controls of Summer Stream Temperature in the Pacific Northwest. *Journal of Hydrology* **2012**, *475*, 323–335, doi:10.1016/j.jhydrol.2012.10.012.
62. Grabowski, Z.J.; Watson, E.; Chang, H. Using Spatially Explicit Indicators to Investigate Watershed Characteristics and Stream Temperature Relationships. *Science of The Total Environment* **2016**, *551–552*, 376–386, doi:10.1016/j.scitotenv.2016.02.042.
63. Isaak, D.J.; Hubert, W.A. A Hypothesis About Factors That Affect Maximum Summer Stream Temperatures Across Montane Landscapes1. *JAWRA Journal of the American Water Resources Association* **2001**, *37*, 351–366, doi:10.1111/j.1752-1688.2001.tb00974.x.
64. Woltemade, C.J.; Hawkins, T.W. Stream Temperature Impacts Because of Changes in Air Temperature, Land Cover and Stream Discharge: Navarro River Watershed, California, USA. *River Res. Applic.* **2016**, *32*, 2020–2031, doi:10.1002/rra.3043.
65. Ebersole, J.L.; Wiginton, P.J.; Leibowitz, S.G.; Van Sickle, J. Predicting the Occurrence of Cold-Water Patches at Intermittent and Ephemeral Tributary Confluences with Warm Rivers. *Freshwater Science* **2014**, *34*, 111–124, doi:10.1086/678127.
66. Johnson, S.L. Factors Influencing Stream Temperatures in Small Streams: Substrate Effects and a Shading Experiment. *Canadian Journal of Fisheries & Aquatic Sciences* **2004**, *61*, 913–923, doi:10.1139/F04-040.
67. Moore, R.D.; Nelitz, M.; Parkinson, E. Empirical Modelling of Maximum Weekly Average Stream Temperature in British Columbia, Canada, to Support Assessment of Fish Habitat Suitability. *Canadian Water Resources Journal / Revue canadienne des ressources hydriques* **2013**, *38*, 135–147, doi:10.1080/07011784.2013.794992.
68. Du, X.; Goss, G.; Faramarzi, M. Impacts of Hydrological Processes on Stream Temperature in a Cold Region Watershed Based on the SWAT Equilibrium Temperature Model. *Water* **2020**, *12*, 1112, doi:10.3390/w12041112.
69. Janisch, J.E.; Wondzell, S.M.; Ehinger, W.J. Headwater Stream Temperature: Interpreting Response after Logging, with and without Riparian Buffers, Washington, USA. *Forest Ecology and Management* **2012**, *270*, 302–313, doi:10.1016/j.foreco.2011.12.035.
70. Poole, G.C.; Berman, C.H. An Ecological Perspective on In-Stream Temperature: Natural Heat Dynamics and Mechanisms of Heat-Caused Thermal Degredation. *Environmental Management* **2001**, *27*, 787–802, doi:10.1007/s002670010188.
71. Caissie, D. The Thermal Regime of Rivers: A Review. *Freshwater Biology* **2006**, *51*, 1389–1406, doi:10.1111/j.1365-2427.2006.01597.x.
72. Horne, J.P.; Hubbart, J.A. A Spatially Distributed Investigation of Stream Water Temperature in a Contemporary Mixed-Land-Use Watershed. *Water* **2020**, *12*, 1756, doi:10.3390/w12061756.
73. He, M.; Hogue, T.S. Integrating Hydrologic Modeling and Land Use Projections for Evaluation of Hydrologic Response and Regional Water Supply Impacts in Semi-Arid Environments. *Environ Earth Sci* **2012**, *65*, 1671–1685, doi:10.1007/s12665-011-1144-3.
74. Borman, M.M.; Larson, L.L. A Case Study of River Temperature Response to Agricultural Land Use and Environmental Thermal Patterns. *Journal of Soil and Water Conservation* **2003**, *58*, 8–12.

75. Johnson, S.L.; Jones, J.A. Stream Temperature Responses to Forest Harvest and Debris Flows in Western Cascades, Oregon. *Canadian Journal of Fisheries and Aquatic Sciences* **2000**, *57*, 30–39, doi:10.1139/cjfas-57-S2-30.
76. Broadmeadow, S.B.; Jones, J.G.; Langford, T.E.L.; Shaw, P.J.; Nisbet, T.R. The Influence of Riparian Shade on Lowland Stream Water Temperatures in Southern England and Their Viability for Brown Trout. *River Res. Applic.* **2011**, *27*, 226–237, doi:10.1002/rra.1354.
77. Gomi, T.; Moore, R.D.; Dhakal, A.S. Headwater Stream Temperature Response to Clear-Cut Harvesting with Different Riparian Treatments, Coastal British Columbia, Canada. *Water Resour. Res.* **2006**, *42*, W08437, doi:10.1029/2005WR004162.
78. Simmons, J.A.; Anderson, M.; Dress, W.; Hanna, C.; Hornbach, D.J.; Janmaat, A.; Kuserk, F.; March, J.G.; Murray, T.; Niedzwiecki, J.; et al. A Comparison of the Temperature Regime of Short Stream Segments under Forested and Non-Forested Riparian Zones at Eleven Sites Across North America. *River Res. Applic.* **2015**, *31*, 964–974, doi:10.1002/rra.2796.
79. Kalny, G.; Laaha, G.; Melcher, A.; Trimmel, H.; Weihs, P.; Rauch, H.P. The Influence of Riparian Vegetation Shading on Water Temperature during Low Flow Conditions in a Medium Sized River. *Knowledge and Management of Aquatic Ecosystems* **2017**, *418*, 1–14.
80. Imholt, C.; Soulsby, C.; Malcolm, I. a.; Gibbins, C. n. Influence of Contrasting Riparian Forest Cover on Stream Temperature Dynamics in Salmonid Spawning and Nursery Streams. *Ecohydrol.* **2013**, *6*, 380–392, doi:10.1002/eco.1291.
81. Zeng, R.; Cai, X. Analyzing Streamflow Changes: Irrigation-Enhanced Interaction between Aquifer and Streamflow in the Republican River Basin. *Hydrol. Earth Syst. Sci.* **2014**, *18*, 493–502, doi:10.5194/hess-18-493-2014.
82. Essaid, H.I.; Caldwell, R.R. Evaluating the Impact of Irrigation on Surface Water - Groundwater Interaction and Stream Temperature in an Agricultural Watershed. *Science of the Total Environment* **2017**, *599–600*, 581–596.
83. Webb, B.W.; Clack, P.D.; Walling, D.E. Water–Air Temperature Relationships in a Devon River System and the Role of Flow. *Hydrological Processes* **2003**, *17*, 3069–3084, doi:10.1002/hyp.1280.
84. van Vliet, M.T.H.; Ludwig, F.; Zwolsman, J.J.G.; Weedon, G.P.; Kabat, P. Global River Temperatures and Sensitivity to Atmospheric Warming and Changes in River Flow. *Water Resour. Res.* **2011**, *47*, W02544, doi:10.1029/2010WR009198.
85. Fullerton, A.H.; Torgersen, C.E.; Lawler, J.J.; Steel, E.A.; Ebersole, J.L.; Lee, S.Y. Longitudinal Thermal Heterogeneity in Rivers and Refugia for Coldwater Species: Effects of Scale and Climate Change. *Aquat Sci* **2018**, *80*, 3, doi:10.1007/s00027-017-0557-9.
86. Allan, J.D. Landscapes and Riverscapes: The Influence of Land Use on Stream Ecosystems. *Annu. Rev. Ecol. Evol. Syst.* **2004**, *35*, 257–284, doi:10.1146/annurev.ecolsys.35.120202.110122.
87. Arismendi, I.; Johnson, S.L.; Dunham, J.B. Technical Note: Higher-Order Statistical Moments and a Procedure That Detects Potentially Anomalous Years as Two Alternative Methods Describing Alterations in Continuous Environmental Data. *Hydrol. Earth Syst. Sci.* **2015**, *19*, 1169–1180, doi:10.5194/hess-19-1169-2015.
88. Arismendi, I.; Groom, J.D. A Novel Approach for Examining Downstream Thermal Responses of Streams to Contemporary Forestry. *Science of The Total Environment* **2019**, *651*, 736–748, doi:10.1016/j.scitotenv.2018.09.208.

89. Isaak, D.J.; Peterson, E.E.; Ver Hoef, J.M.; Wenger, S.J.; Falke, J.A.; Torgersen, C.E.; Sowder, C.; Steel, E.A.; Fortin, M.-J.; Jordan, C.E.; et al. Applications of Spatial Statistical Network Models to Stream Data: Spatial Statistical Network Models for Stream Data. *WIREs Water* **2014**, *1*, 277–294, doi:10.1002/wat2.1023.
90. Neumann, D.W.; Rajagopalan, B.; Zagona, E.A. Regression Model for Daily Maximum Stream Temperature. *J. Environ. Eng.* **2003**, *129*, 667–674, doi:10.1061/(ASCE)0733-9372(2003)129:7(667).
91. Piotrowski, A.P.; Napiorkowski, J.J. Simple Modifications of the Nonlinear Regression Stream Temperature Model for Daily Data. *Journal of Hydrology* **2019**, *572*, 308–328, doi:10.1016/j.jhydrol.2019.02.035.
92. Segura, C.; Caldwell, P.; Sun, G.; McNulty, S.; Zhang, Y. A Model to Predict Stream Water Temperature across the Conterminous USA. *Hydrological Processes* **2015**, *29*, 2178–2195, doi:https://doi.org/10.1002/hyp.10357.
93. Arismendi, I.; Safeeq, M.; Dunham, J.B.; Johnson, S.L. Can Air Temperature Be Used to Project Influences of Climate Change on Stream Temperature? *Environ. Res. Lett.* **2014**, *9*, 084015, doi:10.1088/1748-9326/9/8/084015.
94. Arismendi, I.; Johnson, S.L.; Dunham, J.B.; Haggerty, R.; Hockman-Wert, D. The Paradox of Cooling Streams in a Warming World: Regional Climate Trends Do Not Parallel Variable Local Trends in Stream Temperature in the Pacific Continental United States. *Geophysical Research Letters* **2012**, *39*, doi:https://doi.org/10.1029/2012GL051448.
95. PRISM Climate Group, Oregon State University, Http://Prism.Oregonstate.Edu, Created 1 March 2019.
96. Bradford, J.B.; Schlaepfer, D.R.; Lauenroth, W.K. Ecohydrology of Adjacent Sagebrush and Lodgepole Pine Ecosystems: The Consequences of Climate Change and Disturbance. *Ecosystems* **2014**, *17*, 590–605, doi:10.1007/s10021-013-9745-1.
97. Palmquist, K.A.; Schlaepfer, D.R.; Bradford, J.B.; Lauenroth, W.K. Mid-Latitude Shrub Steppe Plant Communities: Climate Change Consequences for Soil Water Resources. *Ecology* **2016**, *97*, 2342–2354, doi:10.1002/ecy.1457.
98. Abdulla, F.; Eshtawi, T.; Assaf, H. Assessment of the Impact of Potential Climate Change on the Water Balance of a Semi-Arid Watershed. *Water Resour Manage* **2009**, *23*, 2051–2068, doi:10.1007/s11269-008-9369-y.
99. Eckhardt, K.; Ulbrich, U. Potential Impacts of Climate Change on Groundwater Recharge and Streamflow in a Central European Low Mountain Range. *Journal of Hydrology* **2003**, *284*, 244–252, doi:10.1016/j.jhydrol.2003.08.005.
100. Meixner, T.; Manning, A.H.; Stonestrom, D.A.; Allen, D.M.; Ajami, H.; Blasch, K.W.; Brookfield, A.E.; Castro, C.L.; Clark, J.F.; Gochis, D.J.; et al. Implications of Projected Climate Change for Groundwater Recharge in the Western United States. *Journal of Hydrology* **2016**, *534*, 124–138, doi:10.1016/j.jhydrol.2015.12.027.
101. Schlaepfer, D.R.; Lauenroth, W.K.; Bradford, J.B. Consequences of Declining Snow Accumulation for Water Balance of Mid-Latitude Dry Regions. *Global Change Biology* **2012**, *18*, 1988–1997, doi:10.1111/j.1365-2486.2012.02642.x.
102. Konapala, G.; Mishra, A.K.; Wada, Y.; Mann, M.E. Climate Change Will Affect Global Water Availability through Compounding Changes in Seasonal Precipitation and Evaporation. *Nature Communications* **2020**, *11*, 3044, doi:10.1038/s41467-020-16757-w.

103. Bradford, J.B.; Schlaepfer, D.R.; Lauenroth, W.K.; Burke, I.C. Shifts in Plant Functional Types Have Time-Dependent and Regionally Variable Impacts on Dryland Ecosystem Water Balance. *Journal of Ecology* **2014**, *102*, 1408–1418, doi:10.1111/1365-2745.12289.
104. Pierson, F.B.; Jason Williams, C.; Hardegree, S.P.; Clark, P.E.; Kormos, P.R.; Al-Hamdan, O.Z. Hydrologic and Erosion Responses of Sagebrush Steppe Following Juniper Encroachment,Wildfire, and Tree Cutting. *Rangeland Ecology & Management* **2013**, *66*, 274–289, doi:10.2111/REM-D-12-00104.1.
105. Valayamkunnath, P.; Sridhar, V.; Zhao, W.; Allen, R.G. A Comprehensive Analysis of Interseasonal and Interannual Energy and Water Balance Dynamics in Semiarid Shrubland and Forest Ecosystems. *Science of The Total Environment* **2019**, *651*, 381–398, doi:10.1016/j.scitotenv.2018.09.130.
106. Scott, R.L.; Biederman, J.A. Critical Zone Water Balance Over 13 Years in a Semiarid Savanna. *Water Resources Research* **2019**, *55*, 574–588, doi:10.1029/2018WR023477.
107. Lewis, D.; Singer, M.J.; Dahlgren, R.A.; Tate, K.W. Hydrology in a California Oak Woodland Watershed: A 17-Year Study. *Journal of Hydrology* **2000**, *240*, 106–117, doi:10.1016/S0022-1694(00)00337-1.
108. Yang, Y.; Liu, D.L.; Anwar, M.R.; O&amp, G.; apos; Leary; Macadam, I.; Yang, Y. Water Use Efficiency and Crop Water Balance of Rainfed Wheat in a Semi-Arid Environment: Sensitivity of Future Changes to Projected Climate Changes and Soil Type. *Theoretical and Applied Climatology* **2016**, *123*, 565–580, doi:10.1007/s00704-015-1376-3.
109. Kundu, S.; Khare, D.; Mondal, A. Past, Present and Future Land Use Changes and Their Impact on Water Balance. *Journal of Environmental Management* **2017**, *197*, 582–596, doi:10.1016/j.jenvman.2017.04.018.
110. Chauvin, G.M.; Flerchinger, G.N.; Link, T.E.; Marks, D.; Winstral, A.H.; Seyfried, M.S. Long-Term Water Balance and Conceptual Model of a Semi-Arid Mountainous Catchment. *Journal of Hydrology* **2011**, *400*, 133–143, doi:10.1016/j.jhydrol.2011.01.031.
111. Marc, V.; Robinson, M. The Long-Term Water Balance (1972–2004) of Upland Forestry and Grassland at Plynlimon, Mid-Wales. *Hydrol. Earth Syst. Sci.* **2007**, *11*, 44–60, doi:10.5194/hess-11-44-2007.
112. Ward, A.S.; Gooseff, M.N.; Voltz, T.J.; Fitzgerald, M.; Singha, K.; Zarnetske, J.P. How Does Rapidly Changing Discharge during Storm Events Affect Transient Storage and Channel Water Balance in a Headwater Mountain Stream? *Water Resources Research* **2013**, *49*, 5473–5486, doi:https://doi.org/10.1002/wrcr.20434.
113. Wang, D.; Alimohammadi, N. Responses of Annual Runoff, Evaporation, and Storage Change to Climate Variability at the Watershed Scale. *Water Resources Research* **2012**, *48*, doi:https://doi.org/10.1029/2011WR011444.
114. do Nascimento, M.G.; Herdies, D.L.; de Souza, D.O. The South American Water Balance: The Influence of Low-Level Jets. *Journal of Climate* **2016**, *29*, 1429–1449, doi:http://dx.doi.org.ezproxy.proxy.library.oregonstate.edu/10.1175/JCLI-D-15-0065.1.
115. Weltz, M.A.; Blackburn, W.H. Water Budget for South Texas Rangelands. *Journal of Range Management* **1995**, *48*, 45–52, doi:10.2307/4002503.
116. Wilcox, B.P.; Dowhower, S.L.; Teague, W.R.; Thurow, T.L. Long-Term Water Balance in a Semiarid Shrubland. *Rangeland Ecology & Management* **2006**, *59*, 600–606.
117. Bugan, R.; Jovanovic, N.; De Clercq, W. The Water Balance of a Seasonal Stream in the Semi-Arid Western Cape (South Africa). *WSA* **2012**, *38*, 201–212, doi:10.4314/wsa.v38i2.5.

118. Cantón, Y.; Villagarcía, L.; Moro, M.J.; Serrano-Ortíz, P.; Were, A.; Alcalá, F.J.; Kowalski, A.S.; Solé-Benet, A.; Lázaro, R.; Domingo, F. Temporal Dynamics of Soil Water Balance Components in a Karst Range in Southeastern Spain: Estimation of Potential Recharge. *Hydrological Sciences Journal* **2010**, *55*, 737–753, doi:10.1080/02626667.2010.490530.
119. Deus, D.; Gloaguen, R.; Krause, P. Water Balance Modeling in a Semi-Arid Environment with Limited in Situ Data Using Remote Sensing in Lake Manyara, East African Rift, Tanzania. *Remote Sensing* **2013**, *5*, 1651–1680, doi:10.3390/rs5041651.
120. Eilers, V.H.M.; Carter, R.C.; Rushton, K.R. A Single Layer Soil Water Balance Model for Estimating Deep Drainage (Potential Recharge): An Application to Cropped Land in Semi-Arid North-East Nigeria. *Geoderma* **2007**, *140*, 119–131, doi:10.1016/j.geoderma.2007.03.011.
121. Ochoa, C.; Caruso, P.; Ray, G.; Deboodt, T.; Jarvis, W.; Guldan, S. Ecohydrologic Connections in Semiarid Watershed Systems of Central Oregon USA. *Water* **2018**, *10*, 181, doi:10.3390/w10020181.
122. Ray, G.; Ochoa, C.G.; Deboodt, T.; Mata-Gonzalez, R. Overstory–Understory Vegetation Cover and Soil Water Content Observations in Western Juniper Woodlands: A Paired Watershed Study in Central Oregon, USA. *Forests* **2019**, *10*, 151, doi:10.3390/f10020151.
123. Abdallah, M.A.B.; Durfee, N.; Mata-Gonzalez, R.; Ochoa, C.G.; Noller, J.S. Water Use and Soil Moisture Relationships on Western Juniper Trees at Different Growth Stages. *Water* **2020**, *12*, 26.
124. Angell, R.F.; Miller, R.F. Simulation of Leaf Conductance and Transpiration in Juniperus Occidentalis. *Forest Science* **1994**, *40*, 5–17.
125. Scott, R.L. Using Watershed Water Balance to Evaluate the Accuracy of Eddy Covariance Evaporation Measurements for Three Semiarid Ecosystems. *Agricultural and Forest Meteorology* **2010**, *150*, 219–225, doi:10.1016/j.agrformet.2009.11.002.
126. Todd, R.W.; Evett, S.R.; Howell, T.A. The Bowen Ratio-Energy Balance Method for Estimating Latent Heat Flux of Irrigated Alfalfa Evaluated in a Semi-Arid, Advective Environment. *Agricultural and Forest Meteorology* **2000**, *103*, 335–348, doi:10.1016/S0168-1923(00)00139-8.
127. Valayamkunnath, P.; Sridhar, V.; Zhao, W.; Allen, R.G. Intercomparison of Surface Energy Fluxes, Soil Moisture, and Evapotranspiration from Eddy Covariance, Large-Aperture Scintillometer, and Modeling across Three Ecosystems in a Semiarid Climate. *Agricultural and Forest Meteorology* **2018**, *248*, 22–47, doi:10.1016/j.agrformet.2017.08.025.
128. Yeşilırmak, E. Temporal Changes of Warm-Season Pan Evaporation in a Semi-Arid Basin in Western Turkey. *Stoch Environ Res Risk Assess* **2013**, *27*, 311–321, doi:10.1007/s00477-012-0605-x.
129. López-Urrea, R.; Martín de Santa Olalla, F.; Fabeiro, C.; Moratalla, A. Testing Evapotranspiration Equations Using Lysimeter Observations in a Semiarid Climate. *Agricultural Water Management* **2006**, *85*, 15–26, doi:10.1016/j.agwat.2006.03.014.
130. Kume, T.; Otsuki, K.; Du, S.; Yamanaka, N.; Wang, Y.-L.; Liu, G.-B. Spatial Variation in Sap Flow Velocity in Semiarid Region Trees: Its Impact on Stand-Scale Transpiration Estimates. *Hydrological Processes* **2012**, *26*, 1161–1168, doi:https://doi.org/10.1002/hyp.8205.
131. Hargreaves, G.H.; Samani, Z.A. Reference Crop Evapotranspiration from Temperature. *Applied Engineering in Agriculture* **1985**, *1*, 96–99, doi:10.13031/2013.26773.

132. Todorovic, M.; Karic, B.; Pereira, L.S. Reference Evapotranspiration Estimate with Limited Weather Data across a Range of Mediterranean Climates. *Journal of Hydrology* **2013**, *481*, 166–176, doi:10.1016/j.jhydrol.2012.12.034.
133. Raziei, T.; Pereira, L.S. Estimation of ETo with Hargreaves–Samani and FAO-PM Temperature Methods for a Wide Range of Climates in Iran. *Agricultural Water Management* **2013**, *121*, 1–18, doi:10.1016/j.agwat.2012.12.019.
134. Thornthwaite, C.; Mather, J. *The Water Balance, Climatology,VIII(1)*; Centerton, NJ, 1955;
135. Thornthwaite, C.W.; Mather, J.R. Instructions and Tables for Computing Potential Evapotranspiration and the Water Balance: Centerton, N.J., Laboratory of Climatology, Publications in Climatology. **1957**, *10*, 132.
136. Gudulas, K.; Voudouris, K.; Soulios, G.; Dimopoulos, G. Comparison of Different Methods to Estimate Actual Evapotranspiration and Hydrologic Balance. *Desalination and Water Treatment* **2013**, *51*, 2945–2954, doi:10.1080/19443994.2012.748443.
137. Alley, W.M. On the Treatment of Evapotranspiration, Soil Moisture Accounting, and Aquifer Recharge in Monthly Water Balance Models. *Water Resources Research* **1984**, *20*, 1137–1149, doi:https://doi.org/10.1029/WR020i008p01137.
138. Barlow, P.; Leake, S. *Streamflow Depletion by Wells: Understanding and Managing Effects of Groundwater Pumping on Streamflow*; Circular; US Geological Survey Circular 1376: Reston,VA, 2012;
139. Taylor, R.G.; Scanlon, B.; Döll, P.; Rodell, M.; Van Beek, R.; Wada, Y.; Longuevergne, L.; Leblanc, M.; Famiglietti, J.S.; Edmunds, M.; et al. Ground Water and Climate Change. *Nature Climate Change; London* **2013**, *3*, 322–329, doi:http://dx.doi.org.ezproxy.proxy.library.oregonstate.edu/10.1038/nclimate1744.
140. Sophocleous, M. Interactions between Groundwater and Surface Water: The State of the Science. *Hydrogeology Journal* **2002**, *10*, 52–67, doi:10.1007/s10040-001-0170-8.
141. Ochoa, C.G.; Fernald, A.G.; Guldan, S.J.; Tidwell, V.C.; Shukla, M.K. Shallow Aquifer Recharge from Irrigation in a Semiarid Agricultural Valley in New Mexico. *J. Hydrol. Eng.* **2013**, *18*, 1219–1230, doi:10.1061/(ASCE)HE.1943-5584.0000718.
142. Caruso, P.; Ochoa, C.G.; Jarvis, W.T.; Deboodt, T. A Hydrogeologic Framework for Understanding Local Groundwater Flow Dynamics in the Southeast Deschutes Basin, Oregon, USA. *Geosciences* **2019**, *9*, 57, doi:10.3390/geosciences9020057.
143. Seyfried, M.S.; Schwinning, S.; Walvoord, M.A.; Pockman, W.T.; Newman, B.D.; Jackson, R.B.; Phillips, F.M. Ecohydrological Control of Deep Drainage in Arid and Semiarid Regions. *Ecology* **2005**, *86*, 277–287, doi:10.1890/03-0568.
144. Ryel, R.J.; Caldwell, M.M.; Leffler, A.J.; Yoder, C.K. Rapid Soil Moisture Recharge to Depth by Roots in a Stand of Artemisia Tridentata. *Ecology* **2003**, *84*, 757–764, doi:https://doi.org/10.1890/0012-9658(2003)084[0757:RSMRTD]2.0.CO;2.
145. Flerchinger, G.N.; Cooley, K.R. A Ten-Year Water Balance of a Mountainous Semi-Arid Watershed. *Journal of Hydrology* **2000**, *237*, 86–99, doi:10.1016/S0022-1694(00)00299-7.
146. Scanlon, B.R.; Healy, R.W.; Cook, P.G. Choosing Appropriate Techniques for Quantifying Groundwater Recharge. *Hydrogeology Journal* **2002**, 22.
147. Kendy, E.; Gérard-Marchant, P.; Walter, M.T.; Zhang, Y.; Liu, C.; Steenhuis, T.S. A Soil-Water-Balance Approach to Quantify Groundwater Recharge from Irrigated Cropland in the North China Plain. *Hydrological Processes* **2003**, *17*, 2011–2031, doi:https://doi.org/10.1002/hyp.1240.

148. Okumura, A.; Hosono, T.; Boateng, D.; Shimada, J. Evaluations of the Downward Velocity of Soil Water Movement in the Unsaturated Zone in a Groundwater Recharge Area Using Δ18 O Tracer: The Kumamoto Region, Southern Japan. *Geol Cro* **2018**, *71*, 65–82, doi:10.4154/gc.2018.09.
149. Sammis, T.W.; Evans, D.D.; Warrick, A.W. Comparison of Methods to Estimate Deep Percolation Rates1. *JAWRA Journal of the American Water Resources Association* **1982**, *18*, 465–470, doi:https://doi.org/10.1111/j.1752-1688.1982.tb00013.x.
150. Healy, R.W.; Cook, P.G. Using Groundwater Levels to Estimate Recharge. *Hydrogeology Journal* **2002**, *10*, 91–109, doi:10.1007/s10040-001-0178-0.
151. Jassas, H.; Merkel, B. Estimating Groundwater Recharge in the Semiarid Al-Khazir Gomal Basin, North Iraq. *Water* **2014**, *6*, 2467–2481, doi:10.3390/w6082467.
152. Risser, D.W.; Gburek, W.J.; Folmar, G.J. Comparison of Recharge Estimates at a Small Watershed in East-Central Pennsylvania, USA. *Hydrogeology Journal* **2009**, 13.
153. Wang, X.; Zhang, G.; Xu, Y.J. Spatiotemporal Groundwater Recharge Estimation for the Largest Rice Production Region in Sanjiang Plain, Northeast China. *Journal of Water Supply : Research and Technology - AQUA* **2014**, *63*, 630–641, doi:http://dx.doi.org.ezproxy.proxy.library.oregonstate.edu/10.2166/aqua.2014.024.
154. Acharya, B.S.; Kharel, G.; Zou, C.B.; Wilcox, B.P.; Halihan, T. Woody Plant Encroachment Impacts on Groundwater Recharge: A Review. *Water; Basel* **2018**, *10*, doi:http://dx.doi.org.ezproxy.proxy.library.oregonstate.edu/10.3390/w10101466.
155. Moore, G.W.; Barre, D.A.; Owens, M.K. Does Shrub Removal Increase Groundwater Recharge in Southwestern Texas Semiarid Rangelands? *Rangeland Ecology & Management* **2012**, *65*, 1–10, doi:10.2111/REM-D-11-00055.1.
156. Anderson, E.W.; Borman, M.M.; Krueger, W.C. *The Ecological Provinces of Oregon: A Treatise on the Basic Ecological Geography of the State. SR 990, Oregon Agricultural Experiment Station*; 1998;
157. Durfee, N.; Ochoa, C.G.; Mata-Gonzalez, R. The Use of Low-Altitude UAV Imagery to Assess Western Juniper Density and Canopy Cover in Treated and Untreated Stands. *Forests* **2019**, *10*, 296, doi:10.3390/f10040296.
158. Ray, G.L. Long-term Ecohydrologic Response to Western Juniper (Juniperus occidentalis) Control in Semiarid Watersheds of Central Oregon : A Paired Watershed Study. Master's thesis, Oregon State University, 2015.
159. Bates, J.D.; Svejcar, T.; Miller, R.; Davies, K.W. Plant Community Dynamics 25 Years after Juniper Control. *Rangeland Ecology & Management* **2017**, *70*, 356–362, doi:10.1016/j.rama.2016.11.003.
160. Cooperative Climatological Data Summaries, Western Regional Climate Center Available online: http://www.wrcc.dri.edu/cgi-bin/cliMAIN.pl?or0501.
161. Fisher, M. Analysis of Hydrology and Erosion in Small, Paired Watersheds in a Juniper-Sagebrush Area of Central Oregon, Oregon State University: Corvallis, OR, 2004.
162. Soil Survey Staff Natural Resources Conservation Service Official Soil Series Descriptions (OSDs) NRCS Soils Available online: https://www.nrcs.usda.gov/wps/portal/nrcs/detail/soils/home/?cid=nrcs142p2_053587 (accessed on 13 May 2018).

163. USDA Natural Resources Conservation Service. (2021). SNOwpack TELemetry Network (SNOTEL). NRCS Available online: https://data.nal.usda.gov/dataset/snowpack-telemetry-network-snotel (accessed on 18 September 2021).
164. Kilpatrick, F.A.; Schneider, V.R. *Use of Flumes in Measuring Discharge*; Techniques of Water-Resources Investigations; 1983;
165. Samani, Z. Discussion of "History and Evaluation of Hargreaves Evapotranspiration Equation"by George H. Hargreaves and Richard G. Allen. *J. Irrig. Drain Eng.* **2004**, *130*, 447–448, doi:10.1061/(ASCE)0733-9437(2004)130:5(447.2).
166. Dingman, S.L. *Physical Hydrology*; 3rd ed.; Waveland Press, Inc.: Long Grove, IL, 2015;
167. Deboodt, T.L. Watershed response to western juniper control. Doctoral Dissertation, Oregon State University: Corvallis, OR, 2008.
168. Brooks, K.N.; Ffolliott, P.F.; Gregersen, H.M.; Debano, L.F. Groundwater. In *Hydrology and the management of watersheds*; Iowa State Press: Ames, IA, 2003; pp. 107–121.
169. Dilts, T.E.; Weisberg, P.J.; Dencker, C.M.; Chambers, J.C. Functionally Relevant Climate Variables for Arid Lands: A Climatic Water Deficit Approach for Modelling Desert Shrub Distributions. *Journal of Biogeography* **2015**, *42*, 1986–1997, doi:https://doi.org/10.1111/jbi.12561.
170. Lesica, P.; Kittelson, P.M. Precipitation and Temperature Are Associated with Advanced Flowering Phenology in a Semi-Arid Grassland. *Journal of Arid Environments* **2010**, *74*, 1013–1017, doi:10.1016/j.jaridenv.2010.02.002.
171. Niemeyer, R.J.; Link, T.E.; Seyfried, M.S.; Flerchinger, G.N. Surface Water Input from Snowmelt and Rain Throughfall in Western Juniper: Potential Impacts of Climate Change and Shifts in Semi-Arid Vegetation. *Hydrol. Process.* **2016**, *30*, 3046–3060, doi:10.1002/hyp.10845.
172. Yaseef, N.R.; Yakir, D.; Rotenberg, E.; Schiller, G.; Cohen, S. Ecohydrology of a semi-arid forest: partitioning among water balance components and its implications for predicted precipitation changes. *Ecohydrology* **2010**, *3*, 143–154, doi:10.1002/eco.65.
173. Kwon, H.; Pendall, E.; Ewers, B.E.; Cleary, M.; Naithani, K. Spring Drought Regulates Summer Net Ecosystem CO2 Exchange in a Sagebrush-Steppe Ecosystem. *Agricultural and Forest Meteorology* **2008**, *148*, 381–391, doi:10.1016/j.agrformet.2007.09.010.
174. Young, J.A.; Evans, R.A.; Easi, D.A. Stem Flow on Western Juniper (Juniperus Occidentalis) Trees. *Weed Science* **1984**, *32*, 320–327.
175. Sturges, D.L.; Trlica, M.J. Root Weights and Carbohydrate Reserves of Big Sagebrush. *Ecology* **1978**, *59*, 1282–1285.
176. Blarasin, M.; Quinodóz, F.B.; Cabrera, A.; Matteoda, E.; Alincastro, N.; Albo, G. Weekly and Monthly Groundwater Recharge Estimation in A Rural Piedmont Environment Using the Water Table Fluctuation Method. *International Journal of Environmental & Agriculture Research (* **2016**, *2*, 10.
177. Rutledge, A.T. *Computer Programs for Describing the Recession of Ground-Water Discharge and for Estimating Mean Ground-Water Recharge and Discharge from Streamflow Records-Update*; Water-Resources Investigations Report; Supercedes WRI 93-4121.; 1998;
178. Delin, G.N.; Healy, R.W.; Lorenz, D.L.; Nimmo, J.R. Comparison of Local- to Regional-Scale Estimates of Ground-Water Recharge in Minnesota, USA. *Journal of Hydrology* **2007**, *334*, 231–249, doi:10.1016/j.jhydrol.2006.10.010.
179. Arnold, J.G.; Moriasi, D.N.; Gassman, P.W.; Abbaspour, K.C.; White, M.J.; Srinivasan, R.; Santhi, C.; Harmel, R.D.; Griensven, A. van; Liew, M.W.V.; et al. SWAT: Model Use,

Calibration, and Validation. *Transactions of the ASABE* **2012**, *55*, 1491–1508, doi:10.13031/2013.42256.
180. Senay, G.B. Satellite Psychrometric Formulation of the Operational Simplified Surface Energy Balance (SSEBop) Model for Quantifying and Mapping Evapotranspiration. *Applied Engineering in Agriculture* **2018**, *34*, 555–566, doi:10.13031/aea.12614.
181. Senay, G.B.; Bohms, S.; Singh, R.K.; Gowda, P.H.; Velpuri, N.M.; Alemu, H.; Verdin, J.P. Operational Evapotranspiration Mapping Using Remote Sensing and Weather Datasets: A New Parameterization for the SSEB Approach. *JAWRA Journal of the American Water Resources Association* **2013**, *49*, 577–591, doi:10.1111/jawr.12057.
182. Norman, J.M.; Kustas, W.P.; Humes, K.S. A Two-Source Approach for Estimating Soil and Vegetation Fluxes from Observations of Directional Radiometric Surface Temperature. *Agricultural and Forest Meteorology* **1995**, *80*.
183. Zhuang, Q.; Shao, H.; Guan, D. Operational Daily Evapotranspiration Mapping at Field Scale Based on SSEBop Model and Spatiotemporal Fusion of Multi-Source Remote Sensing Data. *PLOS ONE* **2022**, *17*, e0264133, doi:10.1371/journal.pone.0264133.
184. Chen, P.-Y.; Fedosejevs, G.; Tiscareño-LóPez, M.; Arnold, J.G. Assessment of MODIS-EVI, MODIS-NDVI and VEGETATION-NDVI Composite Data Using Agricultural Measurements: An Example at Corn Fields in Western Mexico. *Environ Monit Assess* **2006**, *119*, 69–82, doi:10.1007/s10661-005-9006-7.
185. French, A.N.; Hunsaker, D.J.; Sanchez, C.A.; Saber, M.; Gonzalez, J.R.; Anderson, R. Satellite-Based NDVI Crop Coefficients and Evapotranspiration with Eddy Covariance Validation for Multiple Durum Wheat Fields in the US Southwest. *Agricultural Water Management* **2020**, *239*, 106266, doi:10.1016/j.agwat.2020.106266.
186. Del Grosso, S.J.; Parton, W.J.; Derner, J.D.; Chen, M.; Tucker, C.J. Simple Models to Predict Grassland Ecosystem C Exchange and Actual Evapotranspiration Using NDVI and Environmental Variables. *Agricultural and Forest Meteorology* **2018**, *249*, 1–10, doi:10.1016/j.agrformet.2017.11.007.
187. Van De Griend, A.A.; Owe, M. On the Relationship between Thermal Emissivity and the Normalized Difference Vegetation Index for Natural Surfaces. *International Journal of Remote Sensing* **1993**, *14*, 1119–1131, doi:10.1080/01431169308904400.
188. Gao, B. NDWI—A Normalized Difference Water Index for Remote Sensing of Vegetation Liquid Water from Space. *Remote Sensing of Environment* **1996**, *58*, 257–266, doi:10.1016/S0034-4257(96)00067-3.
189. Wilson, E.H.; Sader, S.A. Detection of Forest Harvest Type Using Multiple Dates of Landsat TM Imagery. *Remote Sensing of Environment* **2002**, *80*, 385–396, doi:10.1016/S0034-4257(01)00318-2.
190. Huang, C.; Li, Y.; Gu, J.; Lu, L.; Li, X. Improving Estimation of Evapotranspiration under Water-Limited Conditions Based on SEBS and MODIS Data in Arid Regions. *Remote Sensing* **2015**, *7*, 16795–16814, doi:10.3390/rs71215854.
191. Liu, C.; Sun, G.; McNulty, S.G.; Noormets, A.; Fang, Y. Environmental Controls on Seasonal Ecosystem Evapotranspiration/Potential Evapotranspiration Ratio as Determined by the Global Eddy Flux Measurements. *Hydrol. Earth Syst. Sci.* **2017**, *21*, 311–322, doi:10.5194/hess-21-311-2017.

192. Peng, L.; Zeng, Z.; Wei, Z.; Chen, A.; Wood, E.F.; Sheffield, J. Determinants of the Ratio of Actual to Potential Evapotranspiration. *Global Change Biology* **2019**, *25*, 1326–1343, doi:10.1111/gcb.14577.
193. Lafleur, P.M.; Hember, R.A.; Admiral, S.W.; Roulet, N.T. Annual and Seasonal Variability in Evapotranspiration and Water Table at a Shrub-Covered Bog in Southern Ontario, Canada. *Hydrol. Process.* **2005**, *19*, 3533–3550, doi:10.1002/hyp.5842.
194. Holzman, M.E.; Rivas, R.E.; Bayala, M.I. Relationship between TIR and NIR-SWIR as Indicator of Vegetation Water Availability. *Remote Sensing* **2021**, *13*, 3371, doi:10.3390/rs13173371.
195. Western Regional Climate Center Available online: https://wrcc.dri.edu/cgi-bin/cliMAIN.pl?or0501.
196. Durfee, N.; Ochoa, C.G. The Seasonal Water Balance of Western Juniper-Dominated and Big Sagebrush-Dominated Watersheds. *Hydrology* **2021**, *8*, 156, doi:10.3390/hydrology8040156.
197. Gorelick, N.; Hancher, M.; Dixon, M.; Ilyushchenko, S.; Thau, D.; Moore, R. Google Earth Engine: Planetary-Scale Geospatial Analysis for Everyone. *Remote Sensing of Environment* **2017**, *202*, 18–27, doi:10.1016/j.rse.2017.06.031.
198. Running, S.W.; Mu, Q.; Zhao, M.; Moreno, A. User's Guide: MODIS Global Terrestrial Evapotranspiration (ET) Product (MOD16A2/A3 and Year-End Gap-Filled MOD16A2GF/A3GF) NASA Earth Observing System MODIS Land Algorithm (For Collection 6). Version 2.2 2019.
199. Ellsäßer, F.; Röll, A.; Stiegler, C.; Hendrayanto; Hölscher, D. Introducing QWaterModel, a QGIS Plugin for Predicting Evapotranspiration from Land Surface Temperatures. *Environmental Modelling & Software* **2020**, *130*, 104739, doi:10.1016/j.envsoft.2020.104739.
200. Timmermans, W.J.; Kustas, W.P.; Andreu, A. Utility of an Automated Thermal-Based Approach for Monitoring Evapotranspiration. *Acta Geophys.* **2015**, *63*, 1571–1608, doi:10.1515/acgeo-2015-0016.
201. Guzinski, R.; Nieto, H.; Jensen, R.; Mendiguren, G. Remotely Sensed Land-Surface Energy Fluxes at Sub-Field Scale in Heterogeneous Agricultural Landscape and Coniferous Plantation. *Biogeosciences* **2014**, *11*, 5021–5046, doi:10.5194/bg-11-5021-2014.
202. Li, F.; Kustas, W.P.; Prueger, J.H.; Neale, C.M.U.; Jackson, T.J. Utility of Remote Sensing–Based Two-Source Energy Balance Model under Low- and High-Vegetation Cover Conditions. *J. Hydrometeor.* **2005**, *6*, 878–891, doi:10.1175/JHM464.1.
203. Norman, J.M.; Kustas, W.P.; Prueger, J.H.; Diak, G.R. Surface Flux Estimation Using Radiometric Temperature: A Dual-Temperature-Difference Method to Minimize Measurement Errors. *Water Resources Research* **2000**, *36*, 2263–2274, doi:https://doi.org/10.1029/2000WR900033.
204. Kustas, W.P.; Daughtry, C.S.T. Estimation of the Soil Heat Flux/Net Radiation Ratio from Spectral Data. *Agricultural and Forest Meteorology* **1990**, *49*, 205–223, doi:10.1016/0168-1923(90)90033-3.
205. An, N.; Hemmati, S.; Cui, Y.-J. Assessment of the Methods for Determining Net Radiation at Different Time-Scales of Meteorological Variables. *Journal of Rock Mechanics and Geotechnical Engineering* **2017**, *9*, 239–246, doi:10.1016/j.jrmge.2016.10.004.
206. Zhuang, Q.; Link to external site, this link will open in a new window; Wang, H.; Xu, Y. Comparison of Remote Sensing Based Multi-Source ET Models over Cropland in a Semi-Humid Region of China. *Atmosphere; Basel* **2020**, *11*, 325, doi:http://dx.doi.org.ezproxy.proxy.library.oregonstate.edu/10.3390/atmos11040325.

207. Al Zayed, I.S.; Elagib, N.A.; Ribbe, L.; Heinrich, J. Satellite-Based Evapotranspiration over Gezira Irrigation Scheme, Sudan: A Comparative Study. *Agricultural Water Management* **2016**, *177*, 66–76, doi:10.1016/j.agwat.2016.06.027.
208. Chun, J.A.; Baik, J.; Kim, D.; Choi, M. A Comparative Assessment of SWAT-Model-Based Evapotranspiration against Regional-Scale Estimates. *Ecological Engineering* **2018**, *122*, 1–9, doi:10.1016/j.ecoleng.2018.07.015.
209. Eliades, M.; Bruggeman, A.; Djuma, H.; Christofi, C.; Kuells, C. Quantifying Evapotranspiration and Drainage Losses in a Semi-Arid Nectarine (Prunus Persica Var. Nucipersica) Field with a Dynamic Crop Coefficient (Kc) Derived from Leaf Area Index Measurements. *Water* **2022**, *14*, 734, doi:10.3390/w14050734.
210. Wang, Y.; Cai, H.; Yu, L.; Peng, X.; Xu, J.; Wang, X. Evapotranspiration Partitioning and Crop Coefficient of Maize in Dry Semi-Humid Climate Regime. *Agricultural Water Management* **2020**, *236*, 106164, doi:10.1016/j.agwat.2020.106164.
211. Wight, J.R.; Hanson, C.L. Crop Coefficients for Rangeland. *Journal of Range Management* **1990**, *43*, 482, doi:10.2307/4002349.
212. Jensen, M.E.; Haise, H.R. Estimating Evapotranspiration from Solar Radiation. *Proceedings of the American Society of Civil Engineers, Journal of the Irrigation and Drainage Division* **1963**, *89*, 15–41.
213. Joiner, J.; Yoshida, Y.; Anderson, M.; Holmes, T.; Hain, C.; Reichle, R.; Koster, R.; Middleton, E.; Zeng, F.-W. Global Relationships among Traditional Reflectance Vegetation Indices (NDVI and NDII), Evapotranspiration (ET), and Soil Moisture Variability on Weekly Timescales. *Remote Sensing of Environment* **2018**, *219*, 339–352, doi:10.1016/j.rse.2018.10.020.
214. Seevers, P.M.; Ottmann, R.W. Evapotranspiration Estimation Using a Normalized Difference Vegetation Index Transformation of Satellite Data. *Hydrological Sciences Journal* **1994**, *39*, 333–345, doi:10.1080/02626669409492754.
215. Huang, S.; Tang, L.; Hupy, J.P.; Wang, Y.; Shao, G. A Commentary Review on the Use of Normalized Difference Vegetation Index (NDVI) in the Era of Popular Remote Sensing. *J. For. Res.* **2021**, *32*, 1–6, doi:10.1007/s11676-020-01155-1.
216. de Souza, R.; Buchhart, C.; Heil, K.; Plass, J.; Padilla, F.M.; Schmidhalter, U. Effect of Time of Day and Sky Conditions on Different Vegetation Indices Calculated from Active and Passive Sensors and Images Taken from UAV. *Remote Sensing* **2021**, *13*, 1691, doi:10.3390/rs13091691.
217. Beneduzzi, H.M.; Souza, E.G.; Bazzi, C.L.; Schenatto, K. Temporal Variability in Active Reflectance Sensor-Measured NDVI in Soybean and Wheat Crops. *Eng. Agríc.* **2017**, *37*, 771–781, doi:10.1590/1809-4430-eng.agric.v37n4p771-781/2017.
218. Rasmussen, J.; Ntakos, G.; Nielsen, J.; Svensgaard, J.; Poulsen, R.N.; Christensen, S. Are Vegetation Indices Derived from Consumer-Grade Cameras Mounted on UAVs Sufficiently Reliable for Assessing Experimental Plots? *European Journal of Agronomy* **2016**, *74*, 75–92, doi:10.1016/j.eja.2015.11.026.
219. Desai, S.; Singh, D.K.; Islam, A.; Sarangi, A. Multi-Site Calibration of Hydrological Model and Assessment of Water Balance in a Semi-Arid River Basin of India. *Quaternary International* **2021**, *571*, 136–149, doi:10.1016/j.quaint.2020.11.032.
220. Uniyal, B.; Jha, M.K.; Verma, A.K. Assessing Climate Change Impact on Water Balance Components of a River Basin Using SWAT Model. *Water Resources Management* **2015**, *29*,

4767–4785, doi:http://dx.doi.org.ezproxy.proxy.library.oregonstate.edu/10.1007/s11269-015-1089-5.
221. Chen, Y.; Marek, G.W.; Marek, T.H.; Porter, D.O.; Brauer, D.K.; Srinivasan, R. Simulating the Effects of Agricultural Production Practices on Water Conservation and Crop Yields Using an Improved SWAT Model in the Texas High Plains, USA. *Agricultural Water Management* **2021**, *244*, 106574, doi:10.1016/j.agwat.2020.106574.
222. Lopes, T.R.; Zolin, C.A.; Mingoti, R.; Vendrusculo, L.G.; Almeida, F.T. de; Souza, A.P. de; Oliveira, R.F. de; Paulino, J.; Uliana, E.M. Hydrological Regime, Water Availability and Land Use/Land Cover Change Impact on the Water Balance in a Large Agriculture Basin in the Southern Brazilian Amazon. *Journal of South American Earth Sciences* **2021**, *108*, 103224, doi:10.1016/j.jsames.2021.103224.
223. Eshtawi, T.; Evers, M.; Tischbein, B. Quantifying the Impact of Urban Area Expansion on Groundwater Recharge and Surface Runoff. *Hydrological Sciences Journal* **2015**, 150527103244004, doi:10.1080/02626667.2014.1000916.
224. Wu, Y.; Li, C.; Zhang, C.; Shi, X.; Bourque, C.P.-A.; Zhao, S. Evaluation of the Applicability of the SWAT Model in an Arid Piedmont Plain Oasis. *Water Science and Technology* **2016**, *73*, 1341–1348, doi:10.2166/wst.2015.609.
225. Kan, G.; He, X.; Ding, L.; Li, J.; Liang, K.; Hong, Y. Study on Applicability of Conceptual Hydrological Models for Flood Forecasting in Humid, Semi-Humid Semi-Arid and Arid Basins in China. *Water* **2017**, *9*, 719, doi:10.3390/w9100719.
226. Pradhan, P.; Tingsanchali, T.; Shrestha, S. Evaluation of Soil and Water Assessment Tool and Artificial Neural Network Models for Hydrologic Simulation in Different Climatic Regions of Asia. *Science of The Total Environment* **2020**, *701*, 134308, doi:10.1016/j.scitotenv.2019.134308.
227. Van Liew, M.W.; Veith, T.L.; Bosch, D.D.; Arnold, J.G. Suitability of SWAT for the Conservation Effects Assessment Project: Comparison on USDA Agricultural Research Service Watersheds. *Journal of Hydrologic Engineering* **2007**, *12*, 173–189, doi:10.1061/(ASCE)1084-0699(2007)12:2(173).
228. Brouziyne, Y.; Abouabdillah, A.; Bouabid, R.; Benaabidate, L.; Oueslati, O. SWAT Manual Calibration and Parameters Sensitivity Analysis in a Semi-Arid Watershed in North-Western Morocco. *Arab J Geosci* **2017**, *10*, 427, doi:10.1007/s12517-017-3220-9.
229. Ghoraba, S.M. Hydrological Modeling of the Simly Dam Watershed (Pakistan) Using GIS and SWAT Model. *Alexandria Engineering Journal* **2015**, *54*, 583–594, doi:10.1016/j.aej.2015.05.018.
230. Kiros, G.; Shetty, A.; Nandagiri, L. Performance Evaluation of SWAT Model for Land Use and Land Cover Changes under Different Climatic Conditions: A Review. *Hydrol Current Res* **2015**, *06*, doi:10.4172/2157-7587.1000216.
231. Gao, J.; Sheshukov, A.Y.; Yen, H.; White, M.J. Impacts of Alternative Climate Information on Hydrologic Processes with SWAT: A Comparison of NCDC, PRISM and NEXRAD Datasets. *CATENA* **2017**, *156*, 353–364, doi:10.1016/j.catena.2017.04.010.
232. Uniyal, B.; Dietrich, J.; Vasilakos, C.; Tzoraki, O. Evaluation of SWAT Simulated Soil Moisture at Catchment Scale by Field Measurements and Landsat Derived Indices. *Agricultural Water Management* **2017**, *193*, 55–70, doi:10.1016/j.agwat.2017.08.002.

233. Parajuli, P.B.; Jayakody, P.; Ouyang, Y. Evaluation of Using Remote Sensing Evapotranspiration Data in SWAT. *Water Resour Manage* **2018**, *32*, 985–996, doi:10.1007/s11269-017-1850-z.
234. Nilawar, A.; Calderella, C.; Lakhankar, T.; Waikar, M.; Munoz, J. Satellite Soil Moisture Validation Using Hydrological SWAT Model: A Case Study of Puerto Rico, USA. *Hydrology* **2017**, *4*, 45, doi:10.3390/hydrology4040045.
235. Abbaspour, K.C.; Yang, J.; Maximov, I.; Siber, R.; Bogner, K.; Mieleitner, J.; Zobrist, J.; Srinivasan, R. Modelling Hydrology and Water Quality in the Pre-Alpine/Alpine Thur Watershed Using SWAT. *Journal of Hydrology* **2007**, *333*, 413–430, doi:10.1016/j.jhydrol.2006.09.014.
236. Abbaspour, K.C.; Rouholahnejad, E.; Vaghefi, S.; Srinivasan, R.; Yang, H.; Kløve, B. A Continental-Scale Hydrology and Water Quality Model for Europe: Calibration and Uncertainty of a High-Resolution Large-Scale SWAT Model. *Journal of Hydrology* **2015**, *524*, 733–752, doi:10.1016/j.jhydrol.2015.03.027.
237. Andrade, C.W.L. de; Montenegro, S.M.G.L.; Montenegro, A.A.A.; Lima, J.R. de S.; Srinivasan, R.; Jones, C.A. Soil Moisture and Discharge Modeling in a Representative Watershed in Northeastern Brazil Using SWAT. *Ecohydrology & Hydrobiology* **2019**, *19*, 238–251, doi:10.1016/j.ecohyd.2018.09.002.
238. Mengistu, A.G.; van Rensburg, L.D.; Woyessa, Y.E. Techniques for Calibration and Validation of SWAT Model in Data Scarce Arid and Semi-Arid Catchments in South Africa. *Journal of Hydrology: Regional Studies* **2019**, *25*, 100621, doi:10.1016/j.ejrh.2019.100621.
239. Rajib, M.A.; Merwade, V.; Yu, Z. Multi-Objective Calibration of a Hydrologic Model Using Spatially Distributed Remotely Sensed/in-Situ Soil Moisture. *Journal of Hydrology* **2016**, *536*, 192–207, doi:10.1016/j.jhydrol.2016.02.037.
240. Kundu, D.; Vervoort, R.W.; van Ogtrop, F.F. The Value of Remotely Sensed Surface Soil Moisture for Model Calibration Using SWAT. *Hydrological Processes* **2017**, *31*, 2764–2780, doi:10.1002/hyp.11219.
241. *Urban Hydrology for Small Watersheds*; U.S. Department of Agriculture, Natural Resources Conservation Service, Conservation Engineering Division, 1986;
242. Ahl, R.S.; Woods, S.W.; Zuuring, H.R. Hydrologic Calibration and Validation of SWAT in a Snow-Dominated Rocky Mountain Watershed, Montana, U.S.A. [1]. *JAWRA Journal of the American Water Resources Association* **2008**, *44*, 1411–1430, doi:10.1111/j.1752-1688.2008.00233.x.
243. Dhami, B.; Himanshu, S.K.; Pandey, A.; Gautam, A.K. Evaluation of the SWAT Model for Water Balance Study of a Mountainous Snowfed River Basin of Nepal. *Environ Earth Sci* **2018**, *77*, 21, doi:10.1007/s12665-017-7210-8.
244. Azimi, M.; Heshmati, Gh.A.; Farahpour, M.; Faramarzi, M.; Abbaspour, K.C. Modeling the Impact of Rangeland Management on Forage Production of Sagebrush Species in Arid and Semi-Arid Regions of Iran. *Ecological Modelling* **2013**, *250*, 1–14, doi:10.1016/j.ecolmodel.2012.10.017.
245. Qiao, L.; Zou, C.B.; Will, R.E.; Stebler, E. Calibration of SWAT Model for Woody Plant Encroachment Using Paired Experimental Watershed Data. *Journal of Hydrology* **2015**, *523*, 231–239, doi:10.1016/j.jhydrol.2015.01.056.
246. White, J.; Stengel, V.; Rendon, S.; Banta, J. The Importance of Parameterization When Simulating the Hydrologic Response of Vegetative Land-Cover Change. *Hydrol. Earth Syst. Sci.* **2017**, *21*, 3975–3989, doi:10.5194/hess-21-3975-2017.

247. Brooks, H.C.; McIntyre, J.R.; Walkter, G.W. *Geology of the Oregon Part of the Baker 1° by 2° Quadrangle*; State of OR Department of Geology and Mineral Industries: Portland, OR, 1976; p. 28;.
248. Walker, G.W.; MacLeod, N.S.; Miller, R.J.; Raines, G.L.; Connors, K.A. *Spatial Digital Database for the Geologic Map of Oregon, Edition 2.0*; U.S. Geologic Survey: Menlo Park, CA, 2003;
249. Ludington, S.; Moring, B.C.; Miller, R.J.; Stone, P.A.; Bookstrom, A.A.; Bedford, D.R.; Evans, J.G.; Haxel, G.A.; Nutt, C.J.; Flyn, K.S.; et al. *Preliminary Integrated Geologic Map Databases of the United States: The Western States: California, Nevada, Arizona, Washington, Idaho, Utah (OFR 2005-1305), Version 1.3*; U.S. Geological Survey, 2003;
250. Bouyoucos, G.J. Hydrometer Method Improved for Making Particle Size Analyses of Soils. *Agron.j.* **1962**, *54*, 464–465, doi:10.2134/agronj1962.00021962005400050028x.
251. Burt, R.; Soil Survey Staff (ed.) *Soil Survey Field and Laboratory Methods Manual; Soil Survey Investigations Report No. 51; Version 2*; U.S. Department of Agriculture, Natural Resources Conservation Service, 2014; p. 487;.
252. van Genuchten, M.Th.; Leij, F.J.; Yates, S.R. *The RETC Code for Quantifying the Hydraulic Functions of Unsaturated Soils*; U.S. Salinity Laboratory, USDA, ARS, Riverside, California, 1991;
253. van Genuchten, M.Th.; Simunek, J.; Sejna, M. RETC for Windows, Version 6.02 2009.
254. Manning, R.; Griffith, J.P.; Pigot, T.F.; Vernon-Harcourt, L.F. On the Flow of Water in Open Channels and Pipes. *Transactions of the Institution of Civil Engineers of Ireland* **1890**, *20*, 161–207.
255. Oregon 10m Digital Elevation Model (DEM) Available online: https://spatialdata.oregonexplorer.info/geoportal/details;id=7a82c1be50504f56a9d49d13c7b4d9aa (accessed on 6 February 2020).
256. National Land Cover Dataset (NLCD) (accessed on 2 February 2020).
257. D. N. Moriasi; J. G. Arnold; M. W. Van Liew; R. L. Bingner; R. D. Harmel; T. L. Veith Model Evaluation Guidelines for Systematic Quantification of Accuracy in Watershed Simulations. *Transactions of the ASABE* **2007**, *50*, 885–900, doi:10.13031/2013.23153.
258. *National Engineering Handbook, Part 630 Hydrology, Chapter 9, Hydrologic Soil-Cover Complexes*; United States Department of Agriculture, National Resources Conservation Service, 2004;
259. Cao, W.; Bowden, W.B.; Davie, T.; Fenemor, A. Multi-Variable and Multi-Site Calibration and Validation of SWAT in a Large Mountainous Catchment with High Spatial Variability. *Hydrological Processes* **2006**, *20*, 1057–1073, doi:10.1002/hyp.5933.
260. X. Zhang; R. Srinivasan; M. Van Liew Multi-Site Calibration of the SWAT Model for Hydrologic Modeling. *Transactions of the ASABE* **2008**, *51*, 2039–2049, doi:10.13031/2013.25407.
261. Athira, P.; Sudheer, K.P. Calibration of Distributed Hydrological Models Considering the Heterogeneity of the Parameters across the Basin: A Case Study of SWAT Model. *Environ Earth Sci* **2021**, *80*, 131, doi:10.1007/s12665-021-09434-8.
262. R. Jiang; Y. Li; Q. Wang; K. Kuramochi; A. Hayakawa; K. P. Woli; R. Hatano Modeling the Water Balance Processes for Understanding the Components of River Discharge in a Non-Conservative Watershed. *Transactions of the ASABE* **2011**, *54*, 2171–2180, doi:10.13031/2013.40656.

263. Le Moine, N.; Andréassian, V.; Perrin, C.; Michel, C. How Can Rainfall-Runoff Models Handle Intercatchment Groundwater Flows? Theoretical Study Based on 1040 French Catchments. *Water Resources Research* **2007**, *43*, doi:10.1029/2006WR005608.
264. Hughes, J.D.; Langevin, C.D.; Banta, E.R. *Documentation for the MODFLOW 6 Framework*; Techniques and Methods; U.S. Geological Survey: Reston, VA, 2017; Vol. 6-A57;.
265. Langevin, C.D.; Hughes, J.D.; Banta, E.R.; Niswonger, R.G.; Panday, S.; Provost, A.M. *Documentation for the MODFLOW 6 Groundwater Flow Model*; U.S. Geological Survey, 2017;
266. Sao, D.; Kato, T.; Tu, L.H.; Thouk, P.; Fitriyah, A.; Oeurng, C. Evaluation of Different Objective Functions Used in the SUFI-2 Calibration Process of SWAT-CUP on Water Balance Analysis: A Case Study of the Pursat River Basin, Cambodia. *Water* **2020**, *12*, 2901, doi:10.3390/w12102901.
267. Pfannerstill, M.; Bieger, K.; Guse, B.; Bosch, D.D.; Fohrer, N.; Arnold, J.G. How to Constrain Multi-Objective Calibrations of the SWAT Model Using Water Balance Components. *JAWRA Journal of the American Water Resources Association* **2017**, *53*, 532–546, doi:10.1111/1752-1688.12524.
268. Her, Y.; Seong, C. Responses of Hydrological Model Equifinality, Uncertainty, and Performance to Multi-Objective Parameter Calibration. *Journal of Hydroinformatics* **2018**, *20*, 864–885, doi:10.2166/hydro.2018.108.
269. Zhang, L.; Xue, B.; Yan, Y.; Wang, G.; Sun, W.; Li, Z.; Yu, J.; Xie, G.; Shi, H. Model Uncertainty Analysis Methods for Semi-Arid Watersheds with Different Characteristics: A Comparative SWAT Case Study. *Water* **2019**, *11*, 1177, doi:10.3390/w11061177.
270. Ficklin, D.L.; Stewart, I.T.; Maurer, E.P. Effects of Climate Change on Stream Temperature, Dissolved Oxygen, and Sediment Concentration in the Sierra Nevada in California. *Water Resources Research* **2013**, *49*, 2765–2782, doi:10.1002/wrcr.20248.
271. Webb, B.W.; Hannah, D.M.; Moore, R.D.; Brown, L.E.; Nobilis, F. Recent Advances in Stream and River Temperature Research. *Hydrological Processes* **2008**, *22*, 902–918, doi:10.1002/hyp.6994.
272. Tague, C.; Farrell, M.; Grant, G.; Lewis, S.; Rey, S. Hydrogeologic Controls on Summer Stream Temperatures in the McKenzie River Basin, Oregon. *Hydrological Processes* **2007**, *21*, 3288–3300, doi:10.1002/hyp.6538.
273. Caldwell, T.G.; Wolaver, B.D.; Bongiovanni, T.; Pierre, J.P.; Robertson, S.; Abolt, C.; Scanlon, B.R. Spring Discharge and Thermal Regime of a Groundwater Dependent Ecosystem in an Arid Karst Environment. *Journal of Hydrology* **2020**, *587*, 124947, doi:10.1016/j.jhydrol.2020.124947.
274. Dugdale, S.J.; Malcolm, I.A.; Kantola, K.; Hannah, D.M. Stream Temperature under Contrasting Riparian Forest Cover: Understanding Thermal Dynamics and Heat Exchange Processes. *Science of The Total Environment* **2018**, *610–611*, 1375–1389, doi:10.1016/j.scitotenv.2017.08.198.
275. Garner, G.; Malcolm, I.A.; Sadler, J.P.; Hannah, D.M. The Role of Riparian Vegetation Density, Channel Orientation and Water Velocity in Determining River Temperature Dynamics. *Journal of Hydrology* **2017**, *553*, 471–485, doi:10.1016/j.jhydrol.2017.03.024.
276. Nusslé, S.; Matthews, K.R.; Carlson, S.M. Mediating Water Temperature Increases Due to Livestock and Global Change in High Elevation Meadow Streams of the Golden Trout Wilderness. *PLOS ONE* **2015**, *10*, e0142426, doi:10.1371/journal.pone.0142426.

277. Oles, K.M.; Weixelman, D.A.; Lile, D.F.; Tate, K.W.; Snell, L.K.; Roche, L.M. Riparian Meadow Response to Modern Conservation Grazing Management. *Environmental Management* **2017**, *60*, 383–395, doi:10.1007/s00267-017-0897-1.
278. Studinski, J.; Hartman, K.; Niles, J.; Keyser, P. The Effects of Riparian Forest Disturbance on Stream Temperature, Sedimentation, and Morphology. *Hydrobiologia* **2012**, *686*, 107–117, doi:10.1007/s10750-012-1002-7.
279. Alger, M.; Lane, B.A.; Neilson, B.T. Combined Influences of Irrigation Diversions and Associated Subsurface Return Flows on River Temperature in a Semi-Arid Region. *Hydrological Processes* **2021**, *35*, e14283, doi:10.1002/hyp.14283.
280. Mayer, T.D. Controls of Summer Stream Temperature in the Pacific Northwest. *Journal of Hydrology* **2012**, *475*, 323–335, doi:10.1016/j.jhydrol.2012.10.012.
281. Gu, C.; Anderson, W.P.; Colby, J.D.; Coffey, C.L. Air-stream Temperature Correlation in Forested and Urban Headwater Streams in the Southern Appalachians. *Hydrological Processes* **2015**, *29*, 1110–1118, doi:10.1002/hyp.10225.
282. Li, H.; Deng, X.; Kim, D.-Y.; Smith, E.P. Modeling Maximum Daily Temperature Using a Varying Coefficient Regression Model. *Water Resources Research* **2014**, *50*, 3073–3087, doi:https://doi.org/10.1002/2013WR014243.
283. Mohseni, O.; Stefan, H.G.; Erickson, T.R. A Nonlinear Regression Model for Weekly Stream Temperatures. *Water Resources Research* **1998**, *34*, 2685–2692, doi:https://doi.org/10.1029/98WR01877.
284. U.S. Department of the Interior *Riparian Area Management: Proper Functioning Condition Assessment for Lotic Areas. Technical Reference 1737-15*; Bureau of Land Management, National Operations Center: Denver, CO, 2015;
285. Rosgen, D.L.; Silvey, H.L. *Applied River Morphology*; Wildland Hydrology Books: Fort Collins, CO, 1996;
286. *Monitoring Manual for Grassland, Shrubland, and Savanna Ecosystems*; Herrick, J.E., Jornada Experimental Range, Eds.; USDA - ARS Jordana Experimental Range ; Distributed by the University of Arizona Press: Las Cruces, N.M. : Tucson, Ariz, 2005; ISBN 978-0-9755552-0-0.
287. Bos, M.G., Replogle, J.A., & Clemmens, A.J. Flow measuring flumes for open channel systems. John Wiley and Sons Inc: New York, NY, USA, 1984; ISBN Z-0471-80637-4
288. National Agriculture Imagery Program Digital Ortho Photo Image 2020.
289. Durfee, N.; Ochoa, C.G.; Jones, G. Stream Temperature and Environment Relationships in a Semiarid Riparian Corridor. *Land* **2021**, *10*, 519, doi:10.3390/land10050519.
290. Pedregosa, F.; Varoquaux, G.; Gramfort, A.; Michel, V.; Thirion, B.; Grisel, O.; Blondel, M.; Prettenhofer, P.; Weiss, R.; Dubourg, V.; et al. Scikit-Learn: Machine Learning in Python. *Machine Learning in Python* **2011**, *12*, 2825–2830.
291. Morrill, J.C.; Bales, R.C.; Conklin, M.H. Estimating Stream Temperature from Air Temperature: Implications for Future Water Quality. *J. Environ. Eng.* **2005**, *131*, 139–146, doi:10.1061/(ASCE)0733-9372(2005)131:1(139).
292. Bowler, D.E.; Mant, R.; Orr, H.; Hannah, D.M.; Pullin, A.S. What Are the Effects of Wooded Riparian Zones on Stream Temperature? *Environmental Evidence* **2012**, *1*, 3, doi:10.1186/2047-2382-1-3.